Department of Electrical and Computer Engineering

MmWave Heterogeneous Cellular Networks and Applications: A Stochastic Geometry Approach

Christodoulos Skouroumounis

A Dissertation

Submitted in Partial Fulfillment of the

Requirements for the Degree of

Doctor of Philosophy

at the University of Cyprus

October, 2019

APPROVAL PAGE

Christodoulos Skouroumounis

MmWave Heterogeneous Cellular Networks and Applications: A Stochastic Geometry Approach

The present Doctorate Dissertation was submitted in partial fulfillment of the requirements for the Degree of Doctor of Philosophy in the Department of Electrical and Computer Engineering, and was approved on October 8, 2019 by the members of the Examination Committee.

Committee Chair _____
Dr. Georgios Ellinas

Research Supervisor _____
Dr. Ioannis Krikidis

Committee Member _____
Dr. Kostas Berberides

Committee Member _____
Dr. Christoforos Hadjicostis

Committee Member _____
Dr. Ghassan Kraidy

Abstract

The widespread use of mobile devices and the emergence of new wireless services have led to an impressive escalation in data traffic demand, which poses extremely huge challenges in current communications systems that operate in sub-6 GHz bands. The investigation of novel paradigms of network deployments and spectrum utilization is required to support the upcoming demands for higher data volume, communication rate as well as system capacity. The deployment of heterogeneous networks (HetNets) operating in the millimeter-wave (mmWave) frequency band has been advocated as one of the most promising enabling technologies to meet these demanding requirements. However, the co-design of mmWave heterogeneous cellular networks with sophisticated communication and signal processing techniques, such as full-duplex (FD) radio, coordinated multi-point (CoMP) transmission, successive interference cancellation (SIC), power control and weighted cell association, has been disregarded. In addition, even though the synergy of communication and radar systems can potentially enhance the network performance in terms of interference mitigation and improved localization, its investigation in the context of mmWave heterogeneous cellular networks has been neglected. To this purpose, this PhD dissertation presents a novel analytical framework based on stochastic geometry to evaluate the achieved performance of the aforementioned techniques in next-generation mmWave heterogeneous cellular networks, from a macroscopic point-of-view.

Firstly in Chapter 3, we investigate the problem of base station (BS) cooperation for the co-design of HetNets and mmWave systems. Specifically, a novel low-complexity BS selection scheme was proposed, and its achieved network performance was evaluated in the context of three well-known association policies. Moreover, we investigate the employment of an ideal SIC scheme for the considered cellular networks to further enhance the achieved network performance. However,

the performance of a user is strongly correlated with its location with respect to the serving BS. Motivated by this, in Chapter 4, we evaluate the performance of mmWave heterogeneous cellular networks for two user location-based classifications, namely cell-center user (CCU) and cell-edge user (CEU). Aiming to further enhance the network's spectral efficiency, both the BSs and the users are able to operate in FD mode. Furthermore, the achieved performance under the utilization of an ideal SIC scheme is investigated. Nevertheless, to achieve the desired ubiquitous coverage in next-generation networks, the heterogeneous deployment of multi-band BSs is required.

In Chapter 5, we further extend our proposed mathematical framework in the context of HetNets sub-6 GHz/mmWave cellular networks, where users are classified either as CCU or CEU. In particular, we propose a novel hybrid cooperation scheme that exploits the CoMP technique in order to enhance the performance of the CEUs and provide ubiquitous connectivity. Finally, driven by the ever-increasing demand for systems with both communication and radar sensing capabilities, in Chapter 6, we study the synergy of communication and radar systems in the context of mmWave heterogeneous cellular networks by exploiting the concept of FD radio. Specifically, we propose a novel cooperative multi-point radar detection (CoMRD) technique, and its achieved detection performance was evaluated in the context of three hard-decision combining rules. Moreover, we study the spatial and temporal interference correlation of the considered network deployment by taking into account a repulsive point process and by investigating the joint detection probability over different time slots, respectively. By leveraging stochastic geometry tools, tractable closed-form expressions for fundamental network performance metrics, such as the coverage probability, network throughput and meta-distribution, are investigated throughout this PhD dissertation. These closed-form expressions provide a quick and convenient methodology of evaluating the system's performance and obtaining insights into how key system parameters affect the performance.

Περίληψη

Η ευρεία χρήση των κινητών συσκευών και η εμφάνιση νέων ασύρματων υπηρεσιών έχουν οδηγήσει σε μια εντυπωσιακή κλιμάκωση της ζήτησης της κυκλοφορίας δεδομένων, η οποία δημιουργεί εξαιρετικά τεράστιες προκλήσεις στα σημερινά συστήματα επικοινωνιών που λειτουργούν σε ζώνες κάτω των 6 GHz. Άρα, είναι απαραίτητη η διερεύνηση καινοτόμων παραδειγμάτων ανάπτυξης δικτύων και χρήσης του φάσματος για να υποστηριχθούν οι επερχόμενες απαιτήσεις για μεγαλύτερο όγκο δεδομένων, ρυθμό επικοινωνίας καθώς και χωρητικότητα του συστήματος. Η ανάπτυξη ετερογενών δικτύων τα οποία λειτουργούν στη ζώνη συχνοτήτων χιλιοστομετρικού κύματος υποστηρίζεται ως μία από τις πιο ελπιδοφόρες τεχνολογίες που επιτρέπουν την ικανοποίηση αυτών των απαιτήσεων. Ωστόσο, ο συν-σχεδιασμός των ετερογενών κυψελωτών δικτύων χιλιοστομετρικού κύματος με εξελιγμένες τεχνικές επικοινωνίας και επεξεργασίας σήματος, όπως την πλήρως αμφίδρομης επικοινωνία, τη συντονισμένη μετάδοση πολλαπλών σημείων, τη διαδοχική ακύρωση παρεμβολών, τον έλεγχος ισχύος και την σταθμισμένη σύνδεση του χρήστη, δεν έχουν ληφθεί υπόψη. Επιπλέον, παρόλο που η συνύπαρξη των συστημάτων επικοινωνίας και ραντάρ μπορεί να ενισχύσει την απόδοση του δικτύου από την άποψη της μείωσης των παρεμβολών και του βελτιωμένου εντοπισμού, η διερεύνησή της παραμελήθηκε στο πλαίσιο των ετερογενών δικτών χιλιοστομετρικού κύματος. Για το σκοπό αυτό, αυτή η διδακτορική διατριβή παρουσιάζει ένα νέο αναλυτικό πλαίσιο βασισμένο στην στοχαστική γεωμετρία για την αξιολόγηση της επιτευχθείσας απόδοσης των προαναφερθεισών τεχνικών στα επόμενης γενεάς ετερογενή δίκτυα χιλιοστομετρικού κύματος, από μακροσκοπική οπτική γωνία.

Acknowledgments

This work was carried out during the years 2014 – 2018 at the KIOS Research and Innovation Center of Excellence and the years 2018 – 2019 at the IRIDA Research Centre for Communication Technologies, Department of Electrical and Computer Engineering of University of Cyprus. These four years of the Ph.D. program has been an incredible journey in my life, and I would like to express my gratitude to many people for their help and supports during this journey.

First and foremost I want to express my deep gratitude to my advisor Prof. Ioannis Krikidis for encouraging my research on wireless cellular networks and for sharing his profound technical and scientific knowledge. While at any time giving me the freedom to pursue topics and ideas that appeared interesting to me, his thorough experience and insight provided an indispensable guideline throughout the course of my doctoral studies. I am extremely grateful for all the guidance and help from my advisor, which have really shaped me into an independent researcher and professional engineer. I also want to thank Dr. Constantinos Psomas for the invaluable comments and discussions, which have inspired me a lot for my research.

My life at both the KIOS and the IRIDA Research Centre for Communication Technologies has been really wonderful and memorable, thanks to my brilliant colleagues and friends. Particular thanks are due to my colleagues for numerous fruitful discussions both on- and off-topic. Their feedback and constructive criticism greatly enhanced the quality of this work.

I would like to thank my parents Antonis and Maria as well as my sisters and brother for their unconditional support and love. I also want to express my gratitude to my friends for being what they are. Finally, i would like to thank my wife, Samantha Mulqueen, for sharing this unbelievable Ph.D. journey with me. Despite the ups and downs, the encouragements from my family have always motivated me to be passionate and confident about my research and life.

Abbreviations

3GPP	**3**rd **G**eneration **P**artnership **P**roject
3D	Three-**D**imensional
4G	Fourth-**G**eneration
5G	Fifth-**G**eneration
ABF	**A**nalog **B**eam**f**orming
ABSF	**A**lmost **B**lank **S**ub-**F**rame
β**-GPP**	β-**G**inibre **P**oint **P**rocess
BS	**B**ase **S**tation
C-RAN	**C**loud-**R**adio **A**ccess **N**etwork
CA	**C**arrier **A**ggregation
CB	**C**oordinated **B**eamforming
CC	**C**omponent **C**arrier
ccdf	**C**omplimentary **C**umulative **D**istribution **F**unction
CCU	**C**ell-**C**enter **U**ser
CEU	**C**ell-**E**dge **U**ser
cdf	**C**umulative **D**istribution **F**unction
CoMP	**Co**ordinated **M**ulti-**P**oint
CoMRD	**Co**ordinated **M**ulti-Point **R**adar **S**ensing
CRE	**C**ell **R**ange **E**xpansion
CS	**C**oordinated **S**cheduling
D2D	**D**evice-to-**D**evice
DBF	**D**igital **B**eam**f**orming
DL	**D**own**l**ink

DPB **D**ynamic **P**oint **b**lanking

DPS **D**ynamic **P**oint **S**election

DUDe **D**ownlink-**U**plink **De**coupling

eICIC **e**nhanced **I**nter-**C**ell **I**nterference **C**oordination

feICIC **f**urther **e**nhanced **I**nter-**C**ell **I**nterference **C**oordination

FC **F**usion **C**enter

FD **F**ull-**D**uplex

FDD **F**requency **D**ivision **D**uplexing

FFR **F**ractional **F**requency **R**euse

GPP **G**inibre **P**oint **P**rocess

HBF **H**ybrid **B**eam**f**orming

HD **H**alf-**D**uplex

HetNet **Het**erogeneous **Net**work

ICI **I**nter-**C**ell **I**nterference

ICIC **I**nter-**C**ell **I**nterference **C**oordination

JCAS **J**oint **C**ommunication **a**nd Radar **S**ensing

JT **J**oint **T**ransmission

LoS **L**ine-**o**f-**S**ight

LTE **L**ong **T**erm **E**volution

M2M **M**achine-to-**M**achine

MCell **M**acro-**Cell**

mgf **M**oment **G**enerating **F**unction

MIMO **M**ultiple **I**nput **M**ultiple **O**utput

mmWave **m**illi**m**eter-**wave**

MUSIC **MU**ltible **SI**gnal **C**lassification

NLoS **N**on-**L**ine-**o**f-**S**ight

NOMA **N**on-**O**rthogonal-**M**ultiple-**A**ccess

NR **N**ew **R**adio

OFDM **O**rthogonal **F**requency **D**ivision **M**ultiplexing

P2P **P**oint-to-**P**oint

pdf **P**robability **D**ensity **F**unction

PGFL **P**robability **G**enerating **F**unctiona**l**

PP **P**oint **P**rocess

PPP **Poisson P**oint **P**rocess

RF **R**adio **F**requency

RRH **R**emote **R**adio **H**ead

RSS **R**eceived **S**ignal **S**trength

SCell **S**mall-**Cell**

SI **S**elf-**I**nterference

SIC **S**uccessive **I**nterference **C**ancellation

SIR **S**ignal-to-**I**nterference **R**atio

SINR **S**ignal-to-**I**nterference-plus-**N**oise **R**atio

SFR **S**oft **F**requency **R**euse

TDD **T**ime **D**ivision **D**ulexing

THz **T**era-**H**er**tz**

UL **U**p**l**ink

WiMAX **W**orldwide **I**nteroperability for **M**icrowave **A**ccess

WLAN **W**ireless **L**ocal **A**rea **N**etwork

WPAN **W**ireless **P**ersonal **A**rea **N**etwork

Publications

Book chapters

1. C. Psomas, **C. Skouroumounis**, and I. Krikidis, *Relay selection in modern communication systems*, chapter in the book titled *Advanced relay technologies in next generation wireless communications*. Editors: I. Krikidis and G. Zheng, IET, 2016.

2. J. M. B. da Silva, **C. Skouroumounis**, I. Krikidis, G. Fodor, and C. Fischione, *Energy efficient full-diplex networks*, chapter in the book titled *Green Communications for Energy-Efficient Wireless Systems and Networks*. Editors: A. Zappone, J. Yang, J. S. Thompson, and H. Suraweera. Eds. IET, 2019.

Published journal publications

1. **C. Skouroumounis**, C. Psomas, and I. Krikidis, "Low-complexity base station selection scheme in mmWave cellular networks," *IEEE Transactions on Communications,* vol. 65, no. 9, pp. 4049–4064, Sept. 2017.

2. **C. Skouroumounis**, C. Psomas and I. Krikidis, "Heterogeneous FD-mm-Wave cellular networks with cell center/edge users," *IEEE Transactions on Communications,* vol. 67, no. 1, pp. 791–806, Jan. 2019

Published conference proceedings

1. C. Psomas, **C. Skouroumounis**, I. Krikidis, A. Kalis, Z. Theodosiou, and A. Kounoudes, "Performance gains from directional antennas in full-duplex systems," in *Proceedings of IEEE International Conference on Microwaves, Communications, Antennas and Electronic Systems (COMCAS)*, Tel Aviv, Israel, Nov. 2015.

2. **C. Skouroumounis**, C. Psomas, and I. Krikidis, "Low complexity base station cooperation in cellular networks with blockages," in *Proceedings of IEEE Wireless Communications and Networking Conference (WCNC)*, Doha, Qatar, Apr. 2016, pp. 1381–1386.

3. **C. Skouroumounis**, C. Psomas, and I. Krikidis, "Low-complexity base station cooperation for mmWave heterogeneous cellular networks," in *Proceedings of IEEE Global Communications Conference (GLOBECOM)*, Washington, DC, Dec. 2016, pp. 1–6.

4. **C. Skouroumounis**, C. Psomas, and I. Krikidis, "FD-mmWave cellular networks with location-based user classification" in *Proceedings of Asilomar Conference on Signals, Systems, and Computers*, Pacific Grove, CA, USA, Oct. 2018.

Unpublished journal publications

1. **C. Skouroumounis**, C. Psomas, and I. Krikidis, "Hybrid cooperation scheme in heterogeneous sub-6 GHz/mmWave cellular networks," submitted in *IEEE Wireless Communications Letters*, Sept. 2019.

2. **C. Skouroumounis**, C. Psomas, and I. Krikidis, "FD-JCAS techniques for mmWave HetNets: Ginibre point process modeling and analysis," submitted in *IEEE Transactions on Wireless Communications*, Sept. 2019.

Unpublished conference publications

1. **C. Skouroumounis**, C. Psomas, and I. Krikidis, "Full-duplex radio in mmWave cellular networks with cell center/edge users" in *Proceedings of IEEE Global Communications Conference (GLOBECOM)* Abu-Dhabi, UAE, Dec. 2018.

2. **C. Skouroumounis**, C. Psomas, and I. Krikidis, "Cooperative detection for mmWave radar cellular networks," submitted in *IEEE International Conference on Communications (ICC)*, Oct.

Contents

List of Figures

Chapter 1

Introduction

Radio transmission has allowed people to communicate without any physical connection for more than a hundred years. In 1895, Guglielmo Marconi opened the way for wireless communications by transmitting the three-dot Morse code for the letter 'S' over a distance of three kilometers using electromagnetic waves. From this beginning, wireless communications have evolved into a key element of modern society, forcing both academia and industry to witness tremendous advances to support practical implementations and satisfy the ever-growing demands. Revolutionary developments in wireless communications, such as multiple-input multiple-output (MIMO) systems, smart antennas, advance coding and orthogonal frequency-division modulation (OFDM), provide high quality mobile broadband services with end-user data rates of several megabits per second over wide areas and tens or even hundreds, of megabits per second locally. From satellite transmission, radio and television broadcasting to the now ubiquitous mobile telephone, wireless communications has revolutionized the way societies function.

1.1 Motivation

Over the last few years, cellular networks have experienced unprecedented growth in the number of mobile subscribers. According to Cisco's latest report [1], more than 27.3 billion handheld or personal mobile-ready devices are expected to utilize the cellular network services by the end of the year 2021, up from 17.1 billion in 2016 (see Figure 1.1). The proliferation of smart devices and the accelerated adoption of data-hungry mobile devices, such as laptops, tablets and smartphones, lead to the dramatic increase in data traffic demand. As reported in [1], the overall

mobile traffic is forecasted to reach 49 exabyte per month by 2021, approximately a sevenfold increase between 2016 and 2021. Furthermore, richer web content, increasing social networking applications, online gaming, audio and high definition video streaming, are factors that will continue raising the amount of data traffic in cellular networks. In addition, the wireless networks are expected to handle and accommodate a vastly diverse range of emerging new services and applications such as, smart personal devices, high mobility users, machine-to-machine (M2M) connections, home automation, self-driving cars, robots and medical monitoring [2–6]. This unprecedented number of connected devices with such diverse requirements are also contributing to the global mobile traffic growth.

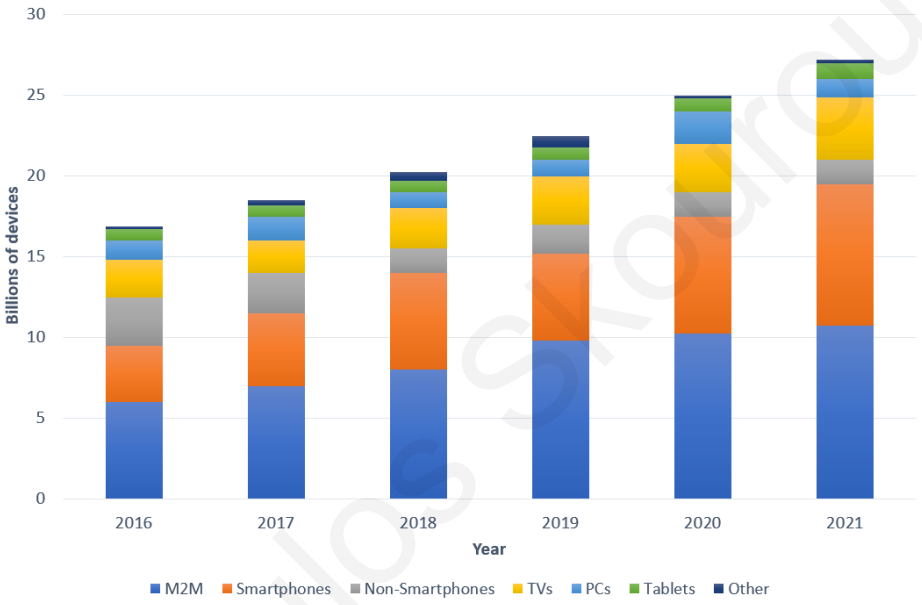

Figure 1.1: Total number of connected devices in the world. (Source: CISCO)

The need to support this traffic explosion along with the ever-fast approaching limits of the current generation of the cellular mobile communications, signals the dawn of the next-generation technology era, commonly known as the beyond fifth-generation (5G) mobile networks. Next-generation technology will enable people to connect with applications and services through flexible, reliable, and secure wireless networks, thus leading the human race into the era of "Everything on Mobile" [7]. In the "Everything on Mobile" era, the mobile networks must meet requirements more diverse than ever, which are summarized in Fig. 1.2. Specifically, next-generation networks are meant to be able to efficiently support 10× to 100× higher number of connected devices [8–10]. Emerging technologies with ultra-low latency and higher data rate requirements, such as augmented reality, 3D gaming and "tactile Inter-

net", will require a 100× increase in achievable data rate and a corresponding 5× to 10× reduction in latency [8, 9]. In addition, services that involve battery operated sensor networks, such as healthcare monitoring devices, laptops and mobile phones, demand 10× longer battery life and a significant cost benefit over the current generation [9, 10]. Moreover, the demand for better quality of service along with the ever-increasing demand for higher data quality transmission (e.g. richer web content, video streaming and 4K video services), pushing the next-generation systems to support data rates of 10 Gbps [9, 10]. Finally, next-generation networks are envisioned to provide ubiquitous connectivity, where the data rate of 95% of the users ranging from 100 Mbps to as much as 1 Gbps.

Figure 1.2: Performance gains for next-generation systems.

Despite the continued evolution of the existing communication systems in terms of standardization, implementation and deployment, addressing all current shortfalls can not be achieved by the implementation of a single communication system [8]. Thus, the next-generation systems will encompass existing technologies enriched with fundamentally new radio concepts in order to meet the new communication requirements. Specifically, it is necessary to meet the very challenging target of 1000-fold network capacity increase. An academic and industry consensus is that, the target of 1000-fold wireless network capacity increase can be achieved by

a combination of techniques and technologies, which are categorized as follows:

- **Spectral efficiency:** An obvious direction towards improving the network capacity is by increasing the spectral efficiency (bps/Hz) of the wireless links by using advanced physical layer techniques, such as MIMO. However, these techniques are already relatively mature, being part of multiple wireless standards such as IEEE 802.11e Worldwide Interoperability for Microwave Access (WiMAX) and 3rd Generation Partnership Project (3GPP) [11–15]. For instance, in case of (MIMO), the current Long-Term Evolution (LTE)-Advance standard already supports 8 antenna elements in the downlink (DL) and 4 in the uplink (UL) [16]. Furthermore, due to adaptive modulation and coding, the wireless links are already operating close to their theoretical limits, which further limits the gains [17]. Motivated by these limitations, the concept of *massive MIMO* was originated. The main idea is the existence of base station (BS) that are equipped with hundreds of antennas, enabling their communication with tens of users simultaneously in each resource block [18, 19]. With the possibility of using the extra degrees of freedom to form very narrow beams, the wireless systems are pushed to operate in a noise-limited environments, achieving theoretical gains in the throughput which are undoubtedly large. Moreover, under the increasingly scarce spectrum, the ability of transmit and receive information over the same RF resources, i.e. FD mode, has become a topic of interest for the next-generation systems [20]. This novel idea may theoretically double the link capacity or reduce by half the allocated frequency band, when it is compared with the current HD mode.

- **Spectrum efficiency:** A potential increase of the transmission bandwidth could enable the increase of both the data rate and the capacity. However, substantial amounts of available spectrum are only likely to be found in the frequency bands above 6 GHz, i.e. *mmWave* band ranging from 6 GHz to 300 GHz, and *Tera-Hz (THz)* band ranging from 300 GHz to 3 THz, which are characterized by their abundant non-congested spectrum resources [21]. mmWave communications constitute an ideal environment for the implementation of various state-of-the-art techniques, such as Massive MIMO, FD radio and HetNets, which can lead to multi-Gbps rates. However, these higher transmission frequencies exhibit very different propagation characteristics, such as

signal attenuation, multipath and reflection, compared to the current sub-6 GHz cellular frequencies, which necessitates fundamental changes in the system design [21]. Additionally, these higher transmission frequencies require significant changes in the hardware, including amplifiers and transceiver architectures [22,23]. Going forward, the THz communications started to receive considerable attention by the research community, which theoretically provide bandwidth up to several THz, resulting in a potential capacity in the order of Tbps [24,25].

- **Spatial efficiency:** Finally, dense deployment is a prerequisite for enhancing the received signal power from the transmitter which increases the achieved SINR. By reducing the size of the cell, the spatial efficiency is increased through higher spectrum reuse, while the link quality can be significantly improved [26]. One of the possible solutions is to deploy HetNets consisting of several tiers of small-cell BSs overlaid within the coverage area of the conventional macro-BSs. Users can thus be offloaded from the overcrowded BSs, resulting in a reduced load-factor that improves the network capacity [26–28]. Furthermore, wireless peer-to-peer communications such as *device-to-device (D2D)* and M2M communication, bypass the BS and the network infrastructure, providing significantly higher data rates and better link quality [29,30].

In particular, the requirements of significant enhancements in the network capacity and the user-experienced data-rates can only be met by massive improvements in all these three directions.

1.2 Thesis Outline and Contribution

This thesis provides insights into the achieved network performance of the mmWave heterogeneous communications with the utilization of sophisticated communication and signal processing techniques, such as FD radio, CoMP transmission,SIC, power control and weighted cell association. Leveraging concepts from stochastic geometry, we establish analytical frameworks that incorporate key features of these cellular networks. The outline of the thesis, together with the publications supporting the contributions, is as follows.

In Chapter 2, we provide preliminaries so that the concepts of this dissertation

are comprehensible. In particular, we introduce the concepts of HetNets and of mmWave communications, focusing on the technical issues and design problems imposed by their integration on cellular networks. Moreover, we introduce state-of-the-art models for the analysis of the HetNets and the mmWave communications. The second part of the chapter focuses on the analysis of these networks with the aid of stochastic geometry, providing key results and important assumptions that are adopted throughout this thesis.

In Chapter 3, we investigate the integration of HetNets deployments in systems operating at the mmWave frequency band. We propose a low-complexity BS selection scheme which provides low computational and implementation complexity without depriving in diversity compared to existing cooperation techniques. Moreover, we consider the case where the users have the ability to employ an ideal interference cancellation technique which provides a significant increase in the network performance. The content of this chapter are based on:

- C. Skouroumounis, C. Psomas, and I. Krikidis, "Low complexity base station cooperation in cellular networks with blockages," in *Proceedings of IEEE Wireless Communications and Networking Conference*, Doha, Qatar, Apr. 2016, pp. 1381–1386.

- C. Psomas, C. Skouroumounis, and I. Krikidis, *Relay selection in modern communication systems*, chapter in the book titled *Advanced relay technologies in next generation wireless communications*. Editors: I. Krikidis and G. Zheng, IET, 2016.

- C. Skouroumounis, C. Psomas, and I. Krikidis, "Low-complexity base station cooperation for mmWave heterogeneous cellular networks," in *Proceedings of IEEE Global Communications Conference*, Washington, DC, Dec. 2016, pp. 1–6.

- C. Skouroumounis, C. Psomas, and I. Krikidis, "Low-complexity base station selection scheme in mmWave cellular networks," *IEEE Transactions on Communications*, vol. 65, no. 9, pp. 4049–4064, Sept. 2017.

In Chapter 4, we assess the effect of FD radio in the context of heterogeneous mmWave cellular networks. Specifically, we propose an analytical framework to evaluate the coverage and sum-rate performance of the considered cellular networks for two user location-based classifications, namely CCUs and CEUs. Our results demonstrate the beneficial combination of FD radio with heterogeneous

mmWave cellular networks, and the trade-off between the coverage and the sum-rate performance is depicted. Moreover, we evaluate the performance of the considered networks with the employment of an ideal interference cancellation scheme, demonstrating the significant performance gains for the CEUs. This chapter includes the material in:

- C. Psomas, C. Skouroumounis, I. Krikidis, A. Kalis, Z. Theodosiou, and A. Kounoudes, "Performance gains from directional antennas in full-duplex systems," in *Proceedings of IEEE International Conference on Microwaves, Communications, Antennas and Electronic Systems*, Tel Aviv, Israel Nov. 2015.

- C. Skouroumounis, C. Psomas, and I. Krikidis, "FD-mmWave cellular networks with location-based user classification" in *Proceedings of Asilomar Conference on Signals, Systems, and Computers,* Pacific Grove, CA, USA, Oct. 2018.

- C. Skouroumounis, C. Psomas, and I. Krikidis, "Full-duplex radio in mmWave cellular networks with cell center/edge users" in *Proceedings of IEEE Global Communications Conference* Abu-Dhabi, UAE, Dec. 2018.

- C. Skouroumounis, C. Psomas and I. Krikidis, "Heterogeneous FD-mm-Wave cellular networks with cell center/edge users," *IEEE Transactions on Communications,* vol. 67, no. 1, pp. 791–806, Jan. 2019.

- J. M. B. da Silva, C. Skouroumounis, I. Krikidis, G. Fodor, and C. Fischione, *Energy efficient full-diplex networks*, chapter in the book titled *Green Communications for Energy-Efficient Wireless Systems and Networks*. Editors: A. Zappone, J. Yang, J. S. Thompson, and H. Suraweera. Eds. IET, 2019.

In Chapter 5, we propose a novel hybrid cooperation scheme in the context of heterogeneous sub-6 GHz/mmWave cellular networks, where users are classified either as CCUs or CEUs. Specifically, our proposed scheme exploits the cooperation technique, aiming at enhancing the performance of the CEUs and providing ubiquitous connectivity. Using stochastic geometry tools, we first establish an analytical and tractable framework to investigate the achieved performance of our proposed scheme in heterogeneous multi-band cellular networks. Based on the proposed framework, analytical expressions for the moments of the conditional success probability are derived for the calculation of the meta-distribution. Finally, a simple approximation of the meta-distribution is calculated, leveraging the

moment-matching method with the Beta-distribution. Our results demonstrate that the cooperation technique is beneficial for the CEUs and that the proposed scheme significantly improves the overall network performance. This chapter is based on:

- C. Skouroumounis, C. Psomas, and I. Krikidis, "Hybrid cooperation scheme in heterogeneous sub-6 GHz/mmWave cellular networks," submitted in *IEEE Wireless Communications Letters*, Sept. 2019.

In Chapter 6, we study the co-design of FD radio with joint communication and radar sensing (JCAS) techniques in mmWave HetNets. Particularly, we propose a novel cooperative detection technique, which exploits the sensing information from multiple BSs, aiming at enhancing the detection performance. Three hard-decision combining rules are considered, namely the *OR*, the *Majority* and the *AND* rule. In real-world network scenarios, the locations of the BSs are spatially correlated, exhibiting a repulsive behavior. Therefore, we model the spatial distribution of the BSs as a β-Ginibre point process (β-GPP), which can characterize the repulsion among the BSs. By using stochastic geometry tools, analytical expressions for the detection performance of β-GPP-based FD-JCAS systems are expressed for each of the considered combining rule. Furthermore, by considering temporal interference correlation, we evaluate the probability of successfully detecting a target over two different time-slots, and provide analytical expressions for each combining rule. Our results demonstrate that our cooperative technique can significantly improve the detection performance when compared to the conventional non-cooperative technique. Moreover, several useful trends in detection performance are illustrated as a function of the repulsion between BSs, the temporal interference correlation and the network characteristics. This chapter includes the material in:

- C. Skouroumounis, C. Psomas, and I. Krikidis, "FD-JCAS techniques for mmWave HetNets: Ginibre point process modeling and analysis," submitted in *IEEE Transactions on Wireless Communications*, Sept. 2019.

- C. Skouroumounis, C. Psomas, and I. Krikidis, "Cooperative detection for mmWave radar cellular networks," submitted in *IEEE International Conference on Communications*, Oct. 2019.

Finally, in Chapter 7 we conclude the thesis with a summary of the main contributions and a discussion on potential directions for future work.

Chapter 2

Background

HetNets and mmWave communications have been identified as promising technologies for handling the explosive growth of data demand over the cellular networks. The integration of HetNets and mmWave communications in cellular networks poses new technical and design issues. In this chapter, we give an overview of the fundamental properties for both the HetNets and mmWave communications, as well as the main challenges in the deployment of HetNet-mmWave cellular networks. Detailed literature review is provided at the end of each section.

2.1 Heterogeneous Networks

Up until recently, the conventional deployment of cellular networks was homogeneous, where an identical set of BSs with similar transmit power levels and similar backhaul links were placed in a planned layout. These BSs, usually referred to as macro-BSs, are high-power tower-mounted transceivers and have service areas called cells of roughly the same size [31]. However, the conventional homogeneous cellular network deployment has reached its fundamental limits in many dense urban areas, while the data traffic is constantly increasing. This limits the options for the cellular operators to increase the most important metric, the *area spectral efficiency*. Unfortunately, the radio link improvements including coding, cognitive transmission, and multiple antennas are also reaching their theoretical limits [26]. Consequently, the further improvement of the system's spectral efficiency is only possible by *network densification* [31]. Following this approach, the deployment of an additional macro-BS in a relatively sparse environment does not severely increase the inter-cell interference (ICI), and solid cell splitting gains are easy to achieve.

However, in the current dense environments, the cell splitting gains are significantly reduced due to the existing severe interference between the cells. Moreover, the cost for site acquisition in a capacity-limited dense urban area can get prohibitively expensive [28]. Hence, the concept of the HetNets deployment was introduced as an flexible, low-cost, and efficient solution to increase the area spectral efficiency.

2.1.1 HetNets technology

The ubiquitous coverage and ever-increasing capacity requirements for current cellular networks are the major drivers for the paradigm of HetNets. The main idea behind a HetNet is to improve the area spectral efficiency with the deployment of a diverse set of low-power nodes, within the areas covered by the existing macro-BSs [27, 32, 33]. The deployment of low-power nodes can be utilized either in the same or in different frequency bands. Both the 3GPP LTE standard and the IEEE WiMAX standard added the notion of "small cell" as an umbrella term for low-cost low-power radio access nodes that operate in a range of several meters to several hundred meters [34–37]. The deployment of these "small cells" focuses on eliminating any coverage hole in outdoor and indoor environments as well as to increase the spatial reuse, resulting in an increased capacity of the network [38, 39]. Thus, while the placement of the macro-BSs in a cellular network is generally based on a careful network planning, the placement of the small cells may be more or less ad-hoc, based on just a rough knowledge of the coverage issues and the traffic density (e.g. hot-spots) in the cellular network. A network, which consists of traditional macro-BSs and embedded small cells, as shown in Figure 2.1, is called heterogeneous cellular network. The different network components depicted in Figure 2.1, can be briefly characterized in the following way

- **Macro-BSs** have typically a high output power (up to 46 dBm [28]) and are deployed in a planned layout to provide basic coverage.

- **Pico-BSs** are deployed both in indoors and outdoors enviroments, transmitting power from 23 dBm to 30dBm and are capable of serving few mobile devices at a distance of less than 300 meters [28]. Their communication with the macro-BS is performed via a dedicated high-bandwidth low-latency backhaul connection.

- **Remote radio head (RRH)/distributed antennas** are connected to the macro-BSs using a dedicated high-bandwidth low-latency backhaul connection; they have minimal autonomous intelligence and act as extensions of the BS antenna ports.

- **Fempto-BSs** are meant for indoor use and their transmit power is less than 23 dBm. Unlike pico-BSs, the femto-BSs may be configured with a restricted association, allowing access only to its closed subscriber group members [38]. A major advantage of the femto-BSs as compared to pico-BSs and RRHs is that they do not need to be planned and maintained by the cellular operators. This is because the fempto-BSs are connected to the core network through a last-mile Internet backhaul connection. The last-mile technology refers to the final leg of the wireless networks that deliver communication services to the users through high-bandwidth cables.

- **Relays** are infrastructure equipment that wirelessly connect to the network backbone and assist in the signal transmission between the macro-BS and the users by receiving and re-transmitting the received signal. Relays offer flexible option where wireline backhaul is unavailable or not economically feasible [40]. Depending on whether the backhaul connection is on the same frequency as the access link or not, the relays are classified as in-band and out-of-band [40].

The heterogeneous deployment of cellular networks brings several benefits for both the mobile users and the network providers. First, the users in isolated areas can now be served by the newly deployed small cells and can experience high data rates, low latency and reduced energy consumption. This is due to the short-range communication with the serving BS and its potentially favorable propagation conditions. Furthermore, since a small cell transmits with much smaller power than the conventional macro-BS, it can opportunistically transmit in the same resource blocks with the macro-BS without creating severe interference to the serving users by the macro-BS. Consequently, the HetNets can provide a more efficient area spectral efficiency (i.e., total number of users served per Hz per unit area). In addition, compared to the macro-BSs, the deployment cost of the small cells can be reduced thanks to the smaller deployment sizes and the flexible backhaul solutions. Finally, the integration of small cells within the network deployment can offload users from

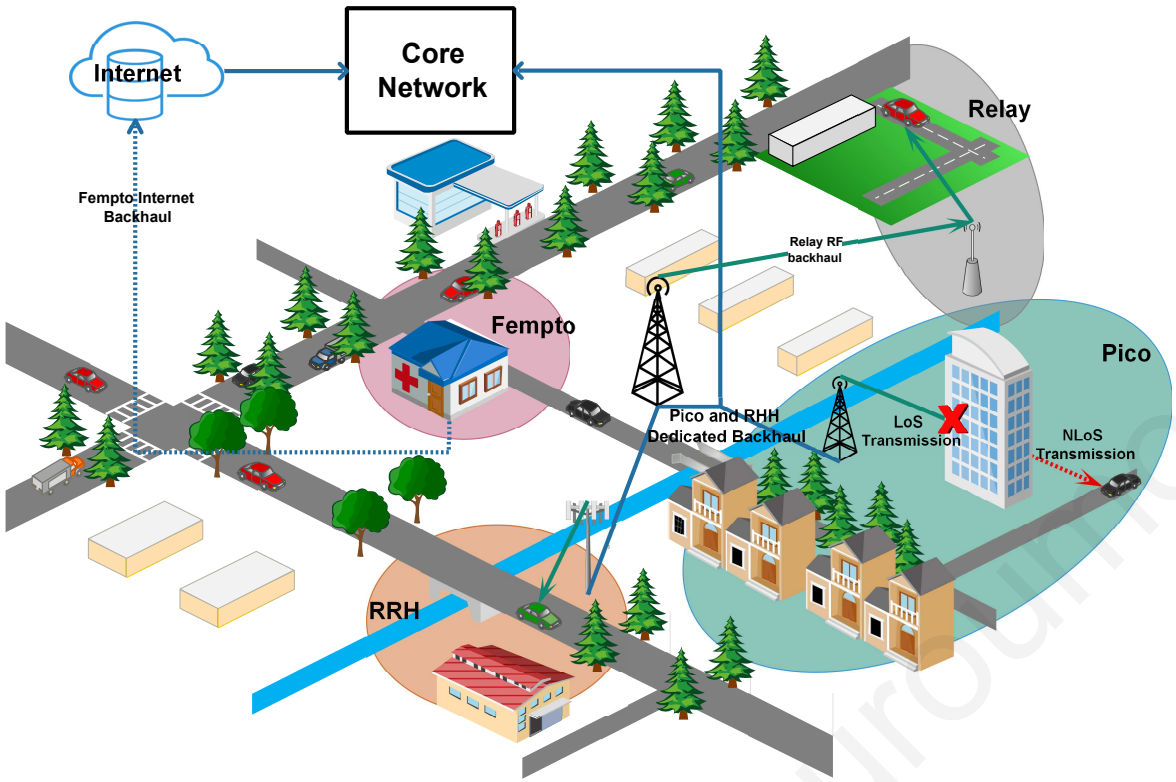

Figure 2.1: HetNet topology consisting of high-power (macro) and low-power BSs.

the congested macro-BSs to enhance their quality of service and increase the overall system capacity.

2.1.2 Design Challenges for HetNets

The existence of large disparities in the transmit power between the nodes of the HetNets impose many challenges. Such power disparities, in general, put the small cells (pico, femto, and relay) at a disadvantage relative to the macro-BSs. In order to overcome the challenges posed by the heterogeneous deployment of the BSs and to fully exploit the benefits of such deployments, several fundamental changes are required in the traditional approaches for modeling, analyzing and designing of the cellular networks. The basic challenges faced by the current wireless communication networks are (*i*) the spatial modeling, (*ii*) the cell association policy, and (*iii*) the interference management.

Spatial Modeling

Until recently, both the academia and the industry were extensively used the hexagonal grid model for the spatial deployment of cellular networks [41]. It is flexible and commonly accepted as a reasonably useful model to represent well-planned homogeneous BS deployments [32, 42]. On the other hand, it is generally not tractable, requiring overly simplistic assumptions and extensive simulations [43, 44]. In addition, with the further densification of cellular networks, the network topology is evolving towards an irregular spatial deployment of the nodes. In the context of HetNets, the small cell deployment is typically beyond the scope of the network planning as it aims to address the coverage issues in the cellular networks, and therefore is a random process [26, 27, 32]. Without prior information, the best statistical model for the deployment of small cells is the uniform distribution, which corresponds to the complete spatial randomness. In that case, the network properties can conveniently be captured by a Point Process (PP) and enable to leverage techniques from the *stochastic geometry*. This powerful mathematical framework recently gained momentum as the only available tool that provides a rigorous approach to model, analyze and design of HetNets [45–47]. Among several PPs, due to its independence property, the Poisson PP (PPP) is the most popular, most tractable, and most important process. Models based on the PPP have been used for large-scale ad-hoc and cellular networks for more than three decades [48, 49], and the performance of PPP-based networks is well characterized and understood. Although, PPP fails to characterize the correlation among the locations of the network's nodes, since the nodes are located independently of each other. However, in many practical networks, the locations of the nodes are determined to alleviate the interference or extend the coverage region, and therefore there exists a form of repulsion among the network's nodes. Recently, the Ginibre PP (GPP) [47,50], which is a type of repulsive point process, has been advocated to model random phenomena where repulsion is observed. The authors in [51] extended the GPP model to a more general class called a β-GPP, where β can be used to control the repulsion between points.

Cell Association

For the conventional homogeneous network deployments comprised only of macro-BSs, the problem of cell association is typically decided based on the maximum

DL receive signal strength (RSS) [43, 52, 53] criterion. However, the assignment of users to a particular BS is a non-trivial problem for HetNet deployments, due to the existence of large disparities in the transmit power between the network's nodes. The significantly larger transmit power of the macro-BSs results in a decidedly larger coverage area compared with that of the small cells. Thus, the above mentioned association criterion leads most of the users to be attracted towards the macro-BSs, while the reduced available power of the small cells attract a limited number of users [26]. This situation might cause the severely congestion of the macro-BSs while the resources at the nearby small cells are underutilized. Thus, even if a user receives the strongest signal from the macro-BS, it is desirable to offload the user to the nearby lightly-loaded small cell which can serve the user with higher data rate by allocating a larger fraction of radio resources [26]. As a consequence, the load in a macro-BS will sufficiently be reduced, allowing the remaining associated users at the macro-BS to be served with improved data rates. Generally, the optimal cell association in a HetNet is the one that can maximize the data rate of all users in the network through balanced distribution of the user loads across all tiers of the BSs.

Interference Management

Since interference is considered as one of the most important limiting factors of the cellular network performance, interference management is a primary concern in any cellular network. For the HetNet topologies, the lack of available spectrum forces the deployment of the small cells in the same frequency band as the macro-BSs, causing additional interference that may compromise the performance of the HetNets [38, 54]. Thus, the interference management is even more important in ultra-dense HetNets deployments. However, the interference scenarios in HetNets are more complex than those in the conventional homogeneous cellular networks and require advanced interference management techniques. For example and as explained above, the users in the HetNets are offloaded from the macro-BSs to the small cells in order to achieve a balanced distribution of user's loads across all tiers. Thus, each offloaded user suffers from severe DL interference because the macro-BS, which transmit the strongest RSS and should have been the serving BS, now acts as an interferer [54]. As a result, the benefits of the load balancing cannot be fully realized unless a suitable interference mitigation technique is employed. In addition,

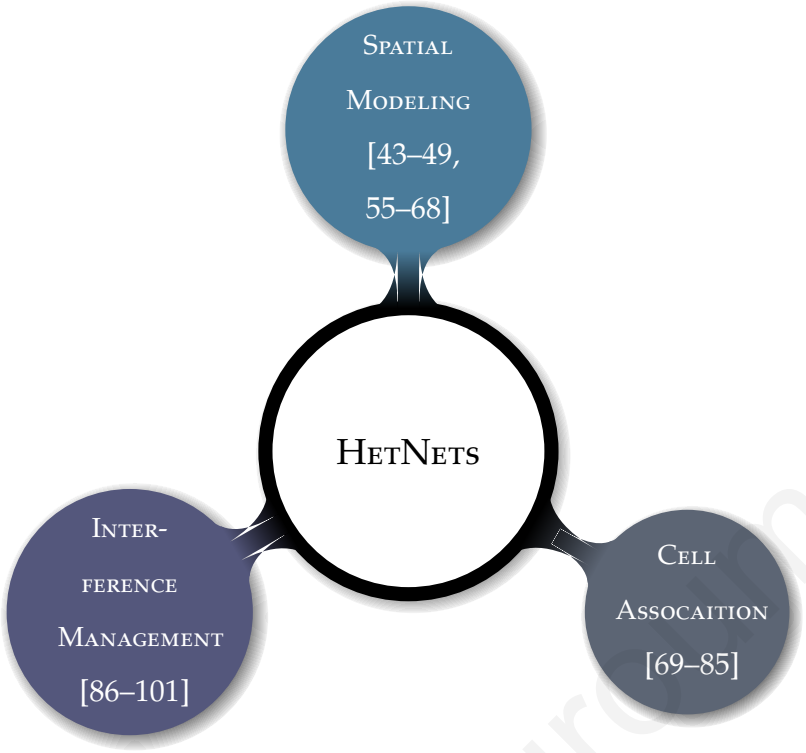

Figure 2.2: The three main problems for the HetNets and some of the related solutions in the literature.

the users that are located in the coverage area of a fempto-BS with restricted access, suffer from severe DL interference from the femto-BS. Meanwhile, the users that are served by the femto-BSs are also severely interfered by these users in the UL.

2.1.3 Related Work

In this section, we present an overview on spatial modeling, cell association, and interference management challenges for HetNets, with some examples of relevant solutions in the literature. Many works in the literature consider the above challenges separately or only partially jointly as illustrated in Figure 2.2.

As previously mentioned, for the spatial modeling of the BS locations in a cellular network, the stochastic geometry approach is widely used in the literature. The approach of analyzing the network performance using stochastic geometry tools has been supported since 1997 [55, 56]. Such an approach seems sensible for the deployment of small cells [57–59] or ad-hoc networks [45,48,49,60], but it is dubious for the deployment of the macro-BSs which is based on a careful network planning. Nevertheless, the difference between randomly placed and actual planned locations may not be as large as expected, even for the macro-BSs deployment. Indeed, the

authors in [43] showed that for a one-tier network, even with the BS locations drawn from a PPP, the resulting network model does not deprived in accuracy compared to the standard grid model. Specifically, the authors showed that the SINR experienced by the users in a simulation with actual BS locations is upper bounded by the SINR of the users in an idealistic grid model, and lower bounded by the SINR of the users in a random network. Interestingly, the random network provides a lower bound that is as tight as the upper bound provided by the idealized grid model [61], and is preferred due to the tractability provided by the stochastic geometry.

Motivated by the mathematical tractability of the PPP models, researchers have recently turned their attention to study the system-level performance of cellular networks with the aid of stochastic geometry. In the context of heterogeneous deployments, which are of interest in the present thesis, the authors in [62, 63] investigated the performance of a two-tier HetNet, consisting of a macro-tier and a femto-tier, using tools from stochastic geometry. For the general deployment of a K-tier HetNet, the authors in [64] developed a tractable model for the DL SINR, where each tier differ in terms of average transmit power, supported data rate and BS density. The aforementioned model was extended in [65, 66], where under certain assumptions, closed-form expressions are derived for the coverage performance. Closed-form expressions are a useful tool to easily obtain insights into how key system parameters affect the system's performance. Interestingly, the insights derived from the closed-form expressions in [65] have been corroborated by the industry field trials [27] and the observations from extremely detailed simulations [28]. Although there has been substantial work studying PPP-distributed wireless networks, few works investigate network deployments that are spatially distributed based on a repulsive PP, i.e. β-GPP. The performance of an energy-harvesting network with repulsive distributed energy sources was studied in [67]. In [68], the performance of cellular networks modeling the locations of base stations as a β-GPP is examined. In the context of HetNets, β parameter can be varied to model both macro-cell BS locations which exhibit high repulsion and small-cell BSs, whose locations exhibit less correlation.

The aforementioned results focused on the DL transmission, where large power disparities exist between the BSs in a HetNet. In contrast, all transmitters in the UL direction can transmit at roughly the same power level. In addition, the DL traffic is typically much heavier than the UL traffic. In view of these asymmetries, the DL and the UL direction need to be considered as two different networks, where different

models for the interference, the cell association, and the throughput are required [26]. Thus, the DL-UL decoupling (DUDe) technique has emerged as an efficient approach to alleviate the DL-UL asymmetry and to improve the UL performance [63]. A tractable model of HetNets was proposed to characterize the network performance with decoupled access in [69], and it is shown that DUDe leads to a significant improvement in the rate coverage probability over the standard coupled association strategy in the HetNets. A complete survey about the DUDe technique can be found in [70], where the authors stated that the DUDe technique could lead to significant gains in the network throughput and the power consumption. A network consisting of hybrid sub-6 GHz macro-BSs and mmWave small cells was studied in [71], where the performance gains with different decoupled association strategies were investigated, and the authors observed that the DUDe approach is a key factor in improving the UL and the DL performance. Finally, in DUDe networks with multi-antenna BSs, offloading the users to small cells is required in order to leverage the benefits of multiple antennas [63].

In contrast to the conventional homogeneous single-tier cellular networks, there are more BSs in the HetNets from which the user can choose to associate with. Therefore, a cell association scheme is an indispensable factor in the heterogeneous wireless networks modeling. Most of the works adopting a stochastic geometry model assume a cell association scheme based on the maximum RSS [66, 69, 72–75]. An alternative cell association scheme is adopted in [64,76,77], where the users associate with the BS that provides the maximum SINR. However, in the heterogeneous cellular networks, choosing the appropriate network tier to associate with, is a non-trivial problem [78], and a simple RSS- or an SINR-based cell association scheme may not be optimal. As mentioned earlier, the large disparities in the transmit power between the elements of the HetNets, brings the unbalanced load distribution between the BSs in different network tiers. Therefore, to enhance the load balancing between the network tiers, a simple technique called *biasing* was proposed in [66, 79, 80], to artificially bias the user association to the small cells. Specifically, the proposed technique virtually increases the relative transmit power of the small cells, biasing the user to associate with a small cell even if it does not provide the strongest RSS (or equivalently the strongest SINR). The biasing technique is also widely known as cell range expansion (CRE) method in the 3GPP standards [81–83]. The authors in [84] developed an analytical framework to evaluate the performance gains achieved with

the implementation of the CRE technique in the context of HetNets. For a two-tier HetNet, in [85], the authors examined different offloading/biasing techniques that can be used to offload users from one network tier to another, in order to efficiently control the load in each tier. Finally, the impact of the biasing technique on the energy efficiency was analyzed in [80] for the heterogeneous cellular deployments. However, although the aforementioned load balancing techniques significantly increase the network capacity, their major drawback is the reduced coverage performance due to the increased ICI [72]. Therefore, the achieved gains from the load balancing techniques could be negated if interference management techniques are not adopted.

In order to address the constraints implied by the ICI, many interference management techniques were investigated during the past decades. Initially, in the 3GPP Release 8 [12] the ICI coordination (ICIC) approach was proposed, which aims to perform interference suppression by allocating different resource blocks to CEUs. Throughout the literature, there are two well-investigated ICIC approaches, namely fractional frequency reuse (FFR) [86, 87] and soft frequency reuse (SFR) [77, 88]. However, this approach is only considered for the interference mitigation in the homogeneous networks [12]. Motivated by this, the enhanced-ICIC (eICIC) approach was firstly introduced in the 3GPP Release 10 [14] and further investigated in the 3GPP Release 11-14 [15, 89–91], which is an advanced version of the ICIC, evolved to support HetNet environments. Such an approach is the CoMP transmission and reception. The main concept of the CoMP approach is the multi-node coordination in such a way that the transmission signals from/to other nodes do not incur serious interference or even can be exploited as a meaningful signal. In the framework of 3GPP, the CoMP transmission is categorized as joint transmission (JT) [75, 92, 93], dynamic point selection (DPS) [75], dynamic point blanking (DPB) [75], and coordinated scheduling/beamforming (CS/CB) [94, 95]. In [93], the authors use stochastic geometry to analyze the JT for the DL heterogeneous cellular networks modeled as multiple tiers of independent PPPs. This work was further extended in [75], where the authors investigated multiple types of CoMP schemes, including JT, DPB, and DPS/DPB, in the context of DL HetNets environments. Another interference management technique for boosting the network performance is the SIC technique [96,97]. A SIC policy is investigated in [98], [99], where the authors evaluate the performance after successfully decoding and canceling the most dominant interfering signals. The deployment of this method in HetNets was investigated in [100], where it is

shown that the main additional gain can be achieved through the cancellation of the strongest interfering signal. In [101], the authors study the employment of a SIC scheme in HetNets and show that the performance benefits decrease with the number of cancellations.

2.1.4 Standardization of HetNets

The transition of the cellular networks from homogeneous to heterogeneous, created the need for an evolved ICIC to mitigate the severe interference observed in HetNet deployments. eICIC was introduced in the 3GPP Release 10 [14], which is an advanced version of the ICIC, evolved to support HetNet environments. The major change is the addition of the time domain ICIC, realized through the use of almost blank subframes (ABSF). Specifically, an ABSF includes only control channel frames and cell-specific reference signals, while it is transmitted with reduced power via OAM or X2 interface [16]. Thus, if the macro-BSs configure ABSFs, then the users served by the pico/femto-BSs can send their data during such ABSF frames and avoid interference from the macro-BS. The ABSF technique was further enriched, in terms of latency, in the 3GPP Release 11 [15], where the ICIC is evolved to further enhanced ICIC (feICIC). However, since the available bandwidth is split in time or frequency domain, the network capacity is significantly reduced. Motivated by this, the carrier aggregation (CA) was also introduced in the 3GPP Release 10 [14] and evolved in the 3GPP Release 12 [89], in order to increase the total bandwidth available and thereby increase the network capacity. The basic idea of the CA is the simultaneous transmission of data via multiple carriers, referred to as component carriers (CC). Based on the 3GPP Release 12 [89], maximum of five CC can be aggregated with each CC having bandwidth of 1.4, 3, 5, 10, 15, or 20 MHz. Thus, with five CC at 20 MHz, a maximum bandwidth of 100 MHz can be achieved. In addition, the CA is available for both the frequency-division duplexing (FDD) and the time-division duplexing (TDD), while it is backward compatible with the 3GPP Release 8 and 9 . Finally, as stated in the 3GPP Release 13 [90], the aggregation of up to 32 CCs is supported and the usage of unlicensed spectrum for the CA is became feasible.

2.2 Millimeter-wave Communications

One of the major challenges that the current fourth generation (4G) LTE networks have had to deal with is the scarcity of available spectrum in the conventional sub-6 GHz frequencies used for the wireless access and backhaul links. Although the introduction of advanced techniques such as enhanced MIMO, CoMP, HetNets, and CA contribute for the increased capacity for the LTE-Advanced implementations, they are not sufficient to cope with the massive data rate demand expected in the near future. On the other hand, mmWave communications offer an alternative and promising solution to support extremely high data rate wireless access, due to the unbounded available bandwidth in the mmWave frequency band.

2.2.1 MmWaves Technology

Up until now, the operation of the wireless networks has been mainly limited to the conventional sub-6 GHz frequency band, which ranges from 300 MHz to 3 GHz [102]. AM radio broadcasting, international shortwave broadcasting, military and ship-to-shore communications are just some examples of wireless services that use the lower end of the spectrum, from the hundreds of KHz to the tens of MHz (e.g., medium-wave and shortwave bands). Television broadcasting is allocated from the tens of MHz to the hundreds of MHz (e.g., VHF and UHF bands). Current cellphones and wireless devices such as tablets and laptops works at carrier frequencies between 700 MHz and 6 GHz, with channel bandwidths of 5 to 100 MHz [102–104]. The remarkable popularity of these wireless services causes device manufacturers and infrastructure developers to continually seek greater radio spectrum for more advanced product offerings. Yet, despite the highly congestion of the wireless services in the sub-6 GHz frequency band, the operating carrier frequency of the mobile communications and the personal area network industries is limited between the frequencies 300 MHz and 3 GHz. In the mmWave spectrum though, ranging from 30-300 GHz which corresponds to wavelengths from 10 mm to 1 mm, the spectrum utilization is much lower [105]. Despite the operating services in the mmWave frequency band such as military transmissions, vehicular radar, and backhaul connections, a vast amount of spectrum is still available at these frequencies [106]. Specifically, the 60 GHz band, also known as the V-Band, ranging between

57 and 66 GHz is characterized by a continuous block of 9 GHz of unlicensed available spectrum. The E-Band, comprised of two blocks of 5 GHz ranging from 71-76 GHz and 81-86 GHz, offers a total of 10 GHz of available spectrum. Other promising mmWave bands are at 28 GHz and 38 GHz, which combined roughly offer 4 GHz of spectrum [105]. Thus, the key question is why the wireless communications did not exploit the mmWave frequency band, since it offers unbounded bandwidth.

The answer has to do with many factors, such as the lack of fundamental understanding of the radio propagation and the cost of designing, fabricating, and deploying new products and infrastructures that support such large bandwidths [107]. Fortunately, recent improvements in the semiconductor technology have facilitated the manufacture of reliable and low-cost radio frequency circuits with gate lengths at or below 30 nm and on-chip antennas systems operating at frequencies much higher than 5 GHz [108]. These advancements have enabled the emergence of the wireless communication operating at the mmWave frequencies band, which represents the most recent game-changing development for the wireless systems [21]. Firstly, as previously mentioned, the available spectrum at the mmWave frequency band is unparalleled compared to the sub-6 GHz frequency band which is used for the conventional cellular and the wireless local area network (WLAN) microwave systems. In particular, all the current commercial wireless systems together have less than two percent of the bandwidth available at the mmWave spectrum [105, 106, 109]. This huge available bandwidth for the wireless communications, even if utilized with a very low spectral efficiency, can easily provide data rate up to Gbps. Secondly, the huge available spectrum resources of mmWave band can be shared among multiple users, allowing for a larger number of simultaneous serving users [103, 104]. Finally, due to the much shorter wavelengths of the mmWave signals, tens-to-hundreds of antenna elements can be integrated onto small-sized chips, thereby producing highly directional antennas [102, 104, 109]. The high directivity not only indicates the high antenna gain for throughput improvement, but also enhances the spatial reuse and mitigates the interference in the presence of concurrent transmissions.

2.2.2 Characteristics of MmWave Communications

The availability of unbounded bandwidth in the mmWave frequency band spurred a great interest in both the academia and industry, as part of the quest for substantial ca-

pacity gains. However, the propagation characteristics of mmWave communications have fundamental differences with the current sub-6 GHz communications [107]. Due to these differences, the mmWave communications exhibit some unique features that are required to be considered in the design of the network architectures and protocols in order to fully exploit their potentials. In this section, the main features of mmWave communications are discussed.

Wireless Channel

The main drawback associated to the mmWave features is the high propagation losses due to the much shorter wavelength compared with the conventional sub-6 GHz communication signals [21]. Its impact can be evaluated by adapting the Friis transmission equation in a free-space scenario, that defines the relationship between the received power P_r and the transmitted power P_t, which can be expressed as

$$P_r(d) = P_t G_r G_t d^{-\nu} \left(\frac{1}{4\pi f} \right)^2, \tag{2.1}$$

where G_t and G_r are the antenna gains of the transmit and the receive antennas respectively, f is the carrier frequency, d is the transmission distance, and ν is the path-loss exponent that is equal to 2 in free-space. Focusing only on the last term with isotropic transmit and receive antennas, i.e. $G_r = G_t = 1$, it emerges how even a little increase of the frequency results in a not negligible reduction of the received power [21]. Specifically, compared to the propagation loss that exists in the sub-6 GHz frequency band, the propagation loss at the mmWave frequency band is significantly higher, e.g., 28 dB higher at 60 GHz than that at 2.4 GHz [102]. Hence, the transition from the current sub-6 GHz frequency band to the mmWave frequency band would lead to a more than 100 times lower receiver power. Other propagation limiting factors of the mmWaves signals are the atmospheric and rain attenuations caused by the gas molecules in the earth's atmosphere, absorbing a certain portion of the radio wave's energy and vibrate with a strength proportional to the carrier frequency [102–104]. Specifically, the impact of the atmospheric and rain attenuation absorption on the mmWave communications is depicted in Fig. 2.3. Such unfavorable propagation characteristics were seen as limitations when considering the development of the mobile networks, leading the mmWave communications to be mainly used for indoor environments [105, 109].

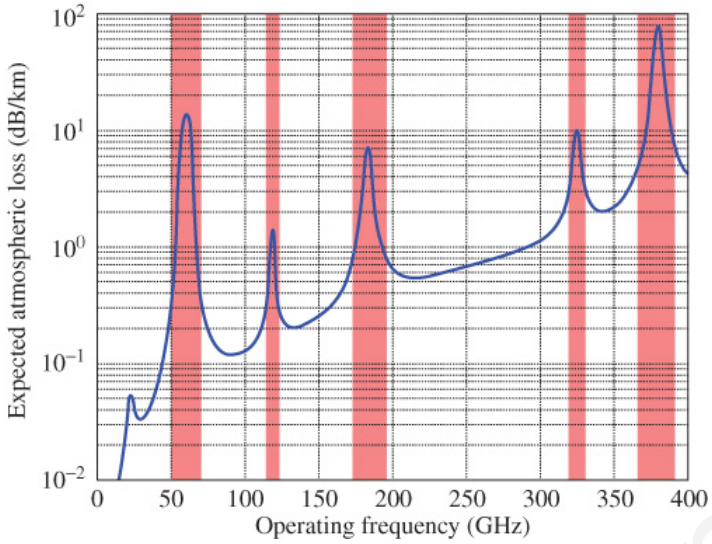

Figure 2.3: Atmospheric absorption of electromagnetic waves. High absorption have resulted in unlicensed short-range applications in the 60 GHz [21].

Directionality and Narrow Beamwidth

Friis equation indicated in Equation (2.1), shows that an easy way to counteract the severe propagation path-losses experienced by the mmWave signals is the exploitation of transmitting and receiving gains, i.e. $G_t > 1$ and $G_r > 1$. Therefore, the beamforming technique becomes extremely important in the system modeling and design of mmWave communications [110]. Conveniently, the small wavelength of the mmmWave signals allows the fabrication of very small antennas and hence providing the ability of stacking tens or even hundreds of them at the transceivers [102, 104, 111]. Thus, the large-scale directional antenna arrays can be leveraged to provide substantial array gains and synthesize highly directional beams. The main idea of the directional antenna arrays is to focus the transmitter's energy towards certain directions, while suppressing it in the direction of the unintended receivers [110]. Hence, the utilization of directional antennas provides to the network increased coverage performance and the interference caused by the nearby sources is significantly reduced. The achieved high array gains help to compensate the severe propagation losses (including the free-space and the atmospheric attenuation losses) that are caused by the ten-fold increase of the carrier frequency, in order to achieve high data rates [112, 113]. Moreover, in contrast to the rich diffraction and scattering environment of the sub-6 GHz systems, the highly directional transmissions will dramatically change the signal as well as the interference power received

by a user within the mmWave systems [112, 114]. Specifically, the utilization of directional antennas in the mmWave systems narrows the transmission beamwidth, allowing more precise targeting of the radio signals and providing a larger resilience against the interference. Therefore, it is necessary and critical to incorporate directional antenna arrays when analyzing mmWave networks in order to fully exploit the benefits of mmWave communications.

Sensitivity to Blockages

Another important feature of the mmWave cellular systems is their vulnerability to blockages. [21]. Specifically, due to the short wavelength of the mmWave frequency band, the multi-path effects in the mmWave wireless communications, e.g., diffraction and higher-order reflection, incur greater attenuation, and the penetration loss of the mmWave signals is significantly higher than the sub-6 GHz counterpart [105,115]. Based on the above, non-line-of-sight (NLoS) transmissions in mmWave channels suffer from significant attenuation and a shortage of multi-paths [28]. Therefore, mmWave systems rely on line-of-sight (LoS) transmissions to achieve the high data rate. Blockages that emerge between the transmitter and the receiver can easily block the LoS transmission, and greatly reduce the transmission data rate. For example, the penetration loss of mmWave signals due to a human body, brick, and glass is estimated at 35 dB, 80 dB and 50 dB, respectively [105]. Such high attenuation makes mmWave connection unavailable sometimes in indoor environments and environments with dense high-rise buildings. In particular, the coverage of indoor wireless systems operating at the sub-6 GHz would encompass a larger area compared to the corresponding coverage area of a wireless system operating at the mmWave frequency band [116]. The high penetration losses of the mmWave signals limit the range of the covered area and emphasize the need for a heterogeneous deployment [28], that can provide coverage for the obstructed areas [21,117–119]. Explicitly, the HetNets allow a wireless system to communicate with a user that suffers from an obstructed mmWave link through a different wireless technology, such as the conventional wireless systems operating in the lower frequency bands [117, 120].

2.2.3 Related Work

Motivated by the mathematical flexibility of the PPP-based abstraction modeling, the research community has recently focuses on the investigation of the system-level performance of the mmWave cellular networks with the aid of stochastic geometry. The aim is to develop mathematical frameworks specifically tailored to account for the peculiarities of the mmWave propagation channels and transmission schemes which were previously mentioned in Section 2.2.2. In fact, the currently available mathematical frameworks for modeling the sub-6 GHz cellular networks are not directly applicable to the mmWave cellular networks. The main reasons are related to the need of incorporating realistic path-loss and blockage models, which are significantly different from the sub-6 GHz communications.

The use of large antenna arrays at both the transmitters and the receivers is a key feature of the mmWave cellular systems and can be applied using digital, analog, or hybrid beamforming techniques [102]. Initially, the digital beamforming (DBF) technique pre-processes the transmitted signal in the digital domain and then post-processes the received signal at the receiver [121]. However, this fully-digital processing is prohibitively complex and costly at the higher frequencies since each antenna element would require its own analog RF chain, which results in a bulkier transceiver and higher power consumption [122, 123]. The solution for overcoming this limitation, is to perform beamforming entirely in the RF domain using analog processing. Specifically, the analog beamforming (ABF) technique forms the beam with only one RF chain and a pair of a digitally controlled phase shifters that are connected to the individual antenna elements at both the transceiver ends [102]. Hence, the ABF technique is considered to be cost-effective and well-fitted for mmWave communications [124–126]. Despite its simplicity, the ABF technique comes at the cost of handling only a single input data stream, which limits the signal processing and multiplexing capability of the system [122]. Consequently, the further enhancement of the mmWave wireless systems is only possible by the utilization of a hybrid beamforming (HBF) technique [127–131]. The HBF technique has been proposed as a possible solution that is able to combine the advantages of both the ABF and DBF techniques. Specifically, the number of analog RF chains is significantly lower than the number of the antenna elements, providing a significant cost reduction and a lower overall power consumption, while there are less degrees of freedom [102].

In the context of stochastic geometry, the utilization of beamforming techniques is well-investigated for mmWave communications [84, 132–134]. In [84], the authors investigate the potential benefits of directional beamforming in mmWave cellular networks and showed that by increasing the main lobe gain results in higher coverage performance. The work in [132], showed that the use of directional antennas at each node of a mmWave communication network along with the use of signals that are inherently directional, reduces the received interference and supports higher densities and larger spectral efficiencies. The authors in [133] investigated the achieved network performance of mmWave cellular networks, where the antenna directionality was approximated by a sectorised antenna model that provides a good approximation of the performance achieved by the actual antenna pattern.

As previously mentioned, mmWave communications suffer from high sensitivity to blockage effects. Recent experimental investigations have shown that the penetration losses through buildings can be as high as 40-80 dB [105], and so the indoor and the outdoor mmWave systems can be considered to be isolated from one another. Moreover, even in outdoor-to-outdoor or indoor-to-indoor communications, blockages such as humans, trees and furnitures can also cause high penetration losses. Hence, the large difference in the path-loss laws between the LoS and the NLoS mmWave links, usually modeled via different path-loss exponents [21]. The authors in [133, 135], showed that the achieved coverage and rate performance by using different path-loss exponents for the LoS and the NLoS mmWave links, can be substantially different from the prior results for the sub-6 GHz systems which assumed a single path-loss exponent value. Therefore, for the investigation of the mmWave network performance, the impact of blockages, such as buildings in urban areas, should be integrated. Throughout the literature, there are two widely-used models for the incorporation of the blockages in the signal propagation, namely *measurement-based models* and *stochastic geometry models*. The most accurate approach in the measurement-based models is the *ray-tracing* approach, where the blockages are characterised explicitly by their sizes, locations, and shapes using a detailed simulation of the actual physical wave propagation process [115, 136]. Ray-tracing approach is a powerful tool for practical system design, however it is not mathematical tractable due to its high complexity [105, 137]. Therefore the utilization of ray-tracing approach for the performance analysis of mmWave networks is limited. On the other hand, in the stochastic geometry models, the statistics of blockages are

drawn randomly according to some distribution. Therefore, this approach is well-investigated in the literature [84,113,115,118,119,138,139], since it can be applied to study system deployments under a variety of blockage parameters, such as size and density, providing a tractable approach to analyze the system performance.

Finally, in order to combat the high penetration losses of mmWave signals, the co-design of mmWave communications and HetNets is crusial [105]. The authors in [140] introduced two different deployment scenarios of heterogeneity in mmWave cellular networks. In the stand-alone scenario, all the tiers will be operating in the mmWave frequency bands, while in the multi-band scenario, the sub-6 GHz network coexists with the mmWave networks. For the first scenario, a general mathematical framework to analyze the heterogeneous mmWave cellular networks was proposed in [141]. Based on this framework, the authors in [84] studied the SINR and the rate coverage performance of heterogeneous DL mmWave cellular networks, and the impact of the biasing factor on the energy efficiency was analyzed. The blockage effect on the connectivity of the mmWave networks in a Manhattan-type urban region was investigated in [138], where the authors quantified the relation between the coverage performance of a mmWave cellular network and the parameters of blockages and BS processes. In [142], the benefits of the BS cooperation technique in the DL of a heterogeneous mmWave cellular system were analyzed. Finally, the impact of D2D communications on the performance of heterogeneous mmWave cellular networks was studied in [68]. For the multi-band scenario, the authors in [71,119] investigated the impact of the DUDe technique on the coverage and the rate performance of a heterogeneous sub-6 GHz/mmWave cellular network. The aforementioned work was further extended in [143], where the authors studied the problem of resource management for both the DL and UL transmissions in concert with the DUDe technique. Finally, the authors in [144] investigated the achieved network performance in the context of cache-enabled heterogeneous mmWave cellular networks, and showed that the multi-band network outperforms the conventional HetNets in terms of the success probability and area spectral efficiency.

2.2.4 Standardization of mmWave communications

In the light of the expected emerging broadband communication demands and the increased challenges of the next-generation networks, 3GPP is working towards

standardizing the mmWave for the 5G New Radio (NR) interface. Regarding the operating frequency band of the 5G NR interface, the 60 GHz band, also known as the V-Band, ranging between 57 and 66 GHz is characterized by a continuous block of 9 GHz of unlicensed available spectrum [145]. In addition, the E-Band, comprised of two blocks of 5 GHz ranging from 71-76 GHz and 81-86 GHz, offers a total of 10 GHz of available spectrum [145]. Other promising mmWave bands are at 28 GHz and 38 GHz, which combined roughly offer 4 GHz of spectrum [105]. Furthermore, the most recent 3GPP Release 14 [91] includes the channel modeling for the frequency band above 6 GHz, which it is defined in 3GPP Specification 38.900/38.901 [146]. Release 15 [147] was concluded at the June 2018 RAN plenary meeting, consisting of the first set of 5G standards. However, some issues still need to be treated and solutions need to be formalized. The commercial use of the unlicensed mmWave band is not a new territory, but the mmWave bands have been used since the 1980s. IEEE 802.11ad/aj for WLAN [148, 149], IEEE 802.15.3c and ECMA-387 for wireless personal area network (WPAN) [150], WirelessHD for video area networking [151] are standards at unlicensed 60 GHz and 45 GHz for providing short-range point-to-point (P2P) communications.

2.3 Other Key-Enabling Technologies

Apart from the **HetNets** and the **mmWave communications** to which this thesis focuses, there are other technologies that are also considered as enabling technologies for the next-generation systems. Specifically, the most widely-accepted candidate technologies for the next-generation systems, are the following

- **Massive-MIMO:** The ability of massive-MIMO to serve multiple users simultaneously within a condensed area while maintaining fast data rates and consistent performance, makes it a suitable technology to address the needs of the forthcoming next-generation era. Early reports point to the considerable capacity improvements, and could potentially yield as much as a 50-fold increase in the future [152–154].

- **Cloud radio access network (C-RAN):** C-RAN is a novel RAN architecture that can address a number of challenges that the operators face while trying to support the growing needs of users, therefore it is seen as a major technological

foundation for the 5G networks [155–157].

- **Non-orthogonal-multiple-access (NOMA):** A candidate technology that focuses into the enhancement of the spectral efficiency and attracts the interest of the wireless community is the NOMA [158–160]. The key idea behind the NOMA technique is to serve multiple users in the same resource block, such as a time slot, sub-carrier, or spreading code, providing low latency, high reliability, massive connectivity, improved fairness, and high throughput.

- **FD radio:** In addition, the potentially double spectral efficiency provided by the simultaneous transmission and reception using non-orthogonal channels, appoints the FD radio as an enabling technology for the next-generation systems. The main drawback of FD radio is the overwhelming negative effect of the selft-interference (SI) at a transceiver. Fortunately, with the recent advancements in transceiver design and signal processing techniques, the SI signal can be successfully suppressed below the noise floor, and therefore the FD technology becomes feasible [161–164]. However, the performance of FD radio in large-scale multi-cell networks is also compromised by the increase of the intra- and out-of-cell co-channel interference. Several research efforts have been carried out to study the effect of multi-user interference on the FD performance for large-scale wireless networks, and several techniques have been proposed to mitigate the additional interference caused by the FD operation [162–164].

  Recent studies [161–164] indicate that the FD systems are feasible and can provide significantly higher data rates than the conventional HD communication systems.

- **D2D communications:** Finally, another candidate technology for the next generation systems is the utilization of the D2D communications. By allowing the D2D communications, that is, the direct transmission between the users, both the efficiency and the scalability of the future networks will be enhanced significantly [165–167].

2.4 Mathematical Modeling

In this section, we will initially introduce some mathematical preliminaries from the stochastic geometry theory that are widely used in the literature, mainly focusing on the spatial modeling of the cellular networks. Moreover, we provide the baseline system model for this thesis, such that extensions to this model are highlighted in the following chapters as needed.

2.4.1 Introduction to point process theory

As previously discussed in this chapter, the stochastic geometry approach is a powerful mathematical framework that recently gained momentum as the only available tool that provides a rigorous approach to model, analyze and design the current cellular networks [45–47]. A wireless communication network can be viewed as a collection of nodes, located in some domain, where each node can be either a transmitter or a receiver. At a generic time instant, several nodes transmit simultaneously, each towards its own receiver. Thus, apart from the transmitted signal from its own transmitter, a receiver also receives the signals from the other transmitters. In addition, the signal power radiated from a point decays in an isotropic way with the distance. Hence, the SINR is a random variable that strongly depends on the network geometry and significantly varies from one receiver to another and from one time instant to another. Based on the above, the geometry of the locations of the nodes plays a key role in the network performance since it determines the SINR at each receiver.

Stochastic geometry tools provide a natural way of defining and computing the macroscopic properties of such networks, by averaging over all potential network topologies weighted by their probability of occurrence. In other words, the stochastic geometry consists in treating such a network as a snapshot of a stationary random model in the whole Euclidean plane or space and analyzing it in a probabilistic way [45]. The most basic stationary random models studied in the stochastic geometry are the multidimensional PPs, which can be depicted as a random collection of points in the d-dimensional space, describing the deployment of the network's nodes [46, 47]. The probabilistic analysis of these PPs provides a way of estimating the spatial averages which often capture the key dependencies of the network performance

characteristics (connectivity, stability, capacity, etc.) as functions of a relatively small number of parameters.

Similar to any random process, a PP can be described in statistical terms by defining the space of possible outcomes and then specifying the probabilities of different events. Let $\mathfrak{N}$ be the set of all point patterns in the d-dimensional Euclidean space $\mathbb{R}^d$, such that any point pattern $\Phi \in \mathfrak{N}$ is (*i*) finite, i.e. any bounded subset $B \subset \mathbb{R}^d$ contains only a finite number of points, and (*ii*) simple, i.e. $x \neq y$ for any $x,\ y \in \Phi$. We use the notation $N(B)$, to denote the number of points of the pattern Φ in the subset B, which is given by

$$N(B) = \sum_{i=1}^{\infty} \mathbb{1}(x_i \in B), \tag{2.2}$$

where $\mathbb{1}(X)$ is an indicator function that is equal to $\mathbb{1}(X) = 1$ if X is true, otherwise $\mathbb{1}(X) = 0$. Finally, let $\mathcal{N}$ be the smallest sigma algebra and $(\Omega, \mathcal{F}, \mathbb{P})$ be a probability space, where Ω denotes the sample space, $\mathcal{F}$ is the set of the events and $\mathbb{P}$ corresponds to the mapping, which assigns probabilities to the events. Based on the aforementioned notation, we first give a formal definition of a PP.

Definition 2.1 (Point Process)**.** *A PP $\Phi = \{x_1, x_2, \cdots\} \subset \mathbb{R}^d$ is a measurable mapping from a probability space $(\Omega, \mathcal{F}, \mathbb{P})$ to $(\mathfrak{N}, \mathcal{N})$, i.e.*

$$\Phi : \Omega \to \mathfrak{N}. \tag{2.3}$$

The definition is referred from [46] and informally describes a PP as a random variable, which takes values from the set of simple and finite sequences $\mathfrak{N}$ on $\mathbb{R}^d$. The average number of the random variables $x_i \in \Phi$ included in a subset $B \subset \mathbb{R}^d$, represents the intensity measure of the PP, and is defined as follows.

Definition 2.2 (Intensity Measure)**.** *The intensity measure Λ of a PP Φ is defined as*

$$\Lambda(B) = \mathbb{E}\left[N(B)\right], \quad \forall B \subset \mathbb{R}^d, \tag{2.4}$$

and if Φ is stationary, the density of the PP Φ, is given by

$$\lambda = \frac{\mathbb{E}\left[N(B)\right]}{|B|},$$

where $|B|$ represents the area of $B \subset \mathbb{R}^d$, which contains only a finite number of points.

It can be easily observed that, the density does not depend on the particular choice of the set B. In addition, the stationarity of the PP implies that the density is constant in the entire d-dimensional space $\mathbb{R}^d$.

In the context of stochastic geometry, there are several basic yet important PPs, however, the most well-studied and most widely used PP is the PPP. Its importance mainly results from its convenient properties as a mathematical model as well as being mathematically interesting [36,45–47]. Motivated by the accurate modeling of real network developments, where the network's nodes exhibit a repulsive behavior in order to alleviate the interference or extend the coverage region, extensions to non-Poisson models are considered. Specifically, the β-GPP, which is a type of repulsive point process with analytical tractability, has been advocated to model random phenomena where repulsion is observed [50, 51, 67, 168]. In the following sections, we introduce the formal definitions of the PPP and the β-GPP, which are extensively used in this thesis.

2.4.2 Poisson Point Process

In this section, we provide definitions and notations to formally define PPPs and give their main characteristics. Initially, the PPP may be defined, studied and used in one dimension (on the real line) where it can be interpreted as a counting process or part of a queuing model [46]; in higher dimensions such as the plane where it plays a key role in the stochastic geometry and the spatial statistics [45–47]; or on more abstract mathematical spaces [45]. The formal definition of a PPP referred from [46] is stated as follows.

Definition 2.3 (Poisson Point Process)**.** *A PPP $\Phi = \{x_1, x_2, \cdots\} \subset \mathbb{R}^d$ with intensity measure Λ is a PP such that:*

- *$\forall B \subset \mathbb{R}^d$, $N(B)$ has a Poisson distribution with mean $\Lambda(B)$. If Λ admits a density λ, we may write*

$$\mathbb{P}(N(B) = k) = \exp\left(-\int_B \lambda(x)dx\right)\frac{\left(\int_B \lambda(x)dx\right)^k}{k!}, \tag{2.5}$$

  where $\lambda(x)$ denotes the density function of the PPP.

- *If $B_1, B_2, \cdots, B_m$ are disjoint bounded subregions of the underlying space, then the number of the points in each bounded subregion, i.e. $N(B_1), N(B_2), \cdots, N(B_m)$, will be*

completely independent to all the others. In other words, there is a lack of interaction between the different regions and the points in general, which motivates the PPP being sometimes called a "completely" random process.

Based on the Definition 2.3, many unique computational properties of the PPP can be derived. Three commonly used properties for analyzing the achieved performance of the cellular networks are provided as follows.

- **Slivnyak's theorem.** For any point $x \in \mathbb{R}^d$ and an event E, the reduced Palm distribution of a PP Φ is defined as $\mathbb{P}^!_{x_0}(E) = \mathbb{P}(\Phi \backslash \{x_0\} \in E | x_0 \in \Phi)$.

  Definition 2.4 (Slivnyak theorem)**.** *A PPP Φ preserves its original distribution under the reduced Palm distribution, which means*

  $$\mathbb{P}^!_{x_0}(E) = \mathbb{P}(\Phi \in E),$$

  if the PP Φ is Poisson distributed.

  An alternative view of the Slivnyak theorem is that the property observed by a typical point x_0 of the PPP Φ, is the same as that observed by x in $\Phi \cup \{x\}$, which means

  $$\mathbb{P}(\Phi \in E | x_0 \in \Phi) = \mathbb{P}(\Phi + \delta_x \in E),$$

  where δ_x is the Dirac measure at x.

- **Laplace Functional.** One of the key transformations in the wireless network modeling and analysis with the stochastic geometry is the Laplace functional. This is because by using the Laplac e functional, the aggregate interference distribution can be uniquely defined.

  Definition 2.5 (Laplace Functional)**.** *For any non-negative function $f(x)$ on $\mathbb{R}^d$, the Laplace functional of a PPP Φ with intensity measure $\Lambda(x)$ is defined as*

  $$\mathbb{E}\left[\exp\left(-\int_{\mathbb{R}^d} f(x)\Phi(dx)\right)\right] = \exp\left(-\int_{\mathbb{R}^d} \left(1 - \exp\left(-f(x)\right)\right)\Lambda(dx)\right).$$

  In the context of wireless communications, the non-negative measurable function $f(x)$, represents the aggregate interference observed at a receiver.

- **Probability Generating Functional.** Another important property for the analysis with the use of stochastic geometry is the calculation of the probability generating functional (PGFL) of a PP $\Phi = \{x : x \in \mathbb{R}^d\}$, that is defined as

$$\mathcal{G}[u] = \mathbb{E}\left[\prod_{x\in\Phi} u(x)\right],$$

where $u(x) : \mathbb{R}^d \to [0, \infty]$.

Definition 2.6 (Probability Generating Functional)**.** *The PGFL of a PPP Φ with intensity measure $\Lambda(x)$, is equal to*

$$\mathcal{G}[u] = \exp\left[-\int_{\mathbb{R}^d} (1 - u(x))\, \Lambda(dx)\right],$$

where $u(x) : \mathbb{R}^d \to [0, \infty]$ is a real value function. If the PPP is stationary, then the PGFL, can be re-written as

$$\mathcal{G}[u] = \exp\left[-\lambda \int_{\mathbb{R}^d} (1 - u(x))\, dx\right].$$

It proves particularly useful to evaluate the Laplace functional of the sum $\sum_{x\in\Phi} f(x)$ using the PGFL as

$$\mathbb{E}\left[\exp\left(-\sum_{x\in\Phi} f(x)\right)\right] = \mathbb{E}\left[\prod_{x\in\Phi} \exp\left(-f(x)\right)\right] = \mathcal{G}\left[\exp(-f(x))\right],$$

which typically appears in the analysis of the aggregate interference.

To develop suitable models for analyzing the network deployments with the aid of PPPs and by using the stochastic geometry, there is a number of useful transformations that can be performed on the PPPs. In the following sections, we briefly introduce the basic PPP transformations that are appeared in this thesis.

Displacement

Firstly, we consider the displacement transformation of a PP. Let a PP $\Phi \subset \mathbb{R}^d$. Consider that the points of the PP Φ, are displaced by a random translation vector V_x, creating a transformed PP, denoted by Φ', which is given by

$$\Phi' = \{x \in \Phi : x + V_x\}.$$

When the displacement transformation is applied to a PPP, the resulting process is again a PPP.

Definition 2.7 (Displacement). *Let a PPP $\Phi \subset \mathbb{R}^d$ with density $\lambda(x)$. If all points are independently displaced such that the distribution of the displaced location of a point at x has probability density $\rho(x, \cdot)$, the displaced points form a PPP Φ' with density*

$$\lambda'(y) = \int_{\mathbb{R}^d} \lambda(x)\rho(x, y)dy.$$

For the case where $\lambda(x) \equiv \lambda$ and $\rho(x, y)$ is a function only of $y - x$, then $\lambda'(x) \equiv \lambda$.

The displacement theorem shows that the PPP is persistent, in the sense that independent displacements preserve the PPP characteristics, which makes it an attractive model when nodes in a wireless network move around independently.

Thinning Transformation

Another important transformation in the context of stochastic geometry, is the thinning transformation. In general, the thinning transformation is the process of removing certain points from a PP, usually according to a probabilistic rule $g : \mathbb{R}^d \to [0, 1]$. If the removal event is independent for all points, the thinning transformation is called *independent*.

Definition 2.8 (Thinning). *Let $g : \mathbb{R}^d \to [0, 1]$ be a thinning function and apply it to a stationary PPP Φ by deleting each point x with probability $1 - g(x)$, independently of all the other points. This thinning procedure generates an inhomogeneous PPP Φ' with density that is equal to*

$$\lambda'(x) = \lambda g(x). \tag{2.6}$$

Mapping Transformation

Another transformation that is considered useful for the analysis of the wireless networks is the mapping transformation. Specifically, the mapping transformation expresses the ability to map each point of the process to another point, possibly in a space of different dimension. When applied to a PPP, the resulting process is still Poisson in many cases.

Definition 2.9 (Mapping). *Let Φ be a PPP on the d-dimensional space $\mathbb{R}^d$ with intensity measure $\Lambda(B)$ and density $\lambda(x)$, and let $f : \mathbb{R}^d \to \mathbb{R}^s$ be a measurable function with the property that $\Lambda\left(f^{-1}(y)\right) = 0,\ \forall y \in \mathbb{R}^s$, such that f does not shrink a non-singleton set to a singleton. Then, the resulting PP $\Phi' = f(\Phi)$ has intensity measure given by*

$$\Lambda'(B') = \Lambda\left(f^{-1}(B')\right) = \int_{f^{-1}(B')} \lambda(x)dx, \qquad \forall B' \subset \mathbb{R}^s, \tag{2.7}$$

where $f^{-1}(B')$ represents the pre-image of the B'.

Superposition operation

Finally, the superposition operation is used to combine two or more PPs together onto one underlying mathematical space.

Definition 2.10 (Superposition)**.** *Let a countable set of PPs $\Phi_1, \Phi_2, \cdots, \Phi_{\mathcal{K}}$ with their corresponding densities $\lambda_1, \lambda_2, \cdots, \lambda_{\mathcal{K}}$. The superposition of these PPs is defined as*

$$\Phi = \bigcup_{k=1}^{\mathcal{K}} \Phi_k,$$

and is also forms a PP.

In other words, any points located in any of the PPs Φ_k will also be located in the superposition of these PPs Φ. In the case where each Φ_k is a PPP, the complete independence offered by such PPs leads to some useful characteristics and results for the superposition property. Specifically, the superposition of the PPPs Φ_i, where $i = \{1, 2, \cdots, \mathcal{K}\}$ and with densities λ_i, is another PPP that is defined as

$$\Phi = \sum_{k=1}^{\mathcal{K}} \Phi_k,$$

with density

$$\lambda = \sum_{k=1}^{\mathcal{K}} \lambda_k.$$

Based on the aforementioned, the PPP-based models for the spatial distribution of the wireless cellular networks often give tractable results. Nevertheless, the PPP-based models may still not be appropriate for realistic network layouts, where clusters or voids of points can be exist. Although there is a rich range of possible PPs, the majority of them unfortunately lack the necessary properties that make them tractable, which partly explains why the clear majority of network models are based on the PPP. Consequently, for the modeling and analysis of repulsive wireless networks with efficient tractability, we confine ourselves in adopting determinantal PPs.

2.4.3 β-Ginibre Point Process

The most tractable determinantal PP is arguably the Ginibre PP, often abbreviated as GPP, which induces a repulsion between points. This repulsion is interpreted by

the probability density to place points. In fact, the probability to draw a point at the same position of an already drawn point is zero. This probability increases by increasing the distance from every existing points.

Let $\mathbb{C}$ denotes the complex plane and $z_1, z_2 \in \mathbb{R}$. We denote by $\bar{z}$ the complex conjugate of a complex number $z = z_1 + jz_2$, i.e. $\bar{z} = z_1 - jz_2$, where $j = \sqrt{-1}$, and by $|z| = \sqrt{z_1^2 + z_2^2}$ the modulus. Consider a Borel set $S \subset \mathbb{R}^d$. For any function $K : S \times S \to \mathbb{C}$, let $[K](x_1, \cdots, x_n)$ be the $n \times n$ matrix with (i, j)-th entry $K(x_i, x_j)$, and $\det A$ be the determinant of a squared matrix A [51]. The product density functions of a GPP, are given by

$$\varrho^{(n)}(x_1, \cdots, x_n) = \det[K](x_1, \cdots, x_n), \tag{2.8}$$

where the kernel function K is the Gaussian kernel, that is given by

$$K(x, y) = \pi^{-1} \exp\left(-\frac{|x|^2 + |y|^2}{2}\right) \exp\left(-x\bar{y}\right), \qquad x, y \in \mathbb{C},$$

with respect to the Lebesgue measure on $\mathbb{C}$. The expression 2.8 highlights that $\varrho^{(n)}(x_1, \cdots, x_n) = 0$ when $x_i = x_j$ for $i \neq j$, which reflects the repulsiveness of a GPP. It also follows that $\mathbb{E}[\Phi(B)] = \int_B \varrho^{(1)}(x)dx = \pi^{-1}|B|$, that is, the density of the GPP is π^{-1}. Furthermore, based on 2.8, the second moment density $\varrho^{(2)}(x, y)$ of the GPP, is given by

$$\varrho^{(2)}(x, y) = \pi^{-2}\left(1 - \exp\left(-|x - y|^2\right)\right),$$

where it is observed that $\varrho^{(2)}(x, y)$ only depends on $|x - y|$, illustrating the motion invariant and repulsive properties of the GPPs.

The standard GPP can be generalized to the β-GPP using independent thinning and rescaling. A β-GPP, where $0 < \beta \leq 1$, is constructed from a GPP by retaining, independently and with probability β, each point of the GPP and then applies an homothety of ratio $\sqrt{\beta}$ to the remaining points. As $\beta \to 0$, the β-GPP converges weakly to the PPP of intensity π^{-1}. Hence, the parameter β can be used to smoothly interpolate between the standard GPP (or 1-GPP) and the PPP.

Regarding modeling network layouts with arbitraty densities $\lambda = c\pi^{-1}$, the β-GPP can be scaled, which results in the scaled kernel

$$K(x, y) = c\pi^{-1} \exp\left(-\frac{c|x|^2 + |y|^2}{2\beta}\right) \exp\left(-\left(\frac{c}{\beta}\right) x\bar{y}\right), \qquad x, y \in \mathbb{C},$$

with respect to the Lebesgue measure on $\mathbb{C}$. The following Proposition states a key result that makes the β-GPP relatively tractable [169].

Proposition 2.1. *Let $\Phi = \{X_i\}$, where $i \in \mathbb{N}^+$, be a scaled β-GPP. For $k \in \mathbb{N}^+$, let B_k be a random variable with propability density*

$$f_{B_k}(x) = \frac{x^{k-1} \exp\left(-\frac{cx}{\beta}\right)}{\left(\frac{\beta}{c}\right)\Gamma[k]},$$

where $B_k \sim \Gamma(k, \beta/c)$, with B_i independent of B_j, if $i \neq j$, and $\Gamma[k]$ represents the gamma function, i.e. $\Gamma[\cdot] = \int_0^\infty x^{k-1}\exp(-x)dx$. Then the set $\{|X_i|^2\}_{i\in\mathbb{N}^+}$ has the same distribution as the set $\widetilde{B}$ obtained by retaining from $\{B_k\}_{k\in\mathbb{N}^+}$ each B_k with probability β independently of everything else.

Therefore, the term $\|x\|^{-a}$ can be represented as $\widetilde{B}_i^{-\frac{a}{2}} = B_i^{-\frac{a}{2}}\Xi_i$, where $\{\Xi_i\}_{i\in\mathbb{N}^+}$ is the set of discrete random variables, such that $\mathbb{P}(\Xi_i = 1) = \beta$ and $\mathbb{P}(\Xi_i = 0) = 1 - \beta$. Regarding the scenario of the 1-GPP, the set of square distances is distributed like a set of independent gamma random variables. For $\beta < 1$, some of the gamma random variables need to be removed. The Palm measure (at the origin) satisfies a similar property, which is stated in the following Proposition.

Proposition 2.2. *The Palm measure of a scaled β-GPP Φ is the law of the PP obtained by adding the origin to Φ and removing the point x, where $|x|^2 = B_1$ (which only exists with probability β).*

It is important to note here that, if the point x with $|x|^2 = B_1$ has been eliminated from Φ, then no point is removed. This is consistent with the fact that as $\beta \to 0$, the β-GPP converges to a PPP, because in this case, the point whose modulus corresponds to B_1 is not present in the GPP with high probability, hence the only difference of the Palm measure is the point at the origin.

In the rest of this chapter, we introduce the baseline system model that is adopted throughout the thesis, with slight modifications that are detailed in each chapter according to the considered network setup.

2.4.4 Topology Model

The network is studied from a large-scale point of view using stochastic geometry. We consider a heterogeneous cellular network composed by $\mathcal{K} = \{1, \ldots, K\}$ network tiers. The BSs belonging to the k-th tier are modeled as a two-dimensional homogeneous PPP Φ_k with spatial density λ_k BS/m^2 and transmission power P_k. Furthermore, the locations of the users follow an arbitrary independent point process Φ_u with spatial density $\lambda_u \gg \sum_{k\in\mathcal{K}} \lambda_k$.

2.4.5 Channel Model

All wireless signals are assumed to experience both large-scale path-loss and small-scale fading effects. It is important to mention here that, we adopt an accurate and general small-scale fading model for the mmWave environments, which is the Nakagami-ν fading, where different links are assumed to be independent and identically distributed. Different parameters of Nakagami fading ν_L and ν_N are assumed for the LoS and the NLoS links. Hence, the power of the channel fading depends on the link's status, $\ell \in \{\mathrm{L}, \mathrm{N}\}$, and is a normalized Gamma random variable with shape parameter ν_ℓ and scale parameter $1/\nu_\ell$. We also consider the scenario where $\nu_\ell = 1$, which corresponds to a simpler channel model. For this case, the channel fading is modeled by Rayleigh fading with unit average power and therefore, the power of the channel fading is an exponential random variable with unit mean, i.e. $h \sim \exp(1)$. For the large-scale path-loss, we assume an unbounded singular path-loss model, $L(X, Y) = \|X - Y\|^{-a}$ which assumes that the received power decays with the distance between the transmitter located at X and the receiver located at Y, where $a > 2$ denotes the path-loss exponent. For simplicity, we denote as $L_0(X) = \|X\|^{-a}$ the path-loss between the transmitter located at X and the receiver located at the origin.

2.4.6 Sectorised Antenna Model

We assume the employment of multiple transmit/receive antennas at both the BSs and the users. To simplify the analysis, we make use of the approximation of an actual beam pattern using a sectorized model. Both the transmit and receive beam patterns are parameterized by three values: main lobe beamwidth $\theta \in [0, 2\pi]$, main lobe gain M, and side lobe gain m [113]. The gain of an interference link seen by the user, is a discrete random variable described by

$$G = \begin{cases} Q^2 & \text{with probability } p_{Q^2} = \left(\frac{\phi}{\pi}\right)^2, \\ Qq & \text{with probability } p_{Qq} = 2\left(\frac{\phi}{\pi}\right)\left(\frac{\pi-\phi}{\pi}\right), \\ q^2 & \text{with probability } p_{q^2} = \left(\frac{\pi-\phi}{\pi}\right)^2, \end{cases} \tag{2.9}$$

where p_G is the probability of a link to have gain equal to $G = \{Q^2, Qq, q^2\}$. We assume that perfect beam alignment can be achieved between each user and its

serving BS using the estimated angles of arrival, resulting in an antenna array gain of Q^2, denoted by G_0.

2.4.7 Blockages Model

A link can be either LoS or NLoS, depending on whether the BS is visible to the user or not. In particular, a transmitter is considered LoS by a receiver, if and only if their communication link of length R is unobstructed by blockages. Under such a scenario, it was shown that the LoS probability function $\mathcal{P}_{\mathrm{L}}(R)$ of a communication link of length R, is given by [133]

$$\mathcal{P}_{\mathrm{L}}(R) = \mathbb{P}[\mathrm{LoS}] = \exp(-\beta R), \tag{2.10}$$

where β is a non-negative blockage constant that models the blockage density and their characteristics [133]. Under the assumption that the BSs are modeled as points of a homogeneous PPP Φ_k and that the events of the BS-to-user links are either in LoS or NLoS independently, the PPP Φ_k can be partitioned into two independent and non-homogeneous PPPs i.e., Φ_k^{L} and Φ_k^{N}, such that $\Phi_k = \Phi_k^{\mathrm{L}} \cup \Phi_k^{\mathrm{N}}$. Specifically, for each network tier $k \in \mathcal{K}$, a PPP Φ_k^{L} with inhomogeneous density $\lambda_k^{\mathrm{L}}(r) = \lambda_k \exp(-\beta r)$ is formed. This originates from the thinning property of the PPPs as we previously discussed in Chapter 2.4.2. The LoS and NLoS links have different path-loss exponents, a_{L} and a_{N}, respectively, and are the same for all network tiers. Hence, the path-loss exponent $a(r)$ for the link between a BS located at distance r from a user, is modeled as a discrete random variable described by

$$a(r) = \begin{cases} a_{\mathrm{L}} & \text{with probability } \mathcal{P}_{\mathrm{L}}, \\ a_{\mathrm{N}} & \text{with probability } \mathcal{P}_{\mathrm{N}} = 1 - \mathcal{P}_{\mathrm{L}}, \end{cases} \tag{2.11}$$

where $\mathcal{P}_{\mathrm{L}}$ is given by expression (2.10).

Chapter 3

Low-complexity base station selection scheme in mmWave cellular networks

In this chapter, we study the performance of HetNet-mmWave cellular networks in the context of a low coordination complexity BS selection scheme. The proposed scheme allows the user to communicate with the BS that provides the maximum SINR from a set formed according to a pre-selection policy. We consider three pre-selection policies based on: 1) the Euclidean distance, 2) the averaged received power, and 3) a random selection. Moreover, we consider the case where the users have the ability to employ the SIC scheme. By using stochastic geometry tools, analytical expressions for the coverage performance are derived for each policy.

3.1 Motivation and Contributions

The wireless industry is currently facing the barrier of limited available spectrum for commercial cellular systems and an increasing demand of data traffic. As a consequence, the research community is directing significant efforts towards advanced communication techniques for the next-generation networks, such as the HetNets and the mmWave communications.

However, the HetNet-mmWave cellular networks have fundamental differences with the current sub-6 GHz cellular networks in terms of the propagation losses and the interference. This leads to the investigation of novel communications techniques in order to address these issues and to fully exploit the benefits of the HetNet-mmWave cellular networks. Throughout the literature, many innovating techniques

were investigated such as the CoMP, the beamforming and the SIC, which can be enable Gb/s-level access speeds with less spectrum usage and lower power consumption. On the other hand, the CoMP technique demands high computational resources for synchronization, channel estimation and data traffic. In contrast, our proposed technique provides low coordination and implementation complexity without depriving in diversity gain compared to the CoMP technique.

In this chapter, we study the DL performance of a HetNet-mmWave cellular network where antenna directionality is employed. We adopt a system-level point of view by taking into account both BS and blockage spatial randomness. We summarize our contributions as follows.

- We propose a BS selection scheme that is based on a two-level procedure: in the first-level, a set of "candidate" BSs is defined and at the second-level, the user selects from this set the BS which provides the highest SINR. The proposed two-level BS selection technique reduces the signaling and thus is attractive for practical and low-coordination implementations.

- We evaluate the achieved performance of our proposed technique in the context of two popular and well investigated BS selection policies. Specifically, the pre-selection is based either on the Euclidean distance or the averaged received signal power. For comparison purposes, we also investigate our proposed technique with a random BS selection policy.

- We investigate the employment of an ideal SIC technique for the DL in the HetNet-mmWave cellular networks to further emphasize the achieved network performance using the proposed technique. With the intention to keep low computational complexity, we assume that the user eliminates only its dominant interferer without depriving from the network to achieve better coverage performance.

- Finally, analytical and asymptotic expressions are derived for the coverage probability for each pre-selection policy by employing Nakagami fading. In addition, analytical expressions of the coverage probability for the case where the users have the ability to perform SIC are also provided for the scenarios considered. These closed-form expressions provide a quick and convenient methodology of evaluating the system's performance and obtaining insights

into how key system parameters affect the performance.

3.2 System Model

Recall that, we consider a heterogeneous cellular network composed by K network tiers of BSs. We assume the BSs are connected by an ideal backhaul network, which provides the ability to the BSs from different tiers to cooperate and jointly transmit data to a user [113]. Each network tier $k \in \{1, \ldots, K\}$ of BSs is modeled by a two-dimensional homogeneous PPP Φ_k with density λ_k and transmission power P_k.

The operation of the considered HetNets in the mmWave frequencies, necessitates the incorporation of the key features of the mmWave communications into the proposed framework. Initially, we assume the employment of multiple transmit/receive antennas at both the BSs and the users, with which adaptive directional beamforming is achieved at each terminal (BS or user). Specifically, we approximate the actual beam pattern by a sectorized model as proposed in [113] and as we previously discussed in Section 2.4. Moreover, the impact of blockages on the network performance is incorporated in the proposed framework. In particular, as we previously discussed in Section 2.4, we assume that a link can be either LoS or NLoS, based on a LoS probability function that is given by $\mathcal{P}_{\mathrm{L}} = \exp(-\beta r)$. Thus, each PPP Φ_k is divided into two independent and non-homogeneous PPPs i.e., Φ_k^{L} and Φ_k^{N}, with densities $\lambda_k^{\mathrm{L}}(r) = \lambda_k \mathcal{P}_{\mathrm{L}}$ and $\lambda_k^{\mathrm{N}}(r) = \lambda_k(1 - \mathcal{P}_{\mathrm{L}})$, respectively.

In terms of the channel modeling, we assume independent Nakagami fading for each link. Different parameters of Nakagami fading ν_L and ν_N are assumed for LoS and NLoS links and so the power of the channel fading depending on the link's status, $\ell \in \{\mathrm{L}, \mathrm{N}\}$, is a normalized Gamma random variable with shape parameter ν_ℓ and scale parameter $1/\nu_\ell$. Furthermore, we assume all wireless links exhibit additive white Gaussian noise with zero mean and variance σ^2.

3.3 BS Selection Technique

Our proposed BS selection (BSS) scheme is based on a two-level procedure. In the first-level phase, a set of K "candidate" BSs is formed based on the adopted pre-selection policy, without taking into consideration the fading channel factor. Specifically, according to the rules of the adopted pre-selection policy, from each

network tier $k \in \{1, \ldots, K\}$, a single BS is selected. The set defined by the pre-selected BSs from all network tiers, represents the set of BSs with which the user is able to communicate, $C \subset \bigcup_{k=1}^{K} \Phi_k$. At the second-level phase, the user selects from the K "candidate" BSs, the one which provides the highest SINR, while the rest of the "candidate" BSs are ignored. Due to the pre-selection of the K "candidate" BS, our proposed selection scheme requires channel estimation for only K links instead of $\sum_{k=1}^{K} N_k$ links, where N_k is a Poisson random variable denoting the number of BSs in the k-th tier.

For comparison purposes, a conventional cooperative scheme, namely the coordinated multi-point (CoMP) technique, where an ideal backhaul network allows a set of randomly located BSs to cooperate and jointly transmit data, is considered. Then, the typical user combines the individual received signals by employing the maximum-ratio combining method, which is the optimum combiner for independent additive white Gaussian noise channels. Therefore, the low coordination complexity of the proposed technique stems from the fact that users connect to a single BS, opposed to the jointly BS transmission technique of the conventional CoMP technique, that demands higher computation and coordination complexity. This is where the novelty of our proposed technique is highlighted. Particularly, by applying the proposed technique, the coordination of implementing BS cooperation in the HetNet-mmWave cellular networks can be significantly decreased.

3.3.1 Closest LoS pre-selection policy (CS)

As a first pre-selection policy, we consider the case where the set of "candidate" BSs, consists of the closest LoS BS from each network tier; Fig. 3.1a schematically depicts the CS policy. This policy requires an a priori knowledge of the location of the BSs, which can be obtained by monitoring the location of the BSs through a low-rate feedback channel or by a global positioning system mechanism. The CS policy does not take into account the instantaneous fading resulting in a low implementation complexity, specifically for scenarios with low mobility. In this case, the set C_{CS} is defined as

$$C_{\mathrm{CS}} = \left\{ u_k^* : u_k^* = \arg\max_{u \in \Phi_k} r_u^{-1}, k \in \{1, \ldots, K\}, r_u \in \Phi^{\mathrm{L}} \right\}. \tag{3.1}$$

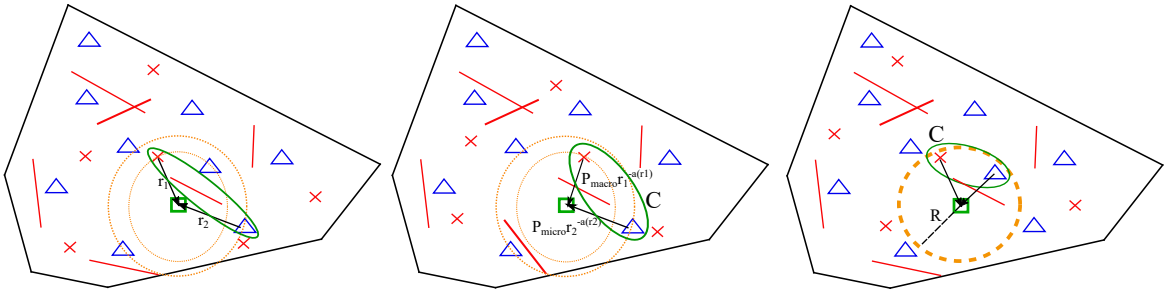

(a) CS Policy (b) SS Policy (c) RS Policy

Figure 3.1: The three considered pre-selection policies.

3.3.2 Strongest pre-selection policy (SS)

For the second pre-selection policy, we consider the case where the set of "candidate" BSs, consists of the BS that provides the strongest RSS from each network tier; Fig. 3.1b schematically depicts the SS policy. Along with the information regarding the BS location, the SS policy also requires the transmit power of the BSs, which can be obtained through a low-rate feedback channel. This case is applicable to wireless networks, where the users keep a list of the neighboring BSs with the strongest RSS to initiate handoff requests. We define the set of "candidate" BSs for this policy as

$$C_{\mathrm{SS}} = \left\{ u_k^* : u_k^* = \arg\max_{u \in \Phi_k} \frac{P_k}{r_u^{a(r_u)}}, k \in \{1, \ldots, K\} \right\}. \tag{3.2}$$

Note that in the case where the transmit power of the BSs of all tiers is the same, the SS policy selects the BSs with the smallest path loss from each network tier k.

3.3.3 Random pre-selection policy (RS)

For comparison reasons, for the final pre-selection policy, we consider the case where the set of "candidate" BSs, consists of a randomly selected BS that is located inside a disk of radius R around its associated user, from each network tier k; Fig. 3.1c depicts the RS policy. The pre-selection of a random BS from the k-th tier is independent of whether the communication link with its associated user is LoS or NLoS. In the case where there is not any available BS inside the disk of radius R, the user is in outage. The absence of need for feedback on the location of the BSs, corresponds to a low implementation complexity approach, which is suitable for the networks with strict power/bandwidth constraints. In this case, the set C_{RS} is defined as

$$C_{\mathrm{RS}} = \left\{ u_k^* : r_{u_k^*} \leq R, k \in \{1, \ldots, K\} \right\}. \tag{3.3}$$

3.3.4 Implementation issues

In this subsection, the potential implementation of the proposed two-level BS selection scheme in the context of the next-generation networks is discussed. Towards this direction, we assume a centralized controller, which takes as input the signal strength of the links between the BSs and the users and implements the proposed selection schemes. This is in line with the C-RAN architecture proposed for the 5G mobile communication systems, where the BSs functionalities from the physical layer to the higher layers are managed by a centralized logic (cloud) [74]. On the other hand, channel estimation in the 5G communication systems exploits the time division duplex reciprocity and is performed in the UL through orthogonal pilots signals. It is worth noting that techniques for estimating the direction of arrival, such as the codebook-based beamforming protocol, the multiple signal classification (MUSIC) or the estimation of signal parameters via rotational invariance techniques [21, Ch. 3], are also used to estimate the beamforming gain. Therefore, the required information (i.e., strength of the links, beamforming gain) is obtained by using the pilot signals. This information is collected and measured by the BSs (i.e., remote radio heads in C-RAN) and is communicated to centralized unit through a fronthaul network.

3.4 Performance Analysis

In this section, we analyze the SINR distribution for the DL of a HetNet-mmWave cellular network, where the terminals employ sectorized antennas in the presence of blockages. We first characterize the overall SINR complimentary cumulative distribution function (ccdf) by analyzing the network when the desired link is either LoS and NLoS and finally we quantify the effect of random distances. Without loss of generality and following Slivnyak's theorem [46], we execute the analysis for a typical user located at the origin but the results hold for all users of the network. Using the proposed two-level BSS technique, the network performance of each policy is derived analytically by using stochastic geometry. Finally, we analytically derive the diversity gain achieved with the SS policy, while the derived result applies for all pre-selection policies.

Let SINR_k, represent the achieved instantaneous SINR when the user communi-

cates with its pre-selected BS from the k-th tier, written as

$$\mathrm{SINR}_k = \frac{G_0 P_k r_{u_k^*}^{-a\left(r_{u_k^*}\right)} h_{u_k^*}}{I + \sigma^2}, \tag{3.4}$$

where $I = \sum_{i=1}^{K} \sum_{G} \sum_{v_i \in \mathcal{Y}} G P_i h_{v_i} r_{v_i}^{-a(r_{v_i})}$ is the total received interfering power from all the active BSs in the i-th tier where $\mathcal{Y} \subset \bigcup_{k=1}^{K} \Phi_k \backslash C$; and $h_{u_k^*}$ is the channel fading between the user and its pre-selected BS, u_k^* from the k-th tier. By using the proposed technique, the controller selects the BS from the set of "candidate" BSs, that provides the maximum SINR i.e., $\mathrm{SINR}^* = \max\{\mathrm{SINR}_k\}$, where $k \in \{1, \ldots, K\}$. The coverage probability $\mathcal{P}^*(T)$ at the user is the probability that the maximum SINR is greater than a predefined threshold T and is given by $\mathcal{P}^*(T) = \mathbb{P}[\mathrm{SINR}^* \geq T]$. Therefore, with uncorrelated branches, the conditional density function (cdf) of SINR^* is

$$\mathbb{P}\left[\mathrm{SINR}^* < T\right] = \prod_{k=1}^{K} \mathbb{P}\left[\mathrm{SINR}_k < T\right] = \prod_{k=1}^{K} \left(1 - \mathcal{P}_k^*(T)\right), \tag{3.5}$$

where $\mathcal{P}_k^*(T)$ denotes the coverage probability of the user communicating with its pre-selected BS from the k-th tier. The link's status ℓ, between each user and its associated BS can be either LoS or NLoS. Hence, for a fixed distance $r_{u_k^*}$, between the user and its associated BS, we can use the law of total probability to expand the SINR ccdf as

$$\mathcal{P}_k^*(T \mid r_{u_k^*}) = \sum_{\ell \in \{\mathrm{L},\, \mathrm{N}\}} \mathcal{P}_\ell \mathcal{P}_k^*(T \mid \ell,\, r_{u_k^*}), \tag{3.6}$$

where $\mathcal{P}_k^*(T \mid \ell,\, r_{u_k^*})$ is the achieved coverage probability of a user connecting with BS u_k^* from the tier k and with link status $\ell \in \{\mathrm{L}, \mathrm{N}\}$ and $\mathcal{P}_\ell$ expresses the probability that the link has status ℓ. By unconditioning on $r_{u_k^*}$, the achieved coverage probability from network tier k is written as

$$\mathcal{P}_k^*(T) = \int_{0 < r_{u_1^*} < \cdots < \infty} \cdots \int \sum_{\ell \in \{\mathrm{L},\, \mathrm{N}\}} \mathcal{P}_\ell \mathcal{P}_k^*\left(T \mid \ell,\, r_{u_k^*}\right) f_\Phi^\Pi(\boldsymbol{r} \mid \ell) d\boldsymbol{r}, \tag{3.7}$$

where $f_\Phi^\Pi(\boldsymbol{r} \mid \ell)$ denotes the joint distribution of $\boldsymbol{r} = \{r_{u_1^*}, \ldots, r_{u_K^*}\}$ for the pre-selection policy $\Pi \in \{\mathrm{CS}, \mathrm{SS}, \mathrm{RS}\}$, given the status of the communication link is $\ell \in \{\mathrm{L}, \mathrm{N}\}$.

Based on the above, in the following subsections, we provide the coverage probability for each pre-selection policy.

3.4.1 CS policy

For the CS policy, the closest LoS BSs from each tier are pre-selected. Therefore, the following lemma provides the density of each tier together with the joint distance

distribution when the CS policy is employed.

Lemma 3.1. *When the CS policy is employed, the density of the i-th tier, is given by*

$$\lambda_i^{\mathrm{CS}}(r \mid \mathrm{L}) = 2\pi\lambda_i r \exp(-\beta r), \tag{3.8}$$

and the joint distance distribution between the user and its pre-selected BSs, is given by

$$f_{\Phi}^{\mathrm{CS}}(\boldsymbol{r} \mid \mathrm{L}) = \prod_{i=1}^{K} 2\pi\lambda_i r_{u_i^*} \exp\left(-\beta r_{u_i^*} - \frac{2\pi\lambda_i}{\beta^2}\left(1 - \exp\left(-\beta r_{u_i^*}\right)(1 + \beta r_{u_i^*})\right)\right). \tag{3.9}$$

Proof. Based on the thinning property as it is previously discussed in Section 2.4.2, the density of the LoS BS from the k-th tier is given by the density of the homogeneous PPP Φ_k, which is equal to $\lambda_k(r) = 2\pi\lambda_k r$, multiplied with the LoS probability $\mathcal{P}_{\mathrm{L}} = \exp(-\beta r)$. Therefore, following the expression (2.7), the intensity measure of the LoS BSs is equal to

$$\Lambda(r) = \frac{2\pi\lambda}{\beta^2}\left(1 - \exp(-\beta r)(1 + \beta r)\right).$$

Hence, based on the Poisson random variable definition given by the expression (2.5), the distribution of the distance R to the closest LoS BS and the probability density function (pdf) of R, are given by

$$\mathbb{P}[R > r] = \exp\left(-\frac{2\pi\lambda}{\beta^2}\left(1 - \exp(-\beta r)(1 + \beta r)\right)\right),$$

and

$$f_{\Phi}(r) = 2\pi\lambda r \exp\left(-\beta r - \frac{2\pi\lambda}{\beta^2}\left(1 - \exp(-\beta r)(1 + \beta r)\right)\right),$$

respectively. The distance distributions are the same for all network tiers, since the network tiers are mutually independent. Therefore, $f_{\Phi_k}(r_k)$ represents the distance distribution of the k-th tier, the joint distance distribution is given by the product of the distance distributions of all the network tiers. □

By using the above lemma, the following theorem provides the coverage probability achieved by the CS policy.

Theorem 3.1. *The coverage probability achieved when the CS policy is employed, is given by*

$$\mathcal{P}^*(T) < 1 - \prod_{k=1}^{K}\left(1 - \sum_{\xi=1}^{\nu_L}(-1)^{\xi+1}\binom{\nu_L}{\xi}\int_{0<r_{u_1^*}<\cdots<\infty}\cdots\int \exp\left(-s_L\sigma^2\right)\mathcal{L}_I(s_{\mathrm{L}})f_{\Phi}^{\mathrm{CS}}(\boldsymbol{r} \mid \mathrm{L})d\boldsymbol{r}\right), \tag{3.10}$$

where $f_{\Phi}^{\mathrm{CS}}(\boldsymbol{r} \mid \mathrm{L})$ *is given by* (3.9)*, and*

$$\mathcal{L}_I(s_{\mathrm{L}}) = \prod_{i=1}^{K} \prod_{G} \exp\left(-p_G \int_{r_{u_i^*}}^{\infty} \left(1 - \left(1 + \frac{s_L G P_i v^{-a_L}}{\nu_{\mathrm{L}}} \right)^{-\nu_{\mathrm{L}}} \right) \lambda_i^{\mathrm{CS}}(v \mid \mathrm{L})\, dv \right), \tag{3.11}$$

where $G \in \{Q^2, Qq, q^2\}$, $s_L = \frac{\eta_L \xi T r_{u_k^*}^{a_L}}{G_0 P_k}$, $\eta_{\mathrm{L}} = \nu_{\mathrm{L}}(\nu_{\mathrm{L}}!)^{-1/\nu_{\mathrm{L}}}$ *and* $\lambda_i^{\mathrm{CS}}(v \mid \mathrm{L})$ *is given by* (3.8)*.*

Proof. Using the proposed BSS technique as described before, the instantaneous coverage probability of the user where the link's status with its associated BS is ℓ, is given by

$$\mathcal{P}_k^*(T \mid \ell,\, r_{u_k^*}) = \mathbb{P}\left[\frac{G_0 P_k h_{u_k^*} r_{u_k^*}^{-a_\ell}}{\sigma^2 + I} \geq T \right] = 1 - \mathbb{P}\left[h_{u_k^*} < \frac{T r_{u_k^*}^{a_\ell}}{G_0 P_k} (\sigma^2 + I) \right]. \tag{3.12}$$

where $h_{u_k^*}$ is a gamma distributed random variable with parameter ν_ℓ. To overcome the difficulty on Nakagami fading, Alzer's Lemma [170] on the ccdf of a gamma random variable with integer parameter can be applied. This relates the cdf of a gamma random variable into a weighted sum of the cdfd of exponential random variables. Hence, we can bound expression (3.12) as

$$\begin{aligned} \mathcal{P}_k^*\left(T \mid \ell,\, r_{u_k^*}\right) &< 1 - \mathbb{E}_{\boldsymbol{r},I}\left[\left(1 - \exp\left(-\frac{\eta_\ell T r_{u_k^*}^{a_\ell}}{G_0 P_k} (\sigma^2 + I) \right) \right)^{\nu_\ell} \right] \\ &= \sum_{\xi=1}^{\nu_\ell} (-1)^{\xi+1} \binom{\nu_\ell}{\xi} \mathbb{E}_I\left[\exp\left(-\frac{\eta_\ell \xi T r_{u_k^*}^{a_\ell}}{G_0 P_k} (\sigma^2 + I) \right) \right], \end{aligned} \tag{3.13}$$

where expression (3.13) is derived with the use of Alzer's Lemma [170] and $\eta_\ell = \nu_\ell(\nu_\ell!)^{-1/\nu_\ell}$. Leveraging tools from stochastic geometry, namely the superposition theorem and the thinning theorem (see Section 2.4.2), the aggregate interference observed by the user can be described as

$$I = \sum_{i=1}^{K} \sum_{G} \sum_{\ell} I_i(v \mid G, \ell),$$

where $I_i(v \mid G, \ell)$ represents the interference caused by the BSs that are in $\ell \in \{\mathrm{L}, \mathrm{N}\}$ with the user, have link gain $G \in \{Q^2, Qq, q^2\}$ and belong in the i-th tier. Hence, the expression (3.13) can be re-written as

$$\mathcal{P}_k^*\left(T|\ell,\, r_{u_k^*}\right) < \sum_{\xi=1}^{\nu_\ell} (-1)^{\xi+1} \binom{\nu_\ell}{\xi} \prod_{i=1}^{K} \prod_{G} \prod_{\ell} \mathbb{E}_{I_i}\left[\exp\left(-s_\ell \left(\sigma^2 + I_i(v|G, \ell) \right) \right) \right], \tag{3.14}$$

It can be easily observed that, each expectation forms the Laplace transform of the associated sub-PPP (Section 2.4.2), $\mathcal{L}_{I_i}(s_\ell \mid G, \ell)$ where $s_\ell = \frac{\eta_\ell \xi T r_{u_k^*}^{a_\ell}}{G_0 P_k}$ and each of these

Laplace transforms are multiplied together. Therefore, (3.14) can be rewritten as,

$$\mathcal{P}_k^*(T \mid \ell,\ r_{u_k^*}) < \sum_{\xi=1}^{\nu_\ell} (-1)^{\xi+1} \binom{\nu_\ell}{\xi} \exp\left(-s_\ell \sigma^2\right) \prod_{i=1}^{K} \prod_{G} \prod_{\ell} \mathcal{L}_{I_i}(s_\ell \mid G, \ell), \tag{3.15}$$

Using stochastic geometry tools, and specifically the probability generating functional of a PPP (see Section 2.4.2), we can analytically represent the Laplace transform for the interference I_i of the associated sub-PPP as

$$\mathcal{L}_{I_i}(s_\ell \mid G, \ell) = \exp\left(-p_G \int_{r_{u_i^*}}^{\infty} \left(1 - \mathbb{E}_h\left[\exp\left(-s_\ell G P_i h v^{-a_\ell}\right)\right]\right) \lambda_i^{\Pi}(v \mid \ell) dv\right), \tag{3.16}$$

where for the considered pre-selection policy $\Pi \in \{\text{CS,SS,RS}\}$, $\lambda_i^{\Pi}(v \mid \ell)$ denotes the density of the BSs of which the link with the user is in a status ℓ and $\mathbb{E}_h[\exp(-xh)]$ corresponds to the moment generating functional of the gamma random variable h with integer parameter ν, and is given by $(1+x)^{-\nu}$. Thus, the Laplace interference function of the associated sub-PPP is given as

$$\mathcal{L}_{I_i}(s_\ell \mid G, \ell) = \exp\left(-p_G \int_{r_{u_i^*}}^{\infty} \left(1 - \left(1 + \frac{s_\ell G P_i v^{-a_\ell}}{\nu_\ell}\right)^{-\nu_\ell}\right) \lambda_i^{\Pi}(v \mid \ell) dv\right). \tag{3.17}$$

Thus, the Laplace transform of interference function, is given by

$$\mathcal{L}_I(s_\ell) = \prod_{i=1}^{K} \prod_{\ell} \prod_{G} \mathcal{L}_{I_i}(s_\ell \mid G, \ell). \tag{3.18}$$

Finally, by substituting the Laplace interference function, into the conditional coverage probability expression (3.15); and by un-conditioning the derived expression using the joint distance distribution (3.9), we conclude to the final expression. □

The above expression provides a general result for the coverage probability when the CS policy is applied. Even from this general expression, we can extract some observations towards its behavior. Initially, we can easily observe that by increasing the Nakagami parameter ν_L, the fading becomes less severe providing a better performance. Moreover, it is clear that by increasing the number of tiers, we can further boost the network performance due to the increase in diversity. In order to gain more insight into the network's performance, we make some additional assumptions in order to further simplify the above expression. Firstly, we assume that the interfering links do not experience any fading. This assumption is based on the fact that small-scale fading has a relatively minor impact in mmWave cellular networks [54]. Also, based on the nature of a mmWave signal, we assume a highly directional beam

pattern with high main-lobe gain i.e., $Q \to \infty$. Finally, we consider the case of an ultra-dense deployment of the BSs. We consider the two extreme cases that provide the bounds of the network performance: *i*) Lower bound: all BSs are in NLoS with the user ($\beta \to \infty$) and *ii*) Upper bound: all BSs are in LoS with the user ($\beta \to 0$). Then, from these assumptions, we can state the following.

Remark: In an ultra-dense network, the coverage probability for the CS policy is given by

$$\mathcal{P}^*(T) < 1 - \prod_{k=1}^{K} \left(1 - \sum_{\xi=1}^{\nu_\ell} \frac{(-1)^{\xi+1}\binom{\nu_\ell}{\xi}}{1 + \eta_\ell \xi T \frac{m^2}{G_0} \Gamma\left[1 - \frac{2}{a_\ell}\right] \frac{\sum_{i=1}^{K} \lambda_i P_i^{\frac{2}{a_\ell}}}{\lambda_k P_k}}\right), \tag{3.19}$$

where $\ell = \mathrm{N}$ for $\beta \to \infty$, $\ell = \mathrm{L}$ for $\beta \to 0$ and $\eta_\ell = \nu_\ell(\nu_\ell!)^{-1/\nu_\ell}$.

Proof. For the case where $\beta \to 0$, the interference at the user is caused only by the side-lobes of the BSs (since $Q \to \infty$) and so the gain of the interfering links is q^2 and $p_{q^2} = 1$, $p_{Q^2} = p_{Qq} = 0$. Then, as we assume the interfering links do not experience fading, the Laplace transform in (3.16) can be written as

$$\mathcal{L}_{I_i}(s_{\mathrm{L}} \mid q^2, \mathrm{L}) = \exp\left(-\int_{r_{u_i^*}}^{\infty} \left(1 - \exp\left(-\frac{s_L q^2 P_i}{v^{a_{\mathrm{L}}}}\right)\right) \lambda_i^{\mathrm{CS}}(v \mid \mathrm{L})\, dv\right), \tag{3.20}$$

Now, for the case $\beta \to 0$, we have $\lambda_i^{\mathrm{CS}}(r \mid \mathrm{L}) = 2\pi\lambda_i r$ and so (3.20) is simplified to

$$\mathcal{L}_{I_i}(s_{\mathrm{L}}|q^2, \mathrm{L}) = \exp\left(\pi\lambda_i \left(r_{u_i^*}^2 + \frac{2}{a_{\mathrm{L}}}(q^2 P_i s_{\mathrm{L}})^{\frac{2}{a_{\mathrm{L}}}} \left(\Gamma\left[-\frac{2}{a_{\mathrm{L}}}\right] - \Gamma\left[-\frac{2}{a_{\mathrm{L}}}, \frac{s_{\mathrm{L}} q^2}{P_i^{-1} r_{u_i^*}^{a_{\mathrm{L}}}}\right]\right)\right)\right), \tag{3.21}$$

where $s_{\mathrm{L}} = \frac{\eta_{\mathrm{L}} \xi T r_{u_k^*}^{a_{\mathrm{L}}}}{G_0 P_k}$, $\eta_\ell = \nu_\ell(\nu_\ell!)^{-1/\nu_\ell}$ and (3.21) follows from [171, 3.326.3]. Then, as the network is ultra-dense, we can assume that the interference-free area around the user is negligible i.e., $r_{u_i^*} \to 0$. Hence, (3.21) can by further simplified to

$$\mathcal{L}_{I_i}(s_{\mathrm{L}} \mid q^2, \mathrm{L}) = \exp\left(-\pi(q^2 P_i s_{\mathrm{L}})^{\frac{2}{a_{\mathrm{L}}}} \lambda_i \Gamma\left[1 - \frac{2}{a_{\mathrm{L}}}\right]\right), \tag{3.22}$$

which follows from the identities $\Gamma[1-a] = -a\Gamma[-a]$ and $\lim_{x\to\infty} \Gamma[a, x] \to 0$. Thus, by substituting the above expression to (3.10), (3.19) follows from [171, 3.326.2]. By following similar steps, we can derive the network performance for the case where $\beta \to \infty$. □

From (3.19) we can easily obtain the same observations as before regarding the number of tiers and the Nakagami parameter. However, from this simplified expression, we can also deduce that the achieved coverage performance increases with the

transmit power of BSs P_k, $k \in \{1, ..., K\}$ until a certain point. By further increasing the transmit power, the ratio $\frac{\sum_{i=1}^{K} P_i^{2/a_L}}{P_k} \to 1$, thus the network performance converges to a constant floor. This observation is due to the increasing interfering power faced by the user which equalizes the desired received signal.

3.4.2 SS policy

We now consider the case where the SS policy is employed. Let $\Psi_k = \left\{ \begin{matrix} r_{u_k^*}^{a\left(r_{u_k^*}\right)} \\ \frac{r_{u_k^*}^{a\left(r_{u_k^*}\right)}}{P_k, u_k^*} \end{matrix} \in \Phi_k \right\}, k \in \{1, \ldots, K\}$, denote the normalized path-loss between each BS in Φ_k and its associated user and let $\gamma_k = r_{u_k}^{a\left(r_{u_k}\right)}/P_k$ be the elements of Ψ_k. The normalized path-loss between the user and its pre-selected BS from tier k is given by γ_k^*. Let $\boldsymbol{\gamma} = (\gamma_1^*, \ldots, \gamma_K^*)$, then by the mapping theorem (See Section 2.4.2), Ψ_k is a PPP with density $\lambda_k(\gamma)$ and joint distribution $f_\Psi(\boldsymbol{\gamma})$ which are given in the following lemma.

Lemma 3.2. *When the SS policy is employed, the density of the tier i is given by*

$$\lambda_i^{\mathrm{SS}}(\gamma \mid \mathrm{L}) = \frac{2\pi\lambda_i}{a_L} P_i^{\frac{2}{a_L}} \gamma^{\frac{2}{a_L}-1} \exp\left(-\beta(P_i\gamma)^{\frac{1}{a_L}}\right) \text{ and} \tag{3.23}$$

$$\lambda_i^{\mathrm{SS}}(\gamma \mid \mathrm{N}) = \frac{2\pi\lambda_i}{a_N} P_i^{\frac{2}{a_N}} \gamma^{\frac{2}{a_N}-1} \left(1 - \exp\left(-\beta(P_i\gamma)^{\frac{1}{a_N}}\right)\right), \tag{3.24}$$

and the joint distance distributions between the user and its pre-selected BSs are given by

$$\begin{aligned} f_\Psi^{\mathrm{SS}}(\boldsymbol{\gamma} \mid \mathrm{L}) = &\prod_{i=1}^{K} \frac{2\pi\lambda_i}{a_L} P_i^{\frac{2}{a_L}} (\gamma_i^*)^{\frac{2}{a_L}-1} \exp\left(-\beta(P_i\gamma_i^*)^{\frac{1}{a_L}}\right) \\ &\times \exp\left(-\frac{2\pi\lambda_i}{\beta^2}\left(1 - \exp\left(-\beta(P_i\gamma_i^*)^{\frac{1}{a_L}}\right)\left(1 + \beta(P_i\gamma_i^*)^{\frac{1}{a_L}}\right)\right)\right), \end{aligned} \tag{3.25}$$

$$\begin{aligned} f_\Psi^{\mathrm{SS}}(\boldsymbol{\gamma} \mid \mathrm{N}) = &\prod_{i=1}^{K} \frac{2\pi\lambda_i}{a_N} P_i^{\frac{2}{a_N}} (\gamma_i^*)^{\frac{2}{a_N}-1} \left(1 - \exp\left(-\beta(P_i\gamma_i^*)^{\frac{1}{a_N}}\right)\right) \\ &\times \exp\left(-\pi\lambda_i(P_i\gamma_i^*)^{\frac{1}{a_N}} - \frac{2\pi\lambda_i}{\beta^2}\left(1 - \exp\left(-\beta(P_i\gamma_i^*)^{\frac{1}{a_N}}\right)\left(1 + \beta(P_i\gamma_i^*)^{\frac{1}{a_N}}\right)\right)\right). \end{aligned} \tag{3.26}$$

Proof. The process $\Psi = \cup_{k=1}^{K} \Psi_k$ is a non-homogeneous PPP with density $\lambda(\gamma) = \sum_{k=1}^{K} \lambda_k(\gamma)$. Using the transformation $r = (\gamma P_k)^{1/a_L}$ and the mapping theorem, the intensity measure of each network tier $k \in \{1, \ldots, K\}$ for LoS and NLoS BSs are given by

$$\begin{aligned} \Lambda_k\left([0, (\gamma P_k)^{1/a_L}] \mid \mathrm{L}\right) &= \int_0^{(\gamma P_k)^{1/a_L}} 2\pi\lambda_k x \exp(-\beta x) dx \\ &= \frac{2\pi\lambda_k}{\beta^2}\left(1 - \exp\left(-\beta(\gamma P_k)^{1/a_L}\right)\left(1 + \beta(\gamma P_k)^{1/a_L}\right)\right), \end{aligned}$$

and

$$\Lambda_k\left([0,(\gamma P_k)^{1/a_{\mathrm{N}}}]\mid \mathrm{N}\right) = \int_0^{(\gamma P_k)^{1/a_{\mathrm{N}}}} 2\pi\lambda_k x(1-\exp(-\beta x))dx$$
$$= \pi\lambda_k(\gamma P_k)^{\frac{1}{a_{\mathrm{N}}}} - \frac{2\pi\lambda_k}{\beta^2}\left(1-\exp\left(-\beta(\gamma P_k)^{\frac{1}{a_{\mathrm{N}}}}\right)\left(1+\beta(\gamma P_k)^{\frac{1}{a_{\mathrm{N}}}}\right)\right),$$

respectively. Then, $\lambda_k((\gamma P_k)^{\frac{1}{a_\ell}}|\ell) = d\Lambda_k\left([0,(\gamma P_k)^{\frac{1}{a_\ell}}]|\ell\right)/d\gamma$ where $\ell \in \{\mathrm{L},\mathrm{N}\}$, gives the density of the BSs. Therefore, the distance distribution of the tier k is given by

$$f_{\Psi_k}((\gamma P_k)^{1/a_\ell}) = \lambda_k((\gamma P_k)^{1/a_\ell})\exp\left(-\Lambda_k[0,(\gamma P_k)^{1/a_\ell}]\right), \tag{3.27}$$

and the joint distance distribution is given by the product of the individual distance distributions due to the independence of the tiers. □

Following a similar methodology as for the CS policy, the Laplace transform for the interference I_i of the BSs that belong in network tier i, can be written as

$$\mathcal{L}_{I_i}(s\mid G,\ell) = \exp\left(-p_G\int_{\gamma_i^*}^{\infty}\left(1-\mathbb{E}_h\left[\exp\left(-s_\ell G h v^{-1}\right)\right]\right)\lambda_i^{\mathrm{SS}}(v\mid\ell)dv\right), \tag{3.28}$$

where $s_\ell = \frac{\eta_\ell \xi T \gamma_k^*}{G_0}$, $\eta_\ell = \nu_\ell(\nu_\ell!)^{-1/\nu_\ell}$ and $\lambda_i^{\mathrm{SS}}(v\mid\ell)$ denotes the density of the BSs of which the link with the user has status $\ell \in \{\mathrm{L},\mathrm{N}\}$. Now, using the moment-generating function (mgf) of the Gamma random variable h as before, the above expression is given by

$$\mathcal{L}_{I_i}(s\mid G,\ell) = \exp\left(-p_G\int_{\gamma_i^*}^{\infty}\left(1-\left(1+\frac{s_\ell G v^{-1}}{\nu_\ell}\right)^{-\nu_\ell}\right)\lambda_i^{\mathrm{SS}}(v\mid\ell)dv\right). \tag{3.29}$$

We can now state the following theorem which provides an the coverage probability achieved by the SS policy.

Theorem 3.2. *The coverage probability achieved when the SS policy is employed, is given by*

$$\mathcal{P}^*(T) < 1-\prod_{k=1}^{K}\left(1-\sum_{\xi=1}^{\nu_L}(-1)^{\xi+1}\binom{\nu_L}{\xi}\int_{0<\gamma_1^*<\gamma_2^*<\cdots<\infty}\cdots\int \exp\left(-s_L\sigma^2\right)\mathcal{L}_I(s_{\mathrm{L}})f_\Psi^{\mathrm{SS}}(\boldsymbol{\gamma}\mid\mathrm{L})d\boldsymbol{\gamma}\right.$$
$$\left.-\sum_{\xi=1}^{\nu_N}(-1)^{\xi+1}\binom{\nu_N}{\xi}\int_{0<\gamma_1^*<\gamma_2^*<\cdots<\infty}\cdots\int \exp\left(-s_N\sigma^2\right)\mathcal{L}_I(s_{\mathrm{N}})f_\Psi^{\mathrm{SS}}(\boldsymbol{\gamma}\mid\mathrm{N})d\boldsymbol{\gamma}\right), \tag{3.30}$$

where $f_\Psi^{\mathrm{SS}}(\boldsymbol{\gamma}\mid\mathrm{L})$ *and* $f_\Psi^{\mathrm{SS}}(\boldsymbol{\gamma}\mid\mathrm{N})$ *are given by* (3.25) *and* (3.26)*, respectively,*

$$\mathcal{L}_I(s_{\mathrm{L}}) = \prod_{i=1}^{K}\prod_{\ell}\prod_{G}\exp\left(-p_G\int_{\gamma_i^*}^{\infty}\left(1-\left(1+\frac{s_L G v^{-1}}{\nu_\ell}\right)^{-\nu_\ell}\right)\lambda_i^{\mathrm{SS}}(v\mid\ell)dv\right), \tag{3.31}$$

and

$$\mathcal{L}_I(s_{\mathrm{N}}) = \prod_{i=1}^{K} \prod_{\ell} \prod_{G} \exp\left(-p_G \int_{\gamma_i^*}^{\infty} \left(1 - \left(1 + \frac{s_N G v^{-1}}{\nu_\ell} \right)^{-\nu_\ell} \right) \lambda_i^{\mathrm{SS}}(v \mid \ell) dv \right), \tag{3.32}$$

where $G \in \{Q^2, Qq, q^2\}$, $\ell \in \{L, N\}$, $s_\ell = \frac{\eta_\ell \xi T \gamma_k^*}{G_0}$, $\eta_\ell = \nu_\ell (\nu_{\ell!})^{-1/\nu_\ell}$ *and* $\lambda_i^{\mathrm{SS}}(v \mid \ell)$ *is given by Lemma 3.2.*

Proof. The proof follows similar methodology as previously described for the CS scenario, but using the Laplace transform of interference function obtained by the multiplication of the associated sub-PPPs that are given by the expression in (3.29). □

The expression in (3.30) provides a general result for the coverage probability when the SS policy is applied. Even from this general expression, we can extract some observations towards its behavior. We can easily observe the positive impact of the number of network tiers and the Nakagami parameter on the network's coverage probability. In order to gain more insight into the network's performance, we make similar assumptions as with the case of CS policy in order to further simplify the above expression. We consider the two extreme cases that provide the bounds of the network performance: *i*) Lower bound: all BSs are in NLoS with the user ($\beta \to \infty$) and *ii*) Upper bound: all BSs are in LoS with the user ($\beta \to 0$). Then, from these assumptions, we can state the following.

Remark: In an ultra-dense network, the coverage probability for the SS policy is given by

$$\begin{aligned} \mathcal{P}^*(T) < 1 - \prod_{k=1}^{K} \Bigg(1 - \sum_{\xi=1}^{\nu_\ell} (-1)^{\xi+1} \binom{\nu_\ell}{\xi} \\ \times \int_0^{\infty} \cdots \int_0^{\infty} \prod_{k=1}^{K} \exp\left(-\pi \lambda_i \left(\frac{\eta_\ell \xi T P_i q^2}{\gamma_i^* G_0} \right)^{\frac{2}{a_\ell}} \Gamma\left[1 - \frac{2}{a_\ell} \right] \right) f_{\Psi}^{\mathrm{SS}}(\boldsymbol{\gamma} \mid \ell) d\boldsymbol{\gamma} \Bigg), \end{aligned} \tag{3.33}$$

where $\ell = \mathrm{N}$ for $\beta \to \infty$, $\ell = \mathrm{L}$ for $\beta \to 0$ and $\eta_\ell = \nu_\ell (\nu_\ell!)^{-1/\nu_\ell}$.

Proof. The proof follows similar steps as for the Remark 3.4.1. □

From (3.33), we can easily the same observations as before regarding the number of tiers and the Nakagami parameter. However, from this simplified expression, we can also deduce that the coverage threshold is inversely proportional to the network performance.

Aiming to measure the reliability of the wireless communication scheme under fading, we study the achieved diversity by employing the SS policy. The standard definition of the diversity is based on the high SINR analysis. For the special case where the Nakagami-m parameters for both LoS and NLoS communication links are assumed equal to $\nu_{\mathrm{L}} = \nu_{\mathrm{N}} = 1$, in the following Remark we derive the diversity order by considering the SS pre-selection policy for the special case where Rayleigh fading is adopted.

Diversity Gain The numerator of (3.4) is an independent exponentially distributed random variable with probability density function $\xi_k \exp(-\xi_k x)$, $x \geq 0$ with $\xi_k = \frac{1}{G_0 \gamma_k^*}$. By letting $I' = I + \sigma^2$, the outage probability is given by

$$\mathbb{P}\left[\mathrm{SINR}^* < T\right] = \prod_{k=1}^{K} \mathbb{P}[\mathrm{SINR}_k < T] = \prod_{k=1}^{K} \mathbb{P}\left[G_0 \gamma_k^* h_{\gamma_k^*} < TI'\right]$$
$$= \prod_{k=1}^{K} \mathbb{E}_{\gamma_{k'}^*, I'}\left[\int_0^{TI'} \xi_k \exp(-\xi_k x)\, dx\right] = T^K \prod_{k=1}^{K} \mathbb{E}_{\gamma_{k'}^*, I'}\left[I' \int_0^1 \xi_k \exp(-\xi_k TI' z)\, dz\right], \quad (3.34)$$

which follows from the change of variable $x = TI'z$. At the high coverage regime i.e., $T \to 0$, we have

$$I' \int_0^1 \xi_k \exp(-\xi_k TI' z)\, dz \sim I' \int_0^1 \xi_k dz.$$

As a result,

$$\mathbb{P}\left[\mathrm{SINR}^* < T\right] \approx T^K \prod_{k=1}^{K} \mathbb{E}_{\gamma_{k'}^*, I'}\left[I' \xi_k\right]. \quad (3.35)$$

By substituting (3.35) into the expression for diversity order of interference-limited networks, we have

$$\lim_{T \to 0} \frac{\log\left(1 - \mathcal{P}^*(T)\right)}{\log(T)} = \lim_{T \to 0} \left(\frac{\log T^K}{\log T} + \frac{\log\left(\prod_{k=1}^{K} \mathbb{E}_{\gamma_{k'}^*, I'}\left[I' \xi_k\right]\right)}{\log T} \right) = K, \quad (3.36)$$

due to the fact that the second term of the equation for $T \to 0$ converges to zero. As a result, the diversity order of the proposed scheme when the user employs the SS policy, is equal to K.

3.4.3 RS policy

The RS scheme randomly pre-selects a BS among the ones located within a disk of radius R around the user. The user is in outage when the disk is empty or when the

selected BS cannot support the target SINR threshold. By considering these events, the coverage probability is given by the following theorem.

Lemma 3.3. *When the RS policy is employed, the density of the tier i is given by*

$$\lambda_i^{\mathrm{RS}}(r \mid \mathrm{L}) = 2\pi\lambda_i r \exp\left(-\beta r\right) \;\; \textit{and} \;\; \lambda_i^{\mathrm{RS}}(r \mid \mathrm{N}) = 2\pi\lambda_i r \left(1 - \exp\left(-\beta r\right)\right), \; r \leq R,$$

and the joint distance distributions between the user and its pre-selected BSs, are given by

$$f_{\Phi}^{\mathrm{RS}}(\boldsymbol{r} \mid \mathrm{L}) = \left(\frac{2}{R^2}\right)^K \prod_{i=1}^{K} r_{u_i^*} \exp\left(-\beta r_{u_i^*}\right), \tag{3.37}$$

$$f_{\Phi}^{\mathrm{RS}}(\boldsymbol{r} \mid \mathrm{N}) = \left(\frac{2}{R^2}\right)^K \prod_{i=1}^{K} r_{u_i^*} \left(1 - \exp\left(-\beta r_{u_i^*}\right)\right). \tag{3.38}$$

Proof. The BSs that belong in the disk of radius R around the user, are uniformly distributed, thus creating a Mattern cluster process [46]. The density function of those points is given by $f(r) = \frac{2r}{R^2}$ and the result follows. □

Theorem 3.3. *The coverage probability achieved when the RS policy is employed, is given by*

$$\begin{aligned}
\mathcal{P}^*(T) <& 1 - \prod_{k=1}^{K} \Bigg(\exp\left(-\lambda_k \pi R^2\right) + \left(1 - \exp\left(-\lambda_k \pi R^2\right)\right) \Bigg(1 \\
&- \sum_{\xi=1}^{\nu_L} (-1)^{\xi+1} \binom{\nu_L}{\xi} \int_{0<r_{u_1^*}<r_{u_2^*}<\cdots<\infty} \cdots \int \exp\left(-s_L \sigma^2\right) \mathcal{L}_I(s_{\mathrm{L}}) f_{\Phi}^{\mathrm{RS}}(\boldsymbol{r} \mid \mathrm{L}) d\boldsymbol{r} \\
&- \sum_{\xi=1}^{\nu_N} (-1)^{\xi+1} \binom{\nu_N}{\xi} \int_{0<r_{u_1^*}<r_{u_2^*}<\cdots<\infty} \cdots \int \exp\left(-s_N \sigma^2\right) \mathcal{L}_I(s_{\mathrm{N}}) f_{\Phi}^{\mathrm{RS}}(\boldsymbol{r} \mid \mathrm{N}) d\boldsymbol{r} \Bigg) \Bigg),
\end{aligned} \tag{3.39}$$

where $f_{\Phi}^{\mathrm{RS}}(\boldsymbol{r} \mid \mathrm{L})$ and $f_{\Phi}^{\mathrm{RS}}(\boldsymbol{r} \mid \mathrm{N})$ are given by (3.37) *and* (3.38)*, respectively,*

$$\mathcal{L}_I(s_{\mathrm{L}}) = \prod_{i=1}^{K} \prod_{\ell} \prod_{G} \exp\left(-p_G \int_{r_{u_k^*}}^{\infty} \left(1 - \left(1 + \frac{s_L G P_i v^{-a_L}}{\nu_\ell}\right)^{-\nu_\ell}\right) \lambda_i^{\mathrm{RS}}(v \mid \ell) dv \right), \tag{3.40}$$

and

$$\mathcal{L}_I(s_{\mathrm{N}}) = \prod_{i=1}^{K} \prod_{\ell} \prod_{G} \exp\left(- \int_{r_{u_k^*}}^{\infty} \left(1 - \left(1 + \frac{s_N G P_i v^{-a_N}}{\nu_\ell}\right)^{-\nu_\ell}\right) \lambda_i^{\mathrm{RS}}(v \mid \ell) dv \right), \tag{3.41}$$

where $G \in \{Q^2, Qq, q^2\}$, $s_\ell = \frac{\eta_\ell \xi T \gamma_k^*}{G_0}$, $\ell \in \{L, N\}$, $\eta_\ell = \nu_\ell (\nu_\ell!)^{-1/\nu_\ell}$ and $\lambda_i^{\mathrm{RS}}(v \mid \ell)$ is given by Lemma 3.3.

Proof. The proof follows the same methodology as previously described for the CS and SS policies, but with the density and joint distribution functions that correspond to the RS policy. Furthermore, the case where the disk of radius R is empty needs to be consider, so the probability of this event occurring is given by $\exp\left(-\lambda_k \pi R^2\right)$ [46]. □

3.5 Successive Interference Cancellation

In this section, we discuss the additional achieved gains on the network performance, by exploiting the ability of the users to perform SIC. Even though SIC is characterized by high computational demand, its application is considered as a special case aiming for the further boost of the network performance. In order to maintain the complexity at a lower level, we assume that the small-scale fading between the user and its associated BS is modeled as Rayleigh fading. Thus, we assume that the Nakagami-m parameters for LoS and NLoS communication links fulfill the expression $\nu_{\mathrm{L}} = \nu_{\mathrm{N}} = 1$. The main idea of SIC is to decode the dominant interference signals and subtract them from the received signal, resulting in an increase of the observed SINR. We assume that each user has the ability to implement an ideal SIC in accordance to [101]. However, extra decoding latency, proportional to the number of canceled signals, is incurred for the entire SIC process. Therefore, the number of interferers that can be canceled is assumed to be limited to $N \in \mathbb{N}$ in order to keep both the computational complexity and power consumption at low levels.

At the beginning, the user attempts to decode the received signal without any interference cancellation. If this attempt is unsuccessful, the user seeks to decode the dominant interfering signal, subtract it from the received signal, and then re-attempt to decode the resulting received signal. We assume that the order statistics of the received interfering signal power do not depend on the fading and are determined by the distances [166]. The received signal power at the user can be ordered as $\{X_{(1)}, X_{(2)}, \dots\}$ such that $X_{(i)} \geq X_{(j)}$, with $i \leq j$ where $X_{(j)}$ represent the received signal from the j-th strongest interfering BS. The previous actions are repeated up to N times until the received signal is decoded, while satisfying the constraint on the maximum number of cancellations; otherwise, the user is considered to be in outage. Hence, the transmission is successful as long as one of the following events is successful

$$
\begin{aligned}
&0 : (\mathrm{SINR}(0) \geq T) \\
&1 : (\mathrm{SINR}(0) < T) \bigcap \left(\frac{X_{(1)}}{I^{(1)} + \sigma^2} \geq T \right) \bigcap (\mathrm{SINR}(1) \geq T) \\
&\quad \vdots \\
&N : \left(\bigcap_{n=0}^{N-1} \mathrm{SINR}(n) < T \right) \bigcap \left(\bigcap_{n=1}^{N} \frac{X_{(n)}}{I^{(n)} + \sigma^2} \geq T \right) \bigcap (\mathrm{SINR}(N) \geq T), \qquad (3.42)
\end{aligned}
$$

where $\mathrm{SINR}(n)$ represents the observed SINR from the user after the cancelation of

the n-th strongest interfering signals and $I^{(n)}$ represents the aggregate interference after the cancellation of the n-th strongest interfering BSs.

The first term in (3.42) represents the outage probability for decoding the received signal, when the user cancels $n-1$ interferers, while the third term denotes the success probability of decoding the received signal after n successful cancellations. Finally, the second term of (3.42) represents the event of successfully canceling the n-th interferer.

For the study of the Laplace transform of the partially canceled interference depending on the pre-selection policy, we state the following Lemma.

Lemma 3.4. *The Laplace transform of the partially canceled interference function $I^{(n)}$ is given by*

$$\mathcal{L}^{\mathrm{CS}}_{I^{(n)}}(s_{\mathrm{L}}) = \prod_{i=1}^{K} \prod_{G} \exp\left(-p_G \int_{R^*(n,k)}^{\infty} \frac{s_{\mathrm{L}} G P_i v^{-a_{\mathrm{L}}}}{1 + s_{\mathrm{L}} G P_i v^{-a_{\mathrm{L}}}} \lambda_i^{\mathrm{CS}}(v \mid \mathrm{L}) dv\right), \tag{3.43}$$

for the CS policy,

$$\mathcal{L}^{\mathrm{SS}}_{I^{(n)}}(s) = \prod_{i=1}^{K} \prod_{\ell} \prod_{G} \exp\left(-p_G \int_{V^*(n,k)}^{\infty} \frac{s G v^{-1}}{1 + s G v^{-1}} \lambda_i^{\mathrm{SS}}(v \mid \ell) dv\right), \tag{3.44}$$

for the SS policy,

$$\mathcal{L}^{\mathrm{RS}}_{I^{(n)}}(s) = \prod_{i=1}^{K} \prod_{\ell} \prod_{G} \exp\left(-p_G \int_{0}^{\infty} \frac{s G P_i v^{-a_\ell}}{1 + s G P_i v^{-a_\ell}} \lambda_i^{\mathrm{RS}}(v \mid \ell) dv\right), \tag{3.45}$$

for the RS policy, where $G \in \{Q^2, Qq, q^2\}$, $s = \{s_{\mathrm{L}}, s_{\mathrm{N}}\} = \{\frac{\eta_{\mathrm{L}} \xi T \gamma_k^*}{G_0}, \frac{\eta_{\mathrm{N}} \xi T \gamma_k^*}{G_0}\}$ takes values depending on whether the direct link is LoS and NLoS, respectively; $R^*(n,k) = \sqrt{\frac{n}{\lambda_k \pi}}$ represents the cancellation radius of the interference-free area around the user, which successfully canceled n interfering BSs from network tier k and $V^*(n,k) = \frac{R^*(n,k)^{a\left(r_{u_k^*}\right)}}{P_k}$ represents the normalised path loss of the cancellation radius.

Proof. The proof follows similar steps as in the proof of Remark 3.4.1, where in this case, we have different regions in which the interfering BSs exist. Specifically, the observed interference originates from BSs which are located outside the interference-free area around the user with cancellation radius $R^*(n,k)$. Hence, the lower limit of the integral of the Laplace transform is defined by the cancellation radius of the user. □

Firstly, we define the probability of successfully decoding the desired signal by the user, after cancelling the n interferers. Given that n interferers have been

canceled, the instantaneous coverage probability of the network tier k can be defined as in the following Lemma.

Lemma 3.5. *Given that n strongest interferers have been canceled, the successful coverage performance, is given by*

$$\mathcal{P}_{\mathcal{S}}(n,T) = 1 - \prod_{k=1}^{K}\Bigg(1 - \int_{0<r_{u_1^*}<r_{u_2^*}<\cdots<\infty}\cdots\int \exp\left(-s\sigma^2\right)\mathcal{L}^{\Pi}_{I^{(n)}}(s_{\mathrm{L}})f^{\Pi}_{\Phi}(\boldsymbol{r}\mid \mathrm{L})d\boldsymbol{r} - \int_{0<r_{u_1^*}<r_{u_2^*}<\cdots<\infty}\cdots\int \exp\left(-s\sigma^2\right)\mathcal{L}^{\Pi}_{I^{(n)}}(s_{\mathrm{N}})f^{\Pi}_{\Phi}(\boldsymbol{r}\mid \mathrm{N})d\boldsymbol{r}\Bigg), \tag{3.46}$$

where $f^{\Pi}_{\Phi}(\boldsymbol{r}\mid \ell)$ is analysed in Lemma 3.2 and it depends on the pre-selection policy $\Pi \in \{CS, SS, RS\}$ and the link status $\ell \in \{L, N\}$, $s_{\mathrm{L}} = \frac{\eta_{\mathrm{L}}\xi T\gamma_k^*}{G_0}$, $s_{\mathrm{N}} = \frac{\eta_{\mathrm{N}}\xi T\gamma_k^*}{G_0}$ and the expressions of $\infty L^{\Pi}_{I^{(n)}}(s_{\mathrm{L}})$ and $\mathcal{L}^{\Pi}_{I^{(n)}}(s_{\mathrm{N}})$ are given by Lemma 3.4 depending on the adopted pre-selection policy.

Proof. We define the instantaneous success probability for the network tier k after successfully canceling n interferers as

$$\begin{aligned}\mathcal{P}_{\mathcal{S}}(n,k,T) &= \mathbb{P}\left[\mathrm{SINR}_k(n) > T\left(I^{(n)}+\sigma^2\right)\right] = \mathbb{P}\left[P_k G_{u_k^*} h_{u_k^*} r_{u_k^*}^{-a\left(r_{u_k^*}\right)} > T\left(I^{(n)}+\sigma^2\right)\right] \\ &= \mathbb{P}\left[h_{u_k^*} > \frac{T r_{u_k^*}^{a\left(r_{u_k^*}\right)}}{P_k G_{u_k^*}}\left(I^{(n)}+\sigma^2\right)\right] = \mathbb{E}_{\boldsymbol{r}}\left[\mathcal{L}_{I^{(n)}}(s)\exp\left(-s\sigma^2\right)\right],\end{aligned} \tag{3.47}$$

which follows from the fact that $h_{u_k^*}$ is an exponentially distributed random variable, hence $P_k G_{u_k^*} h_{u_k^*} r_{u_k^*}^{-a\left(r_{u_k^*}\right)}$ is exponentially distributed with mean $P_k G_{u_k^*} r_{u_k^*}^{-a\left(r_{u_k^*}\right)}$; (3.47) follows with the use of the Laplace transform of $I^{(n)}$ that takes values according to Lemma 3.4. To find the unconditional success probability, we take the expectation over r_k^* and by using the proposed BSS technique, we conclude to (3.46). □

In the following discussion, we derive the success probability of the user to decode and cancel the n-th strongest interferer, with the assumption that the interference for the $n-1$ strongest interfering BSs has been previously canceled.

Lemma 3.6. *The coverage probability of a user attempting to decode the n-th strongest interfering signal, is given by*

$$\mathcal{P}_{\mathcal{S}}(n,T) = 1 - \prod_{k=1}^{K}\Bigg(1 - \int_{0<r_{u_1^*}<r_{u_2^*}<\cdots<\infty}\cdots\int \exp\left(-s\sigma^2\right)\mathcal{L}^{\Pi}_{I^{(n)}}(s_{\mathrm{L}})f_{\Phi}(\boldsymbol{r}, n\mid \mathrm{L})d\boldsymbol{r}$$

$$- \int_{0<r_{u_1^*}<r_{u_2^*}<\cdots<\infty} \cdots \int \exp\left(-s\sigma^2\right) \mathcal{L}^{\Pi}_{I^{(n)}}(s_{\mathrm{N}}) f_{\Phi}(\boldsymbol{r}, n \mid \mathrm{N}) d\boldsymbol{r}\Bigg), \tag{3.48}$$

where $s_{\mathrm{L}} = \frac{\eta_{\mathrm{L}} \xi T \gamma_k^*}{G_0}$, $s_{\mathrm{N}} = \frac{\eta_{\mathrm{N}} \xi T \gamma_k^*}{G_0}$; *the expressions of* $\mathcal{L}^{\Pi}_{I^{(n)}}(s_{\mathrm{L}})$ *and* $\mathcal{L}^{\Pi}_{I^{(n)}}(s_{\mathrm{N}})$ *are given by Lemma 3.4 depending on the adopted pre-selection policy and* $f_{\Phi}(\boldsymbol{r}, n \mid \mathrm{L})$ *and* $f_{\Phi}(\boldsymbol{r}, n \mid \mathrm{N})$ *denote the joint distance distribution between the user and the n-th nearest LoS and NLoS BS from the i-th tier, respectively, and are given by*

$$f_{\Phi}(\boldsymbol{r}, n \mid \mathrm{L}) = \prod_{i=1}^{K} \exp\left(-\Lambda_i(r_n \mid \mathrm{L})\right) \frac{\Lambda_i(r_n \mid \mathrm{L})^n}{n!}, \tag{3.49}$$

and

$$f_{\Phi}(\boldsymbol{r}, n \mid \mathrm{N}) = \prod_{i=1}^{K} \exp\left(-\Lambda_i(r_n \mid \mathrm{N})\right) \frac{\Lambda_i(r_n \mid \mathrm{N})^n}{n!}, \tag{3.50}$$

respectively, where $\Lambda_i(r_n \mid \mathrm{L})$ *and* $\Lambda_i(r_n \mid \mathrm{N})$ *represent the intensity measure of LoS and NLoS BSs in network tier i, respectively.*

Proof. After successfully decoding and subtracting $n-1$ signals from the received signal, the probability of successfully decoding the n-th interfering BS from network tier k, conditioned on its distance, r_n, can be written as

$$\mathcal{P}_{\mathcal{D}}(n, k, T \mid r_n) = \mathbb{P}\left[h_{r_n} > \frac{T\left(I^{(n)} + \sigma^2\right)}{G_0 P_k r_n^{-a(r_n)}}\right] = \exp(-s\sigma^2) \mathcal{L}^{\Pi}_{I^{(n)}}(s), \tag{3.51}$$

where $s = \{s_{\mathrm{L}},\ s_{\mathrm{N}}\} = \left\{\frac{\eta_{\mathrm{L}} \xi T \gamma_k^*}{G_0}, \frac{\eta_{\mathrm{N}} \xi T \gamma_k^*}{G_0}\right\}$ takes value depending on whether the direct link is LoS and NLoS, respectively and the value of $\mathcal{L}^{\Pi}_{I^{(n)}}(s)$ is given based on Lemma 3.4. To find the unconditional success probability, the expectation should be taken with respect to the distance of the n-th interferer with pdf that are given by expressions (3.49) and (3.50), depending on the link's status. Based on the density expressions for each pre-selection policy that are analyzed in Lemma 3.2, the intensity measure is equal to $\Lambda_i(r_n) = \int_0^{r_n} \lambda_i(u) du$. By using the proposed BSS scheme, we conclude to (3.48). □

Note that when $N = 0$ i.e., no interferers have been canceled, the achieved coverage performance with the use of the SIC scheme $\mathcal{P}_{\mathrm{SIC}}(T, N)$ is equal to the coverage probability when no SIC is applied, that is $\mathcal{P}_{\mathrm{SIC}}(T, 0) = \mathcal{P}^*(T)$. We now provide the coverage performance of a receiver with SIC capabilities. Based on the sequence of events in (3.42), the following theorem provides the overall coverage performance.

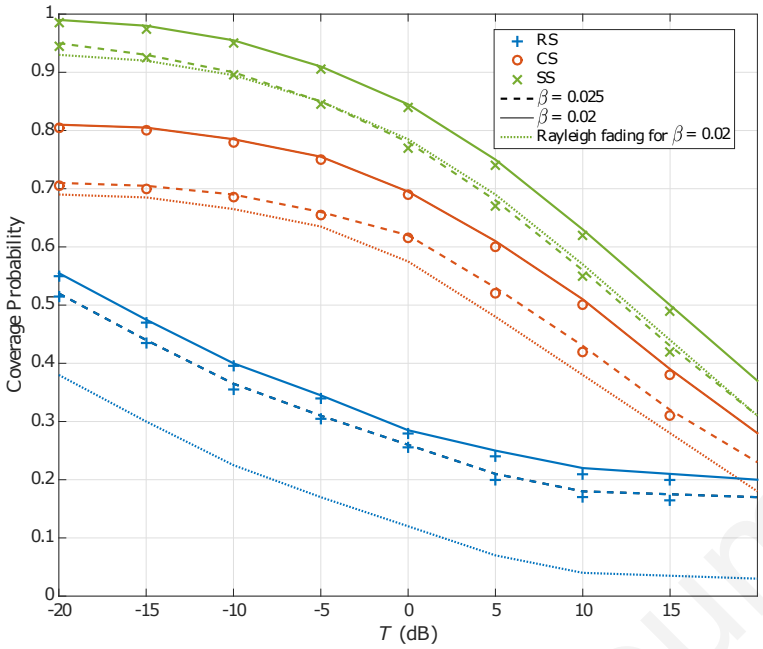

Figure 3.2: Coverage probability versus the threshold T for different values of blockage constant $\beta = \{0.02, 0.025\}$; the lines and markers represent the theoretical and simulation results, respectively.

Theorem 3.4. *The coverage performance $\mathcal{P}_{\text{SIC}}$ for a DL user with the ability to perform SIC to cancel a maximum of N interferers, is given by,*

$$\mathcal{P}_{\text{SIC}}(T,N) = \mathcal{P}^{*}(T) + \sum_{z=1}^{N}\left(\prod_{n=0}^{z-1}(1-\mathcal{P}_{\mathcal{S}}(n,T))\right)\left(\prod_{n=1}^{z}\mathcal{P}_{\mathcal{D}}(n,T)\right)\mathcal{P}_{\mathcal{S}}(z,T). \tag{3.52}$$

Proof. Since the success of SIC occurs as one of the steps described in (3.42), the proof follows directly from the definition of the sequence of events and the derivation of $\mathcal{P}_{\mathcal{S}}(n,T)$ and $\mathcal{P}_{\mathcal{D}}(n,T)$. □

3.6 Numerical Results

In this section, we provide numerical results to verify our model and illustrate the effectiveness and potential benefits of the proposed BSS scheme. We focus on the special case of a heterogeneous network with $K = 2$ tiers i.e., consisting of a macro-tier overlaid with a pico-tier. We assume that the BS density of the first and second tier is $\lambda_1 = 5 \times 10^{-5}$ and $\lambda_2 = 3\lambda_1$, respectively; the transmit power for each network tier is $P_1 = 40$ dB and $P_2 = 20$ dB, respectively. Furthermore, we assume that the non-negative blockage constant is $\beta = 0.02$. The noise power is set to $\sigma^2 = -70$ dB. The Nakagami fading parameters for LoS and NLoS links are set to $\nu_L = 4$ and

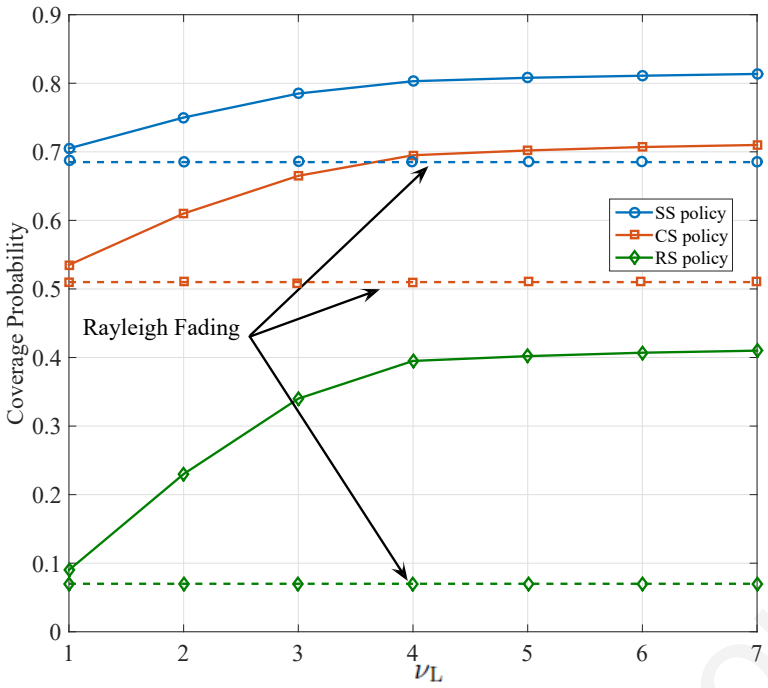

Figure 3.3: Coverage probability versus the Nakagami parameter ν_N for the pre-selection policies; $\nu_L = 2\nu_N$, $T = 5$ dB.

$\nu_N = 2$, while the path loss exponents are set to $a_L = 2$ and $a_N = 4$, respectively. The parameters for the sectorized antenna model are set to $Q = 10$ dB for the main lobe gain, $q = -10$ dB for side lobe gain and $\phi = \frac{\pi}{6}$ for the main lobe beamwidth [113].

Fig. 3.2 illustrates the effects of blockage/obstacles on the network performance for the proposed pre-selection policies. We can first observe that the analytical results provide an upper bound for the network performance given by the simulation results; this is expected due to Alzer's Lemma [170]. Furthermore, it is clear from the figure, that with the increase of blockage density there is a significant loss in coverage performance. This again is expected, since by increasing the blockage density, more and more links between the users and their associated BSs are in NLoS. Therefore, the probability that the user connects to a LoS BS is decreased so the signal at the user becomes weaker and the received SINR is reduced. Another important observation from this figure is that the SS policy achieves a significantly higher network performance, outperforming the other two policies.

In Fig. 3.3, the network coverage performance over Nakagami fading is plotted for all the pre-selection policies. For comparison reasons, the network performance over Rayleigh fading for each pre-selection policy is also displayed in the figure as a dashed line. Based on the figure, we observe that the increase of the Nakagami

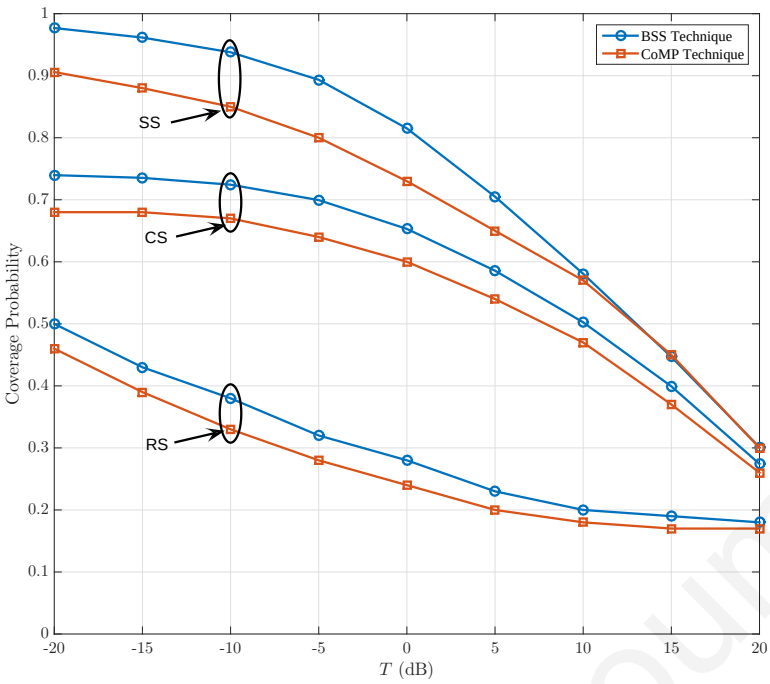

Figure 3.4: Coverage probability versus the threshold T for the BSS and CoMP schemes; $\beta = 0.025$.

parameter ν results in an increase of the coverage probability in all pre-selection policies. This observation can be explained by the fact that by increasing the quality of the communication link, users experience lower fading over their received signal, thus the network performance increase. Furthermore, it can be easily seen that, as $\nu_\ell \to \infty$, the network performance becomes independent of the Nakagami parameter. This was expected due to the fact that, while $\nu_\ell \to \infty$, the fading becomes a deterministic value centered on the mean. Finally, by comparing the achieved network performance between the cases of Nakagami and Rayleigh fading, we noticed that for low Nakagami parameters, the analysis of network performance with the latter case provides a lower bound of the first case. For this reason and for the rest of this chapter, we continue our analysis on the assumption that the attenuation between users and BSs is a Rayleigh fading.

Fig. 3.4 shows the network coverage performance of the proposed BSS technique compared to the conventional coordinated multipoint (CoMP) technique for each pre-selection policy [93]. CoMP technique allows multiple randomly distributed BSs to jointly transmit data to a user. On the other hand, by using BSS technique, each user is able to communicate with the BS that provides the maximum SINR and which belongs in the set of "candidate" BSs. Hence, in order to conduct a fair comparison between the CoMP technique and the BSS technique, we assume that

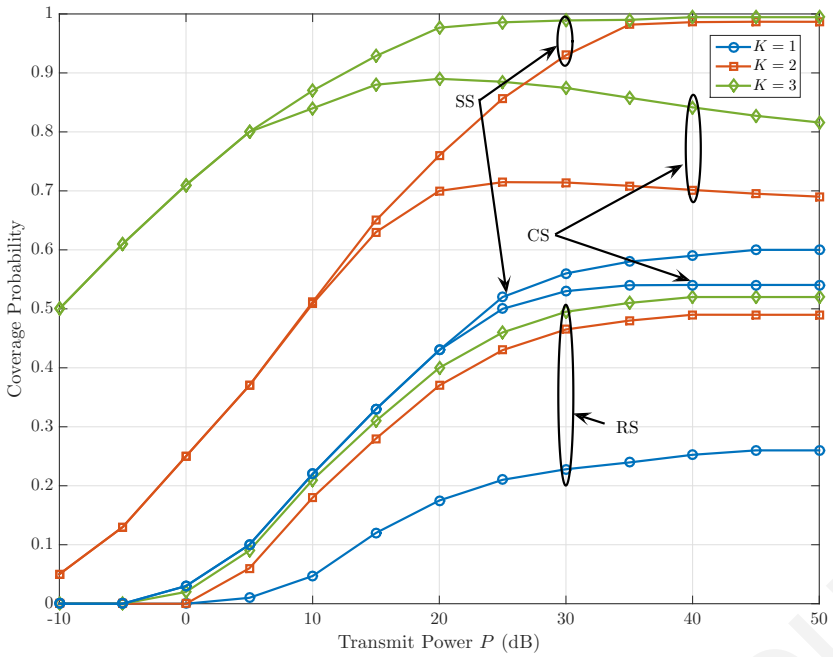

Figure 3.5: Coverage probability versus transmit power for different numbers of tiers; $\lambda_1 = 5 \times 10^{-5}$, $\lambda_2 = 3\lambda_1$, $\lambda_3 = 4\lambda_1$, $P_1 = 3P$ dB, $P_2 = 2P$ dB, $P_3 = P$ dB, and $T = 0$ dB.

the transmit power of the terminals that belong in the network tier k and employ CoMP technique, is equal to $P_k^{\text{CoMP}} = P_k/K$; this assumption ensures the same total transmit power of both techniques. As it can be seen, our proposed technique offers marginal coverage performance gains when compared to the CoMP technique with lower computational demands. Particularly, the selection of a single BS for the communication, opposed to the joint transmission of multiple BSs, reduces the existing interference and thus the network performance is increased.

Fig. 3.5 shows the impact of cooperation on the achieved coverage performance with respect to the BSs' transmit power for $K = \{1, 2, 3\}$. For the cases $K = 2$ and $K = 3$, we assume that the transmit power of the BSs in each tier is inversely proportional to the tier's density. Specifically, we assume $\lambda_1 < \lambda_2 < \lambda_3$ and so $P_1 > P_2 > P_3$. The first main observation is that as the number of network tier increases, the coverage performance improves. This observation has been expected, since as the number of network tier increases, the number of associated BSs with the users increases. As a result, the probability of a user to communicate with a BS that provides higher coverage performance is increased, thus the network performance improves. In addition, as it can be seen in Fig. 3.5, CS and SS schemes outperform the RS scheme independently of the transmit power value. In high and

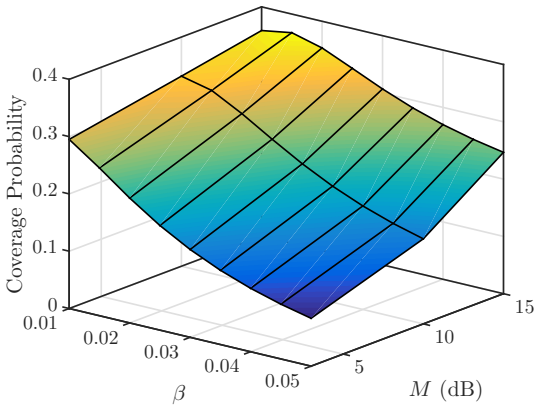

(a) RS user association policy

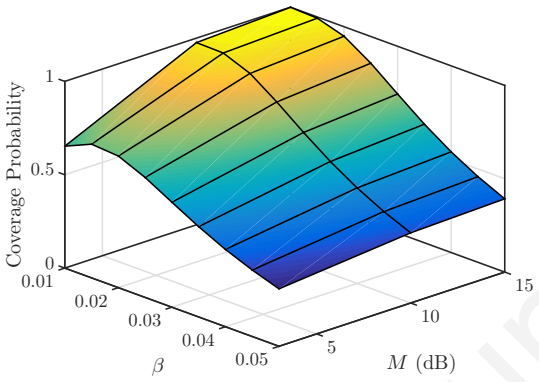

(b) CS user association policy

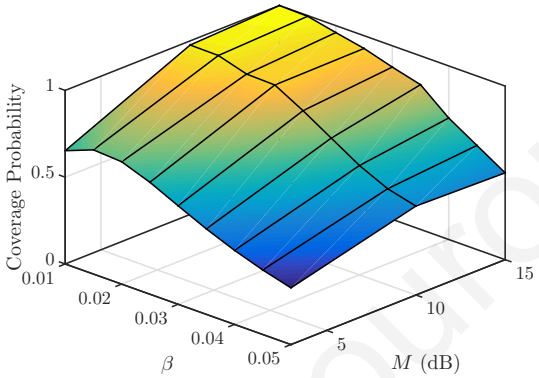

(c) SS user association policy

Figure 3.6: Coverage probability versus blockage constant and main lobe gain; $T = 0$ dB.

moderate transmit power values, the SS scheme outperforms the CS scheme, while in low transmit power values, their difference in terms of coverage performance is negligible. Additionally, it is clear from the plot that the coverage probability for all pre-selection policies converges to a constant value for high transmission powers. This behavior of coverage performance is based on the fact that as the transmission power of the network's nodes increases, the noise in the network becomes negligible.

Fig. 3.6 illustrates the importance of the deployment of sectorized antennas for mmWave networks in order to mitigate the negative effects caused by the blockages on the network performance. For each pre-selection policy, we plot the coverage probability versus the blockage constant and the main lobe gain of sectorized antennas. It can be easily observed that, as the blockage density increases, the network performance decreases independently from the adopted policy. As mentioned before, for high blockage densities, the communication of the users with LoS BSs becomes impossible and thus the coverage probability significantly decreases. In addition, by

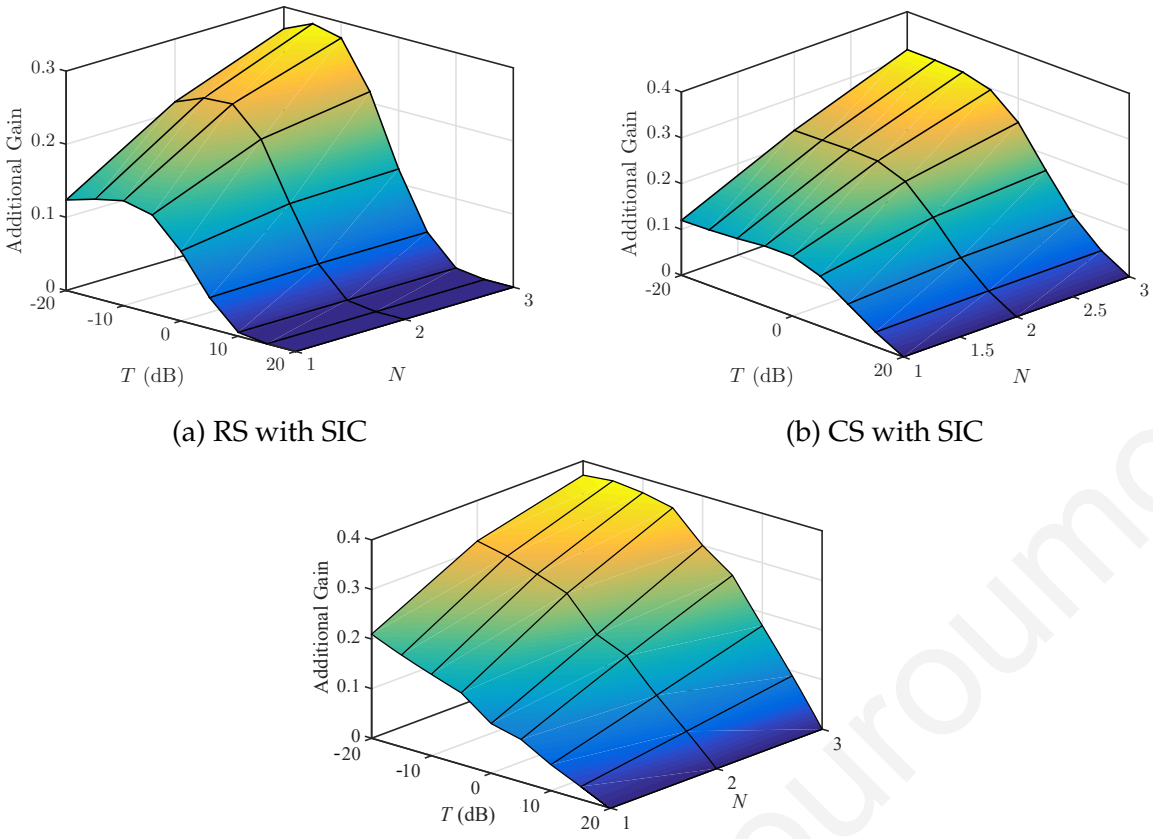

(a) RS with SIC

(b) CS with SIC

(c) SS with SIC

Figure 3.7: Additional gain versus SINR threshold and number of maximum interfering BS cancelations.

narrowing the antenna's main lobe beamwidth, the coverage performance increases. This observation was expected, since by narrowing the main lobe beamwidth, the multi-user interference from interfering BSs is reduced and the observed SINR increases. Hence, it can be easily observed that, while the density of the blockages is increasing, in order to prevent a decrease in the network performance, the antenna's beamwidth should be narrowed. In Fig. 3.7, we plot the additional achieved gain in terms of coverage probability versus the maximum number of cancellations and the SINR threshold. It can be seen that, the coverage probability sharply decreases with N and by increasing the SINR threshold. Specifically, by using the SIC scheme, a considerable improvement on the success probability is observed for SINR threshold values lower than 2 dB, whilst the improvement of the network performance is negligible for higher SINR threshold values. Furthermore, Fig. 3.7 shows that the achieved gain through the cancellation of the strongest interferer, is significantly larger than the gains achieved through the cancellation of higher order interferers. This was expected, due to the fact that by decoding and subtracting the strongest

interfering signal, the users face a noticeable weaker interference resulting in the improvement of observed SINR.

3.7 Summary

In this chapter, we proposed a novel low coordination complexity BS selection scheme in the context of next-generation cellular networks. We assumed that the users and the BSs are equipped with sectorized antennas and the users have the ability to perform SIC. We evaluated the achieved network performance by using our proposed technique in the context of three pre-selection policies that are based on: 1) the Euclidean distance, 2) the averaged received signal power, and 3) random selection. The coverage probability performance of our proposed technique was derived in analytical expressions for the case of Nakagami fading and the impact of blockage density, antenna directionality and number of network tiers has been discussed. Finally, aiming to further boost the achieved performance, a SIC mechanism has been integrated at the user's side to mitigate strong interference terms for the special case of Rayleigh fading. We have shown that the proposed BS selection scheme outperforms conventional CoMP schemes and ensures full diversity gain when the SS policy is employed.

Chapter 4

Heterogeneous FD-mmWave cellular networks with cell center/edge users

In this chapter, we assess the effect of FD radio in HetNet-mmWave communications. Specifically, we propose an analytical framework, based on stochastic geometry, to evaluate the performance of heterogeneous FD-mmWave cellular networks for two user location-based classifications, namely CCUs and CEUs. Moreover, in order to further boost the achieved network performance, the utilization of the SIC technique is considered. Based on the proposed framework, analytical expressions for the coverage and the sum-rate performance are derived.

4.1 Motivation and Contributions

Driven by the demand for increased spectral efficiency in the next-generation systems, the FD radio is identified as a promising solution. FD radio is a well investigated technology which could potentially double the spectral efficiency with respect to the HD counterpart, as it employs simultaneous transmission and reception using non-orthogonal channels [164]. However, the non-orthogonal operation creates a loop-interference (LI) between the input and the output antennas. Motivated by the overwhelming negative effect of the LI at a transceiver, many methods have been developed which successfully mitigate the LI and make the FD technology feasible [161].

The performance of the FD radio in large-scale HetNets is also compromised by the increase of the intra- and out-of-cell co-channel interference [162, 163]. Several

research efforts have been carried out to study the effect of loop- and multi-user interference on the FD performance for large-scale wireless networks, and several techniques have been proposed to alleviate the additional interference caused by the FD operation. Recent studies have shown that, the mitigation of the overall interference can be achieved by exploiting the prominent properties of the mmWave communications [84, 134, 141]. Thus, the co-design of FD radio and mmWave networks is of critical importance in order to combat the severe multi-user interference and increases the network's spectral efficiency.

Furthermore, the majority of works in the literature focus on the average network performance of a user at a random location within a cell. However, the effect of the aforementioned techniques on the user's performance strongly depend on its location [172]. In particular, the users which are located near the serving BS, experience small path-loss attenuation thus the received signal power from the serving BS is significantly higher than the received interference. Nevertheless, the path-loss attenuation becomes more severe as the distance between the user and the serving BS increases, where beyond a critical point the user receives weaker signal power from the serving BS compared to the observed interference. Hence, each cell can be divided into two disjoint sub-regions based on the network topology, namely cell-center region and cell-edge region. The classification of the users into two categories, namely the CCUs and CEUs, is studied in [172] for a grid-based modeled cellular network. In the context of stochastic-based modeled cellular networks, recent studies deal with the classification of the users, which is either based on an SINR ratio threshold [77] or the distance from the serving BS [173]. Even though the technologies of FD radio, mmWave communications and HetNets have been investigated in several works, their co-design, as well as the performance evaluation for different location-based user classifications in a HetNet has been disregarded.

Motivated by the above, in this chapter, we study the achieved coverage and sum-rate performance for each user classification in the context of heterogeneous FD-mmWave cellular networks. We adopt a system-level point of view by taking into account spatial randomness of BSs, users and blockages. Specifically, the main contributions of this chapter are as follows:

- We propose a novel analytical framework based on stochastic geometry, which comprises the co-design of FD radio and HetNet-mmWave cellular networks.

The developed framework takes into account the ability of users to operate either in FD or in HD mode. The users employ distance-proportional fractional power control and are classified either as CCUs or CEUs based on their location within a cell.

- We evaluate the performance of the considered network under an ideal SIC technique for both the DL and UL transmissions, aiming to further enhance the network performance. With the intention of keeping low computational complexity, we assume that only the dominant interferer is eliminated without depriving from the network to achieve better performance.

- Analytical expressions for the coverage and the sum-rate performance are derived for the considered user classifications. Moreover, under specific practical assumptions, closed-form expressions for the Laplace transform of the received interference are derived. Finally, analytical expressions of the coverage and the sum-rate performance for the case where the nodes have the ability to perform SIC are also derived.

The models adopted in this chapter for modeling the mmwave communications were previously introduced in Section 2.4, while some additional preliminaries notions that we will use in the this chapter are introduced in the following section.

4.2 System Model

Recall that, we consider a HetNet composed by K network tiers of BSs. Each network tier $k \in \{1, \ldots, K\}$ of BSs is modeled by a two-dimensional homogeneous PPP Φ_k with density λ_k and transmission power P_k. We consider the scenario where all the BSs operate in FD mode. The users can operate either in FD or in HD mode (e.g. legacy terminals). A user operates in FD mode based on a predefined probability δ^{F}, while an HD user can either operate in DL or UL with probabilities δ^{D} and δ^{U}, respectively. We assume that all FD nodes have both DL and UL communication links.

In terms of channel fading, we consider the scenario where the small-scale fading between two nodes is modeled by Rayleigh fading with unit average power. Hence, the power of the channel fading is an exponential random variable with unit mean. In addition, motivated by the ultra-dense deployment of BSs, we assume that the considered mmWave network deployment operates in the interference-limited

region [174], i.e. thermal noise is neglected. Regarding the LI, we assume that the FD-capable users and BSs employ imperfect cancellation mechanisms [175]. As such, we consider the residual LI channel coefficient to follow a Nagakami-μ distribution with parameters $\left(\mu, \sigma_{\mathrm{LI}}^2\right)$, where $\frac{1}{\sigma_{\mathrm{LI}}^2}$ characterizes the LI cancellation capability of both the BSs and the FD users. Therefore, the power gain of the residual LI channel follows a Gamma distribution with mean μ and variance $\frac{\sigma_{\mathrm{LI}}^2}{\mu}$, i.e. $h_{\mathrm{LI}} \sim \Gamma\left(\mu, \frac{\sigma_{\mathrm{LI}}^2}{\mu}\right)$.

In this chapter, the interference effect from the NLoS signals is ignored, since the dominant interference is caused by the LoS signals [21,115,131]. Thus, for each network tier $k \in \mathcal{K}$, a PPP Φ_k^{L} with inhomogeneous density $\lambda_k^{\mathrm{L}}(r) = \lambda_k \exp(-\beta r)$ is formed, based on the thinning property of the PPPs (See Section 2.4.2). Then, using the expression (2.4), the ff of the distance R to the closest LoS BS from the k-th tier is $\mathbb{P}[R > r] = \exp(-2\pi\lambda_k U(r))$ [115], and the pdf of the distance R, is given by

$$f_R(r) = 2\pi\lambda_k r \exp\left[-\beta r - 2\pi\lambda_k U(r)\right], \tag{4.1}$$

where $U(r) = \frac{1}{\beta^2}\left(1 - \exp\left[-\beta r\right](1 + \beta r)\right)$.

As a result of the scarce power resources of battery-powered devices, the UL power control is of paramount importance in next-generation cellular networks [16]. Hence, we study the utilization of a power control scheme only for the UL transmission, while for the DL transmission we assume a fixed power transmission allocation scheme. We assume that all users utilize distance-proportional fractional power control in order to compensate the large-scale path-loss and maintain the average received signal power at their corresponding serving BSs equal to ρ [163]. To accomplish this, a user, which is at a distance R from its serving BS and with path-loss equal to R^{-a}, adapts its transmitted signal power to $\rho R^{a\epsilon}$, where $0 \leq \epsilon \leq 1$ is the power control fraction. Based on the general UL power control mechanism used in the LTE standard [16], the transmission power allocated to a cellular user can be expressed as $P_u(R) = \min\{\rho R^{a\epsilon},\ P_{\mathrm{m}}\}$, where the users which are unable to fully invert the path-loss, transmit with maximum power P_{m}. It is important to mentioned here that, for the case where $\epsilon = 1$, the path-loss is completely compensated if P_{m} is sufficiently large, and if $\epsilon = 0$, no path-loss inversion is performed and all the users transmit with the same power. The considered distance-proportional UL power control technique only requires the knowledge of the locations of the BSs, opposed to the truncated channel-inversion power control scheme, that demands further computational resources for the channel estimation. This knowledge can be

obtained by monitoring the locations of the BSs through a low-rate feedback channel or by a global positioning system mechanism [19].

4.3 Location-based Classification and Association criteria

In this section, we introduce the location-based classification as well as the association criteria of a user in a cellular network with K-tiers. We provide analytical expressions which will be useful for computing the coverage and the sum-rate performance in Section 4.4. Without loss of generality and by following Slivnyak's theorem [46], the analysis concerns the typical user located at the origin but the results hold for all nodes of the network. Throughout this chapter, we will denote by r_k the distance between the origin and a BS from the k-th tier that is located at $u_k \in \Phi_k^{\mathrm{L}}$, i.e. $r_k = \|u_k\|$.

4.3.1 Location-based Classification

A mmWave channel has fewer multi-path components than a sub-6 GHz channel, hence the small-scale fading has a minor impact on mmWave signals, compared with the ones in the sub-6 GHz channels [21]. As a result, the dominant limiting factor for the performance of mmWave cellular networks is the path-loss attenuation, since the received signal power from a nearby LoS transmitter is almost deterministic [133]. Motivated by this, we adopt a location-based technique for the classification of the users, which provides a low implementation complexity and is not devoid of accuracy. We first define the cell-center and the cell-edge regions of a single-tier cellular network. The spatial partition of a cell into two disjoint sub-regions, center and edge region, aims to classify the users according to their location. The cell-center region is defined as the region in which the user has significantly smaller distance from its serving BS compared to the distance from the dominant interferer. On the other hand, a user is located in the cell-edge region, if the distances from the serving BS and the dominant interferer are relatively equal. For the considered scenario of a K-tier cellular network and due to the independence between the different network tiers, the classification is based on 2^K disjoint sub-regions of a cell. Fig. 4.1a shows a realization of a two-tier FD-mmWave cellular network, where macro-tier BS network

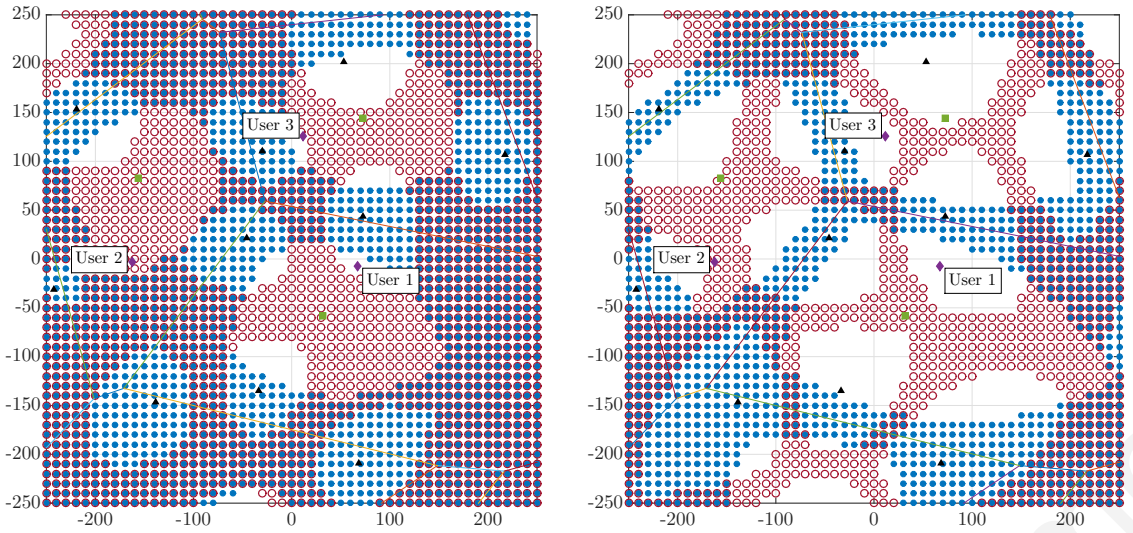

(a) $\zeta = 0.5$ (b) $\zeta = 0.7$

Figure 4.1: The Voronoi tessellation of a two-tier FD-mmWave cellular network, where the macro-BSs, the micro-BSs and the users are represented by triangles, squares and circles, respectively. Points and circles represent the cell-edge regions of macro and micro-tier, respectively.

(represented by rectangles) is overlaid with denser and lower power micro-tier BS network (represented by triangles). Fig 4.1a shows the edge region of the macro-tier network (represented by dots) along with the edge region of the micro-tier network (represented by circles). It can be easily observed that the users (represented by diamonds) can be classified into one of the following disjoint regions of a cell: 1) cell-center for both tiers, 2) cell-edge for both tiers, 3) cell-center for the macro-tier and cell-edge for the micro-tier, and 4) cell-edge for the macro-tier and the cell-center for the micro-tier. For example, *User 1* is classified in the cell-center region for both network tiers, while *User 2* is classified in the cell-center region of the macro-tier and in the cell-edge region of the micro-tier.

We denote as $\mathcal{B}_k$ the region in which a user is classified with respect to the k-th tier. Based on the above, the user's overall classification region $\mathcal{B}$ is defined as the intersection of the regions $\mathcal{B}_k$ in which a user is classified for the k-th tier, i.e. $\mathcal{B} = \cap_{k\in\mathcal{K}}\mathcal{B}_k$. Let C_k and E_k represent the cell-center and the cell-edge regions for the k-th tier, respectively. A user is presumed to be in the cell-edge region for the k-th tier, i.e. $\mathcal{B}_k = E_k$, if its distances from the first and the second closest BSs are relatively equal; otherwise, the user is presumed to be in the cell-center region, i.e. $\mathcal{B}_k = C_k$. Thus, a user is classified as CEU with respect to the k-th tier, if $\frac{R_s}{R_d} > \zeta$

otherwise as CCU, where R_s and R_d denote the distances of the first and the second closest LoS BSs and $\zeta \in [0,1]$ is a predefined fraction. In Fig. 4.1a and Fig. 4.1b, it can be seen that the cell-edge region of the macro-tier and the cell-edge region of the micro-tier, monotonically decrease with the increase of threshold ζ. For example, for the scenario with $\zeta = 0.5$, *User 3* is classified in the cell-center region of the macro-tier and in the cell-edge region of the micro-tier, while for the scenario with $\zeta = 0.7$, *User 3* is classified in the cell-center region of both network tiers. Thus, ζ is a metric that determines the size of the cell-center and the cell-edge regions and consequently the classification of users. By using (4.1), the joint distribution of the distances R_s and R_d for the k-th tier, can be expressed as

$$f_{R_s,R_d}(r_s, r_d) = (2\pi\lambda_k)^2 r_s r_d \exp\left[-\beta r_s - \beta r_d - 2\pi\lambda_k U(r_d)\right]. \tag{4.2}$$

Let $p_{\mathcal{B}_k}$ denote the probability that a user is classified in the region $\mathcal{B}_k$ with respect to the k-th tier. Hence, with the use of (4.2), a user is classified in the cell-center region for the k-th tier with probability

$$p_{C_k} = \mathbb{P}\left[\frac{R_s}{R_d} \leq \zeta\right] = (2\pi\lambda_k)^2 \int_0^\infty r_d U(\zeta r_d) \exp\left[-\beta r_d - 2\pi\lambda_k U(r_d)\right] dr_d, \tag{4.3}$$

while a user is classified in the cell-edge region for the k-th tier with probability

$$p_{E_k} = \mathbb{P}\left[\frac{R_s}{R_d} > \zeta\right] = 1 - p_{C_k}. \tag{4.4}$$

Due to the independence between the network tiers, the overall classification of a user in the region $\mathcal{B}$, occurs with probability $p_{\mathcal{B}}$, which is calculated as $p_{\mathcal{B}} = \prod_{k\in\mathcal{K}} p_{\mathcal{B}_k}$. In the following Lemma, we derive the distance distribution between a user and its serving BS from the k-th tier, given that the user is classified in the region $\mathcal{B}_k$.

Lemma 4.1. *The pdf and the cdf of the distance between a user, which is classified in the region $\mathcal{B}_k$, and its serving BS from the k-th tier are given by*

$$f_R(r|\mathcal{B}_k) = 2\pi\lambda_k r \Omega_k(r, \mathcal{B}_k), \tag{4.5}$$

and

$$F_R(r|\mathcal{B}_k) = 2\pi\lambda_k \int_r^\infty x \Omega_k(x, \mathcal{B}_k)\, dx, \tag{4.6}$$

respectively, where

$$\Omega_k(r, \mathcal{B}_k) = \begin{cases} \frac{\exp[-\beta r]}{p_{C_k}} \left(\exp\left[-2\pi\lambda_k U\left(\frac{r}{\zeta}\right)\right] - \exp\left[-\frac{2\pi\lambda_k}{\beta^2}\right]\right) & \text{if } \mathcal{B}_k = C_k, \\ \frac{\exp[-\beta r]}{p_{E_k}} \left(\exp\left[-2\pi\lambda_k U(r)\right] - \exp\left[-2\pi\lambda_k U\left(\frac{r}{\zeta}\right)\right]\right) & \text{if } \mathcal{B}_k = E_k, \end{cases} \tag{4.7}$$

and p_{C_k} and p_{E_k} are the probabilities that a user is classified in the cell-center and the cell-edge region, respectively.

Proof. Let R_c be the random variable representing the distance of a CCU from the associated BS from the k-th tier. Then, the probability that R_c is greater than r becomes

$$F_R(r|\mathcal{B}_k) = \mathbb{P}\left[R_c > r | R_c < \zeta R_d\right] = \frac{1}{p_{C_k}} \int_r^\infty \int_{\frac{r_c}{\zeta}}^\infty f_{R_c,R_d}(r_c, r_d) dr_d dr_c$$
$$= 2\pi\lambda_k \int_r^\infty r_c \frac{\exp\left[-\beta r\right]}{p_{C_k}} \left(\exp\left[-2\pi\lambda_k U\left(\frac{r}{\zeta}\right)\right] - \exp\left[-\frac{2\pi\lambda_k}{\beta^2}\right]\right) dr_c.$$

Therefore, the pdf of R_c for the k-th tier becomes

$$f_R(r|\mathcal{B}_k) = \frac{d}{dr}\left[1 - F_R(r|\mathcal{B}_k)\right]$$
$$= 2\pi\lambda_k r \frac{\exp\left[-\beta r\right]}{p_{C_k}} \left(\exp\left[-2\pi\lambda_k U\left(\frac{r}{\zeta}\right)\right] - \exp\left[-\frac{2\pi\lambda_k}{\beta^2}\right]\right).$$

Now, let R_e be the distance of a CEU from the associated BS from the k-th tier. The probability that R_e is greater than r becomes

$$F_R(r|\mathcal{B}_k) = \mathbb{P}\left[R_e > r | R_e > \zeta R_d\right] = \frac{1}{p_{E_k}} \int_r^\infty \int_{r_e}^{\frac{r_e}{\zeta}} f_{R_e,R_d}(r_e, r_d) dr_d dr_e$$
$$= 2\pi\lambda_k \int_r^\infty r_e \frac{\exp\left[-\beta r\right]}{p_{E_k}} \left(\exp\left[-2\pi\lambda_k U\left(r\right)\right] - \exp\left[-2\pi\lambda_k U\left(\frac{r}{\zeta}\right)\right]\right) dr_e.$$

Hence, the pdf of R_e for the k-th tier becomes

$$f_R(r|\mathcal{B}_k) = 2\pi\lambda_k r \frac{\exp\left[-\beta r\right]}{p_{E_k}} \left(\exp\left[-2\pi\lambda_k U\left(r\right)\right] - \exp\left[-2\pi\lambda_k U\left(\frac{r}{\zeta}\right)\right]\right). \tag{4.8}$$

Hence the expressions of Lemma 4.1 are derived. □

4.3.2 Association criteria

We consider weighted path-loss user association criteria for both the DL and UL transmissions. In the case where the user operates in FD mode, it can be served either by two different BSs for the DL and UL transmissions or by a single FD BS for both the DL and UL transmissions, i.e. three-node and two-node architectures, respectively [176]. For the DL transmission, we assume that the users are associated with the LoS BS that offers the strongest received power, since by adopting this association policy, the user achieves the highest DL coverage performance. On the other hand, due to the user's limited transmit power, we assume that the users are associated with the closest LoS BS for the UL transmission. Let x_{D}, x_{U} and χ_k denote

the serving BSs for the DL and the UL transmissions and the BS with the minimum path-loss from the k-th tier, respectively. Therefore, the association criteria for both the DL and the UL transmissions, can be described as follows

$$x_{\mathrm{D}} = \arg\min_{x\in\{\chi_k\}} \frac{P_k^{-1}}{L_0(x)}, \text{ and } x_{\mathrm{U}} = \arg\min_{x\in\{\chi_k\}} \frac{\rho}{L_0(x)}, \tag{4.9}$$

where $\chi_k = \arg\min_{x\in\Phi_k^{\mathrm{L}}} L_0(x)^{-1}$. For the case where a user is served by a single BS for both the DL and UL transmissions, this particular BS must satisfy both the expressions in (4.9). The following lemma characterizes the joint DL and UL association probabilities of an FD and an HD user, with respect to the user's classification region.

Lemma 4.2. *An FD user, which is classified in the region $\mathcal{B}$, is served by a BS from the i-th tier for the DL and a BS from the j-th tier for the UL with probability*

$$\Pi_{\mathcal{B}}^{\mathrm{F}}(i,j) = \begin{cases} \int_0^{\infty} \int_{\mathcal{D}_{ij}^{\frac{1}{a}} r_i}^{r_i} f_R(r_i|\mathcal{B}_i) f_R(r_j|\mathcal{B}_j) \prod_{k\in\mathcal{K}\setminus i,j} F_R\left(\max\left\{\mathcal{D}_{ik}^{\frac{1}{a}} r_i, r_j\right\}|\mathcal{B}_k\right) dr_j dr_i, & \text{if } i \neq j, \\ \int_0^{\infty} f_R(r_i,|\mathcal{B}_i) \prod_{k\in\mathcal{K}\setminus i} F_R\left(\max\left\{\mathcal{D}_{ik}^{\frac{1}{a}}, 1\right\} r_i|\mathcal{B}_k\right) dr_i, & \text{if } i = j, \end{cases} \tag{4.10}$$

while for an HD user, the DL and the UL association probabilities are given by

$$\Pi_{\mathcal{B}}^{\mathrm{D}}(i) = \int_0^{\infty} f_R(r_i|\mathcal{B}_i) \prod\nolimits_{k\in\mathcal{K}\setminus i} F_R\left(\mathcal{D}_{ik}^{\frac{1}{a}} r_i|\mathcal{B}_k\right) dr_i, \tag{4.11}$$

and

$$\Pi_{\mathcal{B}}^{\mathrm{U}}(i) = \int_0^{\infty} f_R(r_i|\mathcal{B}_i) \prod\nolimits_{k\in\mathcal{K}\setminus i} F_R\left(r_i|\mathcal{B}_k\right) dr_i, \tag{4.12}$$

respectively, where $\mathcal{D}_{ik} = \frac{P_k}{P_i}$; $f_R(r_i|\mathcal{B}_i)$ and $F_R(r|\mathcal{B}_i)$ denote the pdf and the cdf of the distance between a user and its serving BS from the i-th tier, respectively, which are given in Lemma 4.1.

Proof. We first consider the case when an FD user associates with different BSs for DL and UL. A user associates with different BSs ($x_{\mathrm{D}} \in \Phi_i^{\mathrm{L}}$ and $x_{\mathrm{U}} \in \Phi_j^{\mathrm{L}}$) under the following conditions: (i) x_{D} does not meet the criterion defined for UL $\|x_{\mathrm{D}}\|^a > \|x_{\mathrm{U}}\|^a$, and ($ii$) x_{U} does not meet the criterion defined for DL $P_j^{-1}\|x_{\mathrm{U}}\|^a > P_i^{-1}\|x_{\mathrm{D}}\|^a$. Let $r_i = \|x_{\mathrm{D}}\|$ and $r_j = \|x_{\mathrm{U}}\|$, then by combining the aforementioned conditions we derive

$$\mathcal{D}_{ij}^{\frac{1}{a}} r_i < r_j < r_i, \tag{4.13}$$

where $\mathcal{D}_{ij} = \frac{P_j}{P_i}$. The event that $i \neq j$ can be expressed as

$$\bigcap_{k\in\mathcal{K}\setminus i,j} \left\{\min_{x\in\Phi_k^{\mathrm{L}}} \|x\| > \max\left\{\mathcal{D}_{ij}^{\frac{1}{a}} r_i, r_j\right\} | \mathcal{D}_{ij}^{\frac{1}{a}} r_i < r_j < r_i, \mathcal{B}_k\right\}.$$

Hence, the joint association probability for the event $i \neq j$ is given by

$$\Pi^{\mathrm{F}}_{\mathcal{B}}(i,j) \overset{(a)}{=} \mathbb{E}_{r_i,r_j}\left[\prod_{k\in\mathcal{K}\setminus i,j} F_R\left(\max\left\{\mathcal{D}_{ik}^{\frac{1}{a}} r_i, r_j\right\}|\mathcal{B}_k\right)|\mathcal{D}_{ij}^{\frac{1}{a}} r_i < r_j < r_i, \mathcal{B}_k\right]$$
$$\overset{(b)}{=} \int_0^{\infty}\int_{\mathcal{D}_{ij}^{\frac{1}{a}} r_i}^{r_i} f_R(r_i|\mathcal{B}_i) f_R(r_j|\mathcal{B}_j) \prod_{k\in\mathcal{K}\setminus i,j} F_R\left(\max\left\{\mathcal{D}_{ik}^{\frac{1}{a}} r_i, r_j\right\}|\mathcal{B}_k\right) dr_j dr_i, \tag{4.14}$$

where (a) follows from: (i) the fact that the minimum distance to a BS from a PPP Φ_k is distributed with cdf $\mathbb{P}\left[\min_{x\in\Phi_k^{\mathrm{L}}} \leq t\right] = 1 - F_R(t|\mathcal{B}_k)$ and (ii) the independence between the network tiers, (b) follows since the expectation in (a) is with respect to r_i and r_j, which denote the distances to the serving BSs. Its important to note here, that for the case where $i < j$, the joint association probability is $\Pi^{\mathrm{F}}_{\mathcal{B}}(i,j) = 0$. Assume that the closest BSs of a user from the network tiers Φ_i^{L} and Φ_j^{L} are located at distances r_i and r_j, respectively. Also, let us assume that the user is associated for the UL transmission with the BS from the i-th tier, which is the closest to the user, i.e. $r_i < r_j$. Thus, due to the fact that $P_i > P_j$, the received signal power from the i-th tier is definitely larger than the received signal power from the j-th tier, i.e. $P_i r_i^{-a} > P_j r_j^{-a}$.

The joint association probability of the event $x_{\mathrm{D}} = x_{\mathrm{U}} = x_0$, i.e. $i = j$, given that x_0 belongs to the i-th tier, follows the conditions: (i) $x_{\mathrm{D}} = x_{\mathrm{U}} = x_0$, (ii) x_0 meets the criterion in (4.9) for DL, i.e. $P_i^{-1}\|x_0\|^a < \min_{x\in\Phi_k^{\mathrm{L}}} P_k^{-1}\|x\|^a$, $\forall\, k \neq i$, and (iii) x_0 meets the criterion in (4.9) for UL, i.e. $\|x_0\|^a < \min_{x\in\Phi_k^{\mathrm{L}}} \|x\|^a$, $\forall\, k \neq i$. Thus the probability for the event $i = j$ can be expressed

$$\Pi^{\mathrm{F}}_{\mathcal{B}}(i,i) = \int_0^{\infty} f_R(r_i|\mathcal{B}_i) \prod_{k\in\mathcal{K}\setminus i} F_R\left(\max\left\{\mathcal{D}_{ik'}^{\frac{1}{a}} 1\right\} r_i\right) dr_i. \tag{4.15}$$

Similarly, the DL and UL association probabilities of an HD user can be obtained by investigating the DL and UL transmissions, separately. Regarding the DL association probability, a user associates with a BS $x_{\mathrm{D}} \in \Phi_i^{\mathrm{L}}$, which meets the criterion for DL in (4.9), i.e. $P_i^{-1}\|x_{\mathrm{D}}\|^a < \min_{x\in\Phi_k^{\mathrm{L}}} P_k^{-1}\|x\|^a$ $\forall\, k \neq i$. Thus, the event for the DL association probability can be expressed as

$$\bigcap_{k\in\mathcal{K}\setminus i}\left\{\min_{x\in\Phi_k^{\mathrm{L}}} \|x\| > \mathcal{D}_{ik}^{\frac{1}{a}} r_i \,|\, \mathcal{B}_k\right\}.$$

A similar methodology is followed for obtaining the UL association probability. □

4.4 Heterogeneous FD-mmWave Cellular Network

In this section, we analytically derive both the DL and UL coverage probabilities, as well as the sum-rate performance of a heterogeneous FD-mmWave cellular network for each user classification. Finally, we investigate the additional achieved gains on the network performance, by exploiting the ability of the nodes to perform a SIC technique.

4.4.1 Interference Characterization

Firstly, we investigate the received interference at the typical receiver (i.e., a user or a BS), where analytical and asymptotic expressions for the Laplace transform of the received interference are derived by using stochastic geometry tools. The aggregate interference at the typical receiver can be expressed as follows

$$I^{\mathrm{D}} = \sum\nolimits_{k\in\mathcal{K}} \left(P_k \sum\nolimits_{v\in\Phi_k^{\mathrm{L}}\setminus\{x_{\mathrm{D}}\}} GL_0(v)h_v + \sum\nolimits_{y\in\Psi_k} P_u(\bar{y})GL_0(y)h_y \right),$$

$$I^{\mathrm{U}} = \sum\nolimits_{k\in\mathcal{K}} \left(P_k \sum\nolimits_{v\in\Phi_k^{\mathrm{L}}} GL_0(v)h_v + \sum\nolimits_{y\in\Psi_k\setminus\{x_{\mathrm{U}}\}} P_u(\bar{y})GL_0(y)h_y \right),$$

where $P_u(\bar{y}) = \min\{\rho\bar{y}^{a\epsilon}, P_{\mathrm{m}}\}$ is the transmit power of the interfering user to its serving UL BS that is located at distance $\bar{y}$; h_v and h_y are the channel fadings of the typical receiver with BS at u and user at y, respectively, and Ψ_k is the point process that represents the active LoS users associated with BSs from the k-th tier. The positions of the active users can be seen as a Voronoi perturbed lattice process which is not mathematically tractable. Hence, we adopt the approximation proposed in [69] and characterize the point process Ψ_k as an inhomogeneous PPP with density $\Lambda_k(r)$ which is given by [69]

$$\Lambda_k(r) = \lambda_k^{\mathrm{L}}(r)\left(1 - \exp\left[-2\pi\lambda_k\delta^{\mathrm{U}}U(r)\right]\right), \tag{4.16}$$

where $\lambda_k\delta^{\mathrm{U}}$ denotes the fraction of the BSs that serve their associated users for the UL transmission from the k-th tier and is based on the thinning property of the PPPs (See Section 2.4.2).

In order to characterize the received interference for the DL/UL transmission, it is necessary to define the interference-free areas. For the case of the DL transmission, a user receives interference from both the BSs and the active UL users. From the association criteria in (4.9), we conclude that all BSs that cause interference from the k-th tier to the user have greater path-loss compared to the path-loss of the serving BS

from the i-th tier. Hence, the locations of the interfering BSs from the k-th tier must satisfy the condition $\|x\| > \mathcal{D}_{ik}^{\frac{1}{a}}\|x_{\mathrm{D}}\|$, where $x \in \Phi_k^{\mathrm{L}}$, $x_{\mathrm{D}} \in \Phi_i^{\mathrm{L}}$ and $\mathcal{D}_{ik} = \frac{P_k}{P_i}$. Therefore, we have an interference-free area with radius $r = \mathcal{D}_{ik}^{\frac{1}{a}}\|x_{\mathrm{D}}\|$. On the other hand, a user receives interference from other active users that operate either in FD or in HD UL mode. Due to the assumption that the active interfering users are located outside of the cell, we model this repulsion between the users by assuming that the closest interfering user is at distance b_u [163]. For the case of the UL transmission, there is no exact boundaries for the interference-free area around the typical BS as the users that cause interference can be arbitrarily close. However, with the use of the association criteria in (4.9), we can conclude that for a user which is located at y and is served by a BS from the j-th tier, $\|x_{\mathrm{U}} - y\| < \|x - y\|$ where $x \in \Phi_k^{\mathrm{L}}$ and $x_{\mathrm{U}} \in \Phi_j^{\mathrm{L}}$. Therefore, we have an interference-free area with radius $r = \|x_{\mathrm{U}} - y\|$. Finally, the BS receives interference from all the other BSs in the network. To characterize the interference, in the following Lemma, we compute the Laplace transform of the random variables I^{D} and I^{U} evaluated at s.

Lemma 4.3. *The Laplace transform of the DL interference function, I^{D}, is given by*

$$\mathcal{L}_{I^{\mathrm{D}}}(s) = \prod_{k\in\mathcal{K}}\prod_{G} \exp\left[-2\pi\lambda_k p_G s G\left(P_k \int_{\mathcal{D}_{ik}^{\frac{1}{a}} r_i}^{\infty} \frac{r\mathcal{P}_{\mathrm{L}}(r)}{r^a + sP_kG} dr - \Delta \int_{b_u}^{\infty} \Xi(r) dr\right)\right], \tag{4.17}$$

and for the UL interference function, I^{U}, is given by

$$\mathcal{L}_{I^{\mathrm{U}}}(s) = \prod_{k\in\mathcal{K}}\prod_{G} \exp\left[-2\pi\lambda_k p_G s G\left(P_k \int_{0}^{\infty} \frac{r\mathcal{P}_{\mathrm{L}}(r)}{r^a + sP_kG} dr - \Delta \int_{r_j}^{\infty} \Xi(r) dr\right)\right], \tag{4.18}$$

where

$$\Xi(r) = \left(1 - \exp\left[-2\pi\lambda_k \delta^{\mathrm{U}} U(r)\right]\right) \int_0^{\left(\frac{P_{\mathrm{m}}}{\rho}\right)^{\frac{1}{a\epsilon}}} \frac{\rho r \mathcal{P}_{\mathrm{L}}(r) u^{a\epsilon}}{r^a + sG\rho u^{a\epsilon}} f_R(u) du, \tag{4.19}$$

$\mathcal{P}_{\mathrm{L}}(r) = \exp[-\beta r]$, $\mathcal{D}_{ik} = \frac{P_k}{P_i}$; r_i and r_j are the distances of the serving BSs for the DL and the UL transmission, which belong to the i-th and the j-th tier, respectively, and $\Delta = \delta^{\mathrm{F}} + \left(1 - \delta^{\mathrm{F}}\right)\delta^{\mathrm{U}}$ denotes the fraction of the active interfering users.

Proof. Firstly, we compute the Laplace transform of random variable I^{D} at s conditioned on the random distance $r_{\mathrm{D}} = \|x_{\mathrm{D}}\| \in \Phi_i^{\mathrm{L}}$ to the serving BS from the origin, which we denote as $\mathcal{L}_{I^{\mathrm{D}}}(s)$. The Laplace transform definition yields

$$\mathcal{L}_{I^{\mathrm{D}}}(s) = \mathbb{E}_{\Phi^{\mathrm{L}},\Psi,G,P_u}\left[\exp\left[-s\sum_{k\in\mathcal{K}}\left(P_k \sum_{v\in\Phi_k\setminus\{x_{\mathrm{D}}\}} G_v L_0(v) h_v + P_u(\bar{y}) \sum_{y\in\Psi_k} G_y L_0(y) h_y\right)\right]\right]$$

$$= \prod_{k\in\mathcal{K}} \mathbb{E}_{\Phi_k^{\mathrm{L}},G}\left[\prod_{v\in\Phi_k^{\mathrm{L}}\setminus\{x_{\mathrm{D}}\}} \exp\left[-sG_vP_kL_0(v)h_v\right]\right]$$
$$\times \mathbb{E}_{\Psi_k,G,P_u}\left[\prod_{y\in\Psi_k} \exp\left[-sG_yP_u(\bar{y})L_0(y)h_y\right]\right] \tag{4.20}$$
$$= \prod_{k\in\mathcal{K}} \mathbb{E}_{\Phi_k^{\mathrm{L}}}\left[\prod_{u\in\Phi_k^{\mathrm{L}}\setminus\{x_{\mathrm{D}}\}} \mathbb{E}_{G_v}\left[\exp\left[-sG_vP_kL_0(v)h_v\right]\right]\right]$$
$$\times \mathbb{E}_{\Psi_k}\left[\prod_{y\in\Psi_k} \mathbb{E}_{G_y,P_u}\left[\exp\left[-sG_yP_u(\bar{y})L_0(y)h_y\right]\right]\right]. \tag{4.21}$$

By using the PGFL of PPP and the moment generating function of an exponential random variable (See Section 2.4.2), we obtain the expression (4.17). The Laplace transform of UL transmission can be expressed by following a similar methodology. Hence, the expressions in Lemma 4.3 are derived. □

Recall that $\mathcal{P}_{\mathrm{L}}(r) = \exp\left[-\beta r\right]$ is the LoS probability function defined in Section 4.3, and captures the effect of building blockages. Even through the expressions in Lemma 4.3 can be evaluated using numerical tools, this could be difficult due to the presence of multiple integrals. To address this, we simplify the analysis by considering different practical assumptions.

Special Case for the DL transmission

We consider a step function for the blockage probability [115], i.e. $\mathcal{P}_{\mathrm{L}}(r) = \mathbb{1}_{r<R_B}$ where R_B is the maximum length of an LoS link (i.e. $R_B \approx \sqrt{2}/\beta$ [115]) and assume that the effect of interfering active users is negligible. The validity of the assumptions will be shown in the numerical results. The Laplace transform of the DL interference function for $a = 4$, is given by

$$\mathcal{L}_{I^{\mathrm{D}}}(s) \approx \prod_{k\in\mathcal{K}}\prod_{G} \exp\left[-2\pi\lambda_k p_G sGP_k \int_{\mathcal{D}_{ik}^{\frac{1}{4}} r_i}^{R_B} \frac{r}{r^4 + sP_kG} dr\right]$$
$$\approx \prod_{k\in\mathcal{K}}\prod_{G} \exp\left[-p_G\pi\lambda_k \sqrt{sGP_k}\left(\arctan\left(\frac{\sqrt{sGP_k}}{\mathcal{D}_{ik}^{\frac{1}{2}} r_i^2}\right) - \arctan\left(\frac{\sqrt{sGP_k}}{R_B^2}\right)\right)\right] \tag{4.22}$$
$$\approx \prod_{k\in\mathcal{K}}\prod_{G} \exp\left[-p_G\pi\lambda_k \sqrt{sGP_k}\arctan\left(\frac{\sqrt{sGP_k}\left(R_B^2 - \mathcal{D}_{ik}^{\frac{1}{2}} r_i^2\right)}{sGP_k + R_B^2\mathcal{D}_{ik}^{\frac{1}{2}} r_i^2}\right)\right], \tag{4.23}$$

where (4.22) is derived with the use of [171, 3.194.5]. In order to further simplify the expression, we assume $P_i \gg P_k$ for $k > i$, thus $\mathcal{D}_{ik} \to 0$, and the expression in (4.23)

can be re-written as

$$\mathcal{L}_{I^{\mathrm{D}}}(s) \overset{P_i \gg P_k}{\approx} \prod_{k\in\mathcal{K}} \prod_{G} \exp\left[-p_G \pi \lambda_k \sqrt{sGP_k} \arctan\left(\frac{R_B^2}{\sqrt{sGP_k}}\right)\right]. \tag{4.24}$$

Special Case for the UL transmission

By taking into account the same assumptions as above, the Laplace transform of the UL interference function, can be approximated by

$$\begin{aligned}\mathcal{L}_{I^{\mathrm{U}}}(s) &\approx \prod_{k\in\mathcal{K}} \prod_{G} \exp\left[-2\pi\lambda_k p_G sGP_k \int_0^{R_B} \frac{r}{r^4 + sP_kG} dr\right] \\ &\approx \prod_{k\in\mathcal{K}} \prod_{G} \exp\left[-p_G \pi \lambda_k R_B^2 {}_2F_1\left[1, \frac{1}{2}, \frac{3}{2}, \frac{R_B^4}{sGP_k}\right]\right].\end{aligned} \tag{4.25}$$

where (4.25) is derived with the use of [171, 3.194.1]. We note that the approximated Laplace transform expressions for the observed DL and UL interference provide an upper bound of the actual network performance, since with the aforementioned assumptions the actual aggregate network interference is underestimated. In addition, we can observe that the approximated Laplace transform expressions are relatively efficient to compute as they involve geometrical functions that can be easily evaluated.

Regarding the LI, let $I_{\mathrm{LI}}^{\mathrm{D}}$ and $I_{\mathrm{LI}}^{\mathrm{U}}$ denote the residual interference at the FD users and the FD BSs, respectively, after the LI cancellation. Since the residual LI incurred at a given receiver depends on its own transmit power, we define the residual LI power as follows

$$I_{\mathrm{LI}}^{\mathrm{D}} = \min\{\rho \|x_{\mathrm{D}}\|^{a\epsilon}, P_{\mathrm{m}}\} h_{\mathrm{LI}} \quad \text{and} \quad I_{\mathrm{LI}}^{\mathrm{U}} = P_k h_{\mathrm{LI}}, \tag{4.26}$$

where P_k is the transmit power of a BS in the k-th tier; h_{LI} represents the residual LI channels at both the BSs and the users. We now proceed to the derivation of analytical expressions for the Laplace transform of the LI at the FD receiver for both the DL and UL transmissions.

Lemma 4.4. *The Laplace transform of the observed LI function at an FD user, is given by*

$$\mathcal{L}_{I_{\mathrm{LI}}^{\mathrm{D}}}(s) = \left(\frac{\mu}{\mu + s_{\mathrm{D}}\sigma_{\mathrm{LI}}^2 P_u(r_j)}\right)^{\mu}, \tag{4.27}$$

while the Laplace transform of the observed LI function at an FD BS from the i-th tier, is given by

$$\mathcal{L}_{I_{\mathrm{LI}}^{\mathrm{U}}}(s) = \left(\frac{\mu}{\mu + s_{\mathrm{U}}\sigma_{\mathrm{LI}}^2 P_i}\right)^{\mu}, \tag{4.28}$$

where $r_j = \|x_{\mathrm{U}}\|$; $(\mu, \sigma^2_{\mathrm{LI}})$ *is the fading parameter for the LI channels of the FD BSs and users.*

Proof. The expressions for both the DL and UL transmissions can be obtained: (*i*) by using the definition of the LI for both transmissions, and (*ii*) by applying the Alzer's Lemma [176], in order to approximate the Gamma random variable that represents the LI channel with a weighted sum of the cdfs of exponential random variables. □

4.4.2 SIR Distribution

In this section, we characterize the overall signal-to-interference ratio (SIR) complementary cdf. For the considered system model, the DL and the UL SIR for the typical receiver (i.e. a user or a BS), can be expressed as follows

$$\gamma^{\mathrm{D}}_{ij} = \frac{G_0 P_i L_0\left(x_{\mathrm{D}}\right) h_0}{I^{\mathrm{D}} + \mathbb{1}_{\mathrm{FD}} I^{\mathrm{D}}_{\mathrm{LI}}}, \text{ and } \gamma^{\mathrm{U}}_{ij} = \frac{G_0 P_u(\|x_{\mathrm{U}}\|) L_0\left(x_{\mathrm{U}}\right) \tilde{h}_0}{I^{\mathrm{U}} + I^{\mathrm{U}}_{\mathrm{LI}}}, \tag{4.29}$$

where $x_{\mathrm{D}} \in \Phi^{\mathrm{L}}_i$ and $x_{\mathrm{U}} \in \Phi^{\mathrm{L}}_j$ are the serving BSs for the DL and the UL transmission, respectively, as defined in (4.9); I^{D} and I^{U} are the interferences caused in the DL and the UL transmission, respectively (defined in Section 4.4.1), h_0 and $\tilde{h}_0$ are the channel fadings between the typical receiver and its serving BS and user, respectively, and $\mathbb{1}_{\mathrm{FD}}$ is the indicator function for the event "the typical user is FD-capable". The residual LI observed at the FD users and the BSs are denoted as $I^{\mathrm{D}}_{\mathrm{LI}}$ and $I^{\mathrm{U}}_{\mathrm{LI}}$, which are given by $I^{\mathrm{D}}_{\mathrm{LI}} = P_u(\|x_{\mathrm{U}}\|)h_{\mathrm{LI}}$ and $I^{\mathrm{U}}_{\mathrm{LI}} = P_i h_{\mathrm{LI}}$, respectively, where h_{LI} denotes the power gain of the LI channel. If the typical user operates in HD mode, i.e. $\mathbb{1}_{\mathrm{FD}} = 0$, the observed DL SIR expression for the typical user that is served by a BS from the i-th tier, is denoted as γ^{D}_i. We are now proceed to the derivation of the expressions for the coverage and the sum-rate performance for each user classification.

4.4.3 Coverage and Sum-Rate Performance

We investigate the coverage probability of a user which is classified in the region $\mathcal{B}$, for both the DL and UL transmissions of heterogeneous FD-mmWave cellular networks. The coverage probability for both the DL and UL transmissions, $\mathcal{P}^{\mathrm{D}}(\mathcal{B}, \tau)$ and $\mathcal{P}^{\mathrm{U}}(\mathcal{B}, \tau)$, respectively, is the probability that the SIR is greater than a threshold τ. In the following proposition, the conditional DL and UL coverage probabilities are derived, for an FD user which is served by a BS from the i-th tier for the DL and a BS from the j-th tier for the UL.

Proposition 4.1. *The DL and the UL coverage probabilities of a user, which is classified in the region $\mathcal{B}$, conditioned on the DL and the UL association criteria, are given by*

$$\mathcal{P}_{ij}^{\mathrm{D}}(\mathcal{B},\tau)=\int_0^{\infty}\left(\int_{\mathcal{D}_{ij}^{\frac{1}{a}}r_i}^{r_i}\mathcal{L}_{I^{\mathrm{D}}}(s_{\mathrm{D}})\left(\frac{\mu}{\mu+s_{\mathrm{D}}\sigma_{\mathrm{LI}}^2P_u(r_j)}\right)^{\mu}f_R(r_j|\mathcal{B}_j)dr_j\right)f_R(r_i|\mathcal{B}_i)dr_i, \tag{4.30}$$

and

$$\mathcal{P}_{ij}^{\mathrm{U}}(\mathcal{B},\tau)=\int_0^{\infty}\left(\int_{\mathcal{D}_{ij}^{\frac{1}{a}}r_i}^{r_i}\mathcal{L}_{I^{\mathrm{U}}}(s_{\mathrm{U}})\left(\frac{\mu}{\mu+s_{\mathrm{U}}\sigma_{\mathrm{LI}}^2P_i}\right)^{\mu}f_R(r_j|\mathcal{B}_j)dr_j\right)f_R(r_i|\mathcal{B}_i)dr_i, \tag{4.31}$$

where $\{s_{\mathrm{D}},s_{\mathrm{U}}\}=\left\{\frac{\tau r_i^a}{G_0P_i},\frac{\tau r_j^a}{G_0P_u}\right\}$, $\mathcal{L}_{I^{\mathrm{D}}}(\cdot)$ *and* $\mathcal{L}_{I^{\mathrm{U}}}(\cdot)$ *denote the Laplace transform function of the observed interference for the DL and the UL transmission, respectively, and are given in Lemma 4.3;* $f_R(r_i|\mathcal{B}_i)$ *denotes the distance distributions which is given in Lemma 4.1 and* b_u *is the repulsion parameter [163].*

Proof. First, we focus on the scenario of an FD user that is served by a BS from the i-th tier for the DL and by a BS from the j-th tier for the UL. Let $r_i=\|x_{\mathrm{D}}\|$ and $r_j=\|x_{\mathrm{U}}\|$, then the DL coverage probability is given by

$$\begin{aligned}\mathcal{P}_{ij}^{\mathrm{D}}(\mathcal{B},\tau)&=\mathbb{E}_{r_i,r_j,\mathcal{B}}\left[\mathbb{P}\left[\gamma_{ij}^{\mathrm{D}}>\tau|\mathcal{B}\right]\right]=\int_0^{\infty}\left(\int_{\mathcal{D}_{ij}^{\frac{1}{a}}r_i}^{r_i}\mathbb{P}\left[\gamma_{ij}^{\mathcal{T}}>\tau\right]f_R(r_j|\mathcal{B}_j)dr_j\right)f_R(r_i|\mathcal{B}_i)dr_i\\&=\int_0^{\infty}\left(\int_{\mathcal{D}_{ij}^{\frac{1}{a}}r_i}^{r_i}\mathbb{P}\left[h_0>\frac{\tau L_0^{-1}(r_i)}{G_0P_i}\left(I^{\mathrm{D}}+I_{\mathrm{LI}}^{\mathrm{D}}\right)\right]f_R(r_j|\mathcal{B}_j)dr_j\right)f_R(r_i|\mathcal{B}_i)dr_i.\end{aligned} \tag{4.32}$$

By using the fact that $h_0\sim\exp(1)$, the above expression can be further simplified as

$$\begin{aligned}\mathcal{P}_{ij}^{\mathrm{D}}(\mathcal{B},\tau)&=\int_0^{\infty}\left(\int_{\mathcal{D}_{ij}^{\frac{1}{a}}r_i}^{r_i}\mathbb{E}_{I^{\mathrm{D}}}\left[\exp\left[-s_{\mathrm{D}}I^{\mathrm{D}}\right]\right]\mathbb{E}_{I_{\mathrm{LI}}^{\mathrm{D}}}\left[\exp\left[-s_{\mathrm{D}}I_{\mathrm{LI}}^{\mathrm{D}}\right]\right]f_R(r_j|\mathcal{B}_j)dr_j\right)f_R(r_i|\mathcal{B}_i)dr_i\\&=\int_0^{\infty}\left(\int_{\mathcal{D}_{ij}^{\frac{1}{a}}r_i}^{r_i}\mathcal{L}_{I^{\mathrm{D}}}(s_{\mathrm{D}})\,\mathcal{L}_{I_{\mathrm{LI}}^{\mathrm{D}}}(s_{\mathrm{D}})\,f_R(r_j|\mathcal{B}_j)dr_j\right)f_R(r_i|\mathcal{B}_i)dr_i,\end{aligned} \tag{4.33}$$

where (4.33) follows from the definition of the Laplace transform and $s_{\mathrm{D}}=\frac{\tau L_0^{-1}(r_i)}{G_0P_i}$. The UL coverage probability can be also obtained by following a similar procedure as described above. Hence, the expressions (4.30) and (4.31) are derived. □

Note that, for the scenario of an HD user, $\sigma_{\mathrm{LI}}^2=0$ applies, and thus the term referring to the Laplace transform of the LI function in expression (4.30) becomes zero, and the coverage performance for the considered scenario is denoted as $\mathcal{P}_i^{\mathrm{D}}(\mathcal{B},\tau)$. The following theorem presents the expressions for the DL and the UL coverage probability for the typical user which is classified in the region $\mathcal{B}$.

Theorem 4.1. *The DL coverage probability of a user, which is classified in the region $\mathcal{B}$, is given by*

$$\mathcal{P}^{\mathrm{D}}(\mathcal{B},\tau) = \delta^{\mathrm{F}} \sum\nolimits_{i=1}^{K} \sum\nolimits_{j\geq i} \Pi^{\mathrm{F}}_{\mathcal{B}}(i,j)\mathcal{P}^{\mathrm{D}}_{ij}(\mathcal{B},\tau) + (1-\delta^{\mathrm{F}})\delta^{\mathrm{D}} \sum\nolimits_{i=1}^{K} \Pi^{\mathrm{D}}_{\mathcal{B}}(i)\mathcal{P}^{\mathrm{D}}_{i}(\mathcal{B},\tau)\,, \quad (4.34)$$

while the UL coverage probability is given by

$$\mathcal{P}^{\mathrm{U}}(\mathcal{B},\tau) = \sum\nolimits_{i=1}^{K} \sum\nolimits_{j\geq i} \Pi^{\mathrm{F}}_{\mathcal{B}}(i,j)\mathcal{P}^{\mathrm{U}}_{ij}(\mathcal{B},\tau)\,, \quad (4.35)$$

where $\mathcal{P}^{\mathrm{D}}_{ij}\left(\mathcal{B},\tau^{\mathcal{T}}\right)$ and $\mathcal{P}^{\mathrm{U}}_{ij}\left(\mathcal{B},\tau^{\mathcal{T}}\right)$ denote the coverage probabilities of an FD user for the DL and the UL transmission, respectively, conditioned on the DL and the UL user association criteria and are given in Proposition 4.1.

Proof. We first determine the achieved DL coverage probability of an FD user. The conditional DL coverage probability of an FD user, which is served by a BS from the i-th tier for the DL and a BS from the j-th tier for the UL, is given by (4.30). The sum over all possible association scenarios with their corresponding probabilities provides the achieved DL coverage probability of an FD user. The same is valid for the HD users and the FD BSs, and hence the expressions in Theorem 4.1 are derived. □

It is important to mention here that, as a node's ability to cancel the LI decreases, i.e. $\sigma^2_{\mathrm{LI}} \to \infty$, the LI overcomes the received signal power. For the DL case, this results in a zero coverage probability for the FD users. Specifically, the first term of expression (4.34) becomes zero, and the expression (4.34) is simply given by

$$\mathcal{P}^{\mathrm{D}}(\mathcal{B},\tau) = (1-\delta^{\mathrm{F}})\delta^{\mathrm{D}} \sum\nolimits_{i=1}^{K} \Pi^{\mathrm{D}}_{\mathcal{B}}(i)\mathcal{P}^{\mathrm{D}}_{i}(\mathcal{B},\tau)\,. \quad (4.36)$$

On the other hand, for the UL case, the coverage performance of the BSs, i.e. expression (4.35), is zero since all BSs operate in FD mode.

An equally important metric is the sum-rate performance (bits/sec/Hz). We use the derived SIR distribution framework to obtain analytical expressions for the sum-rate performance of the typical user in the context of the presented heterogeneous FD-mmWave cellular network. Using the coverage probability, we can now derive the average spectral efficiencies achieved by the FD and HD users, which are provided in the following theorem.

Theorem 4.2. *The DL and the UL rate performance of an HD user, which is classified in the region $\mathcal{B}$, can be expressed as*

$$\mathcal{R}^{\mathrm{D}}_{\mathcal{B}} = \frac{1}{\ln(2)} \int_0^{\infty} \frac{\mathcal{P}^{\mathrm{D}}(\mathcal{B},\tau)}{\tau+1} d\tau, \quad (4.37)$$

$$\mathcal{R}_{\mathcal{B}}^{\mathrm{U}} = \frac{1}{\ln(2)} \int_0^{\infty} \frac{\mathcal{P}^{\mathrm{U}}(\mathcal{B}, \tau)}{\tau + 1} d\tau, \tag{4.38}$$

while the sum-rate performance of an FD user, which is classified in the region $\mathcal{B}$, can be expressed as

$$\mathcal{R}_{\mathcal{B}}^{\mathrm{F}} = \mathcal{R}_{\mathcal{B}}^{\mathrm{D}} + \mathcal{R}_{\mathcal{B}}^{\mathrm{U}}, \tag{4.39}$$

where $\mathcal{P}^{\mathrm{D}}(\mathcal{B}, \tau)$ and $\mathcal{P}^{\mathrm{U}}(\mathcal{B}, \tau)$ express the coverage probability for the DL and the UL transmissions, respectively, for a user which is classified in the region $\mathcal{B}$.

4.4.4 Successive Interference Cancellation

In this section, we study how the SIC technique affects the coverage and the sum-rate performance of interference-limited heterogeneous FD-mmWave networks. The analysis will be presented for the DL transmission but the results similarly apply for the UL transmission. We assume that each user has the ability to implement an ideal SIC in accordance to [101]. In addition, due to the weaker transmission power of the users, we assume that the interference effect from neighboring users is negligible and the dominant interference is caused by the BSs. This could also be guaranteed by a protocol that prohibits the selection of active nearby users [130]. Furthermore, we investigate the worst case scenario, where the link between the user and the dominant interfering BS lies in the boresight direction of the antennas of both nodes, resulting in a link gain of Q^2. The main idea of SIC is to decode the dominant interference signals caused by the interfering BSs and subtract them from the received signal, resulting in an increase of the observed SIR. In order to keep both the computational complexity and power consumption at low levels, we assume that SIC is performed to cancel the dominant interferer. Specifically, the user attempts to decode the received signal without any interference cancellation. If this attempt is unsuccessful, the user seeks to decode the dominant interfering signal, subtract it from the received signal, and then re-attempt to decode the resulting received signal. If the user fails to decode the received signal, then the user is considered to be in outage. Based on the sequence of the aforementioned events, the DL coverage performance of a SIC-enabled user which is classified in the region $\mathcal{B}$, conditioned on the user's DL and UL serving BSs, is given by

$$\widehat{\mathcal{P}}_{ij}^{\mathrm{D}}(\mathcal{B}, \tau) = \mathcal{P}_{ij}^{\mathrm{D}}(\mathcal{B}, \tau) + \left(1 - \mathcal{P}_{ij}^{\mathrm{D}}(\mathcal{B}, \tau)\right) \mathcal{P}_{ij}^{\mathrm{D,dec}}(\tau) \mathcal{P}_{ij}^{\mathrm{D,suc}}(\mathcal{B}, \tau), \tag{4.40}$$

where $\mathcal{P}_{ij}^{\mathrm{D,dec}}(\mathcal{B},\tau)$ and $\mathcal{P}_{ij}^{\mathrm{D,suc}}(\mathcal{B},\tau)$ denote the success probability to cancel the strongest signal and the success probability of a link after successfully canceling the dominant interferer, respectively, conditioned on the user classification. Intuitively, since the user is able to successfully cancel the strongest interfering BS, the observed interference by the typical user is changed. Let $\Omega = \bigcup_{k\in\mathcal{K}} \Phi_k \setminus \{x^{\mathrm{D}}\}$ denote the set of interfering BSs. Then the set of interfering nodes after the cancellation of the strongest interfering BS is represented by $\widetilde{\Omega} = \Omega \setminus \{X_{\mathrm{d}}\}$, where X_{d} denotes the location of the strongest interfering BS. In order to show the impact of SIC technique, we consider an ultra-dense scenario, where the radius of interference-free area is derived by using the displacement theorem [168] and is equal to $\lim_{\lambda_k\to\infty} \|X_{\mathrm{d}}\| = (2\pi \sum_{k\in\mathcal{K}} \lambda_k)^{-\frac{1}{2}}$. Hence, the Laplace transform of the aggregate interference after the cancellation of the strongest interferer, denoted as $I_{\widetilde{\Omega}}$, is given by

$$\mathcal{L}_{I_{\widetilde{\Omega}}}(s) = \prod_{k\in\mathcal{K}} \prod_{G} \exp\left[-2\pi\lambda_k p_G s G \left(P_k \int_{\|X_{\mathrm{d}}\|}^{\infty} \frac{r\mathcal{P}_{\mathrm{L}}(r)}{r^a + sP_kG} dr - \Delta \int_{b_u}^{\infty} \Xi(r) dr\right)\right], \tag{4.41}$$

where $\mathcal{P}_{\mathrm{L}}(r) = e^{-\beta r}$, Ξ is given by (4.19) and $\Delta = \delta^{\mathrm{F}} + \left(1-\delta^{\mathrm{F}}\right)\delta^{\mathrm{U}}$.

A SIC-enabled user firstly attempts to decode and cancel the dominant interfering signal. The success probability of a user attempting to decode and cancel the strongest interfering BS, is given by

$$\mathcal{P}_{ij}^{\mathrm{D,dec}}(\tau) = 1 - \prod_{k=1}^{K} \left(1 - \mathcal{P}_{ij}^{\mathrm{D,dec}}(\tau,k)\right), \tag{4.42}$$

where $\mathcal{P}_{ij}^{\mathrm{D,dec}}(\tau,k)$ denotes the probability of a user to successfully decode the dominant interfering BS from the k-th tier that is located at X_{d}. This probability can be calculated as follows

$$\begin{aligned}\mathcal{P}_{ij}^{\mathrm{D,dec}}(\tau,k) &= \mathbb{P}\left[\frac{G_0 P_k L_0^{-1}(X_{\mathrm{d}})}{I_{\widetilde{\Omega}} + I_{\mathrm{LI}}^{\mathrm{D}}} > \tau\right] \\ &= \mathbb{P}\left[h_{X_{\mathrm{d}}} > \frac{\tau L_0^{-1}(X_{\mathrm{d}})}{G_0 P_k}(I_{\widetilde{\Omega}} + I_{\mathrm{LI}}^{\mathrm{D}})\right] = \mathbb{E}_{X_{\mathrm{d}}}\left[\mathcal{L}_{I_{\widetilde{\Omega}}}(s_{\mathrm{D}})\mathcal{L}_{I_{\mathrm{LI}}^{\mathrm{D}}}(s_{\mathrm{D}})\right],\end{aligned} \tag{4.43}$$

where $s_{\mathrm{D}} = \frac{\tau L_0^{-1}(X_{\mathrm{d}})}{G_0 P_k}$. To find the unconditional success probability, the expectation should be taken with respect to the distance to the strongest interferer, i.e. the second-closest BS. The probability that two points are located in a circular area with radius $r_{\mathrm{d}} = \|X_{\mathrm{d}}\|$ around the typical user, i.e. the serving BS and the dominant interferer, is given by [46]

$$\mathbb{P}\left[\mathrm{N}(B(\|X_{\mathrm{d}}\|)) = 2\right] = 1 - \exp\left[-2\pi\lambda_k U(r_0)\right] - 2\pi\lambda_k U(r_1)\exp\left[-2\pi\lambda_k U(r_1)\right]. \tag{4.44}$$

Then, the pdf of the second-closest BS from the k-th tier that is located at X_{d}, is given by,

$$f_{X_{\mathrm{d}}}(r) = \frac{d}{dr}\Big[1 - \mathbb{P}\left[\mathrm{N}(B(\|X_{\mathrm{d}}\|)) = 2\right]\Big] \\ = 2\pi\lambda_k r\left(2\pi\lambda_k U(r) + 1\right)\exp\left[-\beta r - 2\pi\lambda_k U(r)\right].$$

Thus, the success probability of a user to decode the dominant interference from the k-th tier is given by

$$\mathcal{P}_{ij}^{\mathrm{D,dec}}(\tau, k) = \int_0^{\infty}\left(\int_{\mathcal{D}_{ij}^{\frac{1}{\vec{a}}} r_{\mathrm{d}}}^{r_{\mathrm{d}}} \mathcal{L}_{I_{\widetilde{\Omega}}}(s_{\mathrm{D}})\left(\frac{\mu}{\mu + s_{\mathrm{D}}\sigma_{\mathrm{LI}}^2 P_u(r_j)}\right)^{\mu} f_R(r_j|\mathcal{B}_j)dr_j\right) f_{X_{\mathrm{d}}}(r_{\mathrm{d}})dr_{\mathrm{d}}. \quad (4.45)$$

After successfully decoding and canceling the strongest interfering BS, the typical user subtracts it from the received signal and then re-attempts to decode the resulting received signal. The probability of successfully decoding the desired signal, after canceling the strongest interferer, can be derived by following a similar methodology as in Proposition 4.1 and can be expressed as

$$\mathcal{P}_{ij}^{\mathrm{D,suc}}(\mathcal{B}, \tau) = \mathbb{P}\left[\mathrm{SIR}'_{ij} > \tau|\mathcal{B}\right] = \mathbb{P}\left[P_i G_0 L_0(r_i) h_0 > \tau\left(I_{\widetilde{\Omega}} + I_{\mathrm{LI}}^{\mathrm{D}}\right)|\mathcal{B}\right] \\ = \int_0^{\infty}\left(\int_{\mathcal{D}_{ij}^{\frac{1}{\vec{a}}} r_i}^{r_i} \mathcal{L}_{I_{\widetilde{\Omega}}}(s_{\mathrm{D}})\left(\frac{\mu}{\mu + s_{\mathrm{D}}\sigma_{\mathrm{LI}}^2 P_u(r_j)}\right)^{\mu} f_R(r_j|\mathcal{B}_j)dr_j\right) f_R(r_i|\mathcal{B}_i)dr_i, \quad (4.46)$$

where SIR'_{ij} denotes the achieved SIR after the cancellation of the dominant interferer and $s_{\mathrm{D}} = \frac{\tau L_0^{-1}(r_i)}{P_i G_0}$. The same methodology can be performed for the DL coverage probability of an HD user, without the existence of the LI. Due to space limitation, the analysis of this case is omitted. In the following theorems, we define the coverage and the sum-rate performance of a SIC-enabled user in the context of the considered network, for each user classification.

Theorem 4.3. *The DL coverage performance for a SIC-enabled user, which is classified in the region $\mathcal{B}$, is given by*

$$\widehat{\mathcal{P}}^{\mathrm{D}}(\mathcal{B}, \tau) = \delta^{\mathrm{F}}\sum_{i=1}^{K}\sum_{j\geq i}\Pi_{\mathcal{B}}^{\mathrm{F}}(i, j)\widehat{\mathcal{P}}_{ij}^{\mathrm{D}}(\mathcal{B}, \tau) + (1 - \delta^{\mathrm{F}})\delta^{\mathrm{D}}\sum_{i=1}^{K}\Pi_{\mathcal{B}}^{\mathrm{D}}(i)\widehat{\mathcal{P}}_{i}^{\mathrm{D}}(\mathcal{B}, \tau), \quad (4.47)$$

where $\widehat{\mathcal{P}}_{ij}^{\mathrm{D}}(\mathcal{B}, \tau)$ denotes the conditional DL coverage probability of an FD SIC-enabled user, which is classified in the region $\mathcal{B}$, and is given by (4.40)*; $\mathcal{P}_{ij}^{\mathrm{D,dec}}(\mathcal{B}, \tau)$ and $\mathcal{P}_{ij}^{\mathrm{D,suc}}(\mathcal{B}, \tau)$ denote the success probability to cancel the strongest signal and the coverage probability after successfully canceling the dominant interferer, and are given by* (4.45) *and* (4.46)*, respectively; $s_{\mathrm{D}} = \frac{r_i^a \tau}{G_0 P_i}$ and $\mathcal{L}_{I_{\widetilde{\Omega}}}(s_{\mathrm{D}})$ denotes the Laplace transform of the the aggregate interference after the cancellation of the strongest interferer and is given by* (4.41)*.*

Following a similar procedure as described above, the UL coverage probability for a SIC-enabled FD user can be derived. Due to space limitation, the analysis for the UL transmission is omitted. The following Theorem presents the sum-rate performance of an FD and HD link for the case where the user is able to implement the SIC technique for each user classification.

Theorem 4.4. *The DL and UL rate performance of an HD SIC-enabled user, which is classified in the region $\mathcal{B}$, can be expressed as*

$$\widehat{\mathcal{R}}_{\mathcal{B}}^{\mathrm{D}} = \frac{1}{\ln(2)} \int_0^{\infty} \frac{\widehat{\mathcal{P}}^{\mathrm{D}}(\mathcal{B}, \tau)}{\tau + 1} d\tau, \tag{4.48}$$

$$\widehat{\mathcal{R}}_{\mathcal{B}}^{\mathrm{U}} = \frac{1}{\ln(2)} \int_0^{\infty} \frac{\widehat{\mathcal{P}}^{\mathrm{U}}(\mathcal{B}, \tau)}{\tau + 1} d\tau, \tag{4.49}$$

while the sum-rate performance of an FD SIC-enabled user, which is classified in the region $\mathcal{B}$, can be expressed as

$$\widehat{\mathcal{R}}_{\mathcal{B}}^{\mathrm{F}} = \widehat{\mathcal{R}}_{\mathcal{B}}^{\mathrm{D}} + \widehat{\mathcal{R}}_{\mathcal{B}}^{\mathrm{U}}, \tag{4.50}$$

where $\widehat{\mathcal{P}}^{\mathrm{D}}(\mathcal{B}, \tau)$ and $\widehat{\mathcal{P}}^{\mathrm{U}}(\mathcal{B}, \tau)$ express the coverage probability for the DL and the UL transmissions, respectively, of an SIC-enabled user which is classified in the region $\mathcal{B}$.

4.5 Numerical Results

In this section, we provide numerical results to verify our model and illustrate the impact of implementing a heterogeneous FD-mmWave cellular network on the performance of CCUs and CEUs. We focus on the special case of a heterogeneous network with $K = 2$ tiers, where the density of the first and the second tier is $\lambda_1 = 31$ BSs/km^2 and $\lambda_2 = 93$ BSs/km^2, respectively, with transmit power equal to $P_1 = 15$ dBm and $P_2 = 5$ dBm, respectively [115]. For the considered network deployment, a user can be classified as: 1) CCU for both the network tiers (scenario "CC"), 2) CCU for the macro-tier and CEU for the micro-tier (scenario "CE"), 3) CEU for the macro-tier and CCU for the micro-tier (scenario "EC"), and 4) CEU for both the network tiers (scenario "EE"). The path loss exponent is set to $a = 4$. The power control factor is $\epsilon = 0.9$ and all BSs have the same receive sensitivity $\rho = -40$ dB [163]. The SIC capabilities of BSs and users are set to $\sigma_{\mathrm{LI}}^2 = -60$ dB and $\mu = 4$ [163]. The parameters for the sectorized antenna model are set to $Q = 10$ dB, $q = -10$ dB and $\phi = \frac{\pi}{6}$ for the main lobe gain, the side lobe gain and the main

lobe beamwidth, respectively [131]. Unless otherwise specified, the fraction of FD users is set to $\delta^{\mathrm{F}} = 0.8$ and the fractions of HD users that operate in DL and in UL direction are set equal to $\delta^{\mathrm{D}} = \delta^{\mathrm{U}} = 0.5$; $b_u = 40$ m and $\zeta = 0.7$. It is important to note that the selection of these parameter values is for the purpose of presenting the achieved performance of our proposed framework. Using different values will lead to a shifted network performance, but with the same conclusions.

Fig. 4.2a illustrates the achieved coverage performance for both the DL and UL transmissions for all four user classifications. As expected, for the scenario CC, the achieved DL and UL coverage performances are the highest among the four classifications since the serving BSs for the DL and the UL transmission are closer to the user compared to the interfering BSs and users. On the other hand, the scenario EE results in the worst DL and UL coverage performance due to the significantly higher received interference compared to the received signal strength. Furthermore, it is clear from the curves that for the scenarios CC and CE, where the user is classified as CCU for the tier with the highest transmit power, the user achieves significantly higher DL and UL coverage performance compared to the scenarios EC and EE for small coverage thresholds. This observation can be explained by the fact that the dominant interfering BS, which is the BS with the highest transmit power, is at greater distance from the user and thus causes less interference. However, beyond a critical threshold value, the DL and UL coverage performances achieved by a user for the scenarios CE and EC are relatively equal. Finally, the agreement between the theoretical curves (solid and dashed lines) and the simulation results (markers) validates our mathematical analysis.

Fig. 4.2b shows the effect of power control on the achieved sum-rate performance for the considered user classifications. We can easily observe the positive effect of power control on the network's sum-rate performance. As expected, by increasing the power control factor ϵ, the ability of users to compensate the path-loss is also increased that leads to a better UL coverage performance and consequently a significantly increased sum-rate performance. Similarly to the previous figure, Fig. 4.2b also demonstrates the fact that the achieved sum-rate performance of a user for the scenario CC, exceeds the performance of the other user classifications and the achieved sum-rate performance of the scenario EE is the worst. Furthermore, Fig. 4.2b demonstrates the increased sum-rate performance due to the ability of users to implement the SIC technique. This observation has been expected, since by

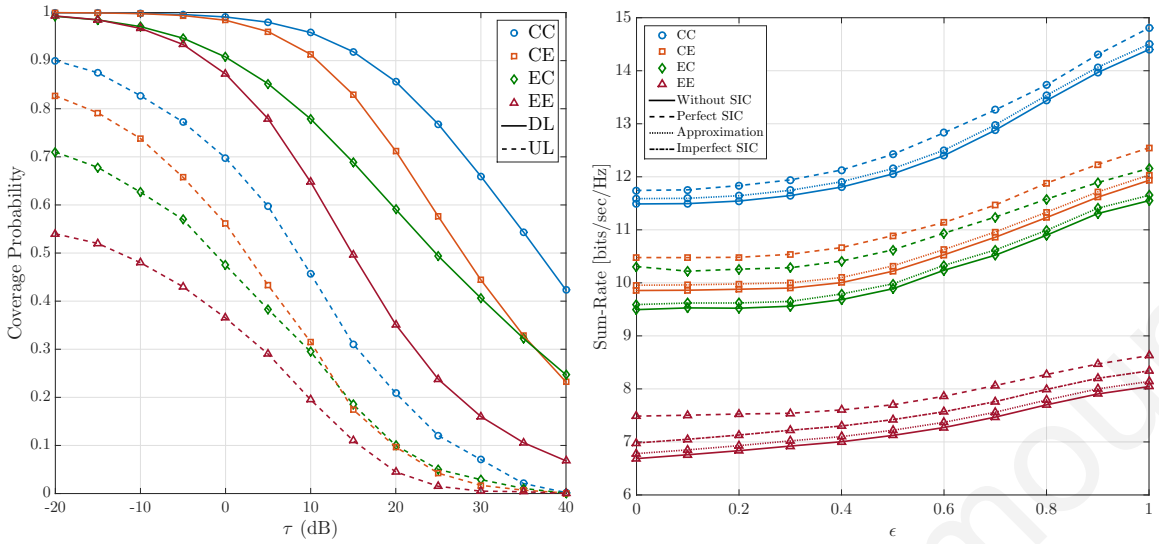

(a) Coverage performance versus the threshold (τ).

(b) Sum-rate performance versus power control factor (ϵ).

Figure 4.2: Coverage and Sum-Rate performance for the considered four user classifications.

decoding and subtracting the strongest interfering signal, the received interference by the users is noticeable weaker resulting in the improvement of the observed SIR. We also numerically investigate an imperfect SIC scheme, where we assume that the interference caused by the dominant BS is canceled imperfectly. As such, we consider the channel coefficient of the residual interference after cancellation, to follow a complex Gaussian distribution with zero mean and variance σ^2_{SIC} (similar to the residual LI [175]). In Fig. 4.2b, we consider $\sigma^2_{\text{SIC}} = -60$ dB and show the achieved sum-rate performance of the imperfect SIC scheme for the EE scenario. As expected, its performance is upper bounded by the achieved performance of the perfect SIC scheme, and lower bounded by the achieved performance without the SIC scheme. Note that the performance of the imperfect SIC scheme will be similar for the other scenarios. Moreover, Fig. 4.2b demonstrates the impact of interfering users on the network performance as well as the adoption of the simplified blockage model. The small deviation from the theoretical curves indicates that, the interference caused by the active users is negligible compared to the interference caused by the interfering BSs due to the user's smaller transmit power. Finally, the adoption of the simplified blockage model provides lower complexity methodology for evaluating the system performance, without being significantly deficient in accuracy.

Fig. 4.3 reveals the impact of blockages on the network's DL coverage perfor-

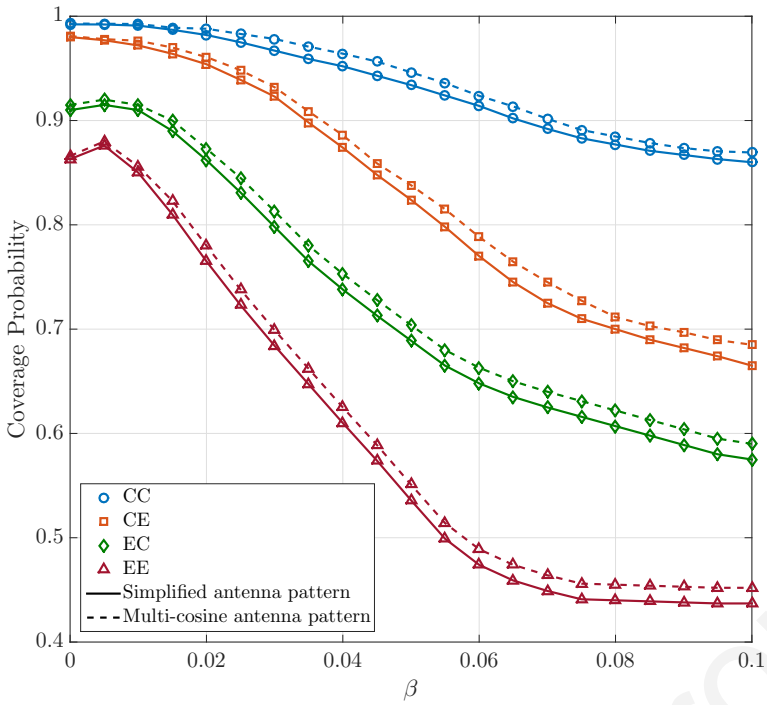

Figure 4.3: DL coverage performance versus blockage constant (β) for the considered user classifications; $\tau = 0$ dB. For the multi-cosine antenna pattern [131], we assume that each network's node is equipped with 256 antenna elements.

mance. It is interesting to note that at low blockage constant values, the existence of blockages improves the network performance. However, by increasing the blockage constant beyond a critical point, the network performance decreases. This observation is based on the fact that at low blockage constants, the interfering signals from LoS BSs are blocked, while the users are still able to communicate with their serving LoS BS. In contrast, for high blockage densities, the communication of the users with LoS BSs becomes impossible and thus the coverage probability significantly decreases. Another important observation is the significant impact of increasing the blockage density on the achieved performance for the EE scenario. This behavior of coverage performance is based on the fact that as the distance between a user and its serving BS increases, user's performance is highly compromised by the increased number of blockages in the area due to the increased probability of the desired links to be blocked. It is important to mention here that the blockage constant has similar effect on the UL coverage performance for all user classifications, thus the curves for the UL transmission are omitted. In addition, we numerically investigate the impact of a more accurate antenna pattern on the coverage performance by using the multi-cosine antenna pattern [131]. As expected, the multi-cosine antenna model outperforms our simplified antenna model, yielding a tight upper bound for the

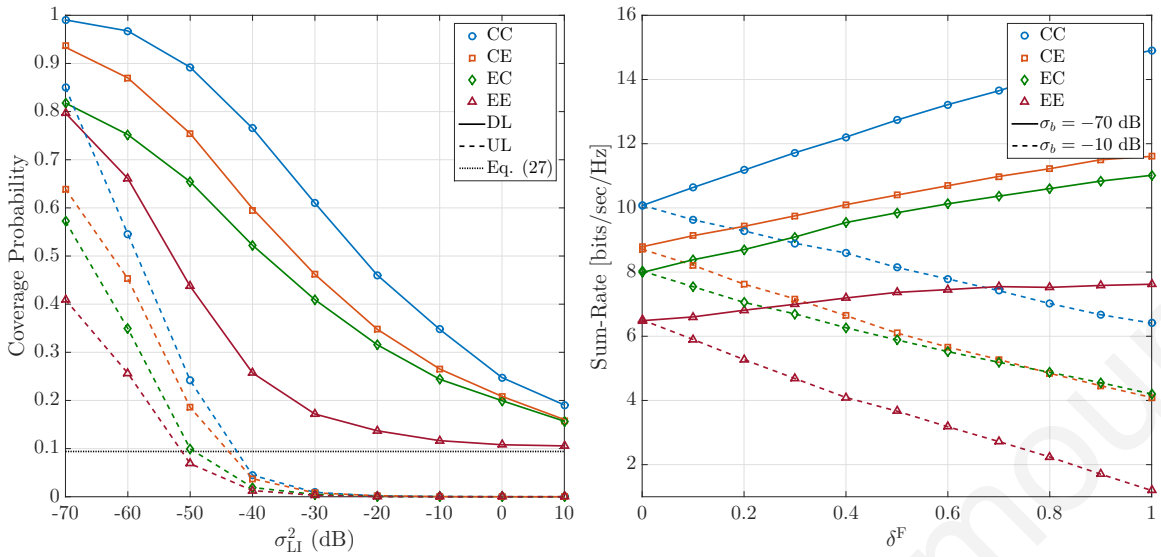

(a) Coverage performance versus the LI cancellation capability (σ^2_{LI}).

(b) Sum-rate versus the fraction of FD users (δ^{F}) for $\sigma^2_{\mathrm{LI}} = \{-70, -10\}$ dB.

Figure 4.4: Coverage and Sum-rate performance for the four user classifications.

achieved coverage performance. This is due to the fact that the simplified antenna model quantizes the continuously varying antenna array gains in a binary manner, overestimating the impact of the observed interference. Finally, it can be easily observed that the achieved performance corresponding to the multi-cosine antenna model follows the same trends with the simplified antenna model, and thus we further support our main conclusions and remarks.

Figs. 4.4a and 4.4b show the effect of the residual LI on the coverage and the sum-rate performance. We can easily observe that by increasing the ability of the users to cancel the LI, i.e. $\sigma^2_{\mathrm{LI}} \to -\infty$, both the coverage and sum-rate performance of the considered network are increased. This observation was expected, since by decreasing the residual LI at the BSs and the users, the aggregate received interference at the nodes is decreased, and therefore an increased SIR is observed. On the other hand, as user's ability to cancel the LI decreases, the DL coverage performance converges to a constant floor while the UL coverage performance becomes zero. This again is expected, since the severe LI causes zero coverage probability when a node operates in the FD mode, thus the overall coverage performance is solely due to the nodes which operate in HD mode. In Fig. 4.4b, we can easily observe that the sum-rate performance is independent from the ability of users to cancel the LI for the case where all the users operate in HD mode, i.e. $\delta^{\mathrm{F}} = 0$. Finally, it is clear from Fig. 4.4b that if the users have high LI cancellation capabilities, the highest sum-rate

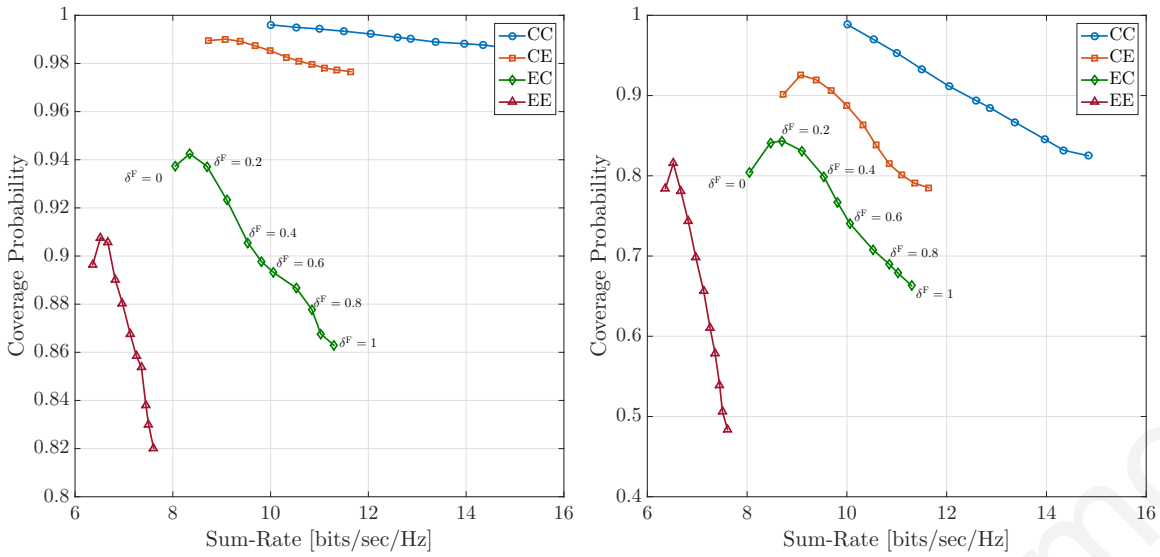

(a) DL coverage performance versus sum-rate performance.

(b) UL coverage performance versus sum-rate performance.

Figure 4.5: Trade-off between the coverage and sum-rate performance for the DL and UL transmission for different fractions of FD users (δ^F).

performance can be achieved, when all the users are operating in FD mode. For the case where the users have low LI cancellation capabilities, all the users must operate in HD mode in order to achieve the highest sum-rate performance.

Figs. 4.5a and 4.5b show the trade-off between the sum-rate performance and the DL and UL coverage performance with respect to the fraction of FD users, respectively. Each point in the curves represents the trade-off between the two performance metrics for a given fraction of FD users. An important observation from these figures is that for the scenarios CE, EC and EE, and at low fraction of FD users, the operation in FD mode improves the coverage performance. This observation can be explained since by increasing the probability of the user to operate in FD mode, the dominant interfering BS tends to become a serving BS, thus the observed SIR is increased due to the reduced interference. However, by increasing the fraction of FD users beyond a critical point, the network performance decreases due to the increased multi-user interference. In addition, the reduction in the DL coverage performance is mainly observed in the scenarios EC and EE, in which the users are more vulnerable in interference changes due to their small distances from the BSs that cause interference. Conversely, the increased number of FD users causes a weak decrease in the DL coverage performance for the scenarios CC and CE. On the other hand, the increased number of transmissions in each direction, positively

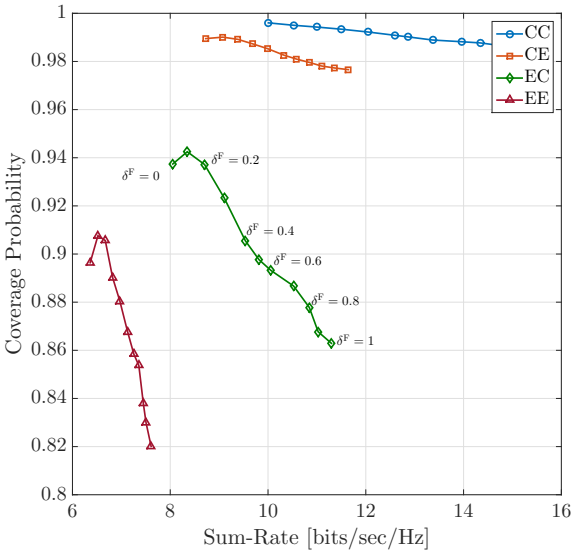

(a) DL coverage performance versus sum-rate performance.

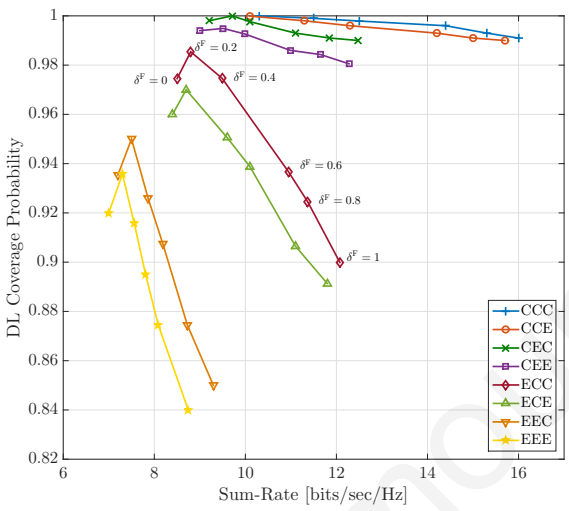

(b) UL coverage performance versus sum-rate performance.

Figure 4.6: Trade-off between the coverage and sum-rate performance for the DL and UL transmission for different fractions of FD users (δ^F).

affects the sum-rate performance. Specifically, the scenarios CC and CE achieve greater sum-rate performance gains compared to the scenarios EC and EE. The same behavior is also observed in Fig. 4.5b, which shows the trade-off between the sum-rate performance and the UL coverage probability. It is important to mention here that, the proposed mathematical framework can capture the performance of HetNets with higher number of network tiers, i.e. $K > 2$. Specifically, for the scenario $K > 2$ and due to the independence between the network tiers, the spatial classification of a user is based on 2^K disjoint sub-regions of a cell. In Fig. 4.6a and Fig. **??**, illustrate the trade-off between the sum-rate performance and the DL coverage performance with respect to the fraction of the FD users with a two-tier ($K = 2$) and a three-tier ($K = 3$) network deployment, respectively. It can be easily observed from the figure that the same conclusions are derived.

4.6 Conclusion

In this chapter, we proposed an analytical framework based on stochastic geometry and studied the performance of heterogeneous FD-mmWave cellular networks. The developed framework takes into account the ability of users to operate either in FD or in HD mode and their classification either as CCUs or CEUs for each network tier.

We derive analytical expressions for both the coverage and sum-rate performance for each user classification and the impact of blockage density, power control, residual LI and fraction of FD users has been discussed. Aiming to further boost the achieved performance, a SIC mechanism has been integrated to mitigate strong interference terms. Our study reveals that HD is beneficial for CEUs since it offers better coverage performance. On the other hand, FD provides a significantly larger sum-rate performance to CCUs, with the cost of a slightly reduced coverage performance. Finally, we have shown that the combination of FD radio with mmWaves provides significant gains to cellular networks, as it can potentially double the network's spectral efficiency as well as mitigate the severe multi-user interference.

Chapter 5

A hybrid cooperation scheme for heterogeneous multi-band cellular networks

In this chapter, we propose a novel hybrid cooperation scheme in the context of heterogeneous sub-6 GHz/mmWave cellular networks, where users are classified either as CCUs or CEUs. Specifically, our proposed scheme exploits the cooperation technique, aiming at enhancing the performance of the CEUs and providing ubiquitous connectivity. Using stochastic geometry tools, we first establish an analytical and tractable framework to investigate the achieved performance of our proposed scheme in heterogeneous multi-band cellular networks. Based on the proposed framework, analytical expressions for the moments of the conditional success probability are derived for the calculation of the meta-distribution. Finally, a simple approximation of the meta-distribution is calculated, leveraging the moment-matching method with the Beta-distribution.

5.1 Motivation and Contribution

As we previously mentioned, mmWave communications is a promising technology for next-generation cellular networks, due to its abundant spectrum resources. However, ubiquitous coverage performance in next-generation networks is not feasible with the deployment of only mmWave BSs [71]. A possible solution is that mmWave BSs will be overlaid on conventional sub-6 GHz HetNets, where the sub-6 GHz BSs

provide general coverage and mmWave BSs provide high capacity to individual users. Even though the utilization of HetNets operating in the same frequency band has been investigated in several works, only limited work has been carried out for heterogeneous multi-band cellular networks. In [71], the authors studied a HetNet consisting of sub-6 GHz macro-cells (MCells) and mmWave small-cells (SCells), and showed that extremely high bias values are desirable for SCells. The authors in [69], proposed a general and tractable framework for characterizing the coverage and rate performance of networks consisting of sub-6 GHz MCells and mmWave SCells, and the analysis indicated that spectral efficiency of mmWave networks increases with the BS density, particularly at the cell edge. A network consisting of sub-6 GHz MCells and mmWave SCells was studied in [119], where the performance gains with different decoupled association strategies were investigated.

The above studies focus on the average network performance of a user at a random location within a cell. However, the link quality of a user is subjected to its location. In particular, the CEUs receive weaker signal power from the serving BS compared to the received interference, resulting in reduced coverage performance. On the other hand, the CCUs experience better coverage performance compared to the CEUs since the received signal power from the serving BS is significantly higher than the received interference. The classification of users into CCUs and CEUs, is studied in [96] for a grid-based modeled cellular network. In the context of stochastic-based modeled cellular networks, recent studies deal with the classification of the users, which are based on an SINR threshold [52] or on distances [173]. Moreover, a fundamental performance metric for the wireless networks is the SINR performance, which indicates the success probability relative to an SINR threshold, evaluated at the typical link. Nonetheless, the performance of the typical link represents an average over all spatial realizations of the PP, which provides very limited information on the individual links [177]. To overcome this limitation, the authors in [75], introduced the concept of meta-distribution, which provides a fine-grained information about the performance of the individual links. Specifically, the standard (mean) success probability defined as the complementary cumulative distribution function of the SINR of the typical user answers the questions "Given a SINR threshold1 θ, what fraction of users in the whole network can achieve successful transmission on average?", while the meta-distribution answers more detailed questions such as "What fraction of users in a cellular network achieve 90% link

reliability given a SINR threshold θ?"

Motivated by the above, in this chapter, we study the meta-distribution of the SINR in the context of heterogeneous multi-band cellular networks. The main contribution of this chapter is the development of a novel hybrid BS cooperation (HC) scheme, aiming at providing an ubiquitous coverage performance. In particular, our proposed scheme exploits the ability of BSs to jointly transmit data in a coherent manner, in order to enhance the CEUs performance. Furthermore, using stochastic geometry tools, we derive the b-th moment of the conditional success probability achieved with the proposed scheme, and a Beta-distribution approximation of the meta-distribution is calculated. Our results illustrate that our cooperative scheme can significantly improve the coverage performance of heterogeneous multi-band cellular networks, when compared to the conventional association scheme for heterogeneous deployments.

5.2 System model

In this section, we provide details of the considered system model. The network is studied from a large-scale point of view using stochastic geometry. We consider a two-tier heterogeneous cellular network consisting of sub-6 GHz MCells overlaid with mmWave SCells. Both the MCells and the SCells are uniformly distributed in $\mathbb{R}^2$ according to independent homogeneous PPPs Φ_{M} and Φ_{S}, with densities λ_{M} and λ_{S}, respectively. We consider a fixed power transmission allocation scheme, i.e. BSs that belong in Φ_i, where $i \in \{\mathrm{M}, \mathrm{S}\}$, transmit with power P_i, where $P_{\mathrm{M}} > P_{\mathrm{S}}$.

In such multi-band deployments, sub-6 GHz BSs are essential in providing ubiquitous coverage to ensure a consistent service for the users. On the other hand, mmWave BSs are mainly used to provide high capacity to individual users. Motivated by this, we assume the employment of omni-directional antennas for all sub-6 GHz BSs, while all mmWave BSs are assumed to be equipped with directional antennas. Furthermore, we assume that the users are equipped with a single omni-directional antenna and are able to work on both sub-6 GHz and mmWave frequencies. For modeling the antenna directionality of the mmWave BSs, we adopt a sectorized antenna model that approximate the actual beam pattern with sufficient accuracy [133]. The antenna array gain is parameterized by three values: 1) main-lobe beamwidth $\phi \in [0, 2\pi]$, 2) main-lobe gain Q (dB), and 3) side-lobe gain q (dB),

where $Q > q$. Thus, the antenna gain between a mmWave BS and a user, is a discrete random variable described by

$$G = \begin{cases} Q & \text{with probability } p_Q = \frac{\phi}{2\pi}, \\ q & \text{with probability } p_q = 1 - \frac{\phi}{2\pi}. \end{cases} \tag{5.1}$$

All users served in mmWave cells are assumed to be in perfect alignment with their serving BSs, whereas the beams of all interfering links are assumed to be randomly oriented with respect to each other and hence the gain on the interfering links is considered to be random.

A blockage model is adopted for the mmWave transmissions to characterize the high path-loss. A mmWave link can be either LoS or NLoS, depending on whether the BS is visible to the user or not, due to the existence of blockages. We consider the case where the LoS probability function is given by $\mathcal{P}_{\mathrm{L}}(R) = \exp(-\beta R)$ [133], where R denotes the distance between the receiver and the transmitter and β is determined by the blockage characteristics. Throughout this work, the interference effect from the NLoS signals is ignored, since the dominant interference is caused by the LoS signals [115]. Thus, regarding the SCells, a PPP $\Phi_{\mathrm{S}}^{\mathrm{L}}$ with inhomogeneous density function $\lambda_{\mathrm{S}}^{\mathrm{L}}(r) = \lambda_{\mathrm{S}} \exp(-\beta r)$ is formed, based on the thinning property of the PPPs [46]. Then, the cdf of the distance R to the closest BS from the i-tier, is given by [115]

$$F_R^{(i)}(r) = \begin{cases} \exp\left(-\pi \lambda_{\mathrm{M}} r^2\right) & \text{if } i = \mathrm{M}, \\ \exp\left(-2\pi \lambda_{\mathrm{S}} U(r)\right) & \text{if } i = \mathrm{S}, \end{cases} \tag{5.2}$$

and the pdf of the distance R is

$$f_R^{(i)}(r) = \begin{cases} 2\pi \lambda_{\mathrm{M}} r \exp\left(-\pi \lambda_{\mathrm{M}} r^2\right), & \text{if } i = \mathrm{M}, \\ 2\pi \lambda_{\mathrm{S}} r \exp\left(-\beta r - 2\pi \lambda_{\mathrm{S}} U(r)\right), & \text{if } i = \mathrm{S}, \end{cases} \tag{5.3}$$

where $U(r) = \frac{1}{\beta^2}\left(1 - \exp\left(-\beta r\right)\left(1 + \beta r\right)\right)$.

All wireless signals are assumed to experience both large-scale path-loss effects and small-scale fading. Specifically, the small-scale fading between two nodes is modeled by Rayleigh fading with unit average power, where different links are assumed to be independent and identically distributed. Hence, the power of the channel fading is an exponential random variable with unit mean, i.e. $|h|^2 \sim \exp(1)$. For the large-scale path-loss, we assume an unbounded singular path-loss model,

$L(X, Y) = \|X - Y\|^{-a}$ which assumes that the received power decays with the distance between the transmitter located at X and the receiver located at Y, where $a > 2$ denotes the path-loss exponent.

5.3 Hybrid cooperation scheme for HetNets

5.3.1 User classification criteria

The adopted classification scheme, spatially separates each cell into two disjoint sub-regions, namely center and edge region, and aims at classifying the users according to their RSS. The cell-center region is defined as the region in which the user observes significantly higher RSS from its serving BS compared with that obtained from the dominant interferer. On the other hand, a user is located in the cell-edge region, if the observed RSSs from the serving BS and the dominant interferer are relatively equal. It is important to mention here that, the serving and the dominant interfering BSs can belong to either MCell or SCell network tier. Nevertheless, regarding the user classification policy, our proposed scheme only requires the investigation of the scenarios where the serving and the dominant interfering BSs belong in the same network tier. Therefore, the classification of the users with respect to a single tier is solely based on the distances from their serving and dominant interfering BSs. Fig. 5.1 shows a realization of a heterogeneous multi-band cellular network, where sub-6 GHz BSs (represented by rectangles) are overlaid with denser and lower power mmWave BSs (represented by dots). Fig. 5.1 shows the center and edge regions of the sub-6 GHz BSs, separated by the dashed lines. In addition, the center and edge regions of the mmWave BSs are also illustrated, and are separated by the dotted lines. Let R_i and $\widetilde{R}_i$ represent the distance of the serving and the dominant interfering BSs, respectively, that belong in the i-th tier, where $i \in \{\mathrm{M}, \mathrm{S}\}$. Thus, a user is classified as CEU, if $\frac{R_i}{\widetilde{R}_i} > \zeta$ otherwise as CCU, where $\zeta \in [0, 1]$ is a predefined fraction. By using (5.3), the joint distribution of the distances R_i and $\widetilde{R}_i$ for the i-th tier, is given by

$$f_{R_i,\widetilde{R}_i}(r_i, \widetilde{r}_i) = \begin{cases} (2\pi\lambda_{\mathrm{M}})^2 r_{\mathrm{M}} \widetilde{r}_{\mathrm{M}} \exp\left(-\pi\lambda_{\mathrm{M}} \widetilde{r}_{\mathrm{M}}^2\right), & \text{if } i = \mathrm{M}, \\ (2\pi\lambda_{\mathrm{S}})^2 r_{\mathrm{S}} \widetilde{r}_{\mathrm{S}} \exp\left(-\beta(r_{\mathrm{S}} + \widetilde{r}_{\mathrm{S}}) - 2\pi\lambda_{\mathrm{S}} U\left(\widetilde{r}_{\mathrm{S}}\right)\right), & \text{if } i = \mathrm{S}. \end{cases} \tag{5.4}$$

Let $\Pi^i_{\mathcal{B}}$ denote the probability that a user is classified as $\mathcal{B} \in \{\mathrm{CCU}, \mathrm{CEU}\}$ with respect to the i-th tier. Hence, with the use of (5.4), a user is classified in the cell-center region

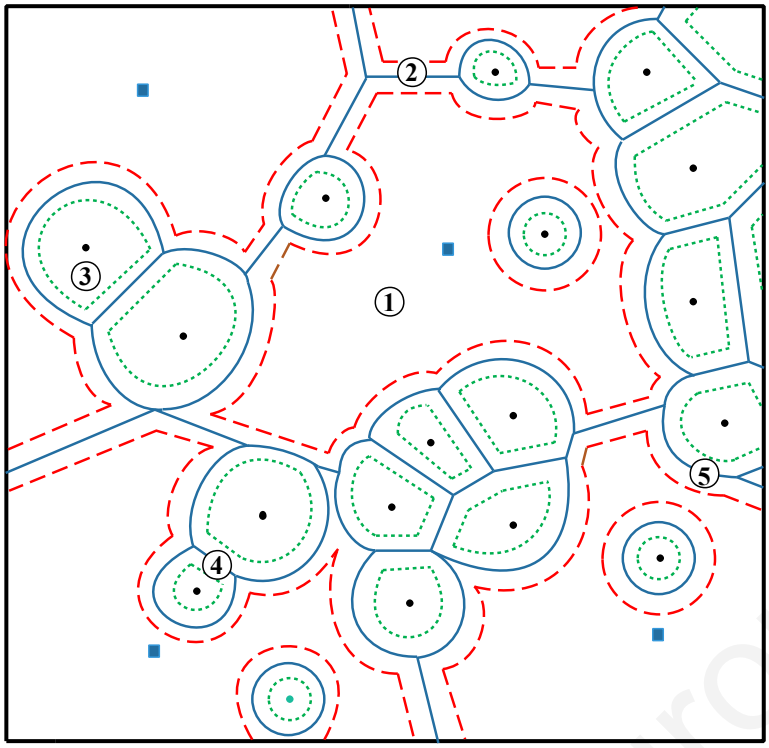

Figure 5.1: The Voronoi tessellation of a two-tier multi-band cellular network, where the MCells and the SCells and the users are represented by rectangles and dots, respectively. Dashed and dotted lines represent the boundaries of the center and edge regions of Mcells and SCells, respectively.

for the i-th tier with probability $\Pi^i_{\mathrm{CCU}} = \mathbb{P}\left[R_i/\widetilde{R}_i \leq \zeta\right]$, that is equal to

$$\begin{aligned}\Pi^i_{\mathrm{CCU}} &= \int_{r_i=0}^{\infty}\left(\int_{\widetilde{r}_i=0}^{r_i\zeta} f_{R_i,\widetilde{R}_i}(r_i,\widetilde{r}_i)d\widetilde{r}_i\right)dr_i \\ &= \begin{cases}\zeta^2, & \text{if } i=\mathrm{M},\\ 2\pi\lambda_{\mathrm{S}}\int_0^{\infty} r_{\mathrm{S}}\exp\left(-\beta r_{\mathrm{S}}-\frac{2\pi\lambda_{\mathrm{S}}}{\beta^2}\right)\left(\exp\left(-2\pi\lambda_{\mathrm{S}}U\left(\frac{r_{\mathrm{S}}}{\zeta}\right)\right)-1\right)dr_{\mathrm{S}}, & \text{if } i=\mathrm{S},\end{cases}\end{aligned}$$

while a user is classified in the cell-edge region for the i-th tier with probability

$$\Pi^i_{\mathrm{CEU}} = 1 - \Pi^i_{\mathrm{CCU}}.$$

5.3.2 Association Policy

For the association policy, we assume that the users are served by the LoS BS that offers the higher RSS. We denote r_{M} and r_{S} the distances between a user and its strongest LoS BSs from the MCell and SCell network tiers, respectively. Let η (dB) denote the predefined bias factor between the MCell and SCell network tiers, which

determines the size of the cell-edge region between the different tiers. The association probabilities of a user are derived in the following Lemma.

Lemma 5.1. *A user is served by a BS from the i-th tier, where* $i \in \{\mathrm{M}, \mathrm{S}\}$*, with probability*

$$\Omega_i = \int_0^{\infty} F_R^{(j)}\left(\left(\frac{P_j \eta}{P_i}\right)^{\frac{1}{a}} x\right) f_R^{(i)}(x) dx, \tag{5.5}$$

where $j \in \{\mathrm{M}, \mathrm{S}\}$ *and* $i \neq j$*.*

Proof. Considering the association criteria, the probability of a user to be served by a BS from the i-th tier, can be expressed as

$$\begin{aligned}\Omega_i &= \mathbb{P}\left[\frac{P_i r_i^{-a}}{P_j r_j^{-a}} > \eta\right] = \mathbb{P}\left[r_j > \left(\frac{P_j \eta}{P_i}\right)^{\frac{1}{a}} r_i\right] \\ &= \int_0^{\infty} \mathbb{P}\left[r_j > \left(\frac{P_j \eta}{P_i}\right)^{\frac{1}{a}} x\right] f_{R_i}(x) dx,\end{aligned}$$

where $\{i, j\} \in \{\mathrm{M}, \mathrm{S}\}$ and $j \neq i$. Hence, by using (5.2) and (5.3), the expression (5.5) is derived. □

5.3.3 Hybrid cooperation Scheme

Our proposed HC scheme aims to provide ubiquitous coverage performance, by allowing the CEUs to jointly receive data from their strongest and second-strongest BSs. As it can be easily observed in Fig. 5.1, a user $u \in \mathbb{R}^2$ can be classified into one of the following disjoint sub-regions of a cell:

- Sub-region 1: $\Re_1$ with probability $\Psi_1 = \Pi_{\mathrm{CCU}}^{\mathrm{M}} \Omega_{\mathrm{M}}$,
- Sub-region 2: $\Re_2$ with probability $\Psi_2 = \Pi_{\mathrm{CEU}}^{\mathrm{M}} \Omega_{\mathrm{M}}$,
- Sub-region 3: $\Re_3$ with probability $\Psi_3 = \Pi_{\mathrm{CCU}}^{\mathrm{S}} \Omega_{\mathrm{S}}$,
- Sub-region 4: $\Re_4$ with probability $\Psi_4 = \Pi_{\mathrm{CEU}}^{\mathrm{S}} \Omega_{\mathrm{S}}$,
- Sub-region 5: $\Re_5$ with probability $\Psi_5 = 1 - \sum_{\kappa=1}^{4} \Psi_\kappa$,

where $\bigcup_\kappa \Re_\kappa = \mathbb{R}^2$ and $\kappa = \{1, \cdots, 5\}$.

In our proposed HC scheme, when a user is classified as CEU, i.e. the RSSs from the serving and the dominant interfering BSs are relatively equal, the user utilize the coordinated multi-point technique. In such a case, the serving and the dominant

interfering BSs jointly transmit data to the user in a synchronous and coherent manner [177]. As we mentioned earlier, the serving and the dominant interfering BSs can belong to either MCell or SCell network tier, independently, therefore a user can be served from either both network tiers or by a single network tier. Let $\text{SINR}_{\{i,j\}}$ represent the observed SINR at a user from its serving BS from the i-th tier and its dominant interfering BS from the j-th tier, where $\{i, j\} \in \{\text{M}, \text{S}\}$. For the scenario where the user is served from both network tiers, i.e. $i \neq j$, the observed SINR is given by

$$\text{SINR}_{\{i,j\}} = \frac{\left| \sum\limits_{k=i,j} \mu_k^{\frac{1}{2}}(Q) P_k^{\frac{1}{2}} \|x_k\|^{-\frac{a}{2}} h_{x_k} \right|^2}{\sum\limits_{k} \sum\limits_{y \in \Phi_k} \mu_k(G) P_k \|y\|^{-a} |h_y|^2 + \sigma_n^2}, \tag{5.6}$$

where $\|x_i\|$ denotes the distance from a user to its strongest BS x_i from the i-th tier; h_x is the channel fading between a receiver and its serving BS located at x; σ_n^2 is the variance of the additive white Gaussian noise at the user and $\mu_k(M)$ is a function where $\mu_k(X) = X$ if $k = \text{S}$, otherwise $\mu_k(X) = 1$. On the other hand, if the user is served by a single network tier, i.e. $i = j$, the observed SINR is given by

$$\text{SINR}_{\{i\}} = \frac{\mu_i(Q) P_i \left| \|x_i\|^{-\frac{a}{2}} h_{x_i} + \mathbb{1}_{\text{CEU}}^{(i)} \|\widetilde{x_i}\|^{-\frac{a}{2}} h_{\widetilde{x_i}} \right|^2}{\sum\limits_{y \in \Phi_i} \mu_i(G) P_i \|y\|^{-a} |h_y|^2 + \sigma_n^2}, \tag{5.7}$$

where $\|\widetilde{x_i}\|$ denotes the distance from a user to its second-strongest BSs $\widetilde{x_i}$ from the i-th tier and $\mathbb{1}_{\text{CEU}}^{(i)}$ is the indicator function, where $\mathbb{1}_{\text{CEU}}^{(i)} = 1$ if the user is classified as CEU with respect to the i-th tier, otherwise $\mathbb{1}_{\text{CEU}}^{(i)} = 0$.

It is important to mention here that, the observed interference for both the CCUs and the CEUs is caused by the network tiers that the user is associated with. In particular, a user that is served by BSs that belong to a single tier, observes interference solely from the BSs that belong to the specific tier. Furthermore, considering $\zeta = 1$ and $\eta = 0$ dB, our proposed cooperation scheme becomes the conventional maximum RSS scheme, which is currently utilized in the HetNets [71].

5.4 Meta-Distribution for HC Scheme

In this section, we study the meta-distribution of the SINR, which is the distribution of the conditional success probability given a realization of the PP, in the context of our proposed HC scheme. Based on [177], the meta-distribution of the SINR is a

two-parameter distribution function defined as

$$\bar{F}_{P_s(\theta)}(x) = \mathbb{P}_o^!\left(P_s(\theta) > x\right), \quad \theta \in \mathbb{R}^+,\ x \in [0,1], \tag{5.8}$$

where $\mathbb{P}_o^!$ denotes the reduced Palm probability conditioning on the typical receiver at the origin o and its corresponding transmitter to be active. Specifically, the meta-distribution of the SINR represents the complementary cdf of the success probability $P_s(\theta)$ conditioned on a PPP Φ, which can be expressed as

$$P_s(\theta) = \mathbb{P}\left[\text{SINR} > \theta | \Phi\right], \tag{5.9}$$

where θ is the SINR threshold. Due to the ergodicity of the point processes, the meta-distribution can be interpreted as the fraction of users in each realization of the point processes that achieve coverage threshold at least θ with probability at least x. The standard coverage probability is the mean of $P_s(\theta)$, obtained by integrating the meta distribution (5.8) over $x \in [0,1]$. Considering the five sub-regions of a cell, we define $P_s^{(\kappa)}(\theta)$ as the success probability of a user that is classified in the sub-region $\Re_\kappa$, where $\kappa = \{1, \cdots, 5\}$, conditioned on the PPP Φ. Thus, from the law of total probability, we have

$$P_s(\theta) = \sum_{\kappa} \Psi_\kappa P_s^{(\kappa)}(\theta). \tag{5.10}$$

5.4.1 Moments of Conditional Success Probability

Since a direct calculation of the meta-distribution is tedious, the characterization of the meta-distribution for our proposed HC scheme will be made through the moments $M_b(\theta) = \mathbb{E}\left[P_s(\theta)\right]$. The moments for each user classification are derived in the following Lemma.

Lemma 5.2. *Given that the typical link is active, the moment $M_b(\theta)$, $b \in \mathbb{C}$, of the conditional success probability in heterogeneous multi-band cellular networks, is given by*

$$M_b(\theta) = \sum_{\kappa} \Psi_\kappa M_b^{(\kappa)}(\theta), \tag{5.11}$$

where $M_b^{(\kappa)}(\theta)$ represents the b-th moment of the conditional success probability within

sub-region $\Re_\kappa$, and is given by

$$M_b^{(\kappa)}(\theta) = \begin{cases} \int_0^\infty \Xi(s_1) e^{\Upsilon_{\mathrm{M}}(s_1,v)} f_{X_1^{\mathrm{M}}}(v)\, dv, & \text{if } \kappa = 1, \\ \int_0^\infty \int_v^{\frac{v}{\zeta}} \Xi(s_2) e^{\Upsilon_{\mathrm{M}}(s_2,t)} f_{X_2^{\mathrm{M}},\widetilde{X}_2^{\mathrm{M}}}(v,t)\, dtdv, & \text{if } \kappa = 2, \\ \int_0^\infty \Xi(s_3) \prod_G e^{\Upsilon_{\mathrm{S}}(s_3,v)} f_{X_3^{\mathrm{S}}}(v) dv, & \text{if } \kappa = 3, \\ \int_0^\infty \int_v^{\frac{v}{\zeta}} \Xi(s_4) \prod_G e^{\Upsilon_{\mathrm{S}}(s_4,t)} f_{X_4^{\mathrm{S}},\widetilde{X}_4^{\mathrm{S}}}(v,t)\, dtdv, & \text{if } \kappa = 4, \\ \int_0^\infty \int_0^\infty \Xi(s_5) e^{\Upsilon_{\mathrm{M}}(s_5,v)} \prod_G e^{\Upsilon_{\mathrm{S}}(s_5,t)} f_{X_5^{\mathrm{M}},X_5^{\mathrm{S}}}(v,t)\, dtdv, & \text{if } \kappa = 5, \end{cases}$$

where

$$\Upsilon_i(s,\delta) = 2\pi\lambda_k \mu_k(p_G) \int_\delta^\infty \left(\left(\frac{1}{1 + s\mu_i(G) P_i r^{-a}} \right)^b - 1 \right) r \mu_k\left(e^{-\beta r}\right) dr, \tag{5.12}$$

$$\Xi(s) = \exp\left(-sb\sigma_n^2\right),$$

and

$$s = \{s_1, s_2, s_3, s_4, s_5\} = \left\{ \frac{\theta x_{\mathrm{M}}^a}{P_{\mathrm{M}}}, \frac{\theta P_{\mathrm{M}}^{-1}}{x_{\mathrm{M}}^{-a} + \widetilde{x}_{\mathrm{M}}^{-a}}, \frac{\theta x_{\mathrm{S}}^a}{P_{\mathrm{S}}}, \frac{\theta P_{\mathrm{S}}^{-1}}{x_{\mathrm{S}}^{-a} + \widetilde{x}_{\mathrm{S}}^{-a}}, \frac{\theta}{\frac{P_{\mathrm{M}}}{x_{\mathrm{M}}^a} + \frac{MP_{\mathrm{S}}}{x_{\mathrm{S}}^a}} \right\}.$$

Proof. Let $X_\kappa^{(i)}$ and $\widetilde{X}_\kappa^{(i)}$ be the random variables representing the distances between a user u within region-$\Re_\kappa$ and its serving and dominant interfering BSs from the i-th tier. Then, the cdf of these distances become

$$\begin{aligned} F_{X_\kappa^{(i)}}(v|\Re_\kappa) &= \frac{\mathbb{P}\left[X_\kappa^{(i)} > v, \Re_\kappa\right]}{\Psi_\kappa}, && \kappa = \{1,3\}, \\ F_{X_\kappa^{(i)},\widetilde{X}_\kappa^{(i)}}(v,t|\Re_\kappa) &= \frac{\mathbb{P}\left[X_\kappa^{(i)} > v, \widetilde{X}_\kappa^{(i)} > t, \Re_\kappa\right]}{\Psi_\kappa}, && \kappa = \{2,4\}, \\ F_{X_\kappa^{(i)},X_\kappa^{(j)}}(v,t|\Re_\kappa) &= \frac{\mathbb{P}\left[X_\kappa^{(i)} > v, X_\kappa^{(j)} > t, \Re_\kappa\right]}{\Psi_\kappa}, && \kappa = \{5\}, \end{aligned}$$

where $i \neq j$. Therefore, similar to the proof of Lemma 5.1, the pdf of the distances becomes

$$\begin{aligned} f_{X_\kappa^{(i)}}(v) &= \frac{d\left[1 - F_{X_\kappa^{(i)}}(v|\Re_\kappa)\right]}{dv}, && \kappa = \{1,3\}, \\ f_{X_\kappa^{(i)},\widetilde{X}_\kappa^{(i)}}(v,t) &= \frac{\partial\left[1 - F_{X_\kappa^{(i)},\widetilde{X}_\kappa^{(i)}}(v,t|\Re_\kappa)\right]}{\partial v \partial t}, && \kappa = \{2,4\}, \\ f_{X_\kappa^{(i)},X_\kappa^{(j)}}(v,t) &= \frac{\partial\left[1 - F_{X_\kappa^{(i)},X_\kappa^{(j)}}(v,t|\Re_\kappa)\right]}{\partial v \partial t}, && \kappa = \{5\}. \end{aligned}$$

Now, we analyze the conditional success probability $P_s^{(\kappa)}(\theta)$. Considering the case where a user is served from both the network tiers, i.e. $i \neq j$, the success probability given the PPP Φ, can be expressed as

$$P_s^{(5)}(\theta) = \mathbb{P}\left[\mathrm{SINR}_{\{i,j\}} > \theta | \Phi\right] = \mathbb{P}\left[\left|\sum_{k=i,j} \mu_k^{\frac{1}{2}}(Q) P_k^{\frac{1}{2}} \|x_k\|^{-\frac{a}{2}} h_{x_k}\right|^2 > \theta\left(I + \sigma_n^2\right)\right]$$

$$= \mathbb{E}_{h_y}\left[\exp\left(-s\left(\sum_k \sum_{y\in\Phi_k} I + \sigma_n^2\right)\right)\middle|\Phi\right] \tag{5.13}$$

$$\stackrel{(a)}{=} \exp\left(-s\sigma_n^2\right) \prod_k \prod_{y\in\Phi_k} \frac{1}{1 + s\mu_k(G) P_k \|y\|^{-a}}, \tag{5.14}$$

where $I = \sum_k \sum_{y\in\Phi_k} \mu_k(G) P_k \|y\|^{-a} |h_y|^2$ denotes the aggregate interference observed by the user, $s = \theta / \left(P_{\mathrm{M}} x_{\mathrm{M}}^{-a} + Q P_{\mathrm{S}} x_{\mathrm{S}}^{-a}\right)$ and (a) follows from the fact that $|h_y|^2$ are independent and identical distributed exponential random variables with unit mean. Hence, the b-th moments of the $P_s^{(5)}(\theta)$, are given by

$$M_b^{(5)}(\theta) = \int_0^\infty \left(\int_0^\infty \exp\left(-sb\sigma_n^2\right) \prod_k \mathbb{E}_{\Phi_k, G} \prod_{y\in\Phi_k} \left(\frac{1}{1 + \frac{s\mu_k(G)P_k}{\|y\|^a}}\right)^b f_{X_5^{\mathrm{M}}, X_5^{\mathrm{S}}}(v,t) dt \right) dv$$

$$\stackrel{(a)}{=} \int_0^\infty \left(\int_0^\infty \exp\left(-sb\sigma_n^2\right) e^{-2\pi\lambda_{\mathrm{M}} \int_v^\infty \left(1 - \left(\frac{1}{1+sP_{\mathrm{M}} r^{-a}}\right)^b\right) r dr} \right.$$

$$\left. \times \prod_G e^{-2\pi\lambda_{\mathrm{S}} p_G \int_t^\infty \left(1 - \left(\frac{1}{1+sGP_{\mathrm{S}} r^{-a}}\right)^b\right) r e^{-\beta r} dr} f_{X_5^{\mathrm{M}}, X_5^{\mathrm{S}}}(v,t) dt \right) dv,$$

where (a) follows from the probability generating functional of a homogeneous PPP Φ. By following a similar methodology as above, the b-th moments of the conditional success probability $P_s^{(\kappa)}(\theta)$ can be also derived, where $\kappa = \{1, \cdots, 5\}$. These proofs are omitted due to the limited available space. □

5.4.2 Beta Approximation of Meta-Distribution

As we previously mention, the numerical calculation of the exact meta-distribution is tedious. Fortunately, as authors showed in [177], the meta-distribution can approximated by matching its first and second moments to the Beta-distribution, resulting in a very tight approximation. The pdf of a random variable X that follows a Beta distribution with shape parameters $\gamma,\ \delta > 0$, is given by

$$f_X(x) = \frac{x^{\gamma-1}(1-x)^{\delta-1}}{B(\gamma,\delta)}, \tag{5.15}$$

where $B(\cdot,\cdot)$ represents the Beta function. The first and second moments of random variable X, are given by

$$M_1 = \frac{\gamma}{\gamma+\delta}, \quad M_2 = \frac{\gamma+1}{\gamma+\delta+1}. \tag{5.16}$$

Hence, the shape parameters of the beta-distribution can be re-written as

$$\gamma = \frac{M_1 M_2 - M_1^2}{M_1^2 - M_2}, \; \delta = \frac{(1-M_1)(M_2-M_1)}{M_1^2 - M_2}. \tag{5.17}$$

The following Theorem provides the meta-distribution of our proposed cooperation scheme for the considered network deployment.

Theorem 5.1. *The approximate meta-distribution for the HC scheme in the context of heterogeneous sub-6 GHz/mmWave cellular networks, is given by*

$$\bar{F}_{P_s(\theta)(x)} = 1 - \frac{1}{B(\gamma,\delta)} \int_0^x t^{\gamma-1}(1-t)^{\delta-1} dt. \tag{5.18}$$

5.5 Numerical Results

In this section, we provide numerical results to verify our model and illustrate the performance of our proposed scheme in heterogeneous sub-6 GHz/mmWave cellular networks. The spatial density of the MCell and the SCell tier is $\lambda_{\mathrm{M}} = 15$ BSs/km^2 and $\lambda_{\mathrm{S}} = 47$ BSs/km^2, respectively, with transmit power equal to $P_{\mathrm{M}} = 30$ dB and $P_{\mathrm{S}} = 20$ dB, respectively. The path loss exponent is set to $a = 4$ and the blockage constant to $\beta = 0.03$. The parameters for the sectorized antenna model are set to $Q = 10$ dB, $q = -10$ dB and $\phi = \frac{\pi}{6}$ [133]. Unless otherwise specified, we set $\zeta = 0.7$, $\eta = 6$ dB and $\sigma_n^2 = -60$ dB. Our results show the good agreement between the theoretical (solid and dashed lines) and the simulation (markers) results, validating our analysis.

Fig. 5.2 illustrates the network performance achieved with the utilization of both the proposed HC scheme and the conventional association scheme ($\zeta = 1$ and $\eta = 0$ dB). For each scheme, we plot the achieved meta-distribution versus the reliability threshold x, for different blockage constants. We can easily observe that, by increasing the blockage constant the achieved network performance decreases for both schemes. This observation is based on the fact that, by increasing the blockage density, the communication of the users with LoS BSs becomes impossible and thus the meta-distribution of the conditional success probability significantly decreases. An important observation from this figure is that, at low reliability threshold values,

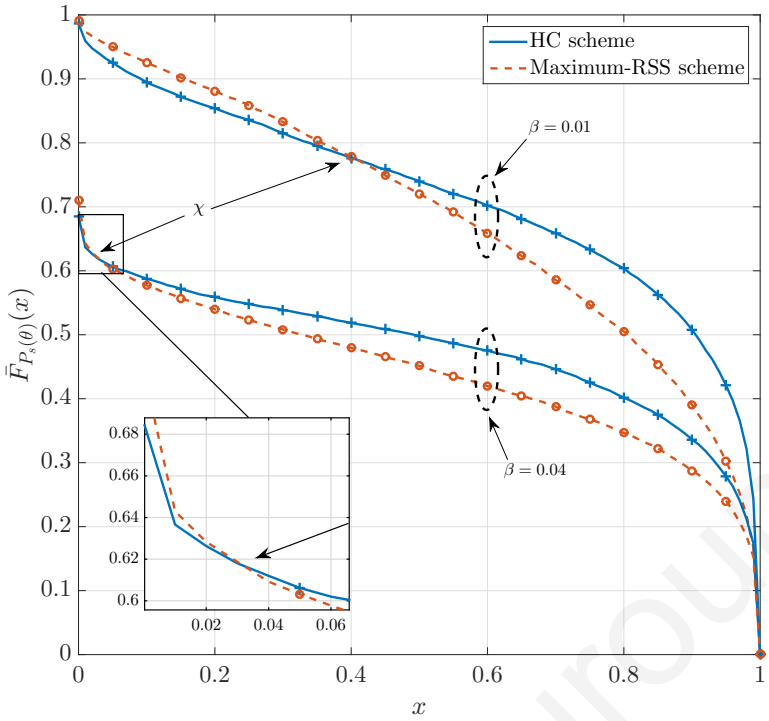

Figure 5.2: Meta-distribution versus x for the HC and maximum-RSS schemes for different β; $\theta = 0$ dB

the conventional scheme provides slightly better network performance compared to the proposed HC scheme. This was expected, since with the utilization of the conventional scheme, a user is served by a single BS and therefore the observed interference is caused by a single network tier. On the other hand, by utilizing the HC scheme, the observed interference can be caused by both network tiers, resulting in a reduced network performance. However, by increasing the reliability threshold beyond a critical point χ, our proposed scheme overcomes the conventional scheme, providing a significantly enhanced network performance. As expected, despite the strong interference observed in HC scheme, the cooperation technique allows a larger fraction of users to achieve the desired reliability given an SINR threshold, providing a significantly improved system performance. Finally, we can easily observe that the critical reliability threshold point χ, reduces with the increase of the blockage constant. It is straightforward that, by increasing the blockage constant, the observed interference is significantly mitigated for both schemes, allowing our proposed HC scheme to overcome the conventional association scheme in lower reliability threshold values, due to the implementation of the cooperation technique.

Fig. 5.3 highlights the impact of the range of the edge-regions on the network

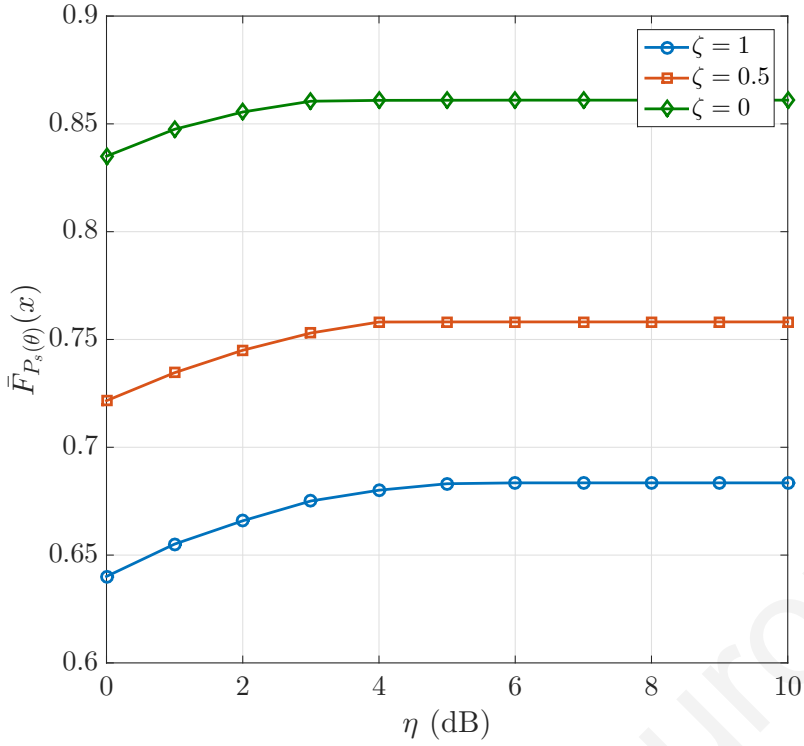

Figure 5.3: Meta-distribution versus η for for different ζ; $\theta = 0$ dB, $x = 0.5$

performance. Specifically, we plot the meta-distribution versus the bias factor η (dB) for different predefined fraction ζ. We can easily observe from the figure that, the meta-distribution increases as the bias factor η increases. This occurs since, larger bias factor leads to a larger edge-region, where a user can achieve higher signal power and lower interference through the implementation of the cooperation technique. Moreover, by further increasing the bias factor, the improvement on meta-distribution becomes marginal. This was expected, since for large bias factor, the signal strength from another BS is significantly weak and therefore, the joint transmission can be neglected. Regarding the predefined fraction ζ, it is clear that, by increasing the edge-region between BSs from a single tier, the achieved meta-distribution also increases due to the utilization of the cooperation technique.

5.6 Conclusion

In this chapter, we proposed a novel hybrid BS cooperation scheme in the context of heterogeneous multi-band cellular networks. Our proposed cooperation scheme exploits the ability of BSs to jointly transmit data in a coherent manner, aiming at enhancing the performance of the CEUs. Using stochastic geometry tools,

the b-th moment of the conditional success probability in the context of our proposed technique was derived in analytical expressions. Motivated by the tedious exact calculation of the meta distribution, an analytical yet simple approximation of the meta-distribution is calculated using the moment-matching method with the beta-distribution. Our numerical results reveals that the proposed HC scheme outperforms the conventional maximum RSS association scheme. A future extension of this work is the investigation of a general heterogeneous K-tier cellular network consisting of BSs that operate in different frequency bands and analyzing the effect of the height difference between the BSs.

Chapter 6

FD-JCAS techniques for mmWave HetNets: Ginibre point process modeling and analysis

In this chapter, we investigate the co-design of FD radio with JCAS techniques in mmWave HetNets. Particularly, we propose a novel cooperative detection technique, which exploits the sensing information from multiple remote radio units (RRUs), aiming at enhancing the detection performance. Three hard-decision combining rules are considered, namely the *OR*, the *Majority* and the *AND* rule. In real-world network scenarios, the locations of the RRUs are spatially correlated, exhibiting a repulsive behavior. Therefore, we model the spatial distribution of the RRUs as a β-GPP, which can characterize the repulsion among the RRUs. By using stochastic geometry tools, analytical expressions for the detection performance of β-GPP-based FD-JCAS systems are expressed for each of the considered combining rule. Furthermore, by considering temporal interference correlation, we evaluate the probability of successfully detecting a target over two different time-slots, and provide analytical expressions for each combining rule.

6.1 Motivation and Contribution

Emerging applications such as smart cars, UAV and enhanced localization, lead to an ever-increasing demand for systems with both communication and radar sensing capabilities [25, 178, 179]. In order to address this demand, JCAS techniques have

been developed, integrating the two operations of communication and sensing over a shared spectrum. The concept of radar sensing refers to the use of radio signals in order to retrieve short-range environmental information through measuring various parameters, such as an object's location, moving speed, and shape [180]. As an emerging research topic, the spectrum sharing of JCAS techniques enables the efficient use of the available spectrum, and provides a new way for designing and modeling novel network architectures and protocols that can benefit from the synergy of communication and radar systems.

The main challenge for the joint operation of communication and radar sensing systems over a shared spectrum is the negative effects of the mutual interference between the two systems, which significantly alleviates the network performance [181]. Therefore, the employment of interference mitigation techniques is of paramount importance in the context of JCAS systems. Nevertheless, the exploitation of cooperative techniques aiming to mitigate the overall interference and enhance the network's detection performance is missing from the current literature.

Efficient spectrum utilization is another key issue for JCAS systems that needs to be addressed. Spectrum efficiency in wireless communication systems can be significantly improved by operating in a FD mode, which is being considered for the next-generation wireless systems. However, as we mentioned in the previous Section, the performance of FD radio in large-scale multi-cell networks is also compromised by the increase of the intra- and out-of-cell co-channel interference. Several research efforts have been carried out to study the effect of multi-user interference on the FD performance for large-scale wireless networks, and several techniques have been proposed to mitigate the additional interference caused by the FD operation [163, 182].

The requirements of next generation cellular networks in massive connectivity and high throughput, motivate the operation of mmWave frequency bands and their heterogeneous deployment. MmWave communications are considered as a suitable environment for integrating FD-JCAS systems due to their unique features, such as the large available bandwidth and the antenna directivity, which can boost the quality of the direct link [178]. In particular, the large available bandwidth of mmWave communications can lead to multi-Gbps rates, which is essential to satisfy the high-capacity requirements of emerging applications in FD-JCAS systems, such as fully-connected vehicles, UAV and robotics [183]. Furthermore, recent studies

have shown that the higher path-losses of the mmWave signals and their sensitivity to blockages, can improve the network performance by mitigating the overall interference [84, 184]. Therefore, the modeling and the analysis of FD-JCAS systems in the context of mmWave cellular networks, is of critical importance in order to support the massive data-rate demands of emerging applications and combat the severe multi-user interference. Even though FD-JCAS systems are well-investigated for sub-6 GHz applications, few works deal with their operation in higher frequency bands, which neglect the negative effects of the SI link on the overall network performance.

Although the PPP has been widely adopted as a model for wireless networks due to its analytical tractability, it fails to characterize the correlation among the locations of the network's nodes, since the nodes are located independently of each other. However, in many practical networks, the locations of the nodes are determined to alleviate the interference or extend the coverage region, and therefore there exists a form of repulsion among the network's nodes. Recently, the GPP [47], which is a type of repulsive point process with analytical tractability, has been advocated to model random phenomena where repulsion is observed. Existing studies have applied the GPP [50], the α-GPP [67], and the β-GPP [185] for modeling the spatial distribution of base stations in conventional wireless networks, analyzing the impact of repulsion between the network's nodes on the achieved performance. In addition to the spatial correlation between the network's nodes, the presence of common randomness in the locations of the interfering nodes induces temporal correlation in the observed interference [186]. Although there has been substantial work quantifying interference correlation in wireless network [186, 187], the investigation of temporal correlation in FD-JCAS systems has been disregarded.

To the best of our knowledge, the spectrum co-existence of FD-JCAS systems in the context of heterogeneous mmWave cellular networks, where the network's nodes experience a repulsion between each other, is overlooked from the literature. In addition, the effect of SI and temporal interference correlation on the achieved performance of the FD-JCAS deployments has not been investigated. Therefore, the aim of this work is to fill this gap by modeling and analyzing such networks and by providing new analytical results for the network performance in a stochastic geometry framework.

The main contributions of this chapter are summarized as follows:

- We develop a novel analytical framework based on stochastic geometry, which comprises the modeling of spectrum sharing FD-JCAS systems in the context of HetNets-mmWave. In particular, we consider a JCAS system, where all RRUs exhibit detection capabilities, of which a fraction also exhibit DL communication capabilities by exploiting the concept of FD radio. We assume that all network's nodes employ directional antennas, whose communication and radar sensing signals are affected by the presence of blockage effects. In addition, since real network deployments form a more regular point pattern than the PPP, the developed framework takes into account the correlation among the locations of the RRUs by modeling their spatial distribution as a β-GPP.

- A novel cooperative multi-point radar detection (CoMRD) technique is proposed, aiming at providing an enhanced detection performance. In particular, our proposed technique exploits the sensing information from a set of preselected RRUs, consisting of the closest RRU to the target from each network tier, in order to alleviate the overall interference of the network. Three hard-decision combining rules, namely the *OR*, the *Majority* and the *AND* rules, are analyzed. Analytical expressions for the detection performance are derived for each of the considered hard-decision combining rules. Moreover, since the β-GPP includes the PPP ($\beta \to 0$) as a special case, we derive simplified analytical expressions for the scenario where the RRUs are independently deployed within the network area. In addition to the spatial correlation of the RRUs, the temporal correlation of the observed interference is also investigated, and analytical expressions of the joint detection probability over different time slots are derived. The derived analytical expressions provide a quick and convenient methodology of evaluating the system's performance and obtaining insights into how key parameters affect the performance.

- The behavior of the detection performance achieved by our proposed technique for the considered combining rules is analyzed for different system parameters such as the total number of network tiers, the repulsion parameter, the blockage density and the fraction of JCAS-enabled RRUs. We demonstrate that our cooperative technique can significantly improve the detection performance in the context of the considered network deployments, when compared to the conventional non-cooperative radar detection technique. In addition, our nu-

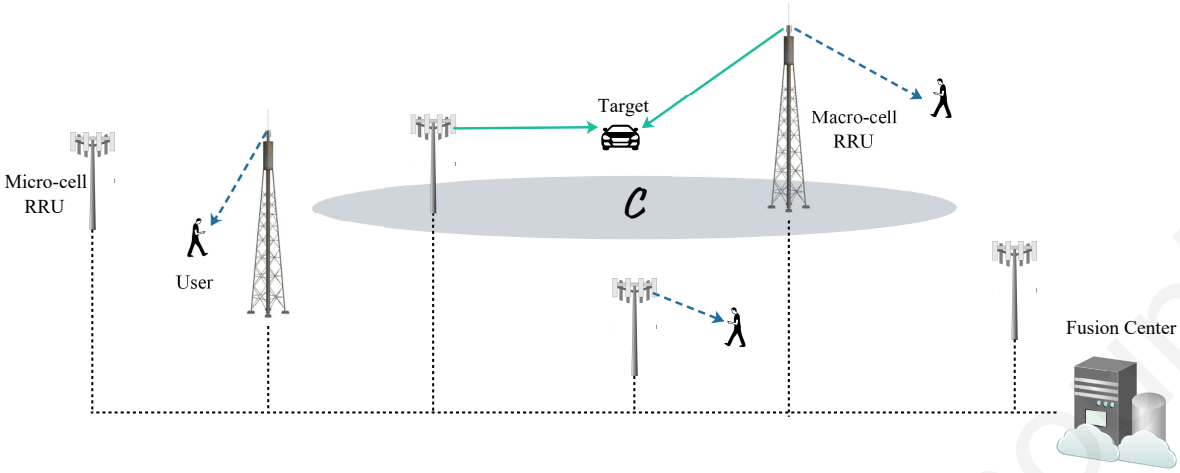

Figure 6.1: Network topology of a two-tier FD-JCAS system in mmWave cellular networks.

merical results illustrate that a repulsive deployment of RRUs is beneficial for the detection performance, since by increasing the distance of an interfering link results in a reduction of the caused interference. We also demonstrate the negative effects of the blockages and the residual SI on the detection performance. Furthermore, we show that the temporal interference correlation significantly impacts the network's detection performance.

6.2 System model

In this section, we provide details of the considered system model. The network is studied from a large-scale point-of-view leveraging tools from stochastic geometry. In order to model and analyze the spectral coexisting communication and radar systems in the context of heterogeneous mmWave cellular networks, an FD-JCAS system is investigated, where the mmWave RRUs have two operations i.e., DL transmission and target detection.

6.2.1 Topology model

In this context, we model the spatial distribution of the RRUs that belong to the k-th tier i.e., $k = \{1, \cdots, \eta\}$, according to a β-GPP denoted as $\Phi_k = \{X_{j,k} \in \mathbb{R}^2, j \in \mathbb{N}^+\}$ with density λ_k and repulsion parameter β_k i.e., $\Phi_k \sim \text{GPP}(\lambda_k, \beta_k)$. We assume that the RRUs are connected to a central unit, also known as fusion center (FC), through an ideal report channel [188]. We denote by $\mathcal{C}$, the set of η cooperative RRUs,

that share their sensing information to the FC for the cooperative detection of a target. We assume that the locations of the targets follow a PPP Φ_t with spatial density $\lambda_t \ll \sum_{k=1}^{\eta} \lambda_k$. Note that, within this chapter, we investigate the detection of a target, which may be a building, a user, an obstacle, etc, depending on the considered application. In addition to the target detection, a fraction of RRUs is also exhibits communication capabilities, serving their associated users in the DL direction by implementing the FD-JCAS scheme. Specifically, an RRU that belongs to the k-th tier, exhibits both communication and radar sensing capabilities based on a predefined probability χ_k, otherwise, it solely exhibits sensing capabilities. Fig. 6.1 shows a realization of a two-tier mmWave cellular network i.e, $\eta = 2$, consisting of macro-cell and micro-cell RRUs, where solid and dashed lines represent the radar sensing and the communication signals of an RRU, respectively. In addition, the set of η cooperative RRUs is illustrated with a shaded area. Based on the stationarity of the β-GPP and without loss of generality [47], we assume the existence of a typical target at the origin.

We adopt a blockage model for modeling the sensitivity of the mmWave signals to the existence of blockages. In particular, we consider the generalized *LoS ball* model proposed in [115], where a link of length R is in LoS state with probability $p(R) = p_{\text{LoS}} \mathbb{1}_{R \leq \Re}$. In this chapter, the interference effect from the NLoS signals is ignored, as we assume the dominant interference is caused by the LoS signals [115]. Regarding modeling the antenna directionality of the RRUs, we adopt an ideal cone antenna pattern [188]. The antenna array gain is parameterized by two values: 1) the main-lobe beamwidth $\phi \in [0, 2\pi]$, and 2) the main-lobe gain G (dB). We assume that perfect beam alignment can be achieved for the links between each target and its cooperative RRUs, using the estimated angles of arrival. Similarly, perfect beam alignment can be also achieved for each user and its serving RRU. On the other hand, the beams of interfering links are assumed to be randomly oriented with respect to each other.

It is important to mention that, an interfering RRU causes interference to another node only if the alignment of their two randomly oriented antenna patterns overlap and their link is LoS; by simple geometrical arguments, this event has probability, $\frac{\phi}{2\pi} p_{\text{LoS}}$. Thus, for each β-GPP Φ_k, where $k = \{1, \cdots, \eta\}$, the active interfering RRUs from that network tier form a β-GPP $\widetilde{\Phi}_k$ with inhomogeneous density function $\widetilde{\lambda}_k(r) = \lambda_k p_{\text{LoS}} \frac{\phi}{2\pi} \mathbb{1}_{r \leq \Re}$ and repulsion parameter β_k i.e., $\widetilde{\Phi}_k \sim \text{GPP}\left(\widetilde{\lambda}_k(r), \beta_k\right)$ [47]. In the context

of the considered system model and based on Section 2.4.3, we denote as $\{\Xi_{j,k}\}_{j\in\mathbb{N}^+}$, the set of discrete random variables for the k-th tier, such that $\mathbb{P}\left(\Xi_{j,k}=1\right)=\beta_k$ and $\mathbb{P}\left(\Xi_{j,k}=0\right)=1-\beta_k$. In addition, for $\widetilde{\Phi}_k$, we define a set of independent Gamma random variables $\{B_{j,k}\}_{j\in\mathbb{N}^+}$, where $B_{j,k}\sim\mathcal{G}\left(j,\beta_k/\left(\pi\widetilde{\lambda}_k(y)\right)\right)$ and $\widetilde{\lambda}_k(y)=\lambda_k p_{\text{LoS}}\frac{\phi}{2\pi}\mathbb{1}_{y\leq\sqrt{\Re}}$. Based on the aforementioned, the pdf of $B_{j,k}$ for the k-th tier is given by the Proposition 2.1.

6.2.2 Channel and power control model

All wireless signals are assumed to experience both large-scale path-loss effects and small-scale fading. We assume that the small-scale fading between two nodes is modeled by Rayleigh fading, where different links are assumed to be independent and identically distributed. Hence, the power of the channel fading at the time slot τ is an exponential random variable with unit mean i.e., $h_\tau\sim\exp(1)$. For the large-scale path-loss between nodes X and Y, we assume a bounded path-loss model, $L(X,Y)=1/\left(\epsilon+\|X-Y\|^a\right)$, where $a>2$ denotes the path-loss exponent and $\epsilon>0$. For simplicity, the path-loss between the node X and the origin is denoted as $L(X)$ i.e., $L(X,0)=L(X)$. The spectrum co-existence of radar and communication systems using non-orthogonal channels causes the existence of SI between the output and the input antennas of the communication and radar systems, respectively. Regarding the channel between radar and communication antennas, we assume that the RRUs employ imperfect cancellation mechanisms [182]. As such, we consider that the residual SI channel coefficient follows a Nagakami-μ distribution with parameters $\left(\mu,\sigma^2_{\text{SI}}\right)$, where $1/\sigma^2_{\text{SI}}$ characterizes the SI cancellation capability of the RRUs. Therefore, the power gain of the residual SI channel follows a Gamma distribution [182] with mean μ and variance σ^2_{SI}/μ i.e., $g_{\text{SI}}\sim\mathcal{G}\left(\mu,\frac{\sigma^2_{\text{SI}}}{\mu}\right)$.

We assume that all RRUs that belong to the k-th tier, where $k=\{1,\cdots,\eta\}$, are allocated with the same transmit power P_k, where $P_k>P_i$ for $k<i$. Due to the overwhelming negative effect of the SI at the radar's receive antenna, the DL power control for the communication system is of paramount importance. Hence, we assume that all RRUs which implement the FD-JCAS scheme, utilize distance-proportional fractional power control for their DL communication with their associated LoS user, which is located at a fixed distance R. The power control scheme aims at compensating the large-scale path-loss and maintaining the average received signal power

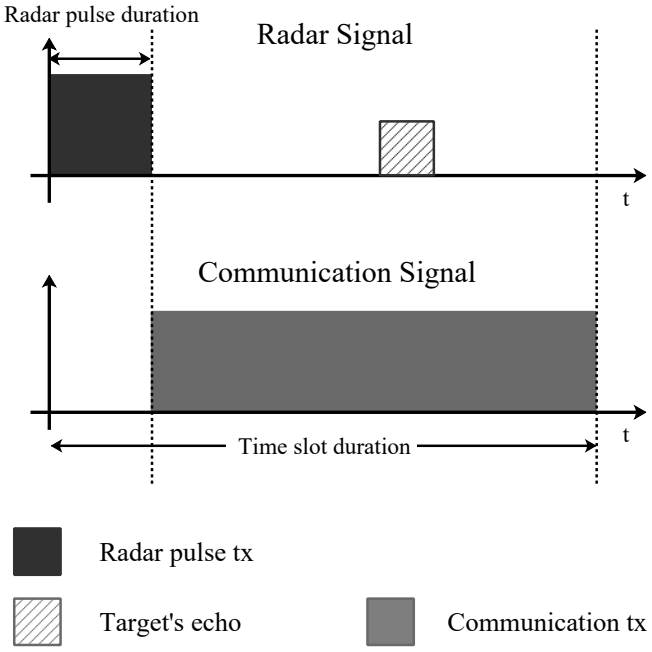

Figure 6.2: The considered FD-JCAS scheme. The first row is the transmitted radar signal and the echo from a target. The second row is the transmitted communication signal.

at their associated LoS user equal to ρ [163]. To accomplish this, an RRU which is at a distance R from its associated LoS user and with path-loss equal to $1/(\epsilon + R^a)$, adapts its transmitted signal power to $\rho\,(\epsilon + R^a)^{\varepsilon}$, where $0 \leq \varepsilon \leq 1$ is the power control fraction. Based on the general power control mechanism, the transmission power allocated to an RRU that belongs in the k-th tier, can be expressed as $\widetilde{P}_k(R) = \min\{\rho\,(\epsilon + R^a)^{\varepsilon}\,,\ P_k\}$, where the RRUs which are unable to fully invert the path-loss, transmit with maximum power P_k. For the detection system, we consider a fixed power transmission allocation scheme i.e., RRUs from the k-th tier transmit with power P_k.

6.2.3 Detection model

As shown in Fig. 6.2, at the beginning of the considered time slot τ, we assume that all cooperative RRUs firstly broadcast a narrow pilot sequence towards their main-lobe direction. Over the subsequent time slot, the cooperative RRUs measure the reflected signal power received within their main-lobe direction. If a cooperative RRU implements the FD-JCAS scheme, this particular RRU also performs DL transmission to satisfy its associated user (see details in Section 6.2.4). Let $\mathrm{SINR}^{\tau}_{j,k}$ represents the effective SINR of the target detection process for the cooperative RRU

$X_{j,k} \in \widetilde{\Phi}_k$, where $j \in \mathbb{N}^+$, at the time slot τ. Then, the SINR of the reflected signal power, is given by

$$\mathrm{SINR}_{j,k}^{\tau} = \frac{\mathcal{S}(X_{j,k}, \tau)}{\mathcal{I}(X_{j,k}, \tau) + I_{\mathrm{SI}}(R, k)\, \mathbb{1}_{\mathrm{JCAS}} + \sigma_n^2}, \tag{6.1}$$

where $\mathcal{S}(X_{j,k}, \tau)$ represents the reflected signal power received at the cooperative RRU $X_{j,k}$, and is equal to $\mathcal{S}(X_{j,k}, \tau) = P_k G^2 \frac{A\ell}{4\pi} h_\tau L^2\left(X_{j,k}\right) \mathbb{1}_{\|X_{j,k}\| \leq \Re}$ based on the well-known range equation [188]; $\ell = c/(4\pi f)^2$, where c is the speed of light, f is the carrier frequency and A is the cross-section area of the typical target; $\mathbb{1}_{\|X_{j,k}\| \leq \Re}$ is the indicator function that models the LoS region, and σ_n^2 denotes the variance of the thermal noise. Moreover, $\mathbb{1}_{\mathrm{JCAS}}$ represents the indicator function of the event "the cooperative RRU $X_{j,k}$ implements the FD-JCAS scheme". Due to the non-orthogonal operation of communication and radar systems, the residual SI observed at the receive antenna of the radar system after the SI cancellation is equal to $I_{\mathrm{SI}}(R, k) = \widetilde{P}_k(R)\, g_{\mathrm{SI}} = \min\{\rho\left(\epsilon + R^a\right)^{\varepsilon}, P_k\} g_{\mathrm{SI}}$, where g_{SI} represents the power gain of the residual SI channel. Regarding the observed interference at the time slot τ i.e., $\mathcal{I}(X_{j,k}, \tau)$, the cooperative RRU at $X_{j,k} \in \widetilde{\Phi}_k$, receives the aggregated interference caused by the nearby RRUs $X_{i,z} \in \widetilde{\Phi}_z$, where $z = \{1, \cdots, \eta\}$. Based on Campbell's theorem [47] and with the aid of the motion-invariant property of the β-GPP [47], we focus on the interference at the cooperative RRU's location $X_{j,k} \in \widetilde{\Phi}_k$, but without considering its contribution to the interference. Specifically, the overall interference observed by the cooperative RRU $X_{j,k}$ at the time slot τ, can be expressed as

$$\mathcal{I}\left(X_{j,k}, \tau\right) = \sum_{z=1}^{\eta} \sum_{i \in \mathbb{N}^+} P_z G^2 \ell g_\tau L\left(X_{i,z}\right) \mathbb{1}_{\|X_{i,z}\| \leq \Re}, \tag{6.2}$$

where g_τ denotes the channel power of the link between the interfering and the cooperative RRUs at the considered time slot τ.

6.2.4 Communication model

Each cooperative RRU implementing the FD-JCAS scheme, performs DL transmission to satisfy its associated user, which is located at a fixed distance R. Regarding the observed interference of a user, we assume that the interference caused by the neighboring targets due to the reflected radar signals is negligible and the dominant interference is caused by the RRUs. This is based on the fact that, the decay of the reflected signal power is higher than the decay of an interfering signal power caused

by an RRU, due to the larger distance the reflection signal must travel. Without loss of generality and by following Slivnyak's theorem, the analysis concerns the typical user located at the origin but the results hold for all nodes of the network. Let $\mathrm{SINR}_k^{\mathrm{D}}$ represents the DL SINR observed by the typical user at the time slot τ, which is associated with a cooperative RRU $X_{j,k} \in \widetilde{\Phi}_k$, where $\|X_{j,k}\| = R$, and is given by

$$\mathrm{SINR}_k^{\mathrm{D}} = \frac{\widetilde{P}_k(R) G^2 \widetilde{h}_\tau L(R)}{\sum\limits_{i \in \mathbb{N}^+ \setminus j} \widetilde{P}_k(R) G^2 \widetilde{g}_\tau L(X_{i,k}) \mathbb{1}_{\mathrm{JCAS}} + \sum\limits_{\substack{z=1 \\ z \neq k}}^{\eta} \sum_{i \in \mathbb{N}^+} \widetilde{P}_z(R) G^2 \widetilde{g}_\tau L(X_{i,z}) \mathbb{1}_{\mathrm{JCAS}} + \sigma_n^2},$$

where $\widetilde{h}_\tau$ and $\widetilde{g}_\tau$ are the power gain of the channels between the typical user and its serving and its interfering RRUs, respectively, and $\widetilde{P}_k(R)$ denotes the transmission power allocated to an RRU that belongs in the k-th tier, based on the power control mechanism. Hence the DL coverage probability of the typical user i.e., $\mathbb{P}[\mathrm{SINR}^{\mathrm{D}} > \theta]$, is evaluated in the following proposition [68].

Proposition 6.1. *The DL coverage probability of the typical user, is given by*

$$\mathbb{P}[\mathrm{SINR}_k^{\mathrm{D}} > \theta] = \exp\left(-\frac{\theta(\epsilon + R^a)\sigma_n^2}{\widetilde{P}_k(R) G^2}\right) \prod_{i \in \mathbb{N}^+} \left(1 - \beta + \int_{\sqrt{R}}^{\sqrt{\Re}} \frac{\beta f_{B_{i,k}}(y)}{1 + \frac{s\widetilde{P}_k(R) G^2}{\left(\epsilon + y^{\frac{a}{2}}\right)}} dy\right)$$
$$\times \prod_{\substack{z=1 \\ z \neq k}}^{\eta} \prod_{i \in \mathbb{N}^+} \left(1 - \beta + \int_{0}^{\sqrt{\Re}} \frac{\beta f_{B_{i,z}}(y)}{1 + \frac{s\widetilde{P}_z(R) G^2}{\left(\epsilon + y^{\frac{a}{2}}\right)}} dy\right),$$

where $f_{B_{i,k}}(u)$ represents the pdf of the β-GPP distributed points, which is given in Proposition 2.1.

In the context of β-GPP deployments, the DL coverage performance is a well-investigated metric within the literature [47, 67, 68]. Therefore, the focus of this chapter lies in evaluating the achieved detection performance of the FD-JCAS systems for the considered network deployments, where the communication operation is indicated by the existence of the residual SI at the cooperative JCAS-enabled RRUs.

6.3 Cooperative multi-point radar detection technique

In this section, we introduce the proposed CoMRD technique in the context of heterogeneous mmWave cellular networks. Our technique exploits the cooperation among

randomly located RRUs that belong in different network tiers, aiming at enhancing the network's detection performance. Specifically, our proposed technique is based on a two-level procedure: (*i*) pre-selection phase, and (*ii*) decision phase, which are described in detail in the following discussion. In addition, analytical expressions are derived which will be useful for evaluating the network's detection performance in Section 6.4. Throughout this chapter, we will denote by r_u the distance between the origin and an RRU that belongs to the k-th tier and is located at $u \in \widetilde{\Phi}_k$ i.e., $r_u = \|u\|$.

6.3.1 Pre-selection Phase

Initially, a set of cooperative RRUs is pre-selected, consisting of the η RRUs that satisfy the rules of the adopted pre-selection policy. Specifically, according to the rules of the adopted pre-selection policy, from each network tier $k \in \{1, \cdots \eta\}$, a single RRU is selected, denoted as $X_k^* \in \widetilde{\Phi}_k$. Hence, the set defined by the pre-selected RRUs from all network tiers, represents the set of cooperative RRUs for the target detection i.e., $C = \{X_k^*, k \in \{1, \cdots, \eta\}\} \subset \cup_{k=1}^{\eta} \widetilde{\Phi}_k$.

In this chapter, we consider the case where the set of cooperative RRUs for the detection of their associated target, consists of the closest LoS RRU to the target from each network tier. This pre-selection policy requires an a priori knowledge of the location of the RRUs, which can be obtained by monitoring the location of the RRUs through a low-rate feedback channel or by a global positioning system mechanism. Hence, the set of η cooperative RRUs, is defined as

$$C = \left\{ X_k^* : X_k^* = \underset{X_{j,k} \in \widetilde{\Phi}_k}{\arg\min} \|X_{j,k}\|, k = \{1, \cdots, \eta\}, j \in \mathbb{N}^+ \right\}, \tag{6.3}$$

where X_k^* represents the location of the closest LoS RRU to the target from the k-th tier. It is worth mentioning that, the adopted pre-selection policy is ideal for scenarios with low mobility, since it does not consider instantaneous fading.

6.3.2 Decision Phase

At the second-level phase, each cooperative RRU takes an independent binary decision regarding the presence of a target based on the observed SINR. Let $\mathcal{H}_0$ and $\mathcal{H}_1$ represent the hypotheses made by each cooperative RRU, when it senses the

absence and the presence of the typical target, respectively. In particular, the cooperative RRU at $X_k^* \in C$ from the k-th tier selects the hypothesis $\mathcal{H}_1$, when the observed SINR exceeds a pre-defined threshold ϑ i.e., $\text{SINR}_{j,k}^{\tau} \geq \vartheta$; otherwise, the cooperative RRU selects the hypothesis $\mathcal{H}_0$. Hence, the binary decision of the cooperative RRU at X_k^*, is defined as

$$\delta_k = \begin{cases} 0, & \text{if } \mathcal{H}_0 \text{ holds,} \\ 1, & \text{if } \mathcal{H}_1 \text{ holds,} \end{cases} \tag{6.4}$$

where $k = \{1, \cdots, \eta\}$.

Thereafter, all local sensing informations from the cooperative RRUs are shared to the FC via an ideal report channel. In order to enhance the overall detection capability of the considered network deployment, the FC makes the final decision by combining all sensing information based on an adopted hard-decision combining rule. Specifically, the FC makes its decision according to the number of RRUs claiming the presence of their associated target. We adopt a generic κ-out-of-η combining rule, where the FC decides that the typical target is present, if and only if the κ or more cooperative RRUs decide the hypothesis $\mathcal{H}_1$. Hence, the final decision of the FC at the time slot τ, conditioned on the cooperative RRUs' locations, is given by

$$\mathcal{P}_d(\vartheta, \kappa, \tau | \mathbf{r}_{X^*}) = \sum_{t=\kappa}^{\eta} \binom{\eta}{t} \prod_{k=1}^{\eta} \mathcal{P}_d^k(\vartheta, \tau | r_{X_k^*})^{\delta_k} \left(1 - \mathcal{P}_d^k(\vartheta, \tau | r_{X_k^*})\right)^{1-\delta_k}, \tag{6.5}$$

where $\kappa \in \mathbb{N}^+$, $\mathbf{r}_{X^*} = \{r_{X_1^*}, \cdots, r_{X_\eta^*}\}$ represents the set of the distances between the typical target and its cooperative RRU from each tier, and $\mathcal{P}_d^k(\vartheta, \tau | r_{X_k^*})$ is the conditional detection probability achieved by the cooperative RRU that belongs to the k-th tier. In this chapter, we assume that the typical target is successfully detected from its cooperative RRU from the k-th tier, if the effective SINR observed at the particular cooperative RRU is greater than a pre-defined threshold ϑ i.e., $\mathcal{P}_d^k(\vartheta, \tau | r_{X_k^*}) = \mathbb{P}\left[\text{SINR}_{j,k}^{\tau} \geq \vartheta\right]$ [48, 74]. Note that, δ_k is the detection decision of the cooperative RRU at $X_k^* \in C$ for the considered combination. It is important to mention here that, if $\kappa = \left\lceil \frac{\eta}{2} \right\rceil$, the rule is referred as the *Majority rule*, if $\kappa = 1$, the rule is referred as the *OR rule*, and if $\kappa = \eta$, the rule is referred as the *AND rule*.

6.4 Detection Performance with CoMRD technique

In this section, we analyze the SINR distribution for the considered mmWave heterogeneous cellular network, where the RRUs from the k-th tier are deployed based on a β-GPP with repulsion parameter β_k, where $k \in \{1, \cdots, \eta\}$. We first define the SINR complementary cumulative distribution function (ccdf), and then the Laplace transform of the overall interference function is characterized. Without loss of generality and following Slivnyak's theorem [47], we execute the analysis for the typical target located at the origin but the results hold for any target in the network. Using the proposed CoMRD technique that is described in the previous section, the network's detection performance of each hard-decision rule is derived analytically by using stochastic geometry theory.

For the considered network deployment, the reflected signal power received at the cooperative RRU $X_{j,k}$ from the k-th tier at time slot τ, can be expressed as

$$\mathcal{S}(\widetilde{B}_{j,k}, \tau) = P_k \omega h_\tau L^2 \left(\widetilde{B}_{j,k}^{\frac{1}{2}}\right) \mathbb{1}_{\widetilde{B}_{j,k} \leq \sqrt{\Re}} = P_k \omega h_\tau L^2 \left(B_{j,k}^{\frac{1}{2}}\right) \Xi_{j,k} \mathbb{1}_{B_{j,k} \leq \sqrt{\Re}}, \tag{6.6}$$

and the observed interference caused by the nearby active interfering RRUs at time slot τ, can be re-written as

$$\begin{aligned} \mathcal{I}\left(\widetilde{B}_{j,k}, \tau\right) &= G^2 \ell g_\tau \sum_{z=1}^{\eta} \sum_{i \in \mathbb{N}^+} P_z L\left(\widetilde{B}_{i,z}^{\frac{1}{2}}\right) \mathbb{1}_{\widetilde{B}_{i,z} \leq \sqrt{\Re}} \\ &= G^2 \ell g_\tau \sum_{z=1}^{\eta} \sum_{i \in \mathbb{N}^+} P_z L\left(B_{i,z}^{\frac{1}{2}}\right) \Xi_{i,z} \mathbb{1}_{B_{i,z} \leq \sqrt{\Re}}, \end{aligned} \tag{6.7}$$

where $k, z \in \{1, \cdots, \eta\}$, $i, j \in \mathbb{N}^+$, $\Xi_{j,k}$ denotes the discrete random variable of the j-th RRU from the k-th tier, i.e $\Xi_{j,k} = \{0, 1\}$, and $\Re$ represents the radius of the LoS region. The following lemma provides the detection probability, $\mathcal{P}_d^k(\vartheta, \tau | B_{j,k})$, achieved by the cooperative RRU $X_{j,k} \in \widetilde{\Phi}_k$ at the time slot τ, in the context of heterogeneous mmWave cellular networks, where the RRUs are deployed based on a β-GPP.

Lemma 6.1. *The conditional detection probability achieved by the cooperative RRU at $X_{j,k} \in \widetilde{\Phi}_k$ at the time slot τ, where the RRUs are distributed according to a β-GPP, is given by*

$$\mathcal{P}_d^k(\vartheta, \tau | B_{j,k}) = \beta_k \exp\left(-s\sigma_n^2\right) \mathcal{L}_I(s, \tau) \left(\chi_k \mathcal{L}_{\mathrm{I_{SI}}}(s) + 1 - \chi_k\right), \tag{6.8}$$

where $\mathcal{L}_I(s, \tau)$ represents the Laplace transform of the overall interference function at the

time slot τ, and is given by

$$\mathcal{L}_{\mathcal{I}}(s,\tau) = \prod_{z=1}^{\eta} \prod_{i\in\mathbb{N}^+} \left(1 - \beta + \int_0^{\sqrt{\Re}} \frac{\beta f_{B_{i,z}}(y)}{1 + \frac{sP_z G^2 \ell}{\left(\epsilon + y^{\frac{a}{2}}\right)}} dy\right), \tag{6.9}$$

and the Laplace transform of the SI, $\mathcal{L}_{I_{\mathrm{SI}}}(s)$, can be expressed as

$$\mathcal{L}_{I_{\mathrm{SI}}}(s) = \left(\frac{\mu}{\mu + s\sigma_{\mathrm{SI}}^2 \min\{\rho\left(\epsilon + R^a\right)^{\varepsilon}, P_k\}}\right)^{\mu}, \tag{6.10}$$

where $s = \frac{\vartheta\left(\epsilon + B_{j,k}^{\frac{a}{2}}\right)^2}{P_k\omega}$ and $f_{B_{j,k}}(u)$ represents the pdf of the β-GPP distributed points, which is given in Proposition 2.1.

Proof. Conditioned on whether the considered RRU $X_{j,k}$ implements the FD-JCAS scheme or not, its achieved detection performance, conditioned on its location, can be expressed as

$$\begin{aligned}
\mathcal{P}_d^k(\vartheta,\tau|B_{j,k}) &= \chi_k \mathbb{P}\left[\frac{P_k\omega h_\tau \left(\epsilon + B_{j,k}^{\frac{a}{2}}\right)^{-2}}{\mathcal{I}(B_{j,k},\tau) + I_{\mathrm{SI}}(R,k) + \sigma_n^2} \geq \vartheta\right] \\
&\quad + (1-\chi_k)\mathbb{P}\left[\frac{P_k\omega h_\tau \left(\epsilon + B_{j,k}^{\frac{a}{2}}\right)^{-2}}{\mathcal{I}(B_{j,k},\tau) + \sigma_n^2} \geq \vartheta\right] \\
&= \chi_k \mathbb{P}\left[\frac{P_k\omega h_\tau \left(\epsilon + B_{j,k}^{\frac{a}{2}}\right)^{-2}}{\mathcal{I}(B_{j,k},\tau) + I_{\mathrm{SI}}(R,k) + \sigma_n^2} \geq \vartheta | \Xi_{j,k} = 1\right] \mathbb{P}[\Xi_{j,k} = 1] \\
&\quad + (1-\chi_k)\mathbb{P}\left[\frac{P_k\omega h_\tau \left(\epsilon + B_{j,k}^{\frac{a}{2}}\right)^{-2}}{\mathcal{I}(B_{j,k},\tau) + \sigma_n^2} \geq \vartheta | \Xi_{j,k} = 1\right] \mathbb{P}[\Xi_{j,k} = 1] \\
&= \chi_k\beta_k \mathbb{P}\left[h_\tau \geq \frac{\vartheta\left(\epsilon + B_{j,k}^{\frac{a}{2}}\right)^2}{P_k\omega}\left(\mathcal{I}(B_{j,k},\tau) + I_{\mathrm{SI}}(R,k) + \sigma_n^2\right)\right] \\
&\quad + (1-\chi_k)\beta \mathbb{P}\left[h_\tau \geq \frac{\vartheta\left(\epsilon + B_{j,k}^{\frac{a}{2}}\right)^2}{P_k\omega}\left(\mathcal{I}(B_{j,k},\tau) + \sigma_n^2\right)\right] \qquad (6.11) \\
&= \chi_k\beta_k \exp\left(-\frac{\vartheta\sigma_n^2\left(\epsilon + B_{j,k}^{\frac{a}{2}}\right)^2}{P_k\omega}\right) \mathcal{L}_{\mathcal{I}}\left(\frac{\vartheta\left(\epsilon + B_{j,k}^{\frac{a}{2}}\right)^2}{P_k\omega}, \tau\right) \mathcal{L}_{I_{\mathrm{SI}}}\left(\frac{\vartheta\left(\epsilon + B_{j,k}^{\frac{a}{2}}\right)^2}{P_k\omega}\right) \\
&\quad + (1-\chi_k)\beta_k \exp\left(-\frac{\vartheta\sigma_n^2\left(\epsilon + B_{j,k}^{\frac{a}{2}}\right)^2}{P_k\omega}\right) \mathcal{L}_{\mathcal{I}}\left(\frac{\vartheta\left(\epsilon + B_{j,k}^{\frac{a}{2}}\right)^2}{P_k\omega}, \tau\right), \qquad (6.12)
\end{aligned}$$

where (6.12) follows from the fact that h_τ is an exponential random variable; $\mathcal{L}_I(\cdot,\tau)$ and $\mathcal{L}_{I_{\text{SI}}}(\cdot)$ are the Laplace transforms of the overall interference function at time slot τ and SI, respectively.

Let $s = \frac{\vartheta\left(\epsilon+B_{j,k}^{\frac{a}{2}}\right)^2}{P_k\omega}$, then the Laplace transform of the overall interference, is

$$\begin{aligned}
\mathcal{L}_{\mathcal{I}}(s,\tau) &= \mathbb{E}\left[\exp\left(-s\left(\sum_{z=1}^{\eta}\sum_{i\in\mathbb{N}^+} P_z G^2 \ell g_\tau L\left(B_{i,z}^{\frac{1}{2}}\right)\Xi_{i,z}\mathbb{1}_{B_{i,z}\le\sqrt{\Re}}\right)\right)\right] \\
&= \prod_{z=1}^{\eta}\prod_{i\in\mathbb{N}^+}\mathbb{E}\left[\exp\left(-sP_z G^2 \ell g_\tau L\left(B_{i,z}^{\frac{1}{2}}\right)\Xi_{i,z}\mathbb{1}_{B_{i,z}\le\sqrt{\Re}}\right)\right] \\
&= \prod_{z=1}^{\eta}\prod_{i\in\mathbb{N}^+}\left(\beta_z\mathbb{E}\left[\exp\left(-sP_z G^2 \ell g_\tau L\left(B_{i,z}^{\frac{1}{2}}\right)\mathbb{1}_{B_{i,z}\le\sqrt{\Re}}\right)\right]+1-\beta_z\right) \qquad (6.13) \\
&= \prod_{z=1}^{\eta}\prod_{i\in\mathbb{N}^+}\left(1-\beta_z+\mathbb{E}\left[\frac{\beta_z}{1+sP_z G^2\ell L\left(B_{i,z}^{\frac{1}{2}}\right)\mathbb{1}_{B_{i,z}\le\sqrt{\Re}}}\right]\right) \qquad (6.14) \\
&= \prod_{z=1}^{\eta}\prod_{i\in\mathbb{N}^+}\left(1-\beta_z+\int_0^{\sqrt{\Re}}\frac{\beta_z f_{B_{i,z}}(y)}{1+\frac{sP_z G^2\ell}{\epsilon+y^{\frac{a}{2}}}}dy\right), \qquad (6.15)
\end{aligned}$$

where (6.13) is derived based on the β-GPP properties, (6.14) is due to the moment generating function of an exponential random variable, and (6.15) uses the distance distribution of β-GPP deployed RRUs, which is calculated in Proposition 2.1. Hence, the expression (6.9) is derived. Regarding the expressions for the Laplace transform of the SI function, it can be expressed as

$$\mathcal{L}_{I_{\text{SI}}}(s) = \mathbb{E}\left[\exp\left(-sI_{\text{SI}}(R,k)\right)\right] = \mathbb{E}\left[\exp\left(-s\min\{\rho\left(\epsilon+R^a\right)^{\varepsilon}, P_k\}g_{\text{SI}}\right)\right], \qquad (6.16)$$

where g_{SI} is the residual SI channel that follows Gamma distribution i.e., $g_{\text{SI}} \sim \mathcal{G}\left(\mu, \frac{\sigma_{\text{SI}}^2}{\mu}\right)$. By applying the Alzer's lemma [47], in order to approximate the Gamma random variable with a weighted sum of the cumulative distribution functions of exponential random variables, we conclude to the expression (6.10) for the Laplace transform of the SI function. □

It is noteworthy to mention that the Laplace transform of the overall interference function in (6.9) is a decreasing function of β. This can be explained by the fact that, the distance between the cooperative RRUs and their interfering RRUs becomes larger as $\beta \to 1$. Specifically, when β becomes larger, the RRUs exhibit more repulsion and tend to be distributed more uniformly. This leads to an increase of the distance between the cooperative RRUs and their interfering RRUs, resulting in a decreased

overall interference. We now state our main result for the detection probability achieved by our proposed CoMRD technique in the context of β-GPP heterogeneous mmWave cellular networks.

Theorem 6.1. *The detection performance achieved by the CoMRD technique at the time slot τ, is given by*

$$\mathcal{P}_d(\vartheta,\kappa,\tau)=\sum_{t=\kappa}^{\eta}\binom{\eta}{t}\prod_{k=1}^{\eta}\left(\sum_{j\in\mathbb{N}^+}\int_0^{\sqrt{\Re}}\mathcal{P}_d^k(\vartheta,\tau|u)^{\delta_k}\left(1-\mathcal{P}_d^k(\vartheta,\tau|u)\right)^{1-\delta_k}f_{B_{j,k}}(u)du\right), \quad (6.17)$$

where $\mathcal{P}_d^k(\vartheta,\tau|u)$ represents the achieved detection performance of the cooperative RRU $X_{j,k}\in\widetilde{\Phi}_k$ at the time slot τ, and $f_{B_{j,k}}(u)$ represents the pdf of the β-GPP distributed points which is given in Proposition 2.1.

Proof. By substituting the expression of Lemma 6.1 in (6.5), and by un-conditioning the derived expression with the pdf given by (2.1), the result in Theorem 6.1 follows. □

To illustrate the effect of repulsion between the RRUs on the achieved detection performance, we also evaluate our proposed technique in the context of PPP heterogeneous mmWave cellular networks. As we previously mentioned, the independent deployment of RRUs i.e., the RRUs are spatially distributed based on a PPP, is a special case of the considered β-GPP deployment, where $\beta\to 0$. Let a PPP $\Psi_k=\{X_k\in\mathbb{R}^2\}$, that denotes the spatial location of RRUs that belong to the k-th tier with density λ_k. Similarly as before, for each PPP Ψ_k, a PPP $\widetilde{\Psi}_k$ with inhomogeneous density function $\widetilde{\lambda}_k(r)=\lambda_k p_{\mathrm{LoS}}\frac{\phi}{2\pi}\mathbb{1}_{r\leq\Re}$ is formed, due to the effects of blockage and the antenna directionality. Hence, the pdf of the distance between the typical target and its closest LoS cooperative RRU X_k from the k-th tier, is given by

$$f_{\widetilde{\Psi}^{\mathrm{L}}}(r)=\lambda_k p_{\mathrm{LoS}}\phi r\exp\left(-\lambda_k p_{\mathrm{LoS}}\frac{\phi}{2}r^2\right)\mathbb{1}_{r\leq\Re}. \quad (6.18)$$

Let r_{X_k} represent the distance between the typical target and its closest LoS cooperative RRU from the k-th tier. In the following corollary, we evaluate the Laplace transform of the overall interference in the context of network deployments without repulsion between the RRUs.

Corollary 6.1. *When $\beta\to 0$, the Laplace transform of the observed interference at the time slot τ, is given by*

$$\widetilde{\mathcal{L}}_{\bar{I}}(s,\tau)=\prod_{z=1}^{\eta}\exp\left(-\lambda_z p_{\mathrm{LoS}}\frac{\phi}{2}\Re^2\left(1-\frac{\epsilon}{Q(s,z)}\right){}_2F_1\left[1,\frac{2}{a},\frac{2+a}{a},-\frac{\Re^a}{Q(s,z)}\right]\right), \quad (6.19)$$

where $Q(s,i) = G^2 \ell P_i s + \epsilon$, $s = \frac{\vartheta\left(\epsilon + r_{X_k}^{a}\right)^2}{P_k \omega}$, *and* $\omega = \frac{A\ell}{4\pi} G^2$.

In the following corollary, we state the achieved detection performance of our proposed technique, when the RRUs are deployed based on a PPP by assuming $\beta \to 0$.

Corollary 6.2. *When* $\beta \to 0$, *the detection performance achieved with the CoMRD technique at the time slot* τ, *is given by*

$$\mathcal{P}_d(\vartheta, \kappa, \tau) = \sum_{t=\kappa}^{\eta} \binom{\eta}{t} \prod_{k=1}^{\eta} \int_0^{\Re} \left(\widetilde{\mathcal{L}}_I(s,\tau) \exp\left(-s\sigma_n^2\right) \left(\chi_k \mathcal{L}_{I_{\mathrm{SI}}}(s) + 1 - \chi_k\right)\right)^{\delta_k} \times \left(1 - \widetilde{\mathcal{L}}_I(s,\tau) \exp\left(-s\sigma_n^2\right) \left(\chi_k \mathcal{L}_{I_{\mathrm{SI}}}(s) + 1 - \chi_k\right)\right)^{1-\delta_k} f_{\overline{\Psi}_k}(u) du, \tag{6.20}$$

where $s = \frac{\vartheta(\epsilon + u^a)^2}{P_k \omega}$, $\omega = \frac{A\ell}{4\pi} G^2$; $\widetilde{\mathcal{L}}_I(\cdot, \tau)$ *and* $\mathcal{L}_{I_{\mathrm{SI}}}(\cdot)$ *represent the Laplace transforms of the observed interference at the time slot* τ *and of the SI, respectively, and* $f_{\overline{\Psi}_k}(u)$ *is given by* (6.18).

6.5 Temporal Correlation of Radar Detection Performance

Even though we assume that the channel fading between different time slots is independent, the interference caused at a certain location is correlated across the time for the same network realization due to the fixed locations of the RRUs. Specifically, by assuming a static target, a fraction of the interfering RRUs at a given time slot might also cause interference at the particular target in future time slots, which introduces a temporal interference correlation that needs to be taken into account. In this section, we study the impact of the temporal correlation between two arbitrary time slots at the typical target. Based on the temporal correlation of the interference, we derive the conditional detection probability achieved with our proposed technique, such that an earlier transmission at the same location was successful. It is important to mention here that, the following analysis captures the pairwise temporal correlation across any two time slots as long as the spatial location of the receiver is fixed.

Consider a *static target* scenario, where the typical target remains static at the origin for multiple time slots. For this scenario, we study the ability of our proposed technique to successfully detect the typical target over different time slots. Let

$\mathcal{P}_d(\vartheta, \tau, \widehat{\tau}|X_{j,k})$ denote the probability of the cooperative RRU $X_{j,k} \in \widetilde{\Phi}_k$ to jointly detect its associated target at both time slots τ and $\widehat{\tau}$, which can be expressed as

$$\mathcal{P}_d(\vartheta, \tau, \widehat{\tau}|X_{j,k}) = \mathbb{P}\left[\mathrm{SINR}^{\tau}_{j,k} \geq \vartheta, \mathrm{SINR}^{\widehat{\tau}}_{j,k} \geq \vartheta\right], \tag{6.21}$$

where $\tau \neq \widehat{\tau}$. In the context of β-GPP heterogeneous mmWave cellular networks, this probability can be expressed as follows

$$\begin{aligned}
\mathcal{P}_d(\vartheta, \tau, \widehat{\tau}|B_{j,k}) &= \mathbb{P}\left[\mathrm{SINR}^{\tau}_{j,k} \geq \vartheta, \mathrm{SINR}^{\widehat{\tau}}_{j,k} \geq \vartheta\right] \\
&= \mathbb{P}\left[\mathrm{SINR}^{\tau}_{j,k} \geq \vartheta, \mathrm{SINR}^{\widehat{\tau}}_{j,k} \geq \vartheta | \Xi_{j,k} = 1\right] \mathbb{P}\left[\Xi_{j,k} = 1\right] \\
&= \beta \mathbb{P}\left[\frac{\mathcal{S}(B_{j,k}, \tau)}{\mathcal{I}(B_{j,k}, \tau) + I_{\mathrm{SI}}(R,k)\mathbb{1}_{\mathrm{JCAS}} + \sigma_n^2} \geq \vartheta, \frac{\mathcal{S}(B_{j,k}, \widehat{\tau})}{\mathcal{I}(B_{j,k}, \widehat{\tau}) + I_{\mathrm{SI}}(R,k)\mathbb{1}_{\mathrm{JCAS}} + \sigma_n^2} \geq \vartheta\right]
\end{aligned} \tag{6.22}$$

where (6.22) is derived by substituting (6.1) for different time instances τ and $\widehat{\tau}$. Since h_τ and $h_{\widehat{\tau}}$ are exponential random variables with unit mean, the joint detection probability, conditioned on whether the considered cooperative RRU $X_{j,k}$ employ the FD-JCAS scheme or not, can be expressed as

$$\begin{aligned}
\mathcal{P}_d(\vartheta, \tau, \widehat{\tau}|B_{j,k}) &= \beta_k \exp\left(-2s\sigma_n^2\right)\left(\chi_k\left(\mathcal{L}_{I_{\mathrm{SI}}}(s)\right)^2 + 1 - \chi_k\right) \\
&\quad \times \mathbb{P}\left[h_\tau \geq s\mathcal{I}(B_{j,k}, \tau), h_{\widehat{\tau}} \geq s\mathcal{I}(B_{j,k}, \widehat{\tau})\right] \\
&= \beta_k \exp\left(-2s\sigma_n^2\right)\left(\chi_k\left(\mathcal{L}_{I_{\mathrm{SI}}}(s)\right)^2 + 1 - \chi_k\right)\mathcal{L}_{\mathcal{I}}(s, \tau, \widehat{\tau}),
\end{aligned} \tag{6.23}$$

where $\mathcal{L}_{\mathcal{I}}(s, \tau, \widehat{\tau})$ is the joint Laplace transform of the interference functions at the time slots τ and $\widehat{\tau}$, and is equal to $\mathcal{L}_{\mathcal{I}}(s, \tau, \widehat{\tau}) = \mathbb{P}\left[h_\tau \geq s\mathcal{I}(B_{j,k}, \tau), h_{\widehat{\tau}} \geq s\mathcal{I}(B_{j,k}, \widehat{\tau})\right]$. In the following lemma, the expression for the joint Laplace transform of the interference functions at the time slots τ and $\widehat{\tau}$ is evaluated.

Lemma 6.2. *The joint Laplace transform of the interference functions at the time slots τ and $\widehat{\tau}$, is given by*

$$\mathcal{L}_{\mathcal{I}}(s, \tau, \widehat{\tau}) = \int_0^{\sqrt{\Re}} \prod_{z=1}^{\eta} \prod_{i \in \mathbb{N}^+} \left(1 - \beta + \frac{\beta}{1 + \frac{sP_z G^2 \ell}{\epsilon + y^{\frac{a}{2}}}}\right)^2 f_{B_{i,z}}(y) dy, \tag{6.24}$$

where $s = \frac{\vartheta\left(\epsilon + B_{j,k}^{\frac{a}{2}}\right)^2}{P_k \omega}$, $\omega = \frac{A\ell}{4\pi} G^2$, and $f_{B_{j,k}}(u)$ represents the pdf of the β-GPP distributed points, which is given in Proposition 2.1.

Proof. Initially, since h_τ and $h_{\widehat{\tau}}$ are independent for $\tau \neq \widehat{\tau}$, the joint Laplace transform of the interference functions at the time slots τ and $\widehat{\tau}$, is given by

$$\mathcal{L}_{\mathcal{I}}(s, \tau, \widehat{\tau}) = \mathbb{E}\left[\exp\left(-s \sum_{z=1}^{\eta} \sum_{i \in \mathbb{N}^+} P_z G^2 \ell g_\tau L\left(B_{i,z}^{\frac{1}{2}}\right) \Xi_{i,z} \mathbb{1}_{B_{i,z} \leq \sqrt{\Re}}\right)\right.$$

$$\times \exp\left(-s\sum_{z=1}^{\eta}\sum_{i\in\mathbb{N}^+} P_z G^2 \ell \mathcal{g}_{\widehat{\tau}} L\left(B_{i,z}^{\frac{1}{2}}\right)\Xi_{i,z}\mathbb{1}_{B_{i,z}\leq\sqrt{\Re}}\right)\Bigg]$$

$$= \mathbb{E}\left[\prod_{z=1}^{\eta}\prod_{i\in\mathbb{N}^+}\left(1-\beta+\frac{\beta}{1+sP_z G^2\ell L\left(B_{i,z}^{\frac{1}{2}}\right)\mathbb{1}_{B_{i,z}\leq\sqrt{\Re}}}\right)^2\right] \tag{6.25}$$

$$= \int_0^{\sqrt{\Re}}\prod_{z=1}^{\eta}\prod_{i\in\mathbb{N}^+}\left(1-\beta+\frac{\beta}{1+\frac{sP_z G^2\ell}{\epsilon+y^{\frac{a}{2}}}}\right)^2 f_{B_{i,z}}(y)dy, \tag{6.26}$$

where $s = \frac{\vartheta\left(\epsilon+B_{j,k}^{\frac{a}{2}}\right)^2}{P_k\omega}$, (6.25) follows from the moment generating functional of the exponential random variables h_τ and $h_{\widehat{\tau}}$, and (6.26) is derived by un-conditioning the expression with the pdf $f_{B_{i,z}}(y)$, which is evaluated in Proposition 6.1. □

By substituting (6.26) in (6.5), and by un-conditioning the derived expression with the pdf given by (2.1), the joint detection probability for the time slots τ and $\widehat{\tau}$ can be expressed as

$$\mathcal{P}_d(\vartheta,\kappa,\tau,\widehat{\tau}) = \sum_{t=\kappa}^{\eta}\binom{\eta}{t}\prod_{k=1}^{\eta}\left(\sum_{j\in\mathbb{N}^+}\int_0^{\sqrt{\Re}}\mathcal{P}_d^k(\vartheta,\tau,\widehat{\tau}|u)^{\delta_k}\left(1-\mathcal{P}_d^k(\vartheta,\tau,\widehat{\tau}|u)\right)^{1-\delta_k} f_{B_{j,k}}(u)du\right), \tag{6.27}$$

where w_k denotes the weight of the cooperative RRU $u \in \widetilde{\Phi}_k$, and $f_{B_{j,k}}(u)$ denotes the distance distribution between the cooperative RRU $u \in \widetilde{\Phi}_k$ and the typical target. The following theorem characterizes the detection probability at the time slot $\widehat{\tau}$, conditioned on the detection probability at the time slot τ, in the context of our proposed technique and in a β-GPP deployment.

Theorem 6.2. *The achieved detection probability with the CoMRD technique at the time slot $\widehat{\tau}$, conditioned on the detection probability at the time slot τ, is given by*

$$\mathcal{P}_d(\vartheta,\kappa,\widehat{\tau}|\tau) = \frac{\mathcal{P}_d(\vartheta,\kappa,\tau,\widehat{\tau})}{\mathcal{P}_d(\vartheta,\kappa,\tau)}, \tag{6.28}$$

where $\mathcal{P}_d(\vartheta,\kappa,\tau)$ and $\mathcal{P}_d(\vartheta,\kappa,\tau,\widehat{\tau})$ are given by (6.17) *and* (6.27)*, respectively.*

In order to illustrate the effect of temporal correlation on the detection performance, we introduce the ratio of the conditional and the unconditional detection probability, that is given by

$$\xi = \frac{\mathcal{P}(\vartheta,\kappa,\widehat{\tau}|\tau)}{\mathcal{P}(\vartheta,\kappa,\tau)} = \frac{\mathcal{P}(\vartheta,\kappa,\tau,\widehat{\tau})}{\mathcal{P}(\vartheta,\kappa,\tau)^2} > 1. \tag{6.29}$$

Remark: From (6.29), if the target detection process succeeds at the time slot τ, there is a higher probability that the target detection process succeeds at future time slots $\widehat{\tau}$.

Remark: From (6.29), we can easily observe that $\mathcal{P}(\vartheta, \kappa, \widehat{\tau}|\tau) > \mathcal{P}(\vartheta, \kappa, \tau)$. Particularly, a failure in the target detection by the CoMRD technique at the time slot τ, results in a more likely target detection failure at future time slots $\widehat{\tau}$.

6.6 Numerical Results

In this section, we plot the analytical results derived in the previous sections along with the simulation results obtained from Monte-Carlo trials. We focus on the special case of a 3-tier HetNet, i.e. $\eta = 3$, where their spatial densities are $\lambda_1 = 1$ RRUs/km^2, $\lambda_2 = 2$ RRUs/km^2, and $\lambda_3 = 4$ RRUs/km^2, respectively, with transmit power equal to $P_1 = 15$ dBm, $P_2 = 10$ dBm, and $P_3 = 5$ dBm, respectively. Regarding the repulsive behavior between the RRUs, we assume that the repulsive parameter of all tiers is equal to $\beta = 0.9$ i.e., $\beta_k = \beta = 0.9$ $\forall k$. For the large-scale path-loss, we assume $a = 4$ and $\epsilon = 1$. The power control factor is $\varepsilon = 0.9$ and all RRUs have the same receive sensitivity $\rho = -40$ dB [163]. The SI capabilities of RRUs are set to $\sigma^2_{\text{SI}} = -60$ dB and $\mu = 4$ [163]. The parameters for the sectorized antenna model are set to $G = 10$ dB and $\phi = \frac{\pi}{6}$ for the main lobe gain and the main lobe beamwidth, respectively [131]. In terms of modeling the blockage sensitivity of mmWave signals, we assume that within a disk of radius $\Re = 400$ m around the typical target, a fraction equal to $p_{\text{LoS}} = 0.7$ of RRUs is in LoS. Unless otherwise specified, the fraction of JCAS-capable RRUs is set to $\chi = 0.8$. Finally, we set $A = 10$ dB, $f = 30$ GHz, and $\sigma^2_n = -60$ dB [188]. It is important to note that the selection of these parameters is for the purpose of presenting the achieved performance of our proposed framework. Using different values will lead to a shifted network performance, but with the same conclusions and remarks.

Fig. 6.3 illustrates the detection performance achieved with our proposed technique for all three hard-decision combining rules and for different repulsion parameter values. An important observation from this figure is that the *OR* combining rule achieves a significantly higher network detection performance, outperforming the other two. This observation is based on the fact that, for the scenario where

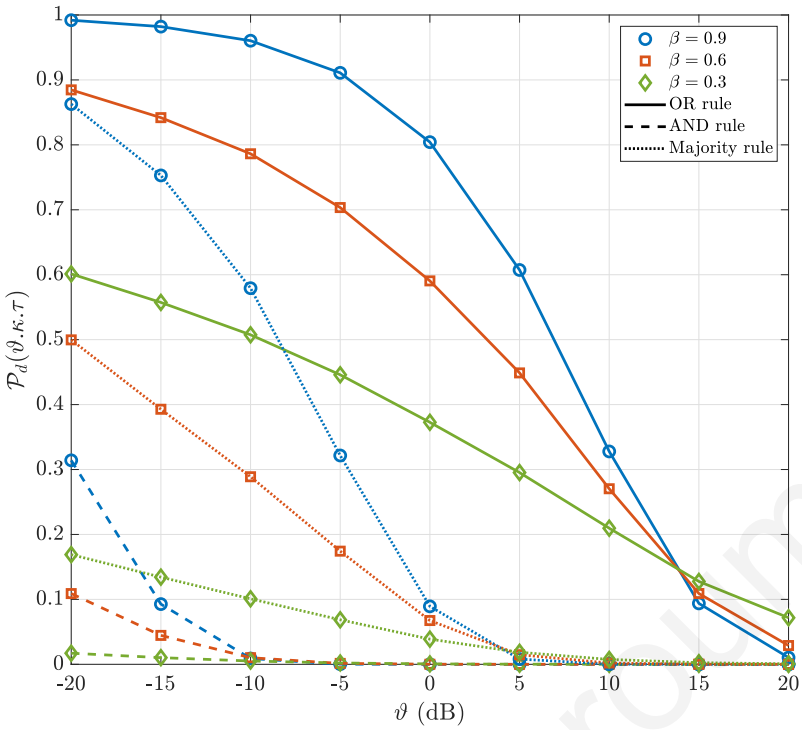

Figure 6.3: Detection probability versus ϑ for the considered combining rules, where $\beta = \{0.3, 0.6, 0.9\}$.

the FC adopts the *OR* rule, the target detection is achieved when at least one of the η cooperative RRUs successfully senses the existence of the particular target. On the other hand, by applying the *Majority* or the *AND* rule, a decreased detection performance is observed since the simultaneous successful detection of the target by the majority or all cooperative RRUs, respectively, is required. Furthermore, Fig. 6.3 demonstrates the impact of the repulsion parameter β on the detection performance achieved with our proposed technique. We can easily observe that, the detection performance $\mathcal{P}_d(\vartheta, \kappa, \tau)$ is an increasing function of β. This is expected, since by increasing the repulsion parameter, the distance between interfering RRUs is increased, achieving a reduced overall interference and an enhanced detection performance. We can finally observe that the analytical results (solid, dashed and dotted lines) agree with the network performance given by the simulation results (markers).

Fig. 6.4 reveals the impact of both the blockage and repulsion parameter on the detection performance achieved by applying the *OR* and the *AND* combining rules and for different number of network tiers. As expected, by increasing the number of network tiers, the number of cooperative RRUs is also increased, and therefore the detection performance achieved by applying the *OR* rule increases, in contrast

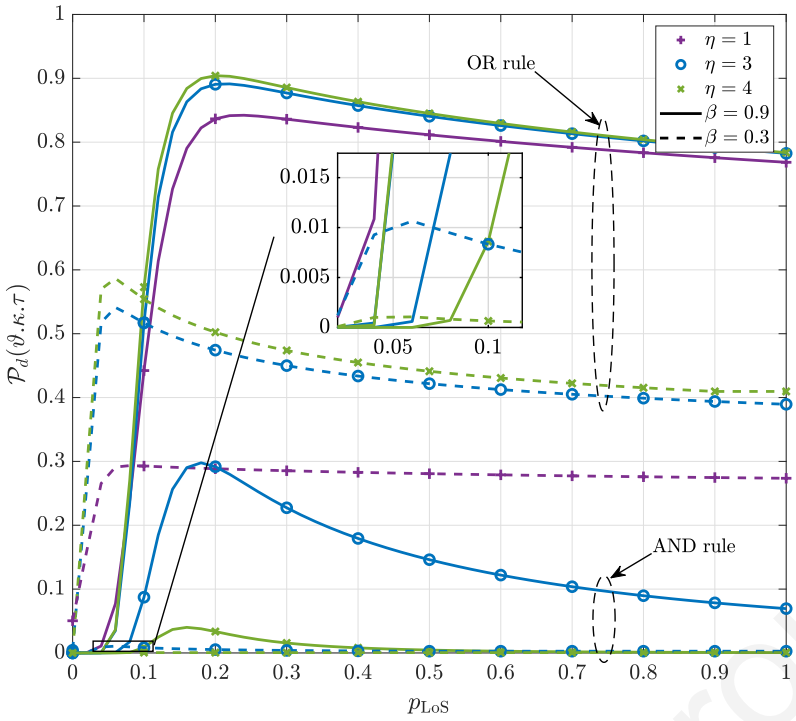

Figure 6.4: Detection probability versus p_{LoS} for the *OR* and *AND* combining rules and for different number of network tiers; $\vartheta = -15$ dB, $\lambda_4 = 6$ RRUs/km^2 and $P_4 = 0$ dBm.

to the decreasing detection performance achieved by applying the *AND* rule. The latter occurs since, as the number of cooperative RRUs increases, the probability of simultaneous successful detection of a target by all cooperative RRUs is decreased. On the other hand, by applying the *OR* rule, the increased number of cooperative RRUs, increases the probability of successfully detecting the target from at least one cooperative RRU. Fig. 6.4 also reveals the impact of blockages on the network's detection performance. As expected, at low LoS constant values, the existence of LoS RRUs improves the network performance, since the cooperative RRUs are able to successfully detect the target. However, by increasing the LoS constant beyond a critical point, which describes the optimal fraction of LoS RRUs that provide the maximum detection performance, the network performance decreases. This observation is based on the fact that, the interference from the LoS RRUs becomes significantly larger than the reflected signal from the target and thus the detection probability significantly decreases. Another important observation is that, the aforementioned critical point depends on the repulsion parameter of the network tiers. Specifically, by enhancing the repulsion behavior between the RRUs, the optimal detection performance is achieved with a larger fraction of LoS RRUs.

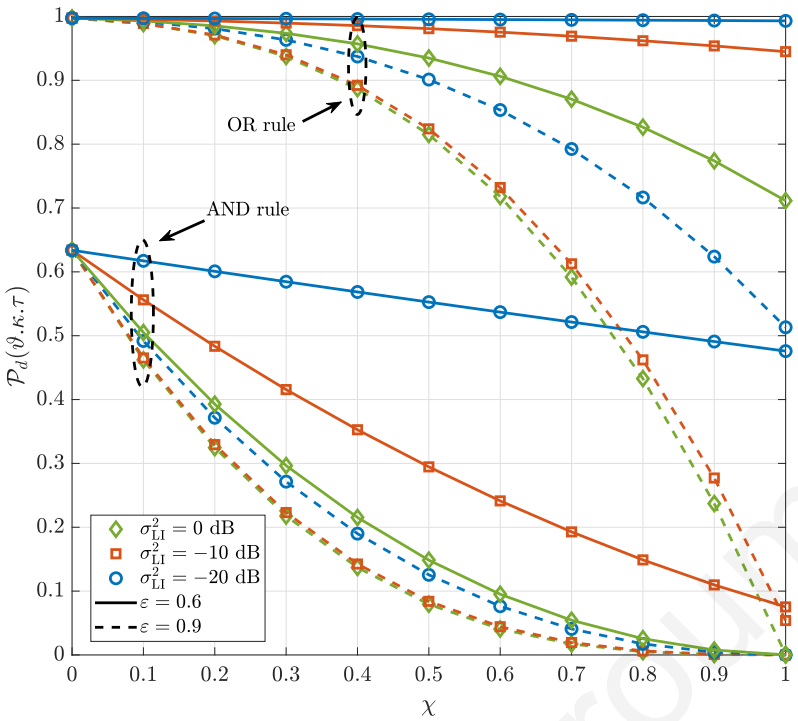

Figure 6.5: Detection probability versus χ for the considered combining rules, where $\sigma^2_{\text{SI}} = \{0,\ -10,\ -20\}$ dB and $\varepsilon = \{0.6\ , 0.9\}$; $\beta = 0.9$, $\vartheta = -20$ dB.

Fig. 6.5 shows the effect of the residual SI on the network's detection performance for the *OR* and the *AND* combining rules. We can easily observe that by increasing the ability of the nodes to cancel the observed SI i.e., $\sigma^2_{\text{SI}} \to -\infty$, the detection performance achieved with our proposed technique is increased for all combining rules. This observation was expected, since by decreasing the residual SI at the RRUs, the aggregate received interference is decreased, and therefore an increased SINR is observed. An important observation from this figure is that the increased fraction of JCAS-enabled RRUs, negatively affects the detection performance. This again is expected, since by increasing the number of RRUs that simultaneously perform both functions i.e., DL transmission and detection, the overall interference increases due to the existence of SI, compromising the observed SINR. We can easily observe from the figure that, the power control can prevent the significant degradation of the network's detection performance by controlling the power control parameter ε. Specifically, by decreasing the power control parameter i.e., $\varepsilon \to 0$, the RRUs' transmit power for the DL communication with their associated users is reduced, resulting in a decreased SI and therefore in an enhanced SINR. It is important to mention here that both the fraction of JCAS-enabled RRUs and the Nakagami-μ fading parameters, have similar effect on the detection performance achieved with

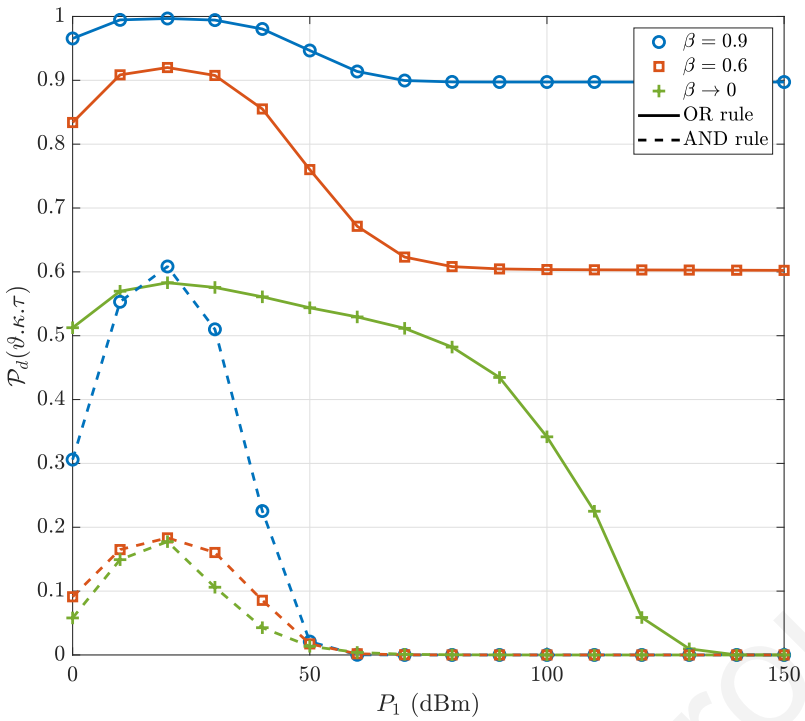

Figure 6.6: Detection probability versus P_1 for the OR and the AND combining rules, where $\beta = \{0, 0.6, 0.9\}$; $P_2 = \frac{P_1}{2}$ dB, $P_3 = \frac{P_1}{3}$ dB and $\chi = 0.3$.

the *Majority* rule, thus the corresponding curves are omitted.

Fig. 6.6 shows the detection performance of the OR and the AND combining rules in terms of the RRUs' transmit power P_1, where $P_2 = \frac{P_1}{2}$ and $P_3 = \frac{P_1}{3}$. We can easily observe from the figure that, by increasing the transmit power of the RRUs can significantly enhance the detection probability of its associated target. This observation is expected since, a larger transmission power by the cooperative RRUs corresponds to receiving a stronger reflected signal power, resulting in an enhanced detection performance. Nevertheless, beyond a critical transmit power level, the increase of the transmission power negatively affects the detection performance. This is again expected, since the residual SI at a receiver becomes larger, and therefore the observed SINR is decreased. Moreover, it can be seen that the detection performance converges to a constant floor in all cases for high transmission powers. This is due to the fact that as the transmission power of the network's RRUs increases, the noise in the network becomes negligible. Fig. 6.6 also illustrates the achieved detection performance of the considered combining rules, for the scenario where the spatial distribution of the RRUs is based on a PPP. It is clear from the figure that, the spatially distributed RRUs based on a repulsive point process can attain better detection performance compared to the randomly deployed RRUs. This is

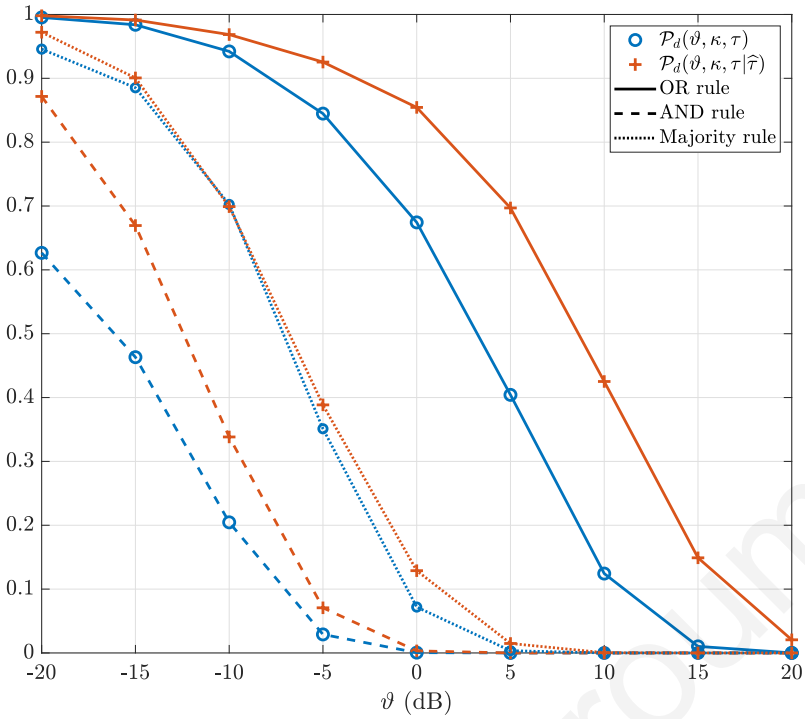

Figure 6.7: Detection probability and conditional detection probability versus ϑ for the considered combining rules; $\beta = 0.9$, $\chi = 0.3$, .

due to the fact that, the distances between a cooperative RRU and its interfering RRUs in a β-GPP-based deployment are greater than the corresponding distances in a PPP-based deployment, resulting in a reduced overall interference.

Finally, Fig. 6.7 highlights the effect of the interference temporal correlation on the network's detection performance between different time slots. Specifically, we plot the conditional and the unconditional target detection probabilities for the three considered combining rules. We can easily observe that the conditional detection probability overcomes the unconditional detection probability. This was expected since, a fraction of interfering RRUs at the time slot τ, in which a static target is successfully detected, also causes interference in future time slots $\widehat{\tau}$. Therefore, as the static target is successfully detected at the time slot τ, the probability of successful detecting the same static target at the time slot $\widehat{\tau}$ is increased. Note that, the aforementioned observation holds for all the considered combining rules and for all the detection thresholds considered.

6.7 Conclusion

In this chapter, we proposed an analytical framework based on stochastic geometry and studied the detection performance of FD-JCAS systems in the context of heterogeneous mmWave cellular networks. In particular, we considered the scenario where all RRUs exhibit detection capabilities, a fraction of which also exhibit DL communication capabilities by exploiting the concept of FD radio. The developed framework takes into account the spatial correlation between the RRUs and the temporal correlation of the interference, by modeling the RRUs' locations as a β-GPP and by analyzing the joint detection probability at two different time slots, respectively. Aiming at enhancing the network's detection performance, a novel cooperative detection technique is proposed, and the achieved network performance is evaluated in the context of three hard-decision combining rules, namely the *OR*, the *Majority* and the *AND* rule. Using stochastic geometry tools, the network's detection performance in the context of our proposed technique was derived in analytical expressions and the impact of blockage characteristics, residual SI, repulsion parameter and fraction of FD-JCAS RRUs have been evaluated. Our study reveals that the proposed technique outperforms the conventional non-cooperative detection technique. Finally, we have shown that the repulsive behavior of the RRUs can provide significantly larger detection performance to the network.

Chapter 7

Conclusion and Future Work

Within the last decade, the intense demand for mobile data traffic has exceeded even the most aggressive predictions. Due to unprecedented growth in the number of mobile subscribers and the accelerated adoption of data-hungry devices, such as smartphones, tablet and laptops, this trend is likely to persist. The need to support this traffic explosion along with the ever-fast approaching limits of the current generation of the cellular mobile communications, signals the dawn of the next-generation technology era, commonly known as the beyond 5G technology. The integration of mmWave communications into cellular HetNets has been advocated as one of the most promising enabling technologies for supporting the increasing demand of data-traffic and for enhancing the performance of next-generation networks. Specifically, the utilization of HetNet deployments provide increased reliability, improved spectrum efficiency, and increased coverage. At the same time, the operation of wireless communications at the mmWave frequency bands can lead to multi-Gbps rates, due to their abundant spectrum resources.

In this thesis, we addressed some of the challenges brought by the integration of HetNets-mmWave networks in cellular systems, and validated the potential of this technology by designing and modeling novel network architectures and protocols. Our main contributions have been in the context of cooperation and resource allocation mechanisms, interference mitigation, and power control techniques. Moreover, we demonstrated that the co-design of HetNets-mmWave cellular networks with other transmission technologies, i.e. FD radio, and JCAS scheme, can further improve of future networks. Leveraging tools from stochastic geometry, we developed a novel analytical framework to evaluate the achieved performance of the

aforementioned techniques in next-generation HetNet-mmWave cellular networks, from a large-scale point-of-view. Tractable closed-form expressions for fundamental network performance metrics, such as the coverage probability, the throughput, detection probability and the meta-distribution, are derived. These closed-form expressions, provide valuable engineering insights to help network operators in the deployment of HetNets in the mmWave bands, and how key system parameters affect the network performance.

7.1 Future Work

Some possible future works are the following:

1. **Extend current system model**: In this Ph.D dissertation we investigated the achieved performance of the considered network deployments in the 2D space, by assuming that all network's nodes are deployed at the same height. However, the heights of blockages, BSs antennas, or even users may have non-negligible impacts on the system performance. In particular, the macro-BSs, which are mainly tower-mounted, are more likely to establish a LoS link towards the users, since their higher height contribute in avoiding the blockages within the network area. On the other hand, high-rise buildings can potentially block all the LoS links between a user and a BS, leading to a significant reduction in the network performance. Thus, it is of interest to incorporate the elevation height in the analysis and extend our proposed framework into 3D space. The 3D model will also make it possible to analyze the performance of the techniques that exploit the spatial degrees of freedom in elevation directions, such as 3D beamforming and vertical sectorization.

   Regarding the classification of users and as discussed in Chapters 4 and 5, we assume that a user can be spatially classified either in the cell-center or the cell-edge region of a communication cell. Specifically, this classification scheme spatially separates a communication cell into two sub-regions. However, the performance of a CCU which is located nearby the cell-edge region, experiences slightly better performance compared to the achieved performance of a CEU, and a significantly lower compared to a CCU near the serving BS. This motivates the investigation of a classification scheme, that spatially separates a

communication cell into multiple sub-regions. With such classification scheme, we can further enhance the performance resolution by capturing the existence of different users' categories, and aiming the enhancement of each category of users with the employment of sophisticated communication techniques.

In Chapter 6, we adopt the β-GPP as an abstraction model for the spatial distribution of wireless networks whose nodes exhibit repulsion, aiming the investigation of the performance of realistic network deployments. Beyond the repulsive behavior, actual network deployments can also exhibit attraction behavior. Such attractive behavior can be observed on larger network deployments, where the BSs within a city are forming a cluster of points, whereas the locations of the points in urban areas are more sparsely located. Therefore, the investigation of a point process that its points exhibit an attractive behavior, such as the Poisson cluster process and the Neyman-Scott process, is an interesting direction for this work.

Moreover, as discussed in Chapter 6, the communication operation in the context of JCAS systems causes a minor degradation on the radar detection operation. The radar detection operation, on the other hand, can provide a significant performance gain on the cellular HetNets operating on the mmWave frequency band. Specifically, the short-range environmental information estimated by the radar detection operation (e.g. blockage detection, channel estimation), can be leveraged by the mmWave BSs (e.g. reconfiguration of the communication beams, handover process) in order to enhance the communication operation.

Finally, throughout this Ph.D. dissertation we derive analytical expressions for important performance metrics for the wireless networks, such as the coverage, the rate and the detection performance. Hence, an important future task is to simplify the expressions, aiming to derive closed-form expressions, by either using some approximations or by considering some special cases. Then, these closed-form expressions can be leveraged in order to study optimization problems for the further enhancement of the network performance and to gain more insights about the impact of key network parameters.

2. **UAVs mmWave communications**: MmWave technology as an important element in the 5G and beyond wireless networks can be used in the UAV com-

munications as well. Indeed, the mmWave technology even sounds more promising for the UAVs as they are deployed at high altitude, offering LoS communication. In addition, the UAVs can be adopted for wireless power transfer (WPT) purposes since they can be easily deployed to provide WPT service in areas without infrastructure (e.g., power beacons) coverage in remote or hazardous environments. However, due to the movement of the UAVs, in order to be able to use mmWave for UAVs communication efficiently, signal blockages, handover effects, fast beamforming training and tracking, and Dopaperpler effects should be addressed properly.

3. **Intelligent reflecting surfaces (IRSs)-aided HetNets-mmWave communications**: An IRS can intelligently control the wireless environment to improve the signal strength received at the destination. Specifically, an IRS consists of many IRS units, each of which can reflect the incident signal at a reconfigurable angle. In other words, the wireless signal travels from the source to the IRS, is optimized at the IRS, and then travels from the IRS to the destination. Such communication method is particularly useful for the HetNets-mmWave systems, where the source and the destination such as the BS and the user have a weak wireless channel in between due to blockages or poor environmental conditions, or they do not have direct LoS. Therefore, IRS-aided HetNets-mmWave communications are envisioned to play a fundamental role in the beyond-5G networks.

4. **Synergy of stochastic geometry and machine learning**: Throughout the literature, many valuable and insightful stochastic geometry-based analytical expressions can be found. However, to ensure tractability, these expressions are based on many simplifying assumptions on the wireless network, which are often unrealistic (i.e., neglect shadowing effects, assume randomly deployed BSs, etc). This is because, the tractable prediction and optimization of the actual network's performance, such as the coverage, the throughput and the spectral efficiency, are very often unfeasible. The aforementioned are even more difficult in the mmWave communications, since the mmWave environments change dynamically and variously due to the mmWave signals' characteristics, such as the high directionality and the sensitivity to blockages. Motivated by the data-driven model adaptation of the machine learning approach, it is interesting to

investigate the machine learning as an enabler of the this challenge.

Chapter 8

List of Publications

1. **Book Chapters**

   - C. Psomas, **C. Skouroumounis**, and I. Krikidis, *Relay selection in modern communication systems*, chapter in the book titled *Advanced relay technologies in next generation wireless communications*. Editors: I. Krikidis and G. Zheng, IET, 2016.
   - J. M. B. da Silva, **C. Skouroumounis**, I. Krikidis, G. Fodor, and C. Fischione, *Energy efficient full-duplex networks*, chapter in the book titled *Green Communications for Energy-Efficient Wireless Systems and Networks*. Editors: A. Zappone, J. Yang, J. S. Thompson, and H. Suraweera. Eds. IET, 2019.

2. **Journal Articles**

   - **C. Skouroumounis**, C. Psomas, and I. Krikidis, "Low-complexity base station selection scheme in mmWave cellular networks," *IEEE Transactions on Communications,* vol. 65, no. 9, pp. 4049–4064, Sept. 2017.
   - **C. Skouroumounis**, C. Psomas and I. Krikidis, "Heterogeneous FD-mmWave cellular networks with cell center/edge users," *IEEE Transactions on Communications,* vol. 67, no. 1, pp. 791–806, Jan. 2019
   - **C. Skouroumounis**, C. Psomas, and I. Krikidis, "Hybrid cooperation scheme in heterogeneous sub-6 GHz/mmWave cellular networks," submitted in *IEEE Wireless Communications Letters*, Sept. 2019.
   - **C. Skouroumounis**, C. Psomas, and I. Krikidis, "FD-JCAS techniques for mmWave HetNets: Ginibre point process modeling and analysis," submitted in *IEEE Transactions on Wireless Communications*, Sept. 2019.

3. **Conference Articles**

- C. Psomas, **C. Skouroumounis**, I. Krikidis, A. Kalis, Z. Theodosiou, and A. Kounoudes, "Performance gains from directional antennas in full-duplex systems," in *Proceedings of IEEE International Conference on Microwaves, Communications, Antennas and Electronic Systems (COMCAS)*, Tel Aviv, Israel, Nov. 2015.
- **C. Skouroumounis**, C. Psomas, and I. Krikidis, "Low complexity base station cooperation in cellular networks with blockages," in *Proceedings of IEEE Wireless Communications and Networking Conference (WCNC)*, Doha, Qatar, Apr. 2016, pp. 1381–1386.
- **C. Skouroumounis**, C. Psomas, and I. Krikidis, "Low-complexity base station cooperation for mmWave heterogeneous cellular networks," in *Proceedings of IEEE Global Communications Conference (GLOBECOM)*, Washington, DC, Dec. 2016, pp. 1–6.
- **C. Skouroumounis**, C. Psomas, and I. Krikidis, "FD-mmWave cellular networks with location-based user classification" in *Proceedings of Asilomar Conference on Signals, Systems, and Computers,* Pacific Grove, CA, USA, Oct. 2018.
- **C. Skouroumounis**, C. Psomas, and I. Krikidis, "Full-duplex radio in mmWave cellular networks with cell center/edge users" in *Proceedings of IEEE Global Communications Conference (GLOBECOM)* Abu-Dhabi, UAE, Dec. 2018.
- **C. Skouroumounis**, C. Psomas, and I. Krikidis, "Cooperative detection for mmWave radar cellular networks," submitted in *IEEE International Conference on Communications (ICC)*, Oct. 2019.

Bibliography

[1] Cisco, "White paper: Cisco visual networking index: Global mobile data traffic forecast update, 2016–2021," tech. rep., Feb. 2017.

[2] M. Corson, R. Laroia, J. Li, V. Park, T. Richardson, and G. Tsirtis, "Towards proximity-aware inter-networking," *IEEE Wireless Commun. Mag.,* vol. 17, no. 6, pp. 26-–33, Dec. 2010.

[3] S. K. Rao and R. Prasad, "Impact of 5G technologies on smart city implementation", in *Wireless Personal Commun.,* vol. 100, no. 1, pp.161–176, May 2018.

[4] G. A. Akpakwu, B. J. Silva, G. P. Hancke, and A. M. Abu-Mahfouz, "A survey on 5G networks for the internet of things: Communication technologies and challenges," *IEEE Access,* vol. 6, pp. 3619–3647, 2018.

[5] N. F. M. Aun, P. J. Soh, A. A. Al-Hadi, M. F. Jamlos, G. A. E. Vandenbosch, and D. Schreurs, "Revolutionizing wearables for 5G: 5G technologies: recent developments and future perspectives for wearable devices and antennas," *IEEE Microwave Mag.,* vol. 18, no. 3, pp. 108–124, May 2017.

[6] J. M. C. Brito, "Trends in wireless communications towards 5G networks – The influence of e-health and IoT applications," in *Proc. Int. Multidisciplinary Conf. Computer and Energy Science ,* Split, pp. 1–7, Jul. 2016.

[7] Huawei " 5G network architecture: A high-level perspective," tech. rep., Jul. 2016.

[8] J. Andrews, S. Buzzi, W. Choi, S. Hanly, A. Lozano, A. Soong, and J. Zhang, "What will 5G be?," *IEEE J. Select. Areas Commun.,* vol. 32, pp. 1065—1082, Jun. 2014.

[9] Ericsson, "5G radio access," tech. rep., Apr. 2016.

[10] 5G-PPP, "5G vision," tech. rep., Feb. 2015.

[11] Q. Li, G. Li, W. Lee, M. Lee, D. Mazzarese, B. Clerckx, and Z. Li, "MIMO techniques in WiMAX and LTE: a feature overview," *IEEE Commun. Mag.,* vol. 48, no. 5, pp. 86-92, May 2010.

[12] 3GPP, "Overview of 3GPP Release 8", Sep. 2008.

[13] 3GPP, "Overview of 3GPP Release 9", Mar. 2009.

[14] 3GPP, "Overview of 3GPP Release 10", Sep. 2011.

[15] 3GPP, "Overview of 3GPP Release 11", Jun. 2013.

[16] S. Sesia, I. Toufik, and M. Baker, *LTE – The UMTS long term evolution: From theory to practice*, in *Wiley*, 2011.

[17] M. Dohler, R. W. Heath, A. Lozano, C. B. Papadias, and R. A. Valenzuela, "Is the PHY layer dead?" *IEEE Commun. Mag.,* vol. 49, no. 4, pp. 159–165, Apr. 2011.

[18] F. Rusek, D. Persson, B. K. Lau, E. G. Larsson, T. L. Marzetta, O. Edfors, and F. Tufvesson, "Scaling up MIMO: Opportunities and challenges with very large arrays," *IEEE Sig. Proc. Mag.,* vol. 30, no. 1, pp. 40-–60, Jan. 2013.

[19] T. L. Marzetta, "Noncooperative cellular wireless with unlimited numbers of base station antennas," *IEEE Trans. Wireless Commun.,* vol. 9, no. 11, pp. 3590–3600, Nov. 2010

[20] M. Heino, D. Korpi, T. Huusari, E. A.-Rodriguez, S. Venkatasubramanian, T. Riihonen, L. Anttila, C. Icheln, K. Haneda, R. Wichman, and M. Valkama, "Recent advances in antenna design and interference cancellation algorithms for in-band full duplex relays,' *IEEE Commun. Mag.,* vol. 53, no. 5, pp. 91–101, May 2015.

[21] T. S. Rappaport, R. C. Daniels, R. W. Heath, and J. N. Murdock, *Millimeter wave wireless communications*, in *Prentice Hall*, 2014.

[22] R. C. Daniels and R. W. Heath, "60 GHz wireless communications: Emerging requirements and design recommendations," *IEEE Veh. Tech. Mag.,* vol. 2, no. 3, pp. 41–50, Sep. 2007.

[23] A. M. Niknejad, "Siliconization of 60 GHz," *IEEE Microwave Mag.,* vol. 11, no. 1, pp. 78–85, Feb. 2010.

[24] K. M. S. Huq, J. M. Jornet, W. H. Gerstacker, A. Al-Dulaimi, Z. Zhou and J. Aulin, "THz communications for mobile heterogeneous networks," *IEEE Commun. Mag.,* vol. 56, no. 6, pp. 94–95, Jun. 2018.

[25] C. Han and Y. Chen, "Propagation modeling for wireless communications in the terahertz band," *IEEE Commun. Mag.,* vol. 56, no. 6, pp. 96–101, June 2018.

[26] J. Andrews, "Seven ways that HetNets are a cellular paradigm shift," *IEEE Commun. Mag.,* vol. 51, no. 3, pp. 136—144, Mar. 2013.

[27] A. Ghosh, J. G. Andrews, N. Mangalvedhe, R. Ratasuk, B. Mondal, M. Cudak, E. Visotsky, T. A. Thomas, P. Xia, H. S. Jo, H. S. Dhillon, and T. D. Novlan, "Heterogeneous cellular networks: From theory to practice," *IEEE Commun. Mag.,* vol. 50, no. 6, pp. 54–64, Jun. 2012.

[28] A. Damnjanovic, J. Montojo, Y. Wei, T. Ji, T. Luo, M. Vajapeyam, T. Yoo, O. Song, and D. Malladi, "A survey on 3GPP heterogeneous networks," *IEEE Wireless Commun.,* vol. 18, no. 3, pp. 10–21, Jun. 2011.

[29] J. Qiao, X. S. Shen, J. W. Mark, Q. Shen, Y. He, and L. Lei, "Enabling device-to-device communications in millimeter-wave 5G cellular networks," *IEEE Commun. Mag.,* vol. 53, no. 1, pp. 209–215, Jan. 2015.

[30] Y. Mehmood, N. Haider, M. Imran, A. Timm-Giel, and M. Guizani, "M2M communications in 5G: State-of-the-art architecture, recent advances, and research challenges," *IEEE Commun. Mag.,* vol. 55, no. 9, pp. 194–201, 2017.

[31] N. Bhushan, J. Li, D. Malladi, R. Gilmore, D. Brenner, A. Damnjanovic, R. Sukhavasi, C. Patel, and S. Geirhofer, "Network densification: the dominant theme for wireless evolution into 5G," *IEEE Commun. Mag.*, vol. 52, pp. 82—89, Feb. 2014.

[32] J. Andrews, H. Claussen, M. Dohler, S. Rangan, and M. Reed, "Femtocells: Past, present, and future," *IEEE J. Sel. Areas Commun.*, vol. 30, no. 3, pp. 497-–508, Apr. 2012.

[33] A. Mesodiakaki, F. Adelantado, L. Alonso, and C. Verikoukis, "Energy-efficient context-aware user association for outdoor small cell heterogeneous networks," in *Proc. IEEE Int. Conf. Commun.*, Sydney, NSW, Australia, June 2014, pp. 1614—1619.

[34] P. Lin, J. Zhang, Y. Chen, and Q. Zhang, "Macro-femto heterogeneous network deployment and management: from business models to technical solutions," *IEEE Wireless Commun.*, vol. 18, no. 3, pp. 64-–70, June 2011.

[35] 3rd Generation Partnership Project (3GPP), "Service requirements for Home Node B (HNB) and Home eNode B (HeNB)," *3rd Generation Partnership Project*, TS 22.220, Oct. 2014.

[36] H. ElSawy, E. Hossain, and M. Haenggi, "Stochastic geometry for modeling, analysis, and design of multi-tier and cognitive cellular wireless networks: A survey," *IEEE Commun. Surveys & Tutorials*, vol. 15, no. 3, pp. 996—1019, June 2013.

[37] L. T. W. Ho and H. Claussen, "Effects of user-deployed, co-channel femtocells on the call drop probability in a residential scenario," in *Proc. IEEE Int. Symp. Personal, Indoor and Mobile Radio Commun.*, Athens, Greece, Sep. 2007.

[38] V. Chandrasekhar, J. Andrews, and A. Gatherer, "Femtocell networks: a survey," *IEEE Commun. Mag.*, vol. 46, pp. 59-–67, Sept. 2008.

[39] R. Bendlin, T. Ekpenyong, and D. Greenstreet, "Paving the path for wireless capacity expansion," tech. rep., Texas Instruments, March 2012.

[40] J. Gora and S. Redana, "In-band and out-band relaying configurations for dual-carrier LTE-advanced system," in *Proc. IEEE 22nd Int. Symposium on Personal, Indoor and Mobile Radio Commun.*, Toronto, 2011, pp. 1820–1824.

[41] T. S. Rappaport, *Wireless Communications: Principles and Practice*, in *New Jersey: Prentice Hall*, 2001.

[42] R. Nasri and A. Jaziri, "Analytical tractability of hexagonal network model with random user location," *IEEE Trans. Wireless Commun.*, vol. 15, no. 5, pp. 3768–3780, May 2016.

[43] J. Andrews, F. Baccelli, and R. Ganti, "A tractable approach to coverage and rate in cellular networks," *IEEE Trans. Commun.*, vol. 59, no. 11, pp. 3122—3134, Nov. 2011.

[44] J. Xu, J. Zhang, and J. Andrews, "On the accuracy of the Wyner model in cellular networks," *IEEE Trans. Wireless Commun.*, vol. 10, no. 9, pp. 3098-–3109, Sep. 2011.

[45] F. Baccelli and B. Blaszczyszyn, *Stochastic Geometry and Wireless Networks: Volume I Theory,* in *Now Foundations and Trends,* Mar. 2009.

[46] M. Haenggi, *Stochastic geometry for wireless networks*, in *Cambridge*, U.K.: Cambridge Univ. Press, 2012.

[47] B. Blaszczyszyn, M. Haenggi, P. Keeler, and S Mukherjee *Stochastic geometry analysis of cellular networks* in *Cambridge*, U.K.: Cambridge Univ. Press, 2018.

[48] T.-C. Hou and V. Li, "Transmission range control in multihop packet radio networks," *IEEE Trans. Commun.,* vol. 34, no. 1, pp. 38–44, Jan. 1986.

[49] E. S. Sousa, "Optimum transmission range in a direct-sequence spread spectrum multihop packet radio network," *IEEE J. Sel. Areas Commun.,* vol. 8, no. 5, pp. 762—771, 1990.

[50] L. Decreusefond, I. Flint, and A. Vergne, "A note on the simulation of the Ginibre point process," *J. Appl. Probab.*, vol. 52, no. 4, pp. 1003–1012, 2015.

[51] N. Deng, W. Zhou, and M. Haenggi, "The Ginibre point process as a model for wireless networks with repulsion," *IEEE Trans. Wireless Commun.*, vol. 14, no. 1, pp. 107–121, Jan. 2015.

[52] T. Novlan, H. Dhillon, and J. Andrews, "Analytical modeling of uplink cellular networks," *IEEE Trans. Wireless Commun.,* vol. 12, no. 6, pp. 2669-–2679, Jun. 2013.

[53] P. Madhusudhanan, J. Restrepo, Y. Liu, T. Brown, and K. Baker, "Stochastic ordering based carrier-to-interference ratio analysis for the shotgun cellular systems," *IEEE Wireless Commun. Lett.,* vol.1, no. 6, pp. 565-–568, Dec. 2012.

[54] M. Haenggi and R. K. Ganti, *Interference in large wireless networks,* in *Now Foundations and Trends,* Feb. 2009, vol. 3.

[55] F. Baccelli, M. Klein, M. Lebourges, and S. Zuyev, "Stochastic geometry and architecture of communication networks," *Telecommun. Syst.,* vol. 7, pp. 209-–227, June 1997.

[56] T. Brown, "Cellular performance bounds via shotgun cellular systems," *IEEE J. Sel. Areas Commun.,* vol. 18, no. 11, pp. 2443—2455, Nov. 2000.

[57] V. Chandrasekhar and J. G. Andrews, "Uplink capacity and interference avoidance for two-tier femtocell networks," *IEEE Trans. Wireless Commun.,* vol. 8, no. 7, pp. 3498-–3509, July 2009.

[58] V. Chandrasekhar and J. G. Andrews, "Spectrum allocation in two-tier networks," *IEEE Trans. Commun.,* vol. 57, no. 10, pp. 3059-–3068, Oct. 2009.

[59] V. Chandrasekhar, M. Kountouris, and J. G. Andrews, "Coverage in multi-antenna two-tier networks," *IEEE Trans. Wireless Commun.,* vol. 8, no. 10, pp. 5314-–5327, Oct. 2009.

[60] M. Haenggi, J. G. Andrews, F. Baccelli, O. Dousse, and M. Franceschetti, "Stochastic geometry and random graphs for the analysis and design of wireless networks," *IEEE J. Sel. Areas Commun.,* vol. 27, no. 7, pp. 1029—1046, Sep. 2009.

[61] A. Guo and M. Haenggi, "Spatial stochastic models and metrics for the structure of base stations in cellular networks," *IEEE Trans. Wireless Commun.*, vol. 12, no. 11, pp. 5800–5812, Nov. 2013.

[62] K. Smiljkovikj, P. Popovski, and L. Gavrilovska, "Analysis of the decoupled access for downlink and uplink in wireless heterogeneous networks," *IEEE Wireless Commun. Lett.*, vol. 4, no. 2, pp. 173—176, Apr. 2015.

[63] M. Bacha, Y. Wu, and B. Clerckx, "Downlink and uplink decoupling in two-tier heterogeneous networks with multi-antenna base stations," *IEEE Trans. Wireless Commun.*, vol. 16, no. 5, pp. 2760–2775, May 2017.

[64] H. S. Dhillon, R. K. Ganti, F. Baccelli, and J. G. Andrews, "Modeling and analysis of K-tier downlink heterogeneous cellular networks," *IEEE Trans. Wireless Commun.*, vol. 30, pp. 550–560, 2012.

[65] S. Mukherjee, "Distribution of downlink SINR in heterogeneous cellular networks," *IEEE J. Sel. Areas Commun.*, vol. 30, no. 3, pp. 575-–585, Apr. 2012.

[66] H.-S. Jo, Y. J. Sang, P. Xia, and J. G. Andrews, "Heterogeneous cellular networks with flexible cell association: a comprehensive downlink SINR analysis," *IEEE Trans. Wireless Commun.*, vol. 11, no. 10, pp. 3484—3495, Oct. 2012.

[67] H. Kong, P. Wang, D. Niyato, and Y. Cheng, "Modeling and analysis of wireless sensor networks with/without energy harvesting using ginibre point processes," *IEEE Trans. Wireless Commun.*, vol. 16, no. 6, pp. 3700–3713, Jun. 2017.

[68] N. Deng, M. Haenggi, and Y. Sun, "Millimeter-wave device-to-device networks with heterogeneous antenna arrays," *IEEE Trans. Commun.*, vol. 66, no. 9, pp. 4271–4285, Sept. 2018.

[69] S. Singh, X. Zhang, and J. G. Andrews, "Joint rate and SINR coverage analysis for decoupled uplink-downlink biased cell associations in HetNets," *IEEE Trans. Wireless Commun.*, vol. 14, no. 10, pp. 5360-–5373, Oct. 2015.

[70] F. Boccardi, J. Andrews, H. Elshaer, M. Dohler, S. Parkvall, P. Popovski, and S. Singh, "Why to decouple the uplink and downlink in cellular networks and how to do it," *IEEE Commun. Mag.*, vol. 54, no. 3, pp. 110—117, Mar. 2016.

[71] H. Elshaer, M. N. Kulkarni, F. Boccardi, J. G. Andrews, and M. Dohler, "Downlink and uplink cell association with traditional macrocells and millimeter wave small cells," *IEEE Trans. Wireless Commun.*, vol. 15, no. 9, pp. 6244—6258, Sep. 2016.

[72] Y. Dhungana and C. Tellambura, "Multichannel analysis of cell range expansion and resource partitioning in two-tier heterogeneous cellular networks," *IEEE Trans. Wireless Commun.*, vol. 15, no. 3, pp. 2394–2406, Mar. 2016.

[73] K. Li, C. Yang, Z. Chen, and M. Tao, "Optimization and analysis of probabilistic caching in N -tier heterogeneous networks," *IEEE Trans. Wireless Commun.*, vol. 17, no. 2, pp. 1283–1297, Feb. 2018.

[74] J. Park, N. Lee, and R. W. Heath, "Feedback design for multi-antenna K-tier heterogeneous downlink cellular networks," *IEEE Trans. Wireless Commun.*, vol. 17, no. 6, pp. 3861–3876, Jun. 2018.

[75] Q. Cui, X. Yu, Y. Wang, and M. Haenggi, "The SIR meta distribution in poisson cellular networks with base station cooperation," *IEEE Trans. Commun.,* vol. 66, no. 3, pp. 1234–1249, Mar. 2018.

[76] P. Madhusudhanan, J. G. Restrepo, Y. Liu, and T. X. Brown, "Analysis of downlink connectivity models in a heterogeneous cellular network via stochastic geometry," *IEEE Trans. Wireless Commun.,* vol. 15, no. 6, pp. 3895-–3907, Jun. 2016.

[77] T. D. Novlan, R. K. Ganti, A. Ghosh, and J. G. Andrews, "Analytical evaluation of fractional frequency reuse for ofdma cellular networks," *IEEE Trans. Wireless Commun.,* vol. 10, no. 12, pp. 4294-–4305, 2011.

[78] R. Trestian, O. Ormond, and G. Muntean, "Game theory-based network selection: Solutions and challenges," *IEEE Commun. Surveys Tutorials,* vol. 14, no. 4, pp. 1212–=1231, Fourth Quarter 2012.

[79] H.S. Jo, Y. Sang, P. Xia, and J. Andrews, "Outage probability for heterogeneous cellular networks with biased cell association," in *Proc. IEEE Global Commun. Conf.,* Houston, TX, USA, Dec. 2011, pp. 1–5.

[80] E. Mugume and D. K. C. So, "User association in energy-aware dense heterogeneous cellular networks," *IEEE Trans. Wireless Commun.,* vol. 16, no. 3, pp. 1713–1726, Mar. 2017.

[81] 3GPP TR 36.942, *Radio Frequency (RF) system scenarios (Release 10),* Dec. 2010.

[82] 3GPP TSG RAN WG1, R1-101506, *Importance of serving cell selection in heterogeneous networks,* Qualcomm Incorporated, San Francisco, Feb. 2010.

[83] N. Trabelsi, C. S. Chen, R. El Azouzi, L. Roullet, and E. Altman, "User association and resource allocation optimization in LTE cellular networks," *IEEE Trans. Net. Service Management,* vol. 14, no. 2, pp. 429–440, June 2017.

[84] E. Turgut and M. C. Gursoy, "Coverage in heterogeneous downlink millimeter wave cellular networks," *IEEE Trans. Commun.,* vol. 65, no. 10, pp. 4463–4477, Oct. 2017.

[85] H. ElSawy, E. Hossain, and S. Camorlinga, "Traffic offloading techniques in two-tier femtocell networks," in *Proc. IEEE Int. Conf. Commun.,* Budapest, 2013, pp. 6086–6090.

[86] T.H. Kim and T.J. Lee. "Throughput enhancement of macro and femto networks by frequency reuse and pilot sensing," in *Proc. IEEE Int. Performance, Computing and Commun. Conf.,* Austin, Texas, 2008, pp. 390–394.

[87] L. Su, C. Yang, and C. L. I, "Energy and spectral efficient frequency reuse of ultra dense networks," *IEEE Trans. Wireless Commun.,* vol. 15, no. 8, pp. 5384–5398, Aug. 2016.

[88] G. Giambene, V. A. Le, T. Bourgeau, and H. Chaouchi, "Iterative multi-level soft frequency reuse with load balancing for heterogeneous LTE-A systems," *IEEE Trans. Wireless Commun.,* vol. 16, no. 2, pp. 924–938, Feb. 2017.

[89] 3GPP, "Overview of 3GPP Release 12", Sep. 2014.

[90] 3GPP, "Overview of 3GPP Release 13", Feb. 2015.

[91] 3GPP, "Overview of 3GPP Release 14", Mar. 2016.

[92] S. Fu, B. Wu, H. Wen, P.-H. Ho, and G. Feng, "Transmission scheduling and game theoretical power allocation for interference coordination in CoMP," *IEEE Trans. Wireless Commun.*, vol. 13, no. 1, pp. 112—123, Jan. 2014.

[93] G. Nigam, P. Minero, and M. Haenggi, "Coordinated multipoint joint transmission in heterogeneous networks," *IEEE Trans. Commun.*, vol. 62, no. 11, pp. 4134—4146, Nov. 2014.

[94] W. Luo, Y. Ji, and A. Guo, "An adaptive ABS-CoMP scheme in LTE advanced heterogeneous networks," in *Proc. IEEE 24th Annual Int. Symp. Personal, Indoor, and Mobile Radio Commun.*, London, 2013, pp. 2769–2773.

[95] M. Hunukumbure and S. Vadgama, "Improving cell edge energy efficiency through CoMP beam-forming," *IEEE Veh. Techn. Conf.*, pp. 1–5, June 2013.

[96] N. H. Mahmood, I. S. Ansari, G. Berardinelli, P. Mogensen, and K. A. Qaraqe, "Analysing self interference cancellation in full duplex radios," in *Proc. IEEE Wireless Commun. Netw. Conf.*, Doha, Qatar, Apr. 2016, pp. 1–6.

[97] E. Björnson, L. Sanguinetti and M. Kountouris, "Deploying dense networks for maximal energy efficiency: small cells meet massive MIMO," *IEEE J. Select. Areas Commun.*, pp. 832–847, Apr. 2016.

[98] G. Zhang and M. Haenggi, "The performance of successive interference cancellation in random wireless networks," *IEEE Trans. Inf. Theory*, vol. 60, pp. 6368-6388, Oct. 2014.

[99] G. Zhang and M. Haenggi, "On decoding the k th strongest user in Poisson networks with arbitary fading distribution," in *Proc. Asilomar Conf. Signals, Systems and Computers*, Pacific Grove, CA, May 2013, pp. 733–737.

[100] G. Zhang and M. Haenggi, "Successive interference cancellation in downlink heterogeneous cellular networks," in *Proc. IEEE Global Commun. Conf.*, Atlanta, GA, Dec. 2013, pp. 730–735.

[101] M. Wildemeersch, T. Q. Quek, M. Kountouris, A. Rabbachin, and C. H. Slump, "Successive interference cancellation in heterogeneous cellular networks," *IEEE Trans. Commun.*, vol. 62, pp. 2006–2021, Jun. 2014.

[102] I. A. Hemadeh, K. Satyanarayana, M. El-Hajjar, and L. Hanzo, "Millimeter-wave communications: Physical channel models, design considerations, antenna constructions, and link-budget," *IEEE Commun. Surveys & Tutorials,* vol. 20, no. 2, pp. 870–913, Second quarter 2018.

[103] M. Marcus and B. Pattan, "Millimeter wave propagation, spectrum management implications," *IEEE Microw. Mag.,* vol. 6, no. 2, pp. 54-–62, Jun. 2005.

[104] D. Liu, L. Wang, Y. Chen, M. Elkashlan, K. K. Wong, R. Schober, and L. Hanzo, "User association in 5G networks: A survey and an outlook," *IEEE Commun. Surveys & Tutorials,* vol. 18, no. 2, pp. 1018–1044, Second quarter 2016.

[105] S. Rangan, T. S. Rappaport, and E. Erkip, "Millimeter-wave cellular wireless networks: Potentials and challenges," in *Proc. IEEE,* vol. 102, no. 3, pp. 366—385, Mar. 2014.

[106] F. Boccardi, R. W. Heath, A. Lozano, T. L. Marzetta, and P. Popovski, "Five disruptive technology directions for 5G," *IEEE Commun. Mag.,* vol. 52, no. 2, pp. 74–80, Feb. 2014.

[107] T. S. Rappaport, Y. Xing, G. R. MacCartney, A. F. Molisch, E. Mellios, and J. Zhang, "Overview of millimeter wave communications for fifth-generation (5G) wireless networks — With a focus on propagation models," *IEEE Trans. Antennas and Propagation,* vol. 65, no. 12, pp. 6213–6230, Dec. 2017.

[108] M. Xiao et al., "Millimeter wave communications for future mobile networks," *IEEE J. Select. Areas Commun.,* vol. 35, no. 9, pp. 1909–1935, Sept. 2017.

[109] S. A. Busari, S. Mumtaz, S. Al-Rubaye, and J. Rodriguez, "5G millimeter-wave mobile broadband: Performance and challenges," *IEEE Commun. Mag.,* vol. 56, no. 6, pp. 137–143, Jun. 2018.

[110] S. Kutty and D. Sen, "Beamforming for millimeter wave communications: An inclusive survey," *IEEE Commun. Surveys Tutorials,* vol. 18, no. 2, pp. 949-–973, Second quarter 2016.

[111] E. Björnson, E. G. Larsson, and T. L. Marzetta, "Massive MIMO: Ten myths and one critical question," *IEEE Commun. Mag.,* vol. 54, no. 2, pp. 114—123, Feb. 2016.

[112] L. Wei, R. Q. Hu, Y. Qian, and G. Wu, "Key elements to enable millimeter wave communications for 5G wireless systems," *IEEE Wireless Commun.,* vol. 21, no. 6, pp. 136–143, Dec. 2014.

[113] A. Thornburg and R. W. Heath, "Ergodic rate of millimeter wave ad hoc networks," *IEEE Trans. Wireless Commun.,* vol. 17, no. 2, pp. 914–926, Feb. 2018.

[114] V. Petrov, M. Komarov, D. Moltchanov, J. M. Jornet, and Y. Koucheryavy, "Interference and SINR in millimeter wave and terahertz communication systems with blocking and directional antennas," *IEEE Trans. Wireless Commun.,* vol. 16, no. 3, pp. 1791–1808, Mar. 2017.

[115] J. G. Andrews, T. Bai, M. N. Kulkarni, A. Alkhateeb, A. K. Gupta, and R. W. Heath, "Modeling and analyzing millimeter wave cellular systems," *IEEE Trans. Commun.,* vol. 65, no. 1, pp. 403–430, Jan. 2017.

[116] S. Nie, G. R. MacCartney, S. Sun, and T. S. Rappaport, "72 GHz millimeter wave indoor measurements for wireless and backhaul communications," in *Proc. IEEE 24th Annual Int. Symp. Personal, Indoor, and Mobile Radio Commun.,* London, 2013, pp. 2429–2433.

[117] G. Yang, M. Xiao, M. Alam, and Y. Huang, "Low-latency heterogeneous networks with millimeter-wave communications," *IEEE Commun. Mag.,* vol. 56, no. 6, pp. 124–129, Jun. 2018.

[118] G. Ghatak, A. De Domenico, and M. Coupechoux, "Coverage analysis and load balancing in HetNets with millimeter wave multi-RAT small cells," *IEEE Trans. Wireless Commun.*, vol. 17, no. 5, pp. 3154–3169, May 2018.

[119] M. Shi, K. Yang, C. Xing, and R. Fan, "Decoupled heterogeneous networks with millimeter wave small cells," *IEEE Trans. Wireless Commun.*, vol. 17, no. 9, pp. 5871–5884, Sept. 2018.

[120] G. Zhang, T. Q. S. Quek, M. Kountouris, A. Huang, and H. Shan, "Fundamentals of heterogeneous backhaul design—Analysis and optimization," *IEEE Trans. Commun.*, vol. 64, no. 2, pp. 876–889, Feb. 2016.

[121] L. Hanzo, M. El-Hajjar, and O. Alamri, "Near-capacity wireless transceivers and cooperative communications in the MIMO era: Evolution of standards, waveform design, and future perspectives," *Proc. IEEE*, vol. 99, no. 8, pp. 1343–1385, Aug. 2011.

[122] W. Roh et al., "Millimeter-wave beamforming as an enabling technology for 5G cellular communications: Theoretical feasibility and prototype results," *IEEE Commun. Mag.*, vol. 52, no. 2, pp. 106–113, Feb. 2014.

[123] S. Hur, T. Kim, D. J. Love, J. V. Krogmeier, T. A. Thomas, and A. Ghosh, "Millimeter wave beamforming for wireless backhaul and access in small cell networks," *IEEE Trans. Commun.*, vol. 61, no. 10, pp. 4391–4403, Oct. 2013.

[124] H. Li, Z. Wang, Q. Liu and M. Li, "Transmit antenna selection and analog beamforming with low-resolution phase shifters in mmWave MISO systems," *IEEE Commun. Lett.*, vol. 22, no. 9, pp. 1878-1881, Sept. 2018.

[125] M. Hashemi, C. E. Koksal, and N. B. Shroff, "Out-of-band millimeter wave beamforming and communications to achieve low latency and high energy efficiency in 5G systems," *IEEE Trans. Commun.*, vol. 66, no. 2, pp. 875–888, Feb. 2018.

[126] L. Zhu, J. Zhang, Z. Xiao, X. Cao, D. O. Wu, and X. Xia, "Joint power control and beamforming for uplink non-orthogonal multiple access in 5G millimeter-wave communications," *IEEE Trans. Wireless Commun.*, vol. 17, no. 9, pp. 6177–6189, Sept. 2018.

[127] M. N. Kulkarni, A. Ghosh, and J. G. Andrews, "A comparison of MIMO techniques in downlink millimeter wave cellular networks with hybrid beamforming," *IEEE Trans. Commun.*, vol. 64, no. 5, pp. 1952–1967, May 2016.

[128] F. Sohrabi and W. Yu, "Hybrid analog and digital beamforming for mmWave OFDM large-scale antenna arrays," *IEEE J. Select. Areas Commun.*, vol. 35, no. 7, pp. 1432–1443, July 2017.

[129] D. Zhang, Y. Wang, X. Li, and W. Xiang, "Hybridly connected structure for hybrid beamforming in mmWave massive MIMO systems," *IEEE Trans. Commun.*, vol. 66, no. 2, pp. 662–674, Feb. 2018.

[130] W. Ni and X. Dong, "Hybrid block diagonalization for massive multiuser MIMO systems," *IEEE Trans. Commun.*, vol. 64, no. 1, pp. 201–211, Jan. 2016.

[131] X. Yu, J.-C. Shen, J. Zhang, and K. Letaief, "Alternating minimization algorithms for hybrid precoding in millimeter wave MIMO systems," *IEEE J. Sel. Topics Signal Process.,* vol. 10, no. 3, pp. 485–500, Apr. 2016.

[132] A. Thornburg, T. Bai, and R. W. Heath, "Performance analysis of outdoor mmWave ad hoc networks," *IEEE Trans. Sign. Proc.*, vol. 64, pp. 4065–4079, Aug. 2016.

[133] T. Bai and R. W. Heath Jr., "Coverage and rate analysis for millimeter wave cellular networks," *IEEE Trans. Wireless Commun.,* vol. 14, no. 2, pp. 1100–1114, Oct. 2014.

[134] X. Yu, J. Zhang, and K. B. Letaief, "Coverage analysis for dense millimeter wave cellular networks: The impact of array size," in *Proc. IEEE Wireless Commun. Netw. Conf.*, Doha, Qatar, Apr. 2016, pp. 1558–2612.

[135] M. Ding, P. Wang, D. Lopez-Perez, G. Mao, and Z. Lin, "Performance impact of LoS and NLoS transmissions in dense cellular networks," *IEEE Trans. Wireless Commun.,* vol. 15, no. 3, pp. 2365–2380, Nov. 2015.

[136] A. Toscano, F. Bilotti, and L. Vegni, "Fast ray-tracing technique for electromagnetic field prediction in mobile communications," *IEEE Trans. Magn.,* vol. 39, no. 3, pp. 1238–1241, May 2003.

[137] K. Rizk, J.-F. Wagen, and F. Gardiol, "Two-dimensional ray-tracing modeling for propagation prediction in microcellular environments," *IEEE Trans. Veh. Technol.,* vol. 46, no. 2, pp. 508–518, May 1997.

[138] K. Han, Y. Cui, Y. Wu, and K. Huang, "The connectivity of millimeter wave networks in urban environments modeled using random lattices," *IEEE Trans. Wireless Commun.,* vol. 17, no. 5, pp. 3357–3372, May 2018.

[139] G. George, K. Venugopal, A. Lozano, and R. W. Heath, "Enclosed mmWave wearable networks: Feasibility and performance," *IEEE Trans. Wireless Commun.,* vol. 16, no. 4, pp. 2300–2313, Apr. 2017.

[140] H. Shokri-Ghadikolaei, C. Fischione, G. Fodor, P. Popovski, and M. Zorzi, "Millimeter wave cellular networks: A MAC layer perspective," *IEEE Trans. Commun.,* vol. 63, no. 10, pp. 3437–3458, Oct. 2015.

[141] M. Di Renzo, "Stochastic geometry modeling and analysis of multi-tier millimeter wave cellular networks," *IEEE Trans. Commun.,* vol. 14, no. 9, pp. 5038–5057, Sep. 2015.

[142] D. Maamari, N. Devroye, and D. Tuninetti, "Coverage in mmWave cellular networks with base station cooperation," *IEEE Trans. Wireless Commun.,* vol. 15, no. 4, pp. 2981–2994, Apr. 2016.

[143] J. Park, S. Kim and J. Zander, "Tractable resource management with uplink decoupled millimeter-wave overlay in ultra-dense cellular networks," *IEEE Trans. Wireless Commun.,* vol. 15, no. 6, pp. 4362–4379, Jun. 2016.

[144] W. Yi, Y. Liu, and A. Nallanathan, "Cache-enabled HetNets with millimeter wave small cells," *IEEE Trans. Commun.*, vol. 66, no. 11, pp. 5497–5511, Nov. 2018.

[145] ETSI, "White paper: E-Band and V-Band - Survey on status of worldwide regulation," tech. rep., Jun. 2015.

[146] 3GPP TR 38.901, http://www.3gpp.org/DynaReport/38901.htm.

[147] 3GPP, "Overview of 3GPP Release 15", Jun. 2018.

[148] E. Perahia, C. Cordeiro, M. Park, and L. L. Yang, "IEEE 802.11ad: Defining the next generation multi-Gbps Wi-Fi," in *Proc. IEEE Consumer Commun. Net. Conf.*, Las Vegas, NV, Aug. 2010, pp. 1–5.

[149] W. Haiming, H. Wei, C. Jixin, S. Bo and P. Xiaoming, "IEEE 802.11aj (45GHz): A new very high throughput millimeter-wave WLAN system," *China Commun.*, vol. 11, no. 6, pp. 51–62, Jun. 2014.

[150] C. W. Pyo and H. Harada, "Throughput analysis and improvement of hybrid multiple access in IEEE 802.15.3c mm-wave WPAN," *IEEE J. Select. Areas Commun.*, vol. 27, no. 8, pp. 1414–1424, Oct. 2009.

[151] K. Venugopal, M. C. Valenti, and R. W. Heath, "Device-to-device millimeter wave communications: Interference, coverage, rate, and finite topologies," *IEEE Trans. Wireless Commun.*, vol. 15, no. 9, pp. 6175–6188, Sept. 2016.

[152] E. G. Larsson, O. Edfors, F. Tufvesson, and T. L. Marzetta, "Massive MIMO for next generation wireless systems," *IEEE Commun. Mag.*, vol. 52, no. 2, pp. 186–195, Feb. 2014.

[153] C. Mollén, J. Choi, E. G. Larsson, and R. W. Heath, "Uplink performance of wideband massive MIMO with one-bit ADCs," *IEEE Trans. Wireless Commun.*, vol. 16, no. 1, pp. 87–100, Jan. 2017.

[154] E. Björnson, J. Hoydis, and L. Sanguinetti, "Massive MIMO has unlimited capacity," *IEEE Trans. Wireless Commun.*, vol. 17, no. 1, pp. 574–590, Jan. 2018.

[155] A. Checko, H. L. Christiansen, Y. Yan, L. Scolari, G. Kardaras, M. S. Berger, and L. Dittmann, "Cloud RAN for mobile networks—A technology overview," *IEEE Commun. Surveys & Tutorials*, vol. 17, no. 1, pp. 405–426, First quarter 2015.

[156] S. Luo, R. Zhang, and T. J. Lim, "Downlink and uplink energy minimization through user association and beamforming in C-RAN," *IEEE Trans. Wireless Commun.*, vol. 14, no. 1, pp. 494–508, Jan. 2015.

[157] C. Pan, M. Elkashlan, J. Wang, J. Yuan, and L. Hanzo, "User-centric C-RAN architecture for ultra-dense 5G networks: Challenges and methodologies," *IEEE Commun. Mag.*, vol. 56, no. 6, pp. 14–20, Jun. 2018.

[158] Y. Liu, G. Pan, H. Zhang, and M. Song, "On the capacity comparison between MIMO-NOMA and MIMO-OMA," *IEEE Access*, vol. 4, pp. 2123–2129, 2016.

[159] Z. Ding, Y. Liu, J. Choi, Q. Sun, M. Elkashlan, Chih-Lin I, and H. V. Poor, "Application of non-orthogonal multiple access in LTE and 5G networks," *IEEE Commun. Mag.*, vol. 55, no. 2, pp. 185–191, Feb. 2017.

[160] Z. Wu, K. Lu, C. Jiang, and X. Shao, "Comprehensive study and comparison on 5G NOMA schemes," *IEEE Access*, vol. 6, pp. 18511–18519, 2018.

[161] H. Alves, R. D. Souza, and M. E. Pellenz, "Brief survey on full-duplex relaying and its applications on 5G," in *Proc. IEEE Int. Workshop Comput. Aided Modeling Anal. Design Commun. Links Netw.,* Guildford, Sept. 2015, pp. 17–21.

[162] S. Wang, V. Venkateswaran, and X. Zhang, "Fundamental analysis of full-duplex gains in wireless networks," *IEEE Trans. Netw.*, vol. 25, pp. 1401–1416, Jun. 2017.

[163] A. H. Sakr and E. Hossain, "On user association in multi-tier full-duplex cellular networks," *IEEE Trans. Commun.*, vol. 65, pp.4080–4095, Sept. 2017.

[164] N. H. Mahmood, M. G. Sarret, G. Berardinelli, and P. Mogensen, "Full duplex communications in 5G small cells," in *Proc. Int. Wireless Commun. Mobile Computing Conf.*, Valencia, Jul. 2017, pp. 1665–1670.

[165] A. Asadi, Q. Wang and V. Mancuso, "A survey on device-to-device communication in cellular networks," *IEEE Commun. Surveys & Tutorials,* vol. 16, no. 4, pp. 1801–1819, Fourth quarter 2014.

[166] Z. Zhang, Z. Ma, M. Xiao, Z. Ding, and P. Fan, "Full-duplex device-to-device-aided cooperative non- orthogonal multiple access," *IEEE Trans. Veh. Tech.,* vol. 66, no. 5, pp. 4467–4471, May 2017.

[167] Y. Pan, C. Pan, Z. Yang, and M. Chen, "Resource allocation for D2D communications underlaying a NOMA-based cellular network," *IEEE Wireless Commun. Lett.,* vol. 7, no. 1, pp. 130–133, Feb. 2018.

[168] F. Baccelli and B. Blaszczyszyn, "Stochastic geometry and wireless networks: Volume I Theory," in *Now Foundations and Trends,* 2010.

[169] Hough, J.B., Krishnapur, M., Peres, Y., and Virág, B. "Zeros of gaussian analytic functions and determinantal point processes" *American Mathematical Society*, Providence, RI (2009)

[170] H. Alzer, "On some inequalities for the incomplete Gamma function," *Mathematics of Computation*, pp. 771–778, 1997.

[171] I. S. Gradshteyn and I. M. Ryzhik, *Table of integrals, series, and products*, in *Elsevier*, Academic Press, 2007.

[172] A. Mahmud and K. A. Hamdi, "A unified framework for the analysis of fractional frequency reuse techniques," *IEEE Trans. Commun.,* vol. 62, pp. 3692–3705, Oct. 2014.

[173] P. D. Mankar, G. Das, and S. S. Pathak, "Load-aware performance analysis of cell center/edge users in random HetNets," *IEEE Trans. Veh. Technology,* vol. 67, pp. 2476–2490, March 2018.

[174] M. Rebato, M. Mezzavilla, S. Rangan, F. Boccardi, and M. Zorzi, "Understanding noise and interference regimes in 5G millimeter-wave cellular networks," in *Proc. European Wireless Conf.,* Oulu, Finland, 2016, pp. 1–5.

[175] T. Riihonen, S. Werner, and R. Wichman, "Hybrid full-duplex/half-duplex relaying with transmit power adaptation," *IEEE Trans. Wireless Commun.,* vol. 10, no. 9, pp. 3074–3085, Sept. 2011.

[176] C. Psomas, M. Mohammadi, I. Krikidis, and H. A. Suraweera, "Impact of directionality on interference mitigation in full-duplex cellular networks," *IEEE Trans. Wireless Commun.*, vol. 16, pp. 487–502, Jan. 2017.

[177] M. Haenggi, "The meta distribution of the SIR in poisson bipolar and cellular networks," *IEEE Trans. Wireless Commun.,* vol. 15, no. 4, pp. 2577–2589, Apr. 2016.

[178] P. Kumari, J. Choi, N. Gonzalez-Prelcic, and R. W. Heath, Jr., "IEEE 802.11ad-based radar: An approach to joint vehicular communication-radar system," *IEEE Trans. Veh. Technol.,* vol. 67, no. 4, pp. 3012–3027, Apr. 2018.

[179] J. Lyu and R. Zhang, "Network-connected UAV: 3D system modeling and coverage performance analysis," *arXiv preprint arXiv:1901.07887*, 2019.

[180] J. A. Zhang, X. Huang, Y,J, Guo, J. Yuan, and R. W. Heath, "Multibeam for joint communication and radar sensing using steerable analog antenna arrays," *IEEE Trans. Veh. Technol.*, vol. 68, no. 1, pp. 671-685, Jan. 2019.

[181] L. Zheng, M. Lops, X. Wang, and E. Grossi, "Joint design of overlaid communication systems and pulsed radars," *IEEE Trans. Sig. Process.,* vol. 66, no. 1, pp. 139–154, Jan, 2018.

[182] T. Riihonen, S. Werner, and R. Wichman, "Hybrid full-duplex/half-duplex relaying with transmit power adaptation," *IEEE Trans. Wireless Commun.*, vol. 10, no. 9, pp. 3074–3085, Sept. 2011.

[183] R. C. Daniels, E. R. Yeh, and R. W. Heath, Jr., "Forward collision vehicular radar with IEEE 802.11: Feasibility demonstration through measurements," *IEEE Trans. Veh. Technol.*, vol. 67, no. 2, pp. 1404-–1416, Feb. 2018.

[184] X. Yu, J. Zhang, and K. B. Letaief, "Coverage analysis for dense millimeter wave cellular networks: The impact of array size," in *Proc. IEEE Wireless Commun. Netw. Conf.*, Doha, Qatar, Sep. 2016, pp. 1558–2612.

[185] H. Deng and B. Himed, "Interference mitigation processing for spectrum-sharing between radar and wireless communications systems," *IEEE Trans. Aerosp. Electron. Syst.*, vol. 49, no. 3, pp. 1911–1919, Jul. 2013.

[186] S. Krishnan and H. S. Dhillon, "Spatio-temporal interference correlation and joint coverage in cellular networks," *IEEE Trans. Wireless Commun.*, vol. 16, no. 9, pp. 5659–5672, Sept. 2017.

[187] G. Nigam, P. Minero, and M. Haenggi, "Spatio-temporal cooperation in heterogeneous cellular networks," *IEEE J. Sel. Areas Commun.*, vol. 33, no. 6, pp. 1253–1265, Jun. 2015.

[188] A. Munari, N. Grosheva, L. Simić, and P. Petri Mähönen, "Performance of radar and communication networks coexisting in shared spectrum bands," *arXiv preprint arXiv:1902.01359*, 2019.